

# Electrochemical sensing and imaging of biological samples

THÈSE N° 6840 (2015)

PRÉSENTÉE LE 10 DÉCEMBRE 2015

À LA FACULTÉ DES SCIENCES DE BASE

LABORATOIRE D'ÉLECTROCHIMIE PHYSIQUE ET ANALYTIQUE

PROGRAMME DOCTORAL EN CHIMIE ET GÉNIE CHIMIQUE

ÉCOLE POLYTECHNIQUE FÉDÉRALE DE LAUSANNE

POUR L'OBTENTION DU GRADE DE DOCTEUR ÈS SCIENCES

PAR

Alexandra BONDARENKO

acceptée sur proposition du jury:

Dr R. Hovius, président du jury  
Prof. H. Girault, Dr F. Cortes Salazar, directeurs de thèse  
Prof. S. Rapino, rapporteuse  
Prof. C. Kranz, rapporteuse  
Prof. Ph. Renaud, rapporteur



ÉCOLE POLYTECHNIQUE  
FÉDÉRALE DE LAUSANNE

Suisse  
2015



*To my family...*

*Посвящается моим родителям...*



*Equipped with his five senses, man explores the universe  
around him and calls the adventure  
Science.*

Edwin Powell Hubble



# Acknowledgements

First and foremost, I would like to acknowledge my thesis advisor Professor Hubert Girault for giving me the opportunity to make my PhD in LEPA. Being a creative and spirited scientist, a successful manager and an exceptional supervisor, Hubert stays the soul of LEPA who always knows how to endorse and motivate everyone in his lab. Working under his leadership was a peerless experience for me including the collaborations with highly professional teams, the access to the state-of-art facilities and the possibility to participate in conferences and workshops. I sincerely thank Hubert for his constant encouragement, optimism and cheerful attitude which were the best motivation for me!

I was lucky to get a co-supervisor Dr. Fernando Cortés Salazar, the person with whom I was discussing, arguing and finding compromises every day. Working in a team with him was a great pleasure! He was always ready to help both with ideas and experimental work and encouraging me to be better than I was. Especially in writing. I am very grateful to Fernando for teaching and supporting me during all these years, for our business trips and dozens of paper drafts, for all his time and effort! Para bailar la bamba, Boss! ;)

It was my honor to have Professor Stefania Rapino, Professor Christine Kranz and Professor Philippe Renaud as the juries and Dr. Rudolf Hovius as the president of the committee of my thesis defense. I highly appreciated their work and I would like to express my gratitude for the fruitful discussion and the suggestions they gave me during the exam.

This work would never be as it is without collaboration with other scientists. Thus, it was a great pleasure to work with Dr. Horst Pick, a highly qualified specialist and also a very nice person, who introduced me to the world of mammalian cancer cells. Moreover, I highly appreciate the joint work with the team of the International Center of Biodynamics (Bucharest, Romania) which was an important part of this work. Furthermore, I would like to thank LEPA SECM team and in particular, Dr. Andreas Lesch, Dr. Dmitrii Momotenko and Tzu-En Lin, as well as MS team and specifically Dr. Liang Qiao, Dr. Yu Lu, Yingdi Zhu and Victor Costa Bassetto for their support, optimism and creativity.

A separate gratitude I would like to express to CMi personal as well as to Electronic and Mechanic workshops and especially to Joffrey Pernollet and Frédéric Gymu for their technical support and help in transforming the ideas into real devices. Moreover, it would be impossible to work without constant support of the chemical shop personal and in particular, Marie Jirousek and Jacques Gremaud who were excellent guides in the area of security and suppliers.

Additionally, it was my pleasure to meet Valérie Devaud who has done a great job in the organization and maintenance of all the working processes in LEPA. I highly appreciate her assistance, enthusiasm and effort to make our work safe and comfortable to everyone.

I would like also to acknowledge Anne Lene Odegaard and Melody Meyer for their help with administrative routine. Special thanks I want to say to Patricia Byron for her kindness, patience and professionalism. Due to her help and buoyancy all the sophisticated organization procedures were transforming into easy and enjoyable tasks.

“A friend is someone who knows all about you and still loves you.” And I was very lucky to have my beloved friends – Natalia and Astrid – working with me in LEPA. Your jokes and tease, your cookies and peanuts, your support and empathy were making my days!

I'm also very grateful for my new friends from all over the world: Ray, Alberto, Daniel, Tibo (Thibault), Marius, Alberto, Olga, Daniel (DAF), Edu, Catarina, Jon, Kristina, Marina and Mitko. You were always around for serious discussions and nonsense dialogues, for dancing and partying, for climbing and hiking, for skydiving and travelling! Gracias! Obrigada! Merci! Danke! Hvala! Благодаря! Спасибо! Un merci tout spécial je voudrais dire à Daniel et Tibo pour me pousser parlant français. Vous êtes très beaucoup joli ;)

Огромное спасибо моим друзьям, приезжавшим в гости: Ольке Кондрашиной, Ксюше Максимовой, Ольке Шуткиной, Ване Палитаю, Мише Маньлову, Ольге Проскуриной, Анечке Чекушиной, Аньке Борзенковой, Иришке Нестеренко, Стасу Конову, Маше Яковлевой, Наташе Белоглазовой и Наташе Бурмистровой. Это были чудесные дни, наполненные чаепитиями и разговорами, прогулками и пробежками, снегопадами и солнечным светом! Не меньшее спасибо тем, кто так и не смог приехать, но всегда оставался на связи: Нафаньке, Димке Сафонову, Мите, Эрдни, Дашке Перевозчиковой, Мише Селиверстову, Лёшке Богданову и Карлсону (да-да, Васильев, это ты!!!). Шутки, ирония, новости, проблемы, возможность смеяться и плакать вместе с вами, – всё это делало мою жизнь настоящей. Отдельное спасибо моим любимым дедам: Леше Кубареву, Виталию Комнатному и Гоше за ежегодные новогодние праздники и дискуссии и за уверенность что некоторые вещи со временем становятся только лучше =)

«Учителя, они как свет в пути!..» Огромное спасибо Учителям и Наставникам, умеющим привить любовь к знаниям, развивающим критическое мышление и подготовившим меня к такому серьёзному решению как получение докторской степени. Рудова Галина Николаевна, Егорова Валентина Ивановна, Южакова Ирина Николаевна, Галин Алексей Михайлович, Коренев Юрий Михайлович, Загорский Вячеслав



Викторович, Менделеева Екатерина Александровна, Морозова Наталья Игоревна, Ливанцова Людмила Ивановна, Знаменков Константин Олегович, Козлова Наталья Александровна и многие другие... Ваш труд и участие без сомнений помогли мне с диссертацией и будут еще не раз помогать по жизни.

И в заключении я бы хотела выразить благодарность всей моей семье! Всем моим родным, живущим в Казахстане, в Германии и в России! Спасибо за то что принимаете меня такой, какая я есть, за заботу и советы, и за все ваши теплые слова!

Для родителей мы всегда остаёмся детьми. И это здорово. И мне бы хотелось, сказать огромное спасибо моим родителям за неустанную заботу, поддержку и любовь, за отличное чувство юмора и бесподобный сарказм, за то что 10 лет назад отпустили и позволили быть самостоятельной, за то что научили никогда не сдаваться и всегда оставаться самой собой, и еще сто тысяч за то что! Вы – самые лучшие и я вас очень люблю =)



# Résumé

L'implémentation des méthodes analytiques pour des échantillons biologiques (comme des bactéries ou des cellules mammifères) est très importante pour le diagnostic et le traitement des diverses maladies ainsi que pour la surveillance d'environnement. Pourtant, l'analyse des échantillons biologiques est une tâche encombrante vu qu'il nécessite de haute sensibilité et de la sélectivité de détection, de la capacité à distinguer des changements dynamiques et spatiaux de concentration et des stratégies de séparation prolongées. Malgré l'apparition de certaines approches développées pour adresser tous ces points, il existe toujours la nécessité d'exploration et de développement des nouvelles plateformes analytiques qui apporteront la contribution à la manipulation des systèmes biologiques. Par conséquent, l'objectif de cette thèse est de proposer, caractériser et intégrer des nouveaux outils analytiques qui peuvent être utilisés pour la perturbation, la détection et l'imagerie d'échantillons biologiques comme des cellules cancéreuses adhérentes.

En premier approche, la microscopie électrochimique à balayage (SECM) a été combinée avec des stratégies de la fixation des cellules pour étudier des différences entre les cellules adhérentes de mélanome correspondant aux diverses stades du cancer. A cet effet, les cellules vivantes, fixées et perméabilisées ont été caractérisées par l'électrochimie. En plus elles ont été immunomarquées pour visualiser par SECM en mode de la hauteur constante la distribution variée de la tyrosinase entre les trois stades de mélanome (*i.e.* Sbc12, WM115 et WM239).

Malgré l'utilisation répandue de SECM en mode de la hauteur constante pour les études des cellules, la topographie complexe des cellules peut influencer considérablement la distance entre la sonde réelle et le substrat en encombrant l'interprétation des données expérimentales obtenues. L'application des sondes de type stylet mou pour le balayage en mode de contact pourrait servir un alternative pour éviter ces limitations, bien qu'ils puissent aussi endommager les échantillons biologiques étudiés. Ensuite, le potentiel de concept des sondes de type stylet mou pour le balayage des cellules adhérentes a été investigué. Des sondes modifiées ultra-moues ont été donc proposées pour le balayage en mode de contact des cellules adhérentes de mélanome d'une manière réussite et sans dommages.

Pendant que la plupart des expériences de SECM avec des cellules adhérentes a été consacrée à « la lecture » d'une réponse biologique, la perturbation du microenvironnement cellulaire par des réactions électrochimiques ou chimiques spatialement localisées est aussi très

importante. Par conséquent, le concept des sondes de type stylet mou a été étendu comme un outil pour altérer localement un microenvironnement de quelques cellules vivantes et adhérentes. La sonde électrochimique push-pull modifiée a été employée pour contrôler avec une grande résolution spatiotemporelle l'espace extracellulaire d'un petit nombre de cellules adhérentes, par exemple avec un marqueur fluorescent ou en modifiant localement le pH.

En dehors de SECM, la spectrométrie de masse est une méthode sensible qui ne nécessite pas de marqueurs, et qui peut aussi être utilisée pour la caractérisation de cellules cancéreuses. En conséquence, dans cette thèse la spectrométrie de masse utilisant une source désorption/ionisation laser assistée par matrice (MALDI-MS) pour des cellules intactes a été combinée avec des diverses techniques de fixation des cellules afin d'obtenir un protocole simple et rapide pour acquérir d'une manière reproductible un spectre de masse spécifique de cellules cancéreuses. Comme résultat, le protocole développé a permis de caractériser et différencier des différents types de mélanome d'une manière simple et rapide, ce qui peut être important pour le diagnostic du cancer.

Au final, l'approche de la détection ampérométrique a été exportée sur une plateforme de jet d'encre multiplexée pour le suivi des échantillons biologiques et environnementaux importants. Avec cet objectif un capteur électrochimique multiplexé a été fabriqué par l'impression jet d'encre séquentielle d'argent, de nanotubes de carbone et d'une couche isolante sur un substrat de polyimide. Le capteur a été couplé avec des différents formats d'immunoessais, *i.e.* concurrent, sandwich et non-concurrent sans marqueur. Une quantification sensible et fiable d'atrazine, d'hormone stimulant de thyroïdes et de bactéries toxiques *Escherichia coli* a été réalisée.

**Mots clés:** microscopie électrochimique à balayage, fixation des cellules, immunomarquage des cellules, stylet mou, balayage en mode de contact, sonde électrochimique push-pull, désorption-ionisation laser assistée par matrice, spectrométrie de masse de la cellule entière, capteur ampérométrique, immunoessais à la base des billes magnétiques, mélanome.

# Abstract

Implementation of analytical methods for biological samples (*e.g.* bacteria or mammalian cells) is of great importance for diagnosis and treatment of various diseases, as well as for environmental monitoring. However, analysing biological samples is a cumbersome task since it requires a high sensitivity and selectivity, a capability to sense dynamic and spatial concentration changes and time-consuming separation strategies. Although several approaches have been proposed to address all these points, there is still room for the exploration and development of new analytical platforms that contribute to the manipulation and understanding of biological systems. The aim of the present thesis is therefore to propose, characterize and implement new analytical tools that can be used for perturbing, sensing, imaging and unravelling of biological samples such as adherent cancer cells.

As a first approach, scanning electrochemical microscopy (SECM) was combined with cell fixations strategies in order to investigate differences between adherent melanoma cells corresponding to various cancer stages. For this purpose, alive, fixed and permeabilized cells were characterized electrochemically and additionally immunostained in order to visualize by constant height mode SECM the different intracellular distribution of tyrosinase among three melanoma cancer stages (*i.e.* Sbc12, WM115 and WM239).

Constant height SECM is widely used for cells investigation, but the intricate cells topography can influence significantly the real probe-substrate distance and thus encumber the interpretation of the obtained experimental data. Applying soft stylus probes in a contact mode could be an alternative to alleviate such a limitation, although it can also introduce damages on the biological samples. Therefore, as the next step the applicability of the soft stylus concept towards the scanning of adherent living cells in a contact mode was investigated. As a result, modified ultra-soft probes were implemented for the successful and damage-free contact mode scanning of adherent melanoma cells.

While the most of the SECM experiments with adherent cells have been devoted to the “reading” of a biological response, the perturbation of the cell microenvironment through spatially localized electrochemical or chemical reactions is also of high importance. Therefore, the SECM soft stylus concept was extended as a tool for locally altering the microenvironment of few adherent living cells. A re-designed electrochemical push-pull probe was employed for controlling with a high spatiotemporal resolution the extracellular

space of a small number of adherent cells, for instance by labelling with a fluorescent dye or by inducing localized pH changes.

Besides SECM, mass-spectrometry (MS) is a sensitive and label-free method which can be also used for cancer cells characterisation. Therefore, in this thesis an intact cell matrix-assisted laser desorption/ionization (MALDI) MS approach was combined with various cell fixation techniques in order to obtain a simple and fast protocol for acquiring in a reproducible manner the MS fingerprint of cancer cells. As a result, the developed protocol allowed the characterization and differentiation of various melanoma cell lines in a fast and simple manner, which can be important for cancer diagnosis.

Finally, the amperometric sensing approach was exported into an inkjet printed multiplexed platform for the monitoring of biological and environmental relevant samples. With this aim, a multiplexed electrochemical sensor device was fabricated by sequential inkjet printing of silver, carbon nanotubes and an insulating layer on a polyimide substrate and coupled to different magnetic beads-based immunoassay formats (*i.e.* competitive and sandwich enzyme as well as label-free non-competitive immunoassays). As a result, reliable and sensitive quantification of atrazine, thyroid-stimulating hormone and noxious *Escherichia coli* bacteria was achieved.

**Key words:** scanning electrochemical microscopy, cells fixation, cells immunostaining, soft stylus, contact mode scanning, electrochemical push-pull probe, matrix-assisted laser desorption/ionization, the whole cell mass spectrometry, amperometric sensors, magnetic beads-based immunoassay, melanoma.

# List of abbreviations

2D	Two dimensional
Abs	Antibodies
AC	Alternating current
AFM	Atomic force microscopy
Ag(s)	Antigen(s)
AJCC	American Joint Committee on Cancer
ALP	Alkaline phosphatase
AO	Acridine orange
ATCC	American Type Culture Collection
ATR	Atrazine
BSA	Bovine serum albumin
CE	Counter electrode
CFU	Colony forming unit
CNTs	Carbon nanotubes
CTCs	Circulating tumour cells
CV	Cyclic voltammetry
CytC	Cytochrome C
DHB	2,5-dihydroxybenzoic acid
DPV	Differential pulse voltammetry
<i>E.coli</i>	<i>Escherichia coli</i>
EGFP	Enhanced green fluorescent protein
EIA	Enzyme immunoassay
EIS	Electrochemical impedance spectroscopy
ELISA	Enzyme-linked immunosorbent assay
FcCOOH	Ferrocene carboxylic acid
FcMeOH	Ferrocene methanol
FCS	Fetal calf serum
FISH	Fluorescent <i>in-situ</i> hybridisation
GC	Gas chromatography
HCCA	$\alpha$ -cyano-4-hydroxycinnamic acid
HEPES	4-(2-hydroxyethyl)-1-piperazineethanesulfonic acid

HPCE	High-performance capillary electrophoresis
HPLC	High-performance liquid chromatography
HRP	Horse radish peroxidase
IHC	Immunohistochemistry
IJP	Inkjet printing
IPTG	Isopropyl-beta-D-thiogalactopyranoside
LB	Lysogeny broth
LC	Liquid chromatography
MALDI	Matrix-assisted laser desorption/ionization
MBs	Magnetic beads
MS	Mass spectrometry
MS/MS	Tandem mass spectrometry
PAPG	4-aminophenyl $\beta$ -D-Galactopyranoside
PAP	4-aminophenol
PAPP	4-aminophenyl phosphate
PIQ	4-aminoquinone
PBS	Phosphate buffer saline
PCR	Polymerase chain reaction
PET	Polyethylene terephthalate
PI	Polyimide
PVDF	Polyvinylidene difluoride
QDs	Quantum dots
QRE	Quasi-reference electrode
RE	Reference electrode
RGP	Radial growth phase
ROS	Reactive oxygen species
RT	Room temperature
S/N	Signal-to-noise ratio
S100	Family of calcium-binding proteins
SA	Sinapinic acid
SECM	Scanning electrochemical microscopy
SG/TC	Substrate generation/tip collection
SICM	Scanning ion-conductive microscopy
SPE	Screen-printed electrode



SPM	Scanning probe microscopy
SWV	Squarewave voltammetry
TG/SC	Tip generation/substrate collection
TMB	3,3',5,5'-tetramethylbenzidine
TOF	Time-of-flight
TSH	Thyroid-stimulating hormone
TyR	Tyrosinase
UME	Ultramicroelectrode
UV	Ultraviolet
VGP	Vertical growth phase
VOCs	Volatile organic compounds
VSM	Voltage-switching mode
WE	Working electrode
$\beta$ -GAL	$\beta$ -Galactosidase



# List of symbols

$A$	Cross sectional surface area of microchannels	$\mu\text{m}^2$
$c$	Concentration	$\text{mol m}^{-3}$
$c_0$	Maximum concentration	$\text{mol m}^{-3}$
$c_{bulk}$	Bulk concentration	$\text{mol m}^{-3}$
$c_i$	Concentration of species $i$	$\text{mol m}^{-3}$
$D$	Diffusion coefficient	$\text{m}^2 \text{s}^{-1}$
$d$	Probe–substrate distance	$\mu\text{m}$
$d_n$	Nozzle diameter	$\mu\text{m}$
$D_i$	Diffusion coefficient of species $i$	$\text{cm}^2 \text{s}^{-1}$
$E_g$	Energy gap between the ground and the first excited level	eV
$F$	Faraday constant (charge on one mole of electrons)	C
flowrate	pushing volume flow rate	$\mu\text{L min}^{-1}$
$h$	Planck constant	J s
$h_A$	Distance from the sample surface to the probe attachment point	$\mu\text{m}$
$h_P$	Real probe–substrate distance for plastic microelectrodes	$\mu\text{m}$
$I$	3x3 identity matrix	none
$i$	Current	nA
$I_T$	Normalized current ( $i_T/i_{T,\infty}$ )	none
$i_T$	Steady–state diffusion current recorded at each point	nA
$i_{T,\infty}$	Steady–state diffusion current recorded at the solution bulk	nA
$k$	Heterogeneous kinetic constant	$\text{m s}^{-1}$
$L$	Normalized distance ( $d/r_T$ )	none
linearFL	Pushing linear flow rate	$\mu\text{m min}^{-1}$
linearFL2	Aspirating linear flow rate	$\mu\text{m min}^{-1}$
$l_T$	Length of the probe in the unbent state	$\mu\text{m}$
$l_{th}$	Thermal penetration depth	nm
$l_\alpha$	Optical penetration depth	nm
$n$	Number of transfer electrons	none
$\mathbf{n}$	Vector normal to the surface	none
$N_i^*$	Normalized number densities of states $i$	none

$O$	Oxidized form of a redox couple	none
$Oh$	Ohnesorge number	none
$R$	Reduced form of a redox couple	none
$Re$	Reynolds number	none
$RG$	The ratio between $r_g$ and $r_T$	none
$r_g$	Insulating glass sheath radius	$\mu\text{m}$
$r$	Radial distance measured from the center of the disk	$\text{nm}$
$r_T$	Tip radius	$\mu\text{m}$
$t$	Time	$\text{s}$
$v$	Velocity	$\text{m s}^{-1}$
$v_{min}$	Minimum velocity (IJP)	$\text{m s}^{-1}$
$We$	Weber number	none
$\alpha$	Probe bending angle	degrees
$a$	Characteristic linear dimension (hydraulic diameter)	$\text{m}$
$\gamma$	Surface tension	$\text{M m}^{-1}$
$\Delta h$	Ablation rate	$\mu\text{m pulse}^{-1}$
$\delta$	Diffusion layer	$\mu\text{m}$
$\eta$	Dynamic viscosity	$\text{Pa s}$
$\Lambda$	Apparent kinetic constant	none
$\nu$	Frequency of light	$\text{s}^{-1}$
$\rho$	Density	$\text{kg m}^3$
$\tau_A$	Time required for initiating a (photo)chemical process	none
$\tau_T$	Thermal relaxation time	$\text{s}$
$\varphi$	Laser fluence	$\text{mJ cm}^{-2}$
$\varphi_{th}$	Fluence threshold of a material	$\text{mJ cm}^{-2}$
$\nabla$	Laplas operator	none

# Table of content

Résumé.....	i
Abstract.....	iii
List of abbreviations .....	v
List of symbols.....	viii
CHAPTER I: Introduction .....	1
1. Living organisms .....	1
1.1. Melanoma .....	1
1.2. <i>Escherichia coli</i> .....	5
2. Analytical methods .....	8
2.1. Scanning Electrochemical Microscopy.....	8
2.2. Immunoassay .....	18
2.3. Matrix-assisted laser desorption ionization .....	23
2.4. Cells fixation methods .....	25
2.5. Microfabrication .....	27
3. Thesis outline .....	31
4. References.....	32
CHAPTER II: Scanning Electrochemical Microscopy of Alive, Fixed and Permeabilized Adherent Melanoma Cells .....	49
1. Introduction.....	50
2. Materials and methods .....	52
2.1. Chemicals.....	52
2.2. Preparation of the polyimide (PI) masks .....	53
2.3. Cell culture and sample preparation .....	53
2.4. Fixation and permeabilization protocol .....	54
2.5. Protocol for TyR immunoassay within adherent cells.....	54
2.6. Immobilization of proteins on PVDF membrane.....	54

2.7. Inkjet printed (IJP) cell-like sample preparation .....	55
2.8. SECM measurements.....	55
3. Results and discussions.....	56
3.1. Influence of cell density on SECM signal .....	56
3.2. SECM of alive, fixed and permeabilized cells. Influence of redox mediator and UME translation rate.....	59
3.3. Inkjet printed cell-like sample .....	63
3.4. SECM of proteins adsorbed on PVDF membrane.....	64
3.5. SECM of different melanoma cell lines.....	65
3.6. Investigation of melanoma-associated tumour antigen TyR expression in adherent cells by SECM .....	66
4. Conclusions.....	70
5. References.....	71
CHAPTER III: Contact Mode Scanning Electrochemical Microscopy of Adherent Cancer Cells .....	75
1. Introduction.....	76
2. Materials and methods .....	77
2.1. Chemicals.....	77
2.2. Soft stylus probe fabrication .....	78
2.3. Cell culture and sample preparation .....	78
2.4. SECM measurements.....	78
3. Results and discussions.....	80
4. Conclusions.....	86
5. References.....	87
CHAPTER IV: Electrochemical Push-Pull Probe for Multimodal Altering of Cell Microenvironment.....	89
1. Introduction.....	90
2. Materials and methods .....	91

2.1. Chemicals.....	91
2.2. Cell culture preparation.....	91
2.3. Electrochemical push-pull probe fabrication.....	92
2.4. Computational model and numerical simulations.....	92
2.5. Local perturbation of adherent cells.....	96
3. Results and discussion.....	98
3.1. Computational model and numerical simulations.....	98
3.2. Experimental perturbation of adherent cancer cells.....	100
4. Conclusions.....	109
5. References.....	111
CHAPTER V: The Intact Cell MALDI-MS of Melanoma.....	113
1. Introduction.....	114
2. Materials and methods.....	115
2.1. Chemicals.....	115
2.2. Cell culture preparation.....	116
2.3. Fixation protocols.....	116
2.4. MALDI experiments.....	116
3. Results and discussion.....	117
4. Conclusions.....	123
Appendix I.....	124
Appendix II.....	125
5. References.....	126
CHAPTER VI: Inkjet Printed Carbon Nanotubes Based Multiplexed Electrochemical Sensor for Environmental and Clinical Applications.....	128
1. Introduction.....	129
2. Materials and methods.....	131
2.1. Chemicals.....	131

2.2. <i>E. coli</i> culturing.....	132
2.3. Microchip fabrication.....	132
2.4. Electrochemical characterization of IJP sensors.....	132
2.5. Electrochemical characterization of MBs by SECM.....	133
2.6. Influence of the enzyme concentration on the electrochemical signal .....	133
2.7. Detection of ATR and TSH .....	134
2.8. <i>E.coli</i> detection protocol .....	135
3. Results and discussions.....	136
3.1. IJP CNTs microchip characterization .....	136
3.2. IJP microchip for ATR immunoassay.....	139
3.3. IJP microchip for TSH immunoassay .....	141
3.4. IJP microchip for <i>E.coli</i> detection .....	143
4. Conclusions.....	144
5. References.....	145
CHAPTER VII: General Conclusions and Future Perspectives .....	148
References.....	151
<i>Curriculum Vitae</i> .....	152



# CHAPTER I

## Introduction

The aim of the present thesis is to propose, characterize and implement new analytical tools that can be used for perturbing, sensing, imaging and unravelling of biological samples such as adherent cancer cells and bacteria.

### 1. Living organisms

#### 1.1. Melanoma

##### *1.1.1. General information*

Cutaneous malignant melanoma originated from melanocytes is one of the most dangerous skin cancers that strikes thousands of people around the world.<sup>1</sup> According to the World Health Organization, about 132'000 new cases of melanoma incidence occur globally every year. The cancer progression from normal melanocytes to malignant melanoma can be described by Clark model (Figure 1.1),<sup>2</sup> distinguishing five cells transformations: *i*) increased proliferation rate of normal melanocytes, *ii*) formation of dysplastic cells and the aberrant cells growth, *iii*) intraepidermal growth during the radial-growth phase (RGP), *iv*) dermal invasion during the vertical-growth phase (VGP) and *v*) metastasis. Another melanoma classification, suggested by the American Joint Commission on Cancer (AJCC), consists of 5 stages: *i*) non-invasive and non-metastasis melanoma, (stage 0); *ii*) the tumour is non-metastatic and does not penetrate into dermis (stage I), *iii*) the tumour is non-metastatic and penetrates into dermis (stage II), *iv*) the tumour produce regional lymph node metastasis (stage III) and *v*) the metastatic tumour spreads across the whole organism (stage IV). While AJCC classification is more frequently used for melanoma diagnosis, Clark model is commonly applied for cells characterisation.

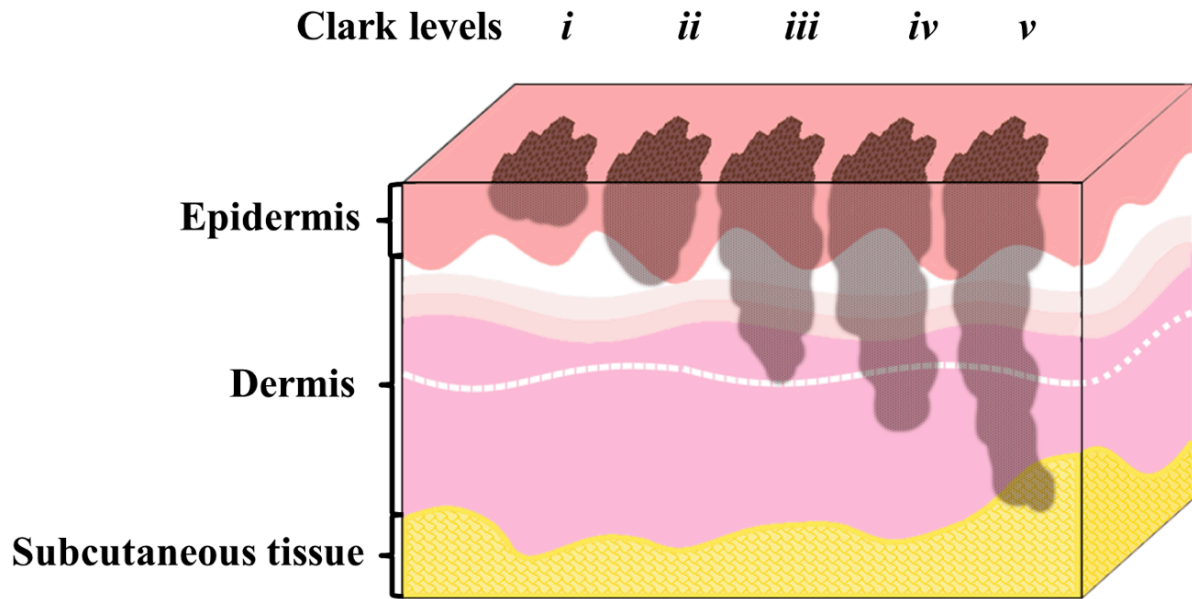


Figure 1.1. Schematic representation of melanoma progression according to Clark model.

Transformation of normal mammalian cells into tumour can be characterised by various hallmarks, including sustaining proliferative signalling, evading growth suppressor, resisting cell death, enabling replicative immortality, inducing angiogenesis, activating invasion and metastasis.<sup>3</sup> This is typically accompanied by interruption of cells processes and production of numerous tumour markers which can be detected in various biological liquids or solid tumours.<sup>4</sup> The earlier these biomarkers are detected, the higher the chances to apply an effective therapy to control the cancer progression. Therefore, development of sensitive and reliable analytical tools for biomarkers detection is of high relevance for cancer diagnosis, prognosis and treatment evaluation.<sup>5</sup>

### ***1.1.2. Melanoma biomarkers in biological fluids and methods of their detection***

Biomarkers, which can be found in biological liquids (*e.g.* blood, serum and urine) are autoantibodies,<sup>6</sup> vascular endothelial growth factor (VEGF),<sup>7,8</sup> tumour necrosis factor alpha (TNF $\alpha$ ),<sup>7</sup> S100 calcium-binding protein B (S100),<sup>7,9</sup> number of interleukins,<sup>7</sup> cluster of differentiation 146 (CD146 or MUC18),<sup>10</sup> 5-S-cysteinyldopa (5-SCD),<sup>11</sup> 6-hydroxy-5-methoxy-indole-2-carboxylic acid (6H5MI2C),<sup>11</sup> 3,4-dihydroxy-l-phenylalanine (l-dopa or DOPA),<sup>12</sup> l-tyrosine (Tyr)<sup>12</sup> and circulating tumour cells (CTCs).<sup>13-15</sup>

Detection of cancer biomarkers in biological liquids typically consists of 2 steps. On the first step, the compound of interest should be selectively captured from the sample by interaction with antibodies (Abs), glycan or specific proteins. Thereafter, the obtained complex can be detected by using various techniques (*e.g.* fluorescent, electrochemical and

mass-spectrometry (MS)). Thus, combination of sandwich immunoassay with fluorescent detection has been introduced for detection of VEGF, interleukins 6, 8 and 10, TNF $\alpha$  and S100B in human serum with a limit of detection (LOD) from 10 to 100 pg/mL,<sup>7</sup> while an immunosensor with amperometric and electrochemical impedance spectroscopy (EIS) were used for the detection of CD146.<sup>10</sup> Additionally, an electrochemical immunosensor based on anti-melanocortin 1 receptor (MC1R) Abs immobilized in silica nanoparticles-polypyrrole (PPy) nanocomposite on a working surface of a carbon screen-printed electrode (SPE) was reported for melanoma CTCs investigation.<sup>14</sup> Besides Abs, specific binding peptides were also reported for S100B capturing and detection by square wave voltammetry (SWV) with a LOD equal to 0.1 nM.<sup>9</sup> Alternatively to Abs and binding proteins, glycoprotein microarray for serum autoantibodies investigation was developed by *Liu et al.* in order to distinguish between the patients with node negative melanoma and node positive melanoma. Glycoproteins were extracted from melanoma cells and the autoantibodies were analysed by immunoassay with fluorescent detection and liquid chromatography coupled with tandem mass spectrometry (LC-MS/MS).<sup>6</sup> High-performance liquid chromatography (HPLC) and gas chromatography (GC) MS analysis of urine and plasma samples was also employed for direct detection of 5-SCD and 6H5MI2C.<sup>11</sup>

Additionally, a glassy carbon electrode modified with 3-amino-5-mercapto-1,2,4-triazole was employed for simultaneous detection of DOPA and Tyr in human blood by differential pulse voltammetry (DPV)<sup>12</sup> and the ion-selective electrode modified with epithelial cells was reported for potentiometric detection of VEGF.<sup>8</sup>

### ***1.1.3. Melanoma biomarkers in tissues and adherent cells and methods of their detection***

Various approaches for cancer biomarkers detection in tissues and cells can be roughly divided into three groups: *i*) labelling (*e.g.* immunohistochemistry (IHC) and fluorescent *in-situ* hybridisation (FISH)), *ii*) MS (*e.g.* LC-MS and GC-MS with different sample pretreatment) and *iii*) non-invasive (*e.g.* infrared, electrical impedance and optical-based) approaches.

The first group consists of various techniques applied for the analysis of skin biopsies. Among them IHC, *i.e.* immunostaining of various tumour biomarkers is the most commonly used due to its simplicity and specificity. The visualisation of the immunostained biomarkers is frequently performed by employing secondary Abs conjugated with horse radish peroxidase (HRP)<sup>16-18</sup> or alkaline phosphatase (ALP)<sup>19,20</sup> that upon enzymatic reaction with the respective substrates leads to the formation of a chromogen. The most recognised tissue

biomarkers for melanoma diagnosis by IHC are calcium-binding proteins S100,<sup>20</sup> glycoprotein 100 (gp100),<sup>20,21</sup> tyrosinase (TyR)<sup>19-21</sup> and MART-1.<sup>20</sup> Additionally, MCAM/MUC18, matrix metalloproteinase-2, Ki-67, proliferating cell nuclear Ag and p16/INK4A and mutated BRAF gen<sup>22-24</sup> were reported.<sup>22-25</sup> Some other possible biomarkers are summarized in reviews.<sup>5,25,26</sup> Besides enzymes, quantum dots (QDs) can be also employed as an IHC label. Thus, conjugation of anti-melanoma Abs with QDs allowed *in vitro* labelling of melanoma cells cocultured with normal melanocytes. The detection of cancer cells was performed optically using confocal laser scanning fluorescence microscope.<sup>27</sup>

In order to facilitate and improve the screening potential of the IHC, tissue microarray assays (TMAs) have been introduced as paraffin blocks with several (up to 1,000) separate tissue cores assembled in array fashion on a single glass slide.<sup>28</sup> The TMAs have been employed for a long list of biomarkers detection, including chromatin assembly factor 1 (CAF-1 p60),<sup>29</sup> nestin,<sup>30,31</sup> CD133,<sup>31</sup> DROSHA protein,<sup>32</sup> CD3, CD8, and CD45RO.<sup>33</sup>

Alternatively to IHC, FISH technique is based on specific binding of the fluorescent labelled oligonucleotides with complementary DNA sequences and enables the direct disclosure and localization of genetic markers in single nuclei.<sup>34</sup> This technique is highly sensitive, and a negative FISH test is a reassuring finding that supports a benign diagnosis, however, a positive FISH test should be carefully interrogated.<sup>35,36</sup> Additionally, various chemical (*e.g.* HPLC and high-performance capillary electrophoresis (HPCE)) and biological (*e.g.* methylation-sensitivity restriction enzymes (MSRE) combined with PCR and genome-wide implemented methods) methods were developed for cell DNA methylation detection and summarised by *Delpu et al.*<sup>37</sup>

The second group (MS-based approaches) have been demonstrated to be useful study the perturbation in glycolysis, tricarboxylic acid cycle, choline and fatty acid metabolism as traits of cancer cells and tissues.<sup>38</sup> For example, by employing nano-LC-MS/MS *Qendro et al.* determined that vimentin and nestin can be used to predict melanoma aggressiveness.<sup>39</sup> *Qiu et al.* developed an approach, which included proteins stable isotope labelling by amino acids in cell culture (SILAC), cell surface biotinylation, affinity peptide purification and LC-MS/MS for the identification and quantification of cell surface membrane proteins of primary and metastatic melanoma.<sup>40</sup> Additionally, generation of proteome reference maps by LC-MS/MS analysis of cancer cells grown *in vitro* with and without normal human cells contact was also applied for biomarkers discovery.<sup>41</sup> Finally, permeabilization of cells membrane in order to obtain the cytosolic cells proteins content with further 2 dimensional LC-MS/MS and 2 dimensional gel electrophoresis MS/MS analysis was suggested by *Mazzucchelli et al.*<sup>42</sup>

Besides proteins, imaging of potential lipid biomarkers in melanoma cells have been also performed, for instance by nanoassisted laser desorption-ionization MS (NALDI-MS).<sup>43</sup> Finally, MS was applied for volatile biomarkers identification by comparing the volatile organic compounds (VOCs) produced by melanoma cells and normal melanocytes cultured *in vivo*. In order to identify the biomarkers, solid-phase micro-extraction, GC-MS and single-stranded DNA-coated carbon nanotubes (DNACNTs) sensors were employed.<sup>44</sup>

Out of the non-invasive methods for melanoma diagnosis, it is worth to notice infrared, electrical impedance and optical-based approaches. Fourier transform infrared (FTIR) imaging of histological sections followed by supervised partial least squares discriminant analysis (PLS-DA) was reported to accurately (>90%) identify the main cell types commonly found in melanoma tumours.<sup>45</sup> Electrical impedance spectroscopy was shown to be a potential adjunct diagnostic tool to help clinicians differentiate between benign and malignant skin lesions without performing biopsy.<sup>46</sup> Additionally, based on the optical images of the skin lesions, various smartphone applications were suggested for the malignancy diagnostic. However, recent studies presented that 3 out of 4 of these applications incorrectly classified 30% or more of melanomas as un concerning.<sup>47</sup>

## **1.2. *Escherichia coli***

### **1.2.1. *General information***

*E. coli* is a bacteria type which contains mostly motile gram-negative bacilli within the family *Enterobacteriaceae* and the tribe *Escherichia*. The Kauffman scheme for *E. coli* strains differentiation is based on their serotype (*i.e.* surface Ag profiles) and determined by the specific combination of O (somatic) and H (flagellar) Ags which can be considered as a virulence marker and lead to the association of the bacteria with certain clinical syndromes. Virulent *E. coli* typically causes the infection evolving through colonization of a mucosal site, evasion of host defenses, multiplication and host damage stages. The infection can result in three different clinical syndromes: *i*) urinary tract infection, *ii*) sepsis/meningitis, and *iii*) enteric/diarrheal disease. Despite most of *E. coli* strains are harmless and widely used in biotechnology<sup>48</sup> the virulent serotypes can cause significant problems for food and medical industry.<sup>49</sup> Additionally, *E. coli* can be found in intestines of large number of warm-blood animals and therefore, it is used as an indicator of water safety regarding fecal contamination.<sup>50</sup> Thus, fast and sensitive methods for *E.coli* detection are of significant interest.

### **1.2.2. Laboratory methods for *E.coli* analysis**

To perform the qualitative analysis of *E. coli* in water special commercially available substrate (Colilert or Colisure test) is frequently used. The presence of total coliforms can be followed by the development of yellow color of the solution due to the cleavage of a chromogenic analog of lactose by bacterial  $\beta$ -galactosidase. As a result, the presence of *E.coli* can be determined by appearing of a blue fluorescence signal under long-wave ultraviolet light due to the bacterial cleavage of 4-methylumbelliferyl  $\beta$ -D-galactopyranoside (MUG). Despite this simple technique has been widely used for establishing the microbiological quality of drinking water, it has significant limitations since 50% of the *E. coli* O157:H7 strains do not cleave MUG and therefore cannot be detected.<sup>51</sup>

The first validated method for *E.coli* quantification was NF ISO 7402, which suggests the enumeration of *Enterobacteriaceae* by *i*) calculation of the most probable number after incubation at 35 °C or 37 °C in liquid medium (MPN technique) or *ii*) by counting colonies in a solid medium after incubation at 35 °C or 37 °C (colony-counting technique). However, nowadays this method is almost completely displaced by colony count technique at 30 °C (method NF V 08-054). The numbers of *E. coli* are typically reported in colony-forming unit (CFU) per mL or per L.

### **1.2.3. Other methods for *E.coli* analysis**

Alternatively to cell culturing, instrumental biochemical techniques for *E. coli* determination are less time-consuming, more precise and can be multiplexed for simultaneous analysis of few pathogen microorganisms. Based on the detection methods, the *E. coli* assays can be divided into three groups: *i*) optical (*e.g.* colorimetric, fluorescent and chemiluminescent), *ii*) electrochemical (*e.g.* amperometry, impedance, voltammetry)<sup>52,53</sup> and *iii*) mass-spectrometric (*e.g.* matrix-assisted laser desorption ionization (MALDI)-MS and electrospray ionization (ESI)-MS).<sup>54</sup> To perform sample pretreatment and bacteria preconcentration different filters as well as micro and nanoparticles (*e.g.* gold, fluorescent silica and quantum dots) and magnetic beads (MBs) can be used as a label for the detection step.<sup>55</sup> Additionally, significant efforts have been done to miniaturize and automate the assay format (*e.g.* by developing biosensors and lab-on-a-chip microfluidic devices)<sup>56,57</sup> and to develop multiplexed systems for simultaneous detection of different bacteria types.<sup>58</sup> In the following text only electrochemical sensors for *E. coli* detection will be discussed in details, other methods can be found in different reviews.<sup>52-55</sup>

Based on the target of the assay, electrochemical sensors for *E.coli* detection can be roughly divided into three groups: *i*) genetic content analysis, *ii*) the whole cell analysis and *iii*) metabolites analysis.<sup>59</sup> The first group includes DNA and RNA hybridization assays which can be additionally combined with amplification techniques, *e.g.* PCR, loop-mediated isothermal amplification (LAMP), helicase-dependent amplification (HDA) and nucleic acid sequence-based amplification (NASBA).<sup>53,59,60</sup> As a detection step in electrochemical genosensors, amperometric<sup>61–64</sup> and voltammetric (*i.e.* SWV,<sup>65,66</sup> alternating current (AC) voltammetry,<sup>67,68</sup> DPV<sup>69,70</sup> and CV<sup>71</sup>) are widely used. Additionally, sensors based on measuring conductivity,<sup>72</sup> chronopotentiometry<sup>73</sup> and impedance<sup>74</sup> have been reported.

The second group (*i.e.* the whole cell *E.coli* sensors) can be designed in both non-specific (*i.e.* physical adsorption) and specific format. The non-specific detection is based on the electrode blocking by the adsorption of the bacteria cells. To perform non-specific bacteria detection, carbon microelectrode arrays with voltammetric detection,<sup>75</sup> as well as Au<sup>76,77</sup> and thin films<sup>78</sup> microelectrodes with impedance monitoring have been reported. Specific whole cell *E.coli* sensors are based on Abs and anti-microbial compounds (*i.e.* concanavalin A,<sup>79–81</sup> lipopolysaccharides,<sup>79</sup> lectins,<sup>82,83</sup> T4-bacteriophage<sup>84</sup> and A-mannoside<sup>85</sup>) capable to recognize and form stable complexes with the bacterial Ags. These capturing agents are typically positioned on the electrodes for the trapping and posterior readout of the bacteria presence, however employing MBs as a carrier for Abs<sup>86–89</sup> and T4-bacteriophage<sup>84</sup> have been also employed. Additionally, the electrochemical signal amplification can be performed by introducing Au nanoparticles (AuNP)<sup>90</sup> and Pt nanochains (PtNCs).<sup>91</sup> Similar to the first group, the detection step can be performed in amperometric,<sup>86,90–93</sup> voltammetric (*i.e.* SWV,<sup>75,79,80</sup> CV<sup>88,94</sup>), impedance,<sup>76–78,84,85,89,95–102</sup> and chronocoulometric<sup>82,83</sup> way. As a label for the whole cell assay, HRP,<sup>90,92,94</sup> glucose oxidase (GOD),<sup>91</sup> AuNPs,<sup>86</sup> polyaniline<sup>88</sup> and Ru complexes<sup>81</sup> were reported. The whole cell sensor approach allows detection of *E.coli* up to 1 CFU/mL.

The third group of *E.coli* detection methods combines different approaches to investigate cells metabolites based on their enzymatic or electrochemical activity. Bacterial lipopolysaccharides can be detected by using concanavalin A<sup>103</sup> and aptamers<sup>104</sup> as capturing agents attached to the electrode surface. Bacterial  $\beta$ -Galactosidase<sup>105–109</sup> and  $\beta$ -D-glucuronidase<sup>105</sup> activity can be monitored by amperometric detection of enzymatic reactions products. Detection of cells biological activity can be also combined with Abs-capturing approach.<sup>107</sup> A brief summary of the developed sensors for the detection of cells metabolism products is given in Table 1.1.

Table 1.3. Biosensors with electrochemical detection based on *E.coli* metabolism

Target	Principle	Immobilization	Detection	Limit of detection	Ref
$\beta$ -Galactosidase $\beta$ -D-glucuronidase	Microbial fuel cell	no	Voltammetry	Not reported	<sup>105</sup>
$\beta$ -Galactosidase	Pt on glass	Collagen gel	Amperometry	$10^3$ CFU	<sup>106</sup>
Lipopolysaccharide	Polyaniline modified steel electrodes	Concanavalin A	Impedance	50 $\mu$ g/mL	<sup>103</sup>
Lipopolysaccharide	Au electrode	Aptamers	Impedance	0.001 ng/mL	<sup>104</sup>
The viable cell based on $\beta$ -Galactosidase	SPE, PAPG substrate	Abs on electrode	Amperometry	$10^3$ CFU/mL	<sup>107</sup>
The viable cell based on $\beta$ -Galactosidase	Tyrosinase composite biosensor, Phenyl-PG substrate	no	Amperometry	1 CFU/100 mL	<sup>108</sup>
The whole cell based on $\beta$ -Galactosidase	Pt coated Au nanoporous film	no	Amperometry	1 CFU/mL	<sup>109</sup>
Polyphenolic metabolites	SAM-bi-enzyme biosensor (HRP and laccase)	no	Amperometry	$9.7 \times 10^2$ CFU/mL	<sup>110</sup>

## 2. Analytical methods

### 2.1. Scanning Electrochemical Microscopy

Scanning electrochemical microscopy (SECM) is a type of scanning probe microscopy (SPM) widely applied for characterization of various substrates topography and reactivity. It is based on recording the current at an ultramicroelectrode (UME) which is positioned or scanned in a proximity to a substrate in the presence of an electrolyte solution.<sup>111</sup> First SECM experiments were presented in 1986<sup>112</sup> and the theory was formulated few years later.<sup>113</sup> During the last 25 years SECM has found a wide application for studying chemical reactions, charge transfer processes at liquid-liquid interface, characterisation of various surfaces reactivity, biotechnological applications and investigation of living cells.<sup>114</sup>

#### 2.1.1. SECM Setup

The SECM setup typically consists of a positioning system, a data acquisition system and the electrochemical cell. The positioning system allows the UME displacement in horizontal ( $x$ ,  $y$ ) and vertical ( $z$ ) directions. The data acquisition system is typically comprised by a bipotentiostat that controls the potentials of the electrochemical cell and measures the current at the working electrodes. The electrochemical cell can consist of three (*i.e.* working UME, reference (RE) and counter (CE) electrodes) or four (*i.e.* working UME, working substrate, RE and CE) electrodes. Finally, the whole SECM setup is controlled by a software that allows the correlation of the recorded current and the position of the UME (Figure 1.2).<sup>114</sup>



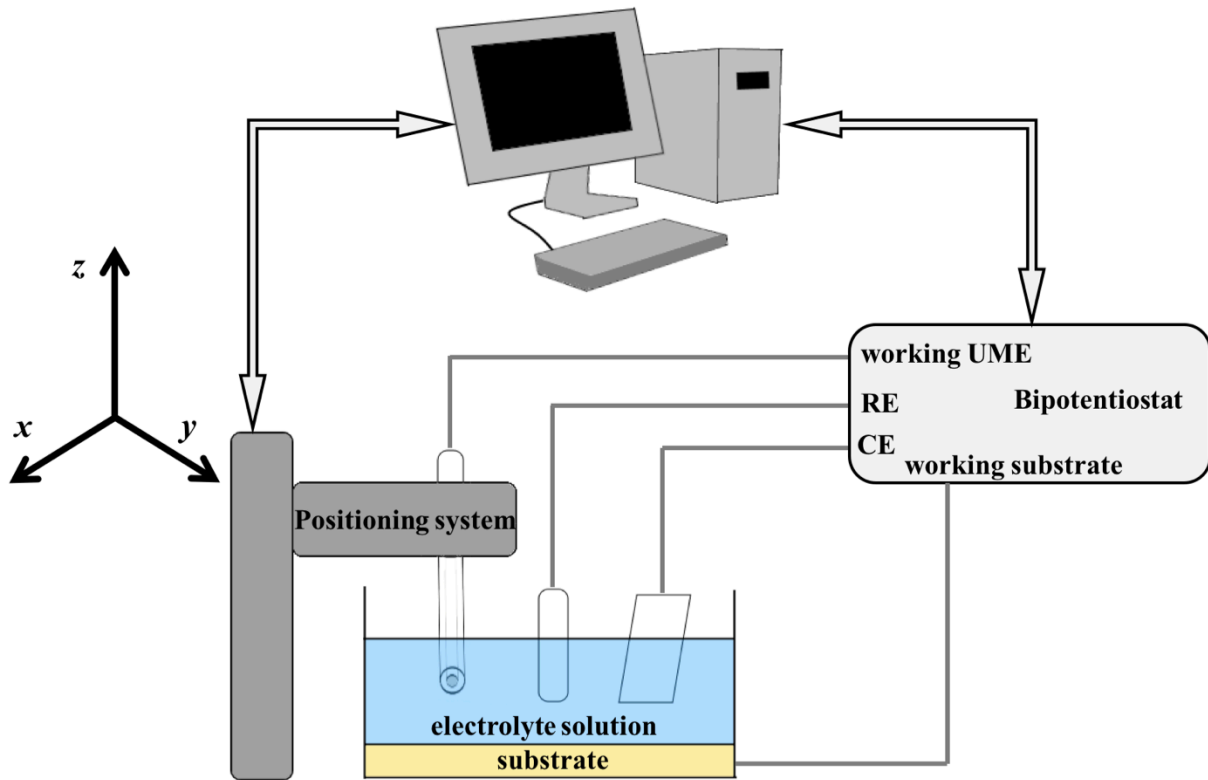


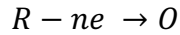
Figure 1.2. Schematic representation of SECM setup

In the present thesis, all SECM experiments were performed with an IVIUM compactstat (IVIUM Technologies, Netherlands) within a three-electrode electrochemical cell with Pt employed as a CE and Ag – as a RE. Soft stylus and glass Pt UME were used as WE. The positioning system from Märzhäuser Wetzlar GmbH & Co KG (Wetzlar, Germany) was combined with a piezoelectric system (PI, GmbH & Co KG, Karlsruhe, Germany) and employed for controlling the probe position. Particularly, the PI system with a travel range of 500  $\mu\text{m}$  and a resolution lower than 1 nm was used to performing more precisely movements in  $z$  direction and the Märzhäuser positioning system with a travel range equal to 10 cm and a resolution of 15 nm – in  $x$  and  $y$  directions. In order to decrease a sample tilt, a tilt table (Zaber Technologies Inc., Vancouver, Canada) was employed allowing the sample levelling with a micrometrical precision. The whole system was isolated from external electric fields with a grounded Faraday cage and placed over a vibration–isolation table in order to increase mechanical stability of the setup.

### 2.1.2. Microelectrodes

Microelectrodes are characterized by having at least one characteristic dimension (*e.g.* radius) in the micrometer scale.<sup>115</sup> In contrast to macroelectrodes where the mass transport controlled by planar diffusion (*i.e.* when an electron transfer process occurring at the electrode is controlled by mass transport), with microelectrodes a hemispherical diffusion profile is

generated (Figure 1.3a) due to the edge effects that became relevant at the micrometer scale. When the UME is positioned in bulk solution in the presence of a redox species R and the constant potential is applied so that the following reaction takes place,



the mass transport at a disk UME is defined by the second law of Fick that in cylindrical coordinates can be written as:

$$\frac{\partial c}{\partial t} = D \left( \frac{\partial^2 c}{\partial z^2} + \frac{\partial^2 c}{\partial r^2} + \frac{1}{r} \frac{\partial c}{\partial r} \right) \quad 1.1$$

where  $D$  is the diffusion coefficient of the redox-active species and  $c$  the concentration of R. In case of steady-state conditions, equation 1.1 can be rewritten as:

$$0 = D \left( \frac{\partial^2 c}{\partial z^2} + \frac{\partial^2 c}{\partial r^2} + \frac{1}{r} \frac{\partial c}{\partial r} \right) \quad 1.2$$

An approximated analytical solution of equation 1.2 has been proposed by *Shoup et al.*<sup>116</sup> and lead to the definition of the steady-state bulk current  $i_{T,\infty}$  as:

$$i_{T,\infty} = 4nFDcr_T \quad 1.3$$

where  $n$  is the number of electrons of the electrochemical reaction taking place at the UME,  $F$  is the Faraday constant and  $r_T$  is the radius of the UME.<sup>117,118</sup>

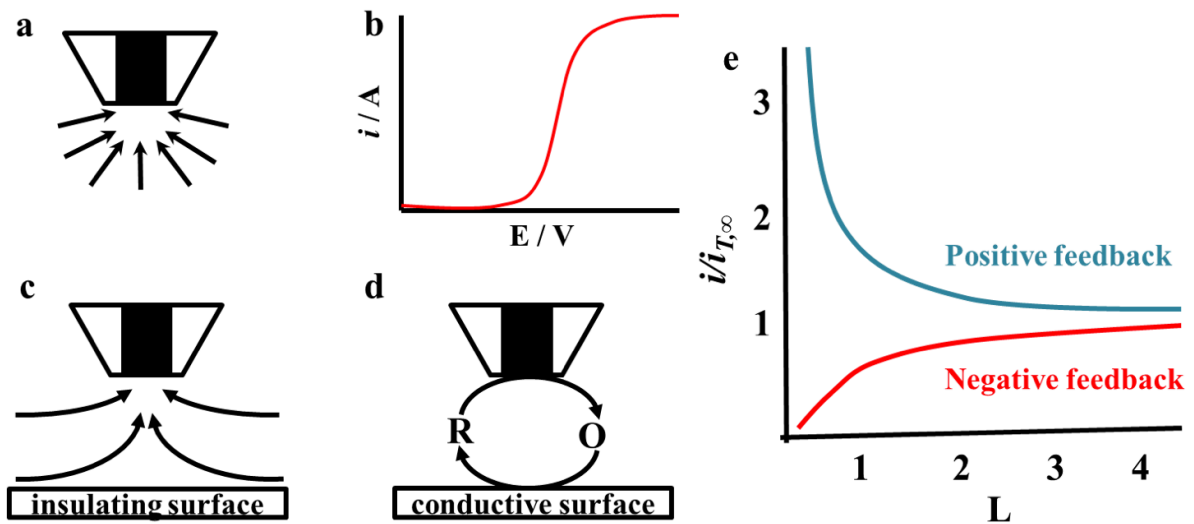


Figure 1.3. Typical cyclic voltammogram recorded at UME (a). Schematic representation of spherical diffusion (b) and hindered diffusion (c) and feedback diffusion (d) towards the UME as well as probe approach curves obtained in case of positive and negative feedback (e).  $L$  is the probe-substrate distance normalized by the electrode radius  $r_T$ .

It is also worth to notice that the equation 1.3 is valid only for electrodes where the  $RG$ , an important UME characteristic widely used in SECM which is defined as  $r_g$  divided by  $r_T$ ,

is lower than 10. Additionally, the time required to achieve steady state conditions is short and approximately equal to  $r_T^2/D$ .<sup>118</sup>

As a result of the fast mass transport achieved at the UME typical CV (Figure 1.3b) represents the flat region in which the current is constant, no matter if the potential is further increased. This potential range should be chosen on order to perform SECM experiments in steady state conditions. Additionally, a small current difference between forward and backward scans indicates a low capacitive current.

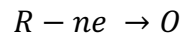
The most classical SECM UMEs are disc electrodes fabricated by encapsulating a microwire (*e.g.* Pt, Au or carbon fiber) within a glass shell.<sup>114,119</sup> The dimensions of these UMEs can be additionally reduced by etching the wire/fiber<sup>120–122</sup> or by pulling metal wires in glass capillaries.<sup>123,124</sup> Carbon microelectrodes can be additionally manufactured by parylene pyrolyzation.<sup>125</sup> Alternatively to glass encapsulation, oxidative electropolymerization,<sup>126</sup> electrophoretic deposition,<sup>121,127</sup> coating with wax<sup>128</sup> and other polymers<sup>125,129–131</sup> have been reported. Atomic force microscopy (AFM)-SECM tips are often manufactured by photolithography<sup>132,133</sup> and focused ion beam<sup>134–136</sup> techniques. Alternatively to disc electrodes, micropipette-based,<sup>137</sup> self-assembled spherical gold (*i.e.* obtained by using gold nanoparticles and thiols cross-linkers),<sup>138</sup> mercury hemisphere,<sup>139</sup> ring<sup>140–142,143</sup> and ring-disk<sup>144</sup> microelectrodes were reported. The main limitation of all UMEs described above is a special attention which has to be paid to the working distance, since any crashes between the hard probe body and the substrate can lead to irreparable damages. To overcome this limitation, soft stylus electrodes<sup>145</sup> have been applied as SECM probes. Soft stylus probes are manufactured by UV-photoablation of polyethylene terephthalate thin films to create microchannels that are filled with carbon paste, cured and posterior Parylene C coated.<sup>145</sup> These probes can be combined with microfluidics to release locally electrolyte solutions in the gap between the sensing UME and the sample area under study as in case of the fountain pen<sup>42</sup> or, additionally, to aspirate the delivered solution as in case of the microfluidic push-pull probe.<sup>43</sup> As a result, the readout of surface reactivity at metal-on-glass structures, human fingerprints, immobilized enzymes and self-assembled monolayers have been demonstrated.<sup>146–148</sup> Furthermore, the electrochemical push-pull scanner (the modified version of the microfluidic push-pull probe) has enabled the coupling of SECM with MS for the extraction of chemical and electrochemical surface information.<sup>146</sup>

### 2.1.3. *SECM modes and methods*

Various electrochemical methods used in SECM can be divided into three groups: *i*) amperometric, *ii*) potentiometric and *iii*) alternating current (AC) impedance. Amperometric methods are based on measurements of electrode current as a function of various parameters (*e.g.* tip-substrate distance and tip-substrate potentials). Analogous to that, potentiometric methods consist in measurements of electrode potential as a function of tip-substrate distance, coordinate or time of the experiment. Alternatively, in AC impedance methods a high-frequency alternating potential is applied to measure the resistance between the tip and a counter electrode in order to provide topography and conductivity of substrates. It also worth to notice that in contrast with other methods, depending on the experimental conditions, both positive and negative feedbacks can be recorded above conductive substrates when AC impedance methods are used.

One of the special features that SECM presents is the capability in which this technique can be adapted to different samples requirements and that have resulted on the development of several operation modes. Out of them, tip generation/substrate collection (TG/SC), substrate generation/tip collection (SG/TC) and feedback modes are most frequently used. In this work, SG/TC and feedback mode were employed and therefore, will be discussed in details.

The feedback mode represents the situation when the tip current is perturbed by reactivity of the monitored surface. Thus, as it was discussed above, when the UME is far from the substrate (*i.e.* in bulk solution) in the presence of a redox species R and the constant potential is applied so that the following reaction is controlled by mass transport,



the current measured at the UME will be equal to  $i_{T,\infty}$ . However, when the UME is approached towards the substrate, the current measured at the UME will vary starting from the probe-substrate distance  $d < 2r_t$  depending on the electrochemical properties of the neighbouring surface. For instance, if the substrate is insulating or not electrochemically active it will simply block the diffusion of the redox mediator towards the UME (Figure 1.3c, hindering diffusion) and as result the tip current will decrease as a consequence of the depletion of species R in the space between the electrode and the substrate (*i.e.* negative feedback). In contrast, if the substrate is conductive or electrochemically active, along with the hindering diffusion, the regeneration of the redox mediator (*i.e.* conversion of O into R) can take place (Figure 1.3d). As a result, the tip current will increase due to the unlimited source of R species (due to its recycling) and the shorter distance that the redox species have

to diffuse between the electrode and the sample substrate (*i.e.* positive feedback). The recycling of R at the substrate is happening due to the local perturbation introduced by the UME positioned close to the sample surface which results in the different potential regions of the conductive surface.<sup>149</sup> The recycling of the redox mediator will depend mainly on the lateral charge transport in the substrate, concentration of the redox mediator, the tip–substrate distance, the size of the sampled area and the rate of the electron transfer.<sup>150</sup>

The current recorded at the UME as a function of the tip-substrate position is called an approach curve. Schematic positive and negative feedbacks approach curves are presented in Figure 1.3e. It is common to represent the approach curves under normalized conditions of current and working distance, with this aim the current measured at the UME ( $i_T$ ) is typically normalized by the steady-state current recorded at the solution bulk ( $i_{T,\infty}$ ), while the tip-substrate distance ( $d$ ) is normalized by the radius of the active electrode area ( $r_T$ ) leading to  $L$  (the normalized working distance).

Since the current monitored during SECM approach curves reflects the combination between the mass-transport and the heterogeneous reaction taking place at the substrate, insights into the kinetics of the investigated process can be obtained by fitting theoretical models with the experimental data. With this aim, different analytical approximations have been derived in order to correlate parameters such as the heterogeneous kinetic constant ( $k$ ) with the experimental  $i_T - d$  profile avoiding the use of complex numerical simulations. For example, *Cornut et al.*<sup>151</sup> reported an approximated analytical expression for quantitative SECM measurements, where the RG of the probe is taken into account:

$$I_T(L, \Lambda, RG) = I_T^{cond} \left( L + \frac{1}{\Lambda}, RG \right) + \frac{I_T^{ins}(L, RG) - 1}{(1 + 2.47RG^{0.31}L\Lambda)(1 + L^{0.006RG + 0.113\Lambda - 0.0236RG + 0.91})} \quad 1.4$$

where  $L$  is the normalized probe-substrate distance and the recorded normalized current for conductive ( $I_T^{cond}$ ) and insulating ( $I_T^{ins}$ ) substrates are equal to

$$I_T^{cond} \left( L + \frac{1}{\Lambda}, RG \right) = \alpha(RG) + \frac{\pi}{4\beta(RG)ArcTan \left( L + \frac{1}{\Lambda} \right)} + (1 - \alpha(RG) - \frac{1}{2\beta(RG)} \frac{2}{\pi} ArcTan \left( L + \frac{1}{\Lambda} \right)) \quad 1.5$$

$$I_T^{ins}(L, RG) = \frac{\frac{2.08}{RG^{0.358}} \left( L - \frac{0.145}{RG} \right) + 1.585}{\frac{2.08}{RG^{0.358}} (L + 0.0023RG) + 1.57 + \frac{\ln RG}{L} + \frac{2}{\pi RG} \ln \left( 1 + \frac{\pi RG}{2L} \right)} \quad 1.6$$

$$\alpha(RG) = \ln 2 + \ln 2 \left( 1 - \frac{2}{\pi} ArcCos \left( \frac{1}{RG} \right) \right) - \ln 2 \left( 1 - \left( \frac{2}{\pi} ArcCos \left( \frac{1}{RG} \right) \right)^2 \right) \quad 1.7$$

$$\beta(RG) = 1 + 0.639 \left( 1 - \frac{2}{\pi} \text{ArcCos} \left( \frac{1}{RG} \right) \right) - 0.186 \left( 1 - \left( \frac{2}{\pi} \text{ArcCos} \left( \frac{1}{RG} \right) \right)^2 \right) \quad 1.8$$

$$\Lambda = \frac{kr_T}{D} \quad 1.9$$

By knowing precisely  $i_{T,\infty}$ ,  $L$ ,  $r_T$ ,  $D$  and  $RG$ ,  $k$  can be extracted from fitting processes. It is important to notice that this expression is valid for  $RG \leq 20$ ,  $L \geq 0.1$  and any  $\Lambda$  value.<sup>151</sup>

SG/TC mode represents the situation when the substrate generates species which will be further detected on the tip. In this case, the study of concentration profiles near the UME as well as detection of enzymatic reactions products can be performed.<sup>111,152</sup>

Along with approach curves, SECM line scans and 2D images are also highly valuable since they permit the mapping of the localized surface reactivity. Since the probe response is influenced not only by the surface reactivity, but also by the topography of the sample, it is important to maintain a constant working distance to avoid any topographic artifacts. For instance, in constant height SECM mode the line scans are performed by positioning the UME at a precise distance above the substrate and recording the signal during its lateral displacement along  $x$ - or  $y$ -axis (Figure 1.4a and b). 2D SECM images are typically constructed from a number of parallel line scans (Figure 1.4c black arrows, high frequency direction) that are separated by a given step towards the perpendicular direction (Figure 1.4c blue arrows, low frequency direction). A schematic 2D SECM image is presented in Figure 1.4d. Additionally, SECM imaging can be carried out using a lift-off routine, *i.e.* after finishing the forward line scan, the UME is retracted at the defined distance (Figure 1.4c dashed arrow 1), moved back to the initial point (Figure 1.4c dashed arrow 2), thereafter displaced to the beginning of the next line scan (Figure 1.4c dashed arrow 3) and finally, approached again towards the sample until the same working distance employed in the previous line scan (Figure 1.4c dashed arrow 4). Line scans and 2D images performed in a constant distance mode will be discussed in details further (*vide infra*).

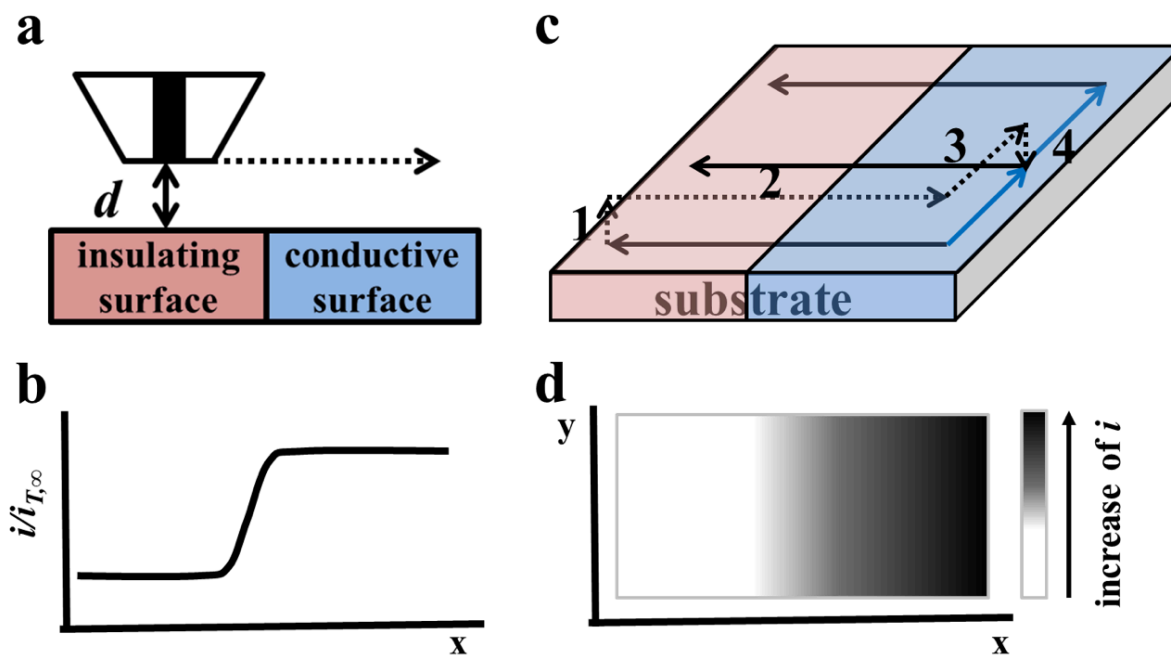


Figure 1.4. Schematic representation of the processes of performing a SECM line scan (a) and 2D image (c) and the results obtained during them ((b) and (d), respectively).

#### 2.1.4. SECM application for cells investigation

Thanks to its high spatial resolution and versatility, SECM has been demonstrated as a useful tool for the electrochemical imaging and intracellular investigation of different living cell types including mammalian cells.<sup>153–158</sup> The most thoroughly studied cells are cervical cancer (HeLa),<sup>158–163</sup> neurons<sup>164–167</sup> and breast cancer cells.<sup>168–170</sup> Typically, SECM experiments are performed using single cells adherently grown on glass or plastic surfaces. However, the investigation of cells layers,<sup>171,172</sup> patterns<sup>163,173,174</sup> and single embryos<sup>175–179</sup> has been also reported. Alternatively to plastic and glass, cells immobilized on collagen substrate,<sup>180</sup> salinized coverslips,<sup>181</sup> as well as in silicon<sup>171</sup> and 3D-printed<sup>182</sup> microstructures were also investigated. Very often cells viability is analyzed directly by following the respiratory activity<sup>175–177,183,184</sup> and production of different compounds, including reactive oxygen species,<sup>185–187</sup> NO<sup>188</sup> and adrenaline,<sup>189</sup> which can be further detected in the extracellular space. Additionally, SECM has been applied for measuring permeation of redox species through living cell membrane<sup>190</sup> and cell monolayers.<sup>172</sup> As a result, charged compounds (*i.e.*  $\text{Fe}(\text{CN})_6^{4-}$ ,  $\text{Fe}(\text{CN})_6^{3-}$ ) presented very low permeability coefficients (*i.e.*  $\leq 10^{-4}$  cm/s), while for ferrocene methanol and p-hydroquinone it was  $5.0 \times 10^{-3}$  and  $2.0 \times 10^{-2}$  cm/s, respectively. It is worth to notice that despite  $\text{Co}(\text{phen})_3^{2+}$  is a charged redox mediator, it was still able to permeate the cell membrane with a permeation coefficient of  $1.0 \times 10^{-3}$  cm/s thanks to the ability of aromatic rings to shield the positive charge.<sup>190</sup> Based on the permeability of cells

membrane for hydrophobic redox mediators (*i.e.* menadione), metastatic and non-metastatic breast cancer cell lines have been differentiated by SECM depending the cells redox response.<sup>129,131,137</sup> Furthermore, it has been shown that FcMeOH<sup>+</sup> can be reduced in cervical cancer cells (HeLa).<sup>159,161,192</sup> Additionally, *Rapino et al.* reported glutathione sulfide/glutathione (GSSG/GSH) balance investigation using breast epithelial MCF10A cells as a model and FcMeOH as a redox mediator.<sup>193</sup> Alternatively, hydrophilic redox mediators that are not able to travel across the cell membrane can be employed to elucidate the cells' topography.<sup>191,194</sup> Besides, double-mediator systems<sup>162</sup> and cell membrane perforation<sup>181</sup> allows the investigation of the intracellular enzymes activity using also hydrophilic redox mediators, although the last can result on the release and dilution of the intracellular content.<sup>181</sup>

In addition to the previous strategies, adherent cells can also be characterized by labelling specific sites with enzymes. Thus, the labelling of single cells was applied by *Xue et al.* for the *in situ* electrochemical imaging of membrane glycan expression in human gastric carcinoma by staining them with HRP-conjugated lectins.<sup>195</sup> Additionally, *Takahashi et al.* presented the immunostaining-based detection of a receptor-mediated endocytosis in Chinese hamster ovaries and human epidermoid carcinoma cells.<sup>196</sup>

As it was discussed above, classical SECM imaging experiments are carried out in constant height mode, where the UME is moved only laterally in the *x* and *y* directions (Figure 1.5a). However, since the feedback SECM signal depends on both working distance and substrate reactivity, the interpretation of adherent cells images can be challenging. Despite of this limitation, various adherent living cells have been investigated by SECM in a constant height mode. For example, interaction of electrochemically generated FcMeOH<sup>+</sup> with HeLa<sup>159,161,192</sup> and MCF10A<sup>193</sup> cells as well as menadione with breast cancer cell lines<sup>129,131,137</sup> was studied by SECM in constant height mode. *Kuss et al.* designed constant height mode SECM experiments for investigation of multidrug resistance protein1 (MRP1) function in cancer cells by performing SECM image of normal HeLa cells and HeLa with overexpressed MRP1.<sup>161</sup> *Zhang et al.* performed a quantitative study of the extracellular ROS profile of T24 cells in different stages and established cisplatin influence on the ROS generation cycle.<sup>186</sup> *Matsumae et al.* reported evaluation of the differentiation status of single embryonic stem cells by monitoring the activity of ALP using SECM in constant height mode.<sup>197</sup> Additionally, the cytotoxicity of menadione on hepatocytes was studied by using the SG/TC mode.<sup>198</sup> Despite of it, few constant height SECM approaches were reported for distinguishing topography and electrochemical activity of cells. As a first approach, a dual Pt microdisc electrode was employed for the simultaneous topography and photosynthetic



activity imaging of a single protoplast by monitoring the oxidation of  $\text{Fe}(\text{CN})_6^{4-}$  at one electrode, while the photosynthetic generated oxygen at the other electrode.<sup>199</sup> The comparison of the response obtained when scanning over alive and killed cells (*e.g.* with KCN) has been also proposed for the separation of cells respiratory activity from cells topography.<sup>158,159,180,184</sup> Additionally, *Salamifar et al.* presented the differentiation between topographical-related and ROS-induced current change on prostate cancer cells (PC3) by comparing the line scans collected at  $-0.65$  (*i.e.* the combined effects of topographical change and ROS release) and  $-0.85$  V (*i.e.* topographical image).<sup>185</sup>

To overcome the limitations of constant height imaging, a variety of approaches for constant distance imaging has been developed based on the monitoring of a distance-dependent signal that is used as feedback to maintain the probe at a constant distance from the substrate surface during the scanning process (Figure 1.5b). The distance-dependent signal can be electrochemical-related or based on a physical interaction between the tip and substrate. For instance, the voltage-switching mode SECM (VSM-SECM) monitors the faradaic current and the hindered diffusion feedback signal (for distance control and topographical imaging) by switching the potential during the scanning. Thus, simultaneous topographical and electrochemical images of single cells were obtained for rat adrenal pheochromocytoma cells (PC12) neurotransmitters detection using a nanometer sized carbon UME.<sup>164</sup> Combination of SECM with scanning ion-conductive microscopy (SICM) has been also successfully implemented to perform mapping of adherent cells by using various tip designs.<sup>141,200</sup> A nanopipette/nanoring electrode probe was employed for acquiring highly resolved topographic and reactivity images of cells. This technique was also applied for the characterization of electroactive species permeation through cellular membranes.<sup>141</sup> Double-barrel carbon nanoprobes (DBCNPs) were also reported for the investigation of rat adrenal PC12 as well as for the localized chemical stimulation and detection of neurotransmitter release from them.<sup>200</sup> Modification of commercial atomic force microscope allowed the alternating current SECM (AC-SECM) investigation of African green monkey kidney cells (*Cos-7*) metabolic activity.<sup>201</sup> Combination of amperometry and constant-impedance was employed for the constant-distance mode imaging of undifferentiated and differentiated PC12 cells using carbon ring and carbon fiber tips.<sup>202</sup> Constant distance SECM of cells has also been demonstrated by using a shear force-based mechanism.<sup>189</sup> The principle of this methodology consists in positioning a vibrating SECM probe near the surface so that the tip–substrate distance is controlled by monitoring the damping of the oscillations due to shear

forces between the tip and the sample surface.<sup>203</sup> Shear-force SECM was also applied for cells investigation, *e.g.* for measurements of ALP in gene-transfected single HeLa cells,<sup>135</sup> detection of reactive oxygen species<sup>187</sup> and nitric oxide<sup>188</sup> released from live cells, or cellular respiratory activity.<sup>204</sup>

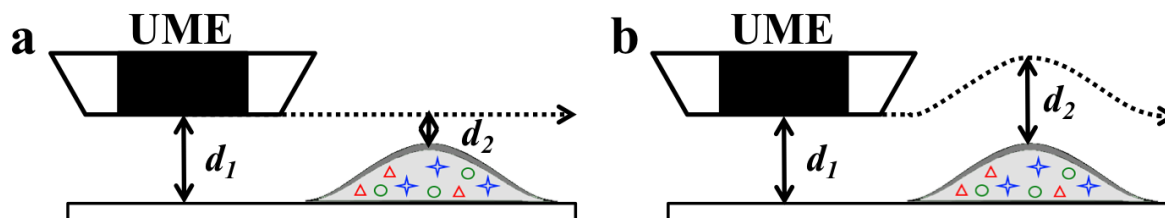
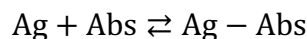


Figure 1.5. Schematic representation of SECM line scan performed in contact-height (a) and contact-distance (b) format.

## 2.2. Immunoassay

### 2.2.1. Immunoreagents

One of the biggest challenges in analytical chemistry is developing fast, high sensitive and selective methods for clinical and environmental monitoring. To achieve such requirements, naturally occurring ability of Abs to recognize Ag and bind it with a high affinity degree into a stable immunocomplex have shown to be a very promising strategy:



Abs are glycoproteins, produced in serum by the adaptive immune system as a response to Ag action. Ag is a substance of any chemical structure, which can induce the Abs production. Based on the structural and biological properties, mammalian Abs are classified within an immunoglobulin superfamily and can be divided into five classes: IgA, IgD, IgE, IgG and IgM. Among them the IgG class is the most widely used due to their stability during the isolation and purification processes. The structure of IgG can be described as a Y-shape molecule containing two heavy and two light chains connected by disulphide bonds and the special hypervariable regions which are responsible for the Ag recognition.<sup>205,206</sup> Abs can be produced naturally against molecules such as proteins, nucleic acids, polysaccharides, lipopolysaccharides, cells of different viruses and bacteria, however the substances with molecular weight less than 10 kDa cannot induce Abs production in organism by themselves and should be first conjugated with carrier proteins such as bovine serum albumin (BSA), soybean trypsin inhibitor, ovalbumin *etc.* The Abs produced in mammals (*e.g.* rabbit or sheep) are called polyclonal. They consist of a number of immunoglobulins with different binding constants for Ag-Abs interaction (affinity constants) and ability to recognize and bind

different parts of Ag, called epitope or Ag determinant. Due to the heterogeneity of binding sites, a different selectivity of polyclonal Abs for different Ags can be observed. In order to avoid this limitation, monoclonal Abs can be used. Monoclonal Abs are characterized by having equal affinity constants and provide unique specificity by recognizing only one epitope on an Ag, allowing development of highly sensitive immunomethods. To produce highly specific and homogeneous monoclonal Abs, a long list of methods have been suggested during the last 20 years, such as cloning, B-cell immortalization, display or hybridoma technologies,<sup>207,208</sup> that allowed a wide range of applications such as immunoassays,<sup>209</sup> affinity chromatography,<sup>205</sup> cell mapping,<sup>210</sup> western blot<sup>211</sup> cancer diagnose and treatment.<sup>212</sup> Additionally to the Abs produced against targeted Ag (*i.e.* primary Abs), Abs against Abs (*i.e.* secondary Abs) can be also obtained. The secondary Abs are typically named by the host animal and source of the primary Abs (*e.g.* rabbit anti-mouse, sheep anti-rabbit, *etc.*).

### **2.2.2. Immunoassay**

Immunoassay is an analytical method based on Ag-Abs interaction.<sup>213</sup> The first variant of immunoassays was described in the work of Berson and Yalow in 1959<sup>214</sup> and since then it has been improved and modified widely. Nowadays, all the immunoassay formats can be roughly divided into 2 main groups: those, which require special equipment for the quantitative analysis of providing the exact concentration of Ag, and those, which can answer if there is the Ag in the concentration higher than a predetermined level or not and where typically a visual detection is used. The first group of methods comprises enzyme immunoassay (EIA), radioimmunoassay, fluorescence polarization immunoassay (FPIA), a wide range of immunosensors and capillary electrophoresis (CE) immunoassay. The second group is intended for on-site applications and for immunochromatographic and immunofiltration tests and columns.<sup>213,215</sup> Different quantitative immunoassay techniques have become useful tools for cosmetology, food industry, environmental monitoring and clinical tests. A significant part of them are based on heterogeneous EIA, in particular on enzyme-linked immunosorbent assay (ELISA) due to its ability to analyse complex samples, such as blood or urine, without significant pretreatment coupled with low analysis cost and rather high sensitivity.<sup>216</sup>

The basic principles of ELISA are: *i)* separation of the target compound from the sample by physical adsorption or by interaction with capturing reactants fixed on a solid phase, such as polystyrene plate, cellulose membrane, gel or MBs and *ii)* detection an enzymatic reaction.

To date, a great number of different ELISA configurations have been reported. In general, all of them are based on one of the following methods: *i*) direct ELISA, *ii*) indirect ELISA and *iii*) sandwich ELISA. Additionally, competitive and non-competitive formats can be used as well. To simplify the classification, the description of the methods will be given regarding Ag detection however, Abs can be also a target for ELISA (*e.g.* allergy test). In case of direct noncompetitive ELISA, the target analyte, which is adsorbed on the solid surface, is detected by addition of the primary Abs, conjugated with an enzyme (Figure 1.6a). The direct adsorption can be done mainly with proteins and is almost impossible for low-mass Ags. Indirect noncompetitive ELISA differs from the direct approach by employing label-free primary Abs and secondary Abs conjugated with an enzyme (Figure 1.6b). Thus, the detection step for this method can be universal for many Ags if the primary Abs are obtained from the same source (*i.e.* the host animal). Sandwich noncompetitive ELISA is based on the variability of primary Abs against large molecules (*i.e.* different epitopes within the same molecule). In this case one type of primary Abs is adsorbed on a solid surface to assure the binding of the target Ag. On the next step another type of primary Abs is added and in presence of the Ag the sandwich complex is produced: Ab<sub>1</sub>-Ag-Ab<sub>2</sub>. If on the last step the primary Abs are conjugated with an enzyme, the method is called direct noncompetitive sandwich ELISA (Figure 1.6c); if not – the additional step of incubation with secondary Abs conjugated with an enzyme is necessary and the method is called indirect noncompetitive sandwich ELISA.

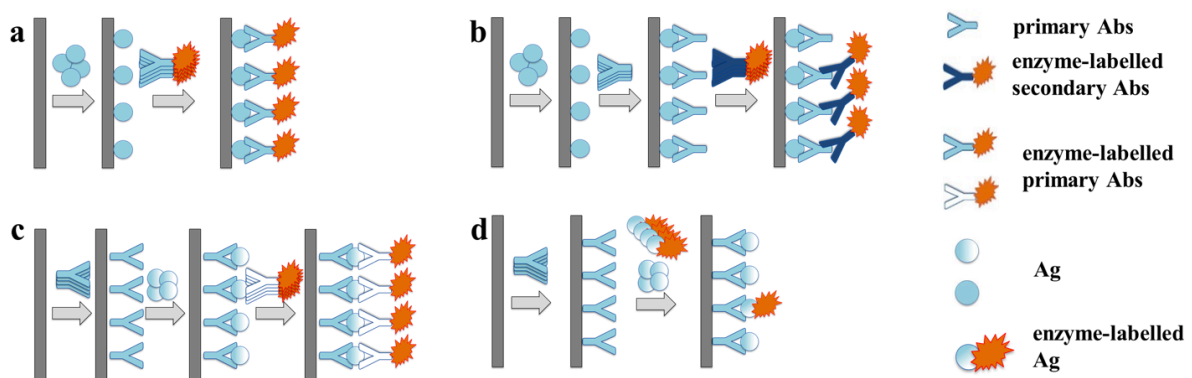


Figure 1.6. Noncompetitive formats of immunoassay: (a) direct ELISA, (b) indirect ELISA, (c) sandwich ELISA. Competitive indirect immunoassay (d).

Competitive ELISA presents the competition between the target Ag present in the sample and the one labelled or adsorbed Ag which concentration is always fixed, for binding with the Abs (Figure 1.6d). Competitive format is typically used for indirect assay however, it can be also applied for sandwich method in an inhibition format.<sup>216,217</sup>

Historically, the first reported immunoassay technique was developed using radioactive label  $I^{131}$  (*i.e.* radioimmunoassay, RIA) for the detection of plasma insulin in human subjects.<sup>214</sup> However, the instability of reagents and safety issues restricted the wide application of the technique. To overcome these limitations, the application of enzymes, which activity or quantity can be easily measured by different means was suggested. Depending on the type of enzyme and the enzymatic substrate employed, different detection strategies can be proposed in order to quantify the products of the enzymatic reaction, such as colorimetric,<sup>218</sup> fluorescence (FL),<sup>219</sup> chemiluminescence (CL)<sup>220</sup> or electrochemical detection methods.<sup>221</sup> Despite the colorimetric detection has the worst reported sensitivity, it has found a wide range of applications in commercial ELISA kits. Colorimetric detection is most frequently based on the reaction between hydrogen peroxide and 3,3',5,5'-tetramethylbenzidine (TMB) in presence of HRP. As a consequence, HRP mediates the combined TMB oxidation and hydrogen peroxide reduction, leading to the formation of 3,3',5,5'-tetramethylbenzidine diimine (TMB<sub>ox</sub>), which absorbs light at 370 and 652 nm (Figure 1.7). The enzymatic reaction can be stopped by the addition of sulphuric acid, which also stabilizes the diimine structure, changing the colour of the solution from blue to yellow with the maximum absorbance at 450 nm (pH<1).<sup>222</sup>

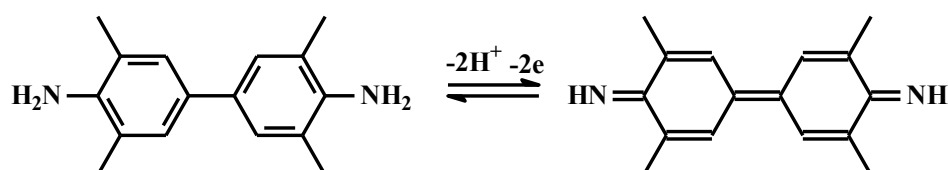


Figure 1.7. The conversion of 3,3',5,5'-tetramethylbenzidine into 3,3',5,5'-tetramethylbenzidine diimine in the process of hydrogen peroxide reducing by HRP.

Fluorescent detection presents a higher sensitivity in comparison with colorimetric methods in addition to the possibility for developing multi analysis methodologies, although it requires a rather complex read-out equipments.<sup>223,224</sup> Chemiluminescence immunoassay (CLIA) has attracted significant interest because of its high sensitivity, which is close to RIA,<sup>209</sup> wide linear range and faster procedure. The most widely used enzyme for CLIA is HRP and the most common substrate is luminol with hydrogen peroxide. The scheme of the luminol transformation during the enzymatic reaction is shown in Figure 1.8. To improve the sensitivity of CLIA, a wide range of luminol-signal enhancers have been suggested, *i.e.* 4-methoxyphenol, 4-(1-imidazolyl)-phenol, 4-iodophenol, 4-hydroxybiphenyl and 4-(1H-pyrrol-1-yl)-phenol. CLIA can be also performed using non-enzymatic labels, such as luminol, isoluminol, aromatic acridinium esters and some other organic compounds. Additionally, amplification of the chemiluminescent signal can be achieved by using

nanoparticles of Au, Ag or QDs.<sup>225,226</sup>

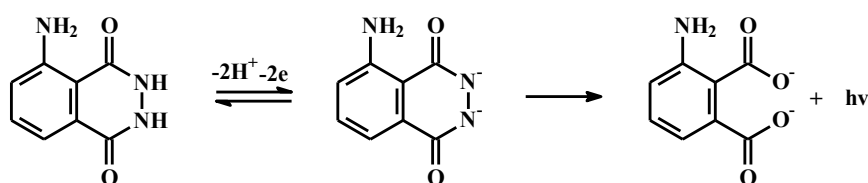


Figure 1.8. Scheme of chemiluminescent transformation of luminol in the presence of hydrogen peroxide and HRP.

Electrochemical detection is less applied for immunoassay despite it is a fast, reliable and high-sensitive method, allowing miniaturization of the analytical strategies.<sup>227</sup> The electrochemical immunoassay is usually based on the detection of an electroactive product, which is generated during the enzymatic reaction. HRP, ALP,  $\beta$ -galactosidase and glucose oxidase can be used with a large number of substrates to generate an electroactive signal. Both 2-electrode and 3-electrode electrochemical cells can be employed. Among different electrodes used for ELISA, SPEs have attracted significant attention because of their low cost, simple fabrication and convenience for on-site applications. They can be easily miniaturized allowing low sample volume without any diminution on analytical characteristics. Different types of electrochemical cells can be employed to improve electrochemical immunoassays, such as multiplexed electrochemical detectors with 8, 32 or 48 independent electrodes for high throughput amperometric detection on a classical or customized microwell plates. However, all these methods require the transformation of the enzymatic products (*e.g.* electroactive species) from the plate into the electrochemical cell that can influence negatively on the reproducibility of the analysis. To avoid this situation, different configurations can be used, such as fluidic systems with directly injected ELISA contents or MBs as a solid surface for the easier manipulation of the immobilized immunoreagents.<sup>228,229</sup>

### 2.2.3. Magnetic beads for immunoassay

MBs have been widely used because of their chemical and physical stability and high surface to volume ratio in comparison with a planar solid phase, which can be easily modified with biomolecules. The small size of MBs ensures a fast equilibrium between Ag and Abs, and thereby fast immunoassays protocols. Moreover, MBs are compatible with miniaturized systems due to their high degree of freedom and easy manipulation with an external magnetic field.<sup>230</sup>

MBs are commercially available and typically covered with the hydrophilic polymers in order to prevent their aggregation and with different surface functionalization including protein A, protein G, amine, carboxylic acid, epoxy, tosyl-activated, silane and streptavidine

groups. MBs can be easily modified with Abs or other biomolecules allowing a wide range of applications as a solid phase for immunoassays. However, due to the ability of the beads to absorb light, application of MBs on immunoassays with optical detection can cause some problems. Still some successful examples for CL detection have been reported.<sup>231,232</sup> As a result the use of MBs for immunoassay with an electrochemical detection represents the most promising strategy.

Electrochemical immunosensors based on the immobilization of Abs or Ags on the surface of the electrode present good reproducibility and sensitivity due to the fact that the enzymatic reaction and its products are close to the surface. However, coating the electrode with immunoreagents can generate electrode passivation and decreasing on the electrochemical signal. Thus, introducing MBs as a solid phase for immunoassays that are readout by electrochemical means seems to be a good match, especially if the functionalized MBs are attracted to the surface of the electrode *via* an external magnetic field.<sup>228</sup>

### **2.3. Matrix-assisted laser desorption ionization**

MS is a label-free technique where the analytical signal depends on the molecular weight and charge of the analysed species after they are ionized.<sup>233–236</sup> Thus, the most of the MS experiments consist of 2 steps, *i.e.* sample ionization and mass-to-charge ratio ( $m/z$ ) detection. As a result, highly accurate molecular weight of intact molecules presented in the sample can be obtained.

When speaking about MS of biomolecules two soft (*i.e.* without ions fragmentation) ionization techniques namely, electrospray ionization (ESI)<sup>237</sup> and matrix-assisted laser desorption/ionization (MALDI)<sup>238,239</sup> are typically used. For the  $m/z$  detection ion trap (IT), orbitrap, ion cyclotron resonance (ICR), quadrupole (Q) and time-of-light (TOF) detectors can be used. Herein, only MALDI-TOF-MS concept will be reviewed in details, since it was the MS technique employed on this thesis.

The concept of MALDI was initially introduced by F. Hillenkamp and M. Karas in 1988.<sup>240</sup> It consists on the deposition of the sample of interest together with a special matrix on a conductive plate, drying it and further ionization with laser pulses (Figure 1.9). It requires high-vacuum for the ionization process, and besides, the sample should be placed onto a special plate, mixed with a special matrix and then dried before the analysis can be done. The matrix acts a proton donor or receptor helping the analyte ionization and prevents sample damage by consuming part of the laser energy. The most typical matrixes used in MALDI are 2,5-dihydroxybenzoic acid (DHB),  $\alpha$ -cyano-4-hydroxycinnamic acid (HCCA),

sinapinic acid (SA) and 3-hydroxypicolinic acid (HPA).<sup>241</sup> The ionization mechanism is not completely established however, three different concepts have been proposed, namely *i*) photochemical ionization (*i.e.* the ions are produced by protonation or deprotonation between sample and matrix in the gas phase),<sup>242,243</sup> *ii*) cluster ionization (*i.e.* laser adsorption causes ion desorption by desolvation of matrix molecules)<sup>244</sup> and *iii*) pseudo-proton transfer (*i.e.* ions are produced during crystallization process) model.<sup>245</sup>

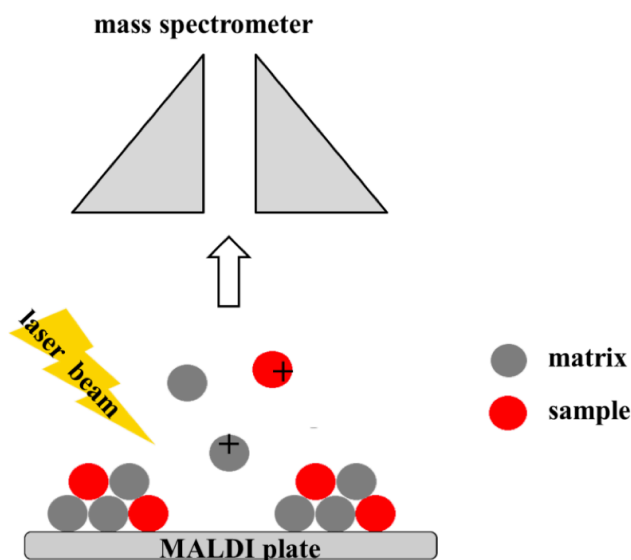


Figure 1.9. The principle of matrix-assisted laser desorption/ionization time of flight mass spectrometer (MALDI-TOF-MS).

Out of various analyzers combined with MALDI ionization source, time-of-flight (TOF) analyzer is the most widely used. Different concepts, *i.e.* linear TOF, tandem TOF/TOF and reflectron TOF can be employed. The principle of MALDI-TOF is based on accelerating ions in a constant electric field region and their separation in a field-free time-of-flight tube. While all the ions have the same energy from the electric field, they would reach the detector at different times because of their different masses. Tandem TOF/TOF analyzer consists of two consecutive TOF mass spectrometers, where the first one isolates precursor ions of choice using a velocity filter, and the second one analyses the fragmented ions. The reflectron TOF uses a constant electrostatic field to reflect the ion beam toward the detector. The more energetic ions penetrate deeper into the reflectron, and take a slightly longer path to the detector. Less energetic ions of the same mass-to-charge ratio penetrate a shorter distance into the reflectron and, correspondingly, take a shorter path to the detector. As a result, an increase of MS resolution is achieved however, a decrease in sensitivity ( $\leq 10$  kDa) is also observed. In this thesis MALDI-TOF-MS concept was used.



MALDI-MS found wide applications, for example for molecular imaging of biological samples<sup>246–251</sup> and *in vitro* cultured mammalian cells characterisation.<sup>252–257</sup> The MALDI configuration allows direct cells positioning on a target plate and therefore, the intact-cell analysis in order to obtain cells fingerprints can be performed. In this case cells can be either grown directly on a MALDI target plate<sup>252</sup> or collected by centrifugation after culturing in a classical Petri dish.<sup>253–257</sup> The latter allows cells pellets to be either transferred directly to the target plate, where it is dried and covered with a matrix solution,<sup>256</sup> or mixed with a matrix solution prior to be transferred.<sup>254,255,257</sup> As a result, instead of individual protein peaks, a number of signals representing the MS fingerprint of mammalian cells can be obtained.<sup>253</sup> This approach was successfully applied for the identification of two different pancreatic cell lines,<sup>256</sup> differentiation of stimulated and non-stimulated macrophages,<sup>254</sup> prediction of mammalian cells phenotype<sup>255</sup> and to characterize neural cell types.<sup>257</sup>

## 2.4. Cell fixation methods

### 2.4.1. General information

Fixation is a process commonly used in biology that eliminates the biological activity inside cells and tissues, but preserves cellular ultrastructure as well as proteins, carbohydrates and other bio-active moieties in their original spatial organization within the cells.<sup>258</sup> Additionally, depending on the thickness or type of the sample a longer or modified protocol might be needed as in the case of tissues samples. Different approaches and types of fixatives have been developed and tested throughout the years. Fixatives which crosslinks proteins are called additives and those, which precipitate proteins are called coagulants.<sup>258</sup> Finally, the fixation mechanisms can be categorized as *i*) cross-linkers, *ii*) dehydrates and *iii*) heat effects and their combinations thereof.

### 2.4.2. Crosslinking fixatives

Among crosslinking fixatives formaldehyde and glutaraldehyde are the most frequently used compounds however, genipin can be also employed. The fixation action of formaldehyde consists on the formation of new chemical bonds through the interaction between amino and imino groups, mostly lysine and arginine.<sup>259</sup> As a result formaldehyde can create methylene bridges between amino acids in proteins that were in a close proximity ( $\sim 2\text{\AA}$ ). Additionally, DNA and RNA can be also involved in the formaldehyde network, *e.g.* through the amino group on cytosine.<sup>260</sup> In its turn, glutaraldehyde crosslinks proteins mostly *via* reacting with  $\epsilon$ -amino groups of amino acids.<sup>261</sup> Genipin is a naturally occurring crosslinking agent extracted

from the fruits of *Gardenia jasminoides Ellis*. It can spontaneously react with amino acids and proteins and form both intramolecular and intermolecular crosslinks with cyclic structure. Additionally, genipin is less cytotoxic than synthetic crosslinkers.<sup>262,263</sup>

### **2.4.3. Dehydrates**

Organic solvents and alcoholic fixatives are the most typical dehydrators. They can be used as pure compounds (*e.g.* methanol, ethanol, acetone, *etc.*) or in mixtures. Thus, Camoy's fixative consists of ethanol (60%), chloroform (30%) and glacial acetic acid (10%); Methacam fixative consists of methanol (60%), chloroform (30%) and glacial acetic acid (10%). AMeX fixation represents the consequent fixation of biological material with acetone and cleaning with methylbenzoate and xylene. Additionally, HOPE (HEPES-glutamic acid buffer-mediated organic solvent protection effect) fixation is performed by immersing the tissue sample in the protection buffer before dehydrating it with acetone.<sup>258</sup> Additionally to fixation, organic solvents and alcohols increase permeability of cells membranes.<sup>264</sup> *Noguchi et al.* tested the fixation with methanol, acetone and ethanol reporting that 100% methanol fixation did not cause regional differences due to artificial tissue shrinkage.<sup>265</sup> Additionally, it provides the best preservation of morphology and the lowest fluorescent background and therefore, permits flow cytometric analysis of immunofluorescent stained intracellular antigens.<sup>266,267</sup>

### **2.4.4. Heat effects**

Microwave irradiation was used to fix a wide range of surgical and autopsy specimens as well as tissue from freshly killed rats. Heating up to 58 °C tissues submerged in normal saline solutions resulted in tissue fixation of a quality comparable with that produced by conventional fixation with 10% formalin.<sup>268</sup> Used alone this method has such advantages as keeping the sample non-contaminated with other chemicals however, often leads to shrinkage and sponginess of tissues. Combination with other methodologies such as chemical fixation can help to overcome this limitation.<sup>258</sup> Additionally to fixation with heat, freezing can be also implemented. This type of fixation is called cryofixation and consists in uniform and sufficiently rapid freezing of the biological sample, which does not allow material to move. This technique is widely used for electron microscopy.<sup>269,270</sup>

### **2.4.5. Cells fixation for SPM and MALDI**

Crosslinking reagents have been already applied to the study of biological subjects by using SPM techniques. Thus, combination of AFM with cross-linking fixation approach,

allowed not only escape topographical changes during the image, but also presented significant changes in membrane elasticity (typical values of the elastic modulus are around 2 kPa for the living cell and more than 100 kPa for the fixed cell).<sup>271,272</sup> It was also shown that AFM resolution in alive cells is generally poor compared with the one achieved after cells fixation.<sup>272,273</sup> Moreover, glutaraldehyde followed by paraformaldehyde fixation was employed for identification of actin-based structures on the surface of cells derived from the VGP of melanoma progression by combination of laser-scanning confocal microscopy and AFM.<sup>274</sup> An interesting result obtained during AFM investigation of fixed samples with glutaraldehyde is that cells topography did not present significant changes in comparison to their alive state.<sup>271</sup> Besides AFM, SICM has also been combined with fixation strategies for the cell volume measurement of epithelial kidney cells fixed with formaldehyde.<sup>275</sup> Comparison of AFM and SICM approaches was also performed using fixed epithelial cells.<sup>276</sup> Due to the preservation of cells architecture, fixation methodologies have also found a wide application in MALDI-MS imaging of tissues<sup>246–248</sup> and cells.<sup>249–251,277</sup> Particularly, all fixation approaches were tested as a sample pretreatment. For example, acetone,<sup>249</sup> formaldehyde,<sup>250</sup> glutaraldehyde<sup>277</sup> and cryofixation<sup>251</sup> were reported for cells, while tissue samples are typically fixed by cryofixation or formalin. Additionally, the influence of fixatives (acetone, ethanol, methanol, xylene, isopropanol, hexane, tert-butyl methyl ether, ethanol/acetic acid) on MS signal provided by tissues was investigated by *Seeley et al.*<sup>246</sup>

## **2.5. Microfabrication**

Microfabrication techniques have made possible to bring analytical methodologies into a new level and has allowed to fit the nowadays requirements, such as high throughput, low cost, point of care, on-site and on-line, disposable, *etc.* In the present thesis microfabrication techniques such as IJP and laser ablation have been employed to develop different analytical tools for biological and environmental monitoring, as well as, for scanning cells in contact mode.

### **2.5.1. Inkjet printing**

Inkjet printing (IJP) is a technology that has been around for quite some time especially for the graphic industry. However, recently along the 3D printing hype it has been redesigned as a manufacturing technique for functional materials deposition due to its more efficient material use, non-contact and mask-free printing strategy, among other advantages. IJP can be experimentally implemented in different ways, namely *i)* continuous and *ii)* drop-on-demand

IJP. In continuous IJP, a force is applied to a liquid jet to induce the stream breakup into a series of droplets of uniform size and speed. Since these droplets are charged, they can be redirected at convenience as they pass through an electric field and steered onto the desired location on the substrate to form the printed image. In drop-on-demand IJP ink droplets are only formed and ejected when required by using *i*) thermal, *ii*) squeeze-mode, *iii*) bend-mode, *iv*) push mode or *v*) shear mode print heads. The thermal IJP is based on the localized overheating of the ink to generate a bubble formation, which induces the change in volume within the print head chamber and forces the ink out of the nozzle, thereby forming a droplet. In a squeeze-mode IJP a voltage is applied to parallel piezoelectric elements within a nozzle causing them to squeeze the ink chamber and force a droplet out of the nozzle. Similarly, in bend-mode print heads, the bending of the ink chamber wall induces droplet ejection. In the push mode print heads an electrical excitation of the membrane causes it to expand and push against the ink chamber wall thereby expelling a droplet. Finally, shear mode print heads are designed such that shear deformation in the piezoelectric element is used to deform the upper half of the channels, which is mirrored in the lower half of the channel forcing the channel into a chevron shape. This flexing of the channel induces droplet ejection. Piezoelectric print heads are the most commonly used print heads for printing functional materials, as there is no risk of thermal degradation of the ink or need to use only solvents with a specific nucleation temperature. The drop-on-demand IJP process consists of five stages, namely drop ejection, drop flight, drop impact, drop spreading and drop solidification.<sup>278</sup> The performance of the droplet ejection process can be characterized by responses such as the droplet velocity, volume, consistency, shape and directionality. These parameters are affected by factors such as waveform, print head geometry, propagation of the sound in the ink media, nozzle size, fluid viscosity and surface tension, among others.<sup>279,280</sup>

The behaviour of liquid drops can be characterized by a number of dimensionless groupings of physical constants, namely the Reynolds ( $Re$ ), Weber ( $We$ ), and Ohnesorge ( $Oh$ ) numbers:

$$Re = \frac{v\rho a}{\eta} \quad 1.10$$

$$We = \frac{v^2\rho a}{\gamma} \quad 1.11$$

$$Oh = \frac{\sqrt{We}}{Re} = \frac{\eta}{(\gamma\rho a)^{1/2}} \quad 1.12$$

where  $\rho$ ,  $\eta$ , and  $\gamma$  are the density, dynamic viscosity, and surface tension of the fluid respectively,  $v$  is the velocity, and  $a$  is a characteristic length.

*Reis et al.* proposed that for stable drop formation  $Z = 1/Oh$  should be in the range  $10 > Z > 1$ .<sup>281</sup> *Duineveld et al.*<sup>282</sup> suggested that a minimum velocity for drop ejection should be:

$$v_{min} = \left(\frac{4\gamma}{\rho d_n}\right)^{1/2} \quad 1.13$$

where  $d_n$  is the nozzle diameter.

Equation 1.13 can be reformulated in terms of the Weber number:

$$We = v_{min} \left(\frac{\rho d_n}{\lambda}\right)^{1/2} > 4 \quad 1.14$$

Finally, there is a well-established experimental threshold for the onset of splashing, first proposed by *Stow et al.*<sup>283</sup> as a critical dimensionless grouping of variables:

$$We^{1/2} Re^{1/4} > f(R) \quad 1.15$$

where  $f(R)$  is a function of surface roughness only and for flat and smooth surfaces it is equal to 50.<sup>284</sup> Still, there are other parameters that can affect drastically the print quality, such as droplet-substrate distance, porosity and temperature of the substrate, printing strategy and post-processing techniques. The gist in IJP is to be able to get a compromise among all these parameters that allows you to obtain the functionality and other features that the foreseen application requires.

Out of the functional materials suitable for IJP the most frequently used are nanoparticles, organometallic, conductive polymers, graphene oxide and carbon nanotubes (CNTs).<sup>285,286</sup> As a result, IJP has been used for the fabrication of (bio)chemical sensors on paper<sup>287,288</sup> and polymeric substrates,<sup>289,290</sup> in a single<sup>291</sup> or multiplexed concept,<sup>290</sup> designed for the simultaneous detection of one<sup>287</sup> or multiple analytes<sup>292</sup> and combined with other microfabrication techniques.<sup>293,294</sup>

CNTs consist of  $sp^2$ -hybridised, tubular carbon networks and can be of single wall (SWNT), double wall (DWNT) or multi wall (MWNT) type.<sup>295</sup> Differences in their electrochemical behavior normally occur due to the nature of the CNTs, present functional groups, employed synthesis strategy, cleaning procedures and remaining metallic and carbonaceous impurities, storage conditions and aging.<sup>296,297</sup> CNTs have attracted a lot of attention due to their high surface area, mechanical stability, electrical conductivity and electrochemical reactivity.<sup>295-297</sup> Despite the current debate whether CNTs represent efficient electrocatalysts as stand-alone films,<sup>298-300</sup> this material has been widely used as active layer in electronic and electrochemical devices. For instance, flexible stand-alone CNTs electrodes were fabricated recently by a multilayer IJP process showing a catalytic effect and faster kinetics compared to carbon paste electrodes for the amperometric detection of antioxidants in blood bags.<sup>289</sup>

### 2.5.2. Laser ablation

Laser ablation is the microfabrication method that has been widely used for bioanalytical application. Thus, various polyimide microchips were fabricated in order to be coupled with electrospray ionization (ESI) MS approach<sup>301–308</sup> and to obtain water-in-oil droplet systems.<sup>309</sup> Additionally, UV-photoablation of polyethylene terephthalate (PET) was widely used to manufacture soft UMEs as well as microarrays.<sup>145–148,310,311</sup>

The principle of material removal by laser ablation has not been completely established however there are two possible phenomena taking place, namely *i*) thermal and *ii*) photochemical ablation. The main difference between these mechanisms consists in the magnitude of the absorbed energy and the time scale of the different process that can take place inside the material (*i.e.* photons absorption, emission and a non-radiative transition). When a material absorbs energy, it allows its promotion from the ground state to a first excited state. The difference between the states can be described by the energy ( $E_g$ ) equal to  $h\nu$ , where  $h$  is Planck constant and  $\nu$  is a frequency of light. Thereafter, relaxation processes will take place due to the electronic and vibrational transitions among the different electronic states. Material ablation can take place by desorption of molecules in both ground and excited states (photochemical ablation) or during the non-radiative transitions which leads to the local increment of temperature, generating the ejection of melted or vaporized sample (photothermal ablation).

The total ablation rate ( $\Delta h$ ) expressed as the ablated depth per pulse can be approximated as:

$$\Delta h = v_A N_A^*(0) + v_{A^*} N_{A^*}^*(0) + v_D N_D^*(0) \quad 1.16$$

where  $v_i$  represent the rate constants for thermally activated desorption and  $N_i^*$  are the normalized number densities of states  $i$ . Based on the equation 1.16, purely thermal effects will be observed if  $\tau_T \ll \tau_A^*$  and  $\tau_A \ll \tau_{A^*}^*$ , while pure photochemical effect will be observe if  $\tau_T > \tau_A^*$  and  $\tau_A \gg \tau_{A^*}^*$ , where  $\tau_T$ ,  $\tau_A$  and  $\tau_{A^*}^*$  are thermal relaxation time, time for initiation photochemical desorption and chemical reaction, respectively.

The ablation rate can be defined by the logarithmic law:

$$\Delta h(\varphi) = l_\alpha \ln \left( \frac{\varphi}{\varphi_{th}} \right) \quad 1.17$$

where  $l_\alpha$  is the optical penetration depth,  $\varphi$  is the energy given to the substrate and  $\varphi_{th}$  is the minimum energy required for photoablation of a specific material. Based on the equation 1.17 it can be conclude that materials with low  $\varphi_{th}$  and big  $l_\alpha$  are the most likely material to be employed for laser ablation.<sup>312</sup>

In present thesis laser ablation was performed with an excimer (*abbr.* of excited dimer) laser, in which an excited state complex is formed by the interaction of two monomers. The excited complexes present a short lifetime (*e.g.* nanoseconds), and as a consequence decay to its ground state emitting laser light, along with the complex dissociation. The laser wavelength depends on the mixture employed, which typically consists of a noble gas and a halogen species. Herein, ArF laser with  $\lambda$  equal to 193 nm was employed.<sup>313</sup> The whole setup devoted to microfabrication purposes consisted of a pulsed laser source, a metallic mask and an  $x, y$ -table (perpendicular to the laser beam). Due to the fact that the area of the produced laser beam is around 1 cm<sup>2</sup>, a mask consisted of a metallic sheet (*e.g.* molybdenum) with an overture is needed to project the shape and the size of the ablated area. The size of the ablated area corresponds approximately to one tenth of the overture in the mask.

### **3. Thesis outline**

This thesis presents the development of various analytical tools and approaches for fast sensing and imaging of adherent cancer cells and *E.coli*. In Chapter II the potential of SECM combined with cells fixation approaches was tested on adherent melanoma cells. This approach was fulfilled by differentiation of melanoma stages by immunostaining of TyR expression and SECM imaging in the SG/TC mode. In Chapter III the potential of the soft stylus probe concept towards the scanning of adherent living cells in a contact mode was studied using WM-115 melanoma adherent cells as a model. Chapter IV is devoted to the characterisation and implementation of an electrochemical push-pull probe as a tool for studying adherent cancer cells through the control over the chemical composition of the extracellular space with high spatiotemporal resolution. As a proof of concept, localized fluorescent labelling and pH changes were purposely demonstrated. Chapter V illustrates an intact cell MALDI-MS protocol for characterizing the differences in the high-abundant proteins content of mammalian cancer cells derived from different cancer stages. In Chapter VI a fast, simple and cost-efficient way of manufacturing a multiplexed electrochemical sensor device that enables the reproducible implementation of a broad spectrum of immunoassays with amperometric detection was presented and implemented for detection of various targeted analytes including *E.coli*. Finally, Chapter VII presents the general conclusions of this thesis and outlines future perspectives.

#### 4. References

- (1) Taylor, J.-S. *Science* **2015**, *347*, 824.
- (2) Miller, A. J.; Mihm, M. C. *N. Engl. J. Med.* **2006**, *355*, 51–65.
- (3) Hanahan, D.; Weinberg, R. A. *Cell* **2011**, *144*, 646–674.
- (4) Lindblom, A.; Liljegren, A. *Clin. Rev.* **2000**, *320*, 424–427.
- (5) Tandler, N.; Mosch, B.; Pietzsch, J. *Amino Acids* **2012**, *43*, 2203–2230.
- (6) Liu, Y.; He, J.; Xie, X.; Su, G.; Teitz-Tennenbaum, S.; Sabel, M. S.; Lubman, D. M. *J. Proteome Res.* **2010**, *9*, 6044–6051.
- (7) Domnanich, P.; Peña, D. B.; Preininger, C. *Biosens. Bioelectron.* **2011**, *26*, 2559–2565.
- (8) May, K. M. L.; Vogt, A.; Bachas, L. G.; Anderson, K. W. *Anal. Bioanal. Chem.* **2005**, *382*, 1010–1016.
- (9) Wang, X.; Li, H.; Li, X.; Chen, Y.; Yin, Y.; Li, G. *Electrochem. commun.* **2014**, *39*, 12–14.
- (10) Ren, X.; Yan, T.; Zhang, Y.; Wu, D.; Ma, H.; Li, H.; Du, B.; Wei, Q. *Biosens. Bioelectron.* **2014**, *58*, 345–350.
- (11) Hartleb, J.; Arndt, R. *J. Chromatogr. B Biomed. Sci. Appl.* **2001**, *764*, 409–443.
- (12) Revin, S. B.; John, S. A. *Sensors Actuators B. Chem.* **2013**, *188*, 1026–1032.
- (13) Vendittelli, F.; Paolillo, C.; Autilio, C.; Lavieri, M. M.; Silveri, S. L.; Capizzi, R.; Capoluongo, E. *Clin. Chim. Acta* **2015**, *444*, 242–249.
- (14) Seenivasan, R.; Maddodi, N.; Setaluri, V. *Biosens. Bioelectron.* **2015**, *68*, 508–515.
- (15) Stoitchkov, K.; Letellier, S.; Garnier, J.-P.; Toneva, M.; Naumova, E.; Peytcheva, E.; Tzankov, N.; Bousquet, B.; Morel, P.; Le Bricon, T. *Clin. Chim. Acta* **2001**, *306*, 133–138.
- (16) Zhang, S.; Yang, J.; Lin, J. *Bioelectrochemistry* **2008**, *72*, 47–52.
- (17) Cao, C.; Sim, S. J. *Biosens. Bioelectron.* **2007**, *22*, 1874–1880.
- (18) Bobrow, M. N.; Shaughnessy, K. J.; Litt, G. J. *J. Immunol. Methods* **1991**, *137*, 103–112.
- (19) Hofbauer, G. F. L.; Kamarashev, J.; Geertsen, R.; Böni, R.; Dummer, R. *J. Cutan. Pathol.* **1998**, *25*, 204–209.
- (20) De Vries, T. J.; Smeets, M.; De Graaf, R.; Hou-Jensen, K.; Bröcker, E. B.; Renard, N.; Eggermont, A. M. M.; Van Muijen, G. N. P.; Ruiter, D. J.; Vries, T. J. De; Smeets, M.;



- Graaf, R. De; Hou-Jensen, K.; Bro, E. B.; Renard, N.; Eggermont, A. M. M.; Muijen, G. N. P. Van; Ruiters, D. J. J. *J. Pathol.* **2001**, *193*, 13–20.
- (21) Boyle, J. L.; Haupt, H. M.; Stern, J. B.; Multhaupt, H. A. B. *Arch. Pathol. Lab. Med.* **2002**, *126*, 816–822.
- (22) Boursault, L.; Haddad, V.; Vergier, B.; Cappellen, D.; Verdon, S.; Bellocq, J.-P.; Jouary, T.; Merlio, J. P. *PLoS One* **2013**, *8*, e70826.
- (23) Tetzlaff, M. T.; Pattanaprichakul, P.; Wargo, J.; Fox, P. S.; Patel, K. P.; Estrella, J. S.; Broaddus, R. R.; Williams, M. D.; Davies, M. A.; Routbort, M. J.; Lazar, A. J.; Woodman, S. E.; Hwu, W.-J.; Gershenwald, J. E.; Prieto, V. G.; Torres-Cabala, C. A.; Curry, J. L. *Hum. Pathol.* **2015**, *46*, 1101–1110.
- (24) Wilmott, J. S.; Menzies, A. M.; Haydu, L. E.; Capper, D.; Preusser, M.; Zhang, Y. E.; Thompson, J. F.; Kefford, R. F.; Von Deimling, A.; Scolyer, R. A.; Long, G. V. *Br. J. Cancer* **2013**, *108*, 924–931.
- (25) Rothberg, B. E. G.; Bracken, M. B.; Rimm, D. L. *J. Natl. Cancer Inst.* **2009**, *101*, 452–474.
- (26) Weinstein, D.; Leininger, J.; Hamby, C.; Safai, B. *J. Clin. Aesthet. Dermatol.* **2014**, *7*, 13–24.
- (27) Kim, M. J.; Lee, J. Y.; Nehrbass, U.; Song, R.; Choi, Y. *Analyst* **2012**, *137*, 1440–1445.
- (28) Kononen, J.; Bubendorf, L.; Kallioniemi, A.; Bärklund, M.; Schraml, P.; Leighton, S.; Torhorst, J.; Mihatsch, M. J.; Sauter, G.; Kallioniemi, O. P. *Nat. Med.* **1998**, *4*, 844–847.
- (29) Mascolo, M.; Ilardi, G.; Merolla, F.; Russo, D.; Vecchione, M. L.; De Rosa, G.; Staibano, S. *Int. J. Mol. Sci.* **2012**, *13*, 11044–11062.
- (30) Ladstein, R. G.; Bachmann, I. M.; Straume, O.; Akslen, L. A. *Mod. Pathol.* **2014**, *27*, 396–401.
- (31) Sabet, M. N.; Rakhshan, A.; Erfani, E.; Madjd, Z. *Asian Pacific J. Cancer Prev.* **2014**, *15*, 8161–8169.
- (32) Jafarnejad, S. M.; Sjoestroem, C.; Martinka, M.; Li, G. *Mod. Pathol.* **2013**, *26*, 902–910.
- (33) Zlobec, I.; Koelzer, V. H.; Dawson, H.; Perren, A.; Lugli, A. *J. Transl. Med.* **2013**, *11*, 104.
- (34) Caria, P.; Vanni, R. *Mol. Cytogenet.* **2014**, *7*, 56.

- (35) Minca, E. C.; Tubbs, R. R.; Portier, B. P.; Wang, Z.; Lanigan, C.; Aronow, M. E.; Triozzi, P. L.; Singh, A.; Cook, J. R.; Sauntharajah, Y.; Plesec, T. P.; Schoenfield, L.; Cawich, V.; Sulpizio, S.; Schultz, R. A. *Cancer Genet.* **2014**, *207*, 306–315.
- (36) Tetzlaff, M. T.; Wang, W.-L.; Milless, T. L.; Curry, J. L.; Torres-Cabala, C. A.; McLemore, M. S.; Ivan, D.; Bassett, R. L.; Prieto, V. G. *Am. J. Surg. Pathol.* **2013**, *37*, 1783–1796.
- (37) Delpu, Y.; Cordelier, P.; Cho, W. C.; Torrisani, J. *Int. J. Mol. Sci.* **2013**, *14*, 15029–15058.
- (38) Patel, S.; Ahmed, S. *J. Pharm. Biomed. Anal.* **2015**, *107*, 63–74.
- (39) Qendro, V.; Lundgren, D. H.; Rezaul, K.; Mahony, F.; Ferrell, N.; Bi, A.; Lati, A.; Chowdhury, D.; Gygi, S.; Haas, W.; Wilson, L.; Murphy, M.; Han, D. K. *J. Proteome Res.* **2014**, *13*, 5031–5040.
- (40) Qiu, H.; Wang, Y. *J. Proteome Res.* **2008**, *7*, 1904–1915.
- (41) Paulitschke, V.; Kunstfeld, R.; Mohr, T.; Slany, A.; Micksche, M.; Drach, J.; Zielinski, C.; Pehamberger, H.; Gerner, C. *J. Proteome Res.* **2009**, *8*, 2501–2510.
- (42) Mazzucchelli, G. D.; Cellier, N. A.; Mshviladzade, V.; Elias, R.; Shim, Y.-H.; Touboul, D.; Quinton, L.; Brunelle, A.; Laprévotte, O.; De Pauw, E. A.; De Pauw-Gillet, M. C. A. *J. Proteome Res.* **2008**, *7*, 1683–1692.
- (43) Tata, A.; Fernandes, A. M. A. P.; Santos, V. G.; Alberici, R. M.; Araldi, D.; Parada, C. A.; Braguini, W.; Veronez, L.; Silva Bisson, G.; Reis, F. H. Z.; Alberici, L. C.; Eberlin, M. N. *Anal. Chem.* **2012**, *84*, 6341–6345.
- (44) Kwak, J.; Gallagher, M.; Ozdener, M. H.; Wysocki, C. J.; Goldsmith, B. R.; Isamah, A.; Faranda, A.; Fakharzadeh, S. S.; Herlyn, M.; Johnson, A. T. C.; Preti, G. *J. Chromatogr. B Anal. Technol. Biomed. Life Sci.* **2013**, *931*, 90–96.
- (45) Wald, N.; Goormaghtigh, E. *Analyst* **2015**, *140*, 2144–2155.
- (46) Mohr, P.; Birgersson, U.; Berking, C.; Henderson, C.; Trefzer, U.; Kemeny, L.; Sunderkötter, C.; Dirschka, T.; Motley, R.; Frohm-Nilsson, M.; Reinhold, U.; Loquai, C.; Braun, R.; Nyberg, F.; Paoli, J. *Ski. Res. Technol.* **2013**, *19*, 75–83.
- (47) Wolf, J. A.; Moreau, J. F.; Akilov, O.; Patton, T.; English, J. C.; Ho, J.; Ferris, L. K. *JAMA dermatology* **2013**, *149*, 422–426.
- (48) Belkin, S. *Curr. Opin. Microbiol.* **2003**, *6*, 206–212.
- (49) Nataro, J. P.; Kaper, J. B. *Clin. Microbiol. Rev.* **1998**, *11*, 142–201.
- (50) Lopez-Roldan, R.; Tusell, P.; Courtois, S.; Cortina, J. L. *Trends Anal. Chem.* **2013**, *44*, 46–57.

- (51) Straub, T. M.; Chandler, D. P. *J. Microbiol. Methods* **2003**, *53*, 185–197.
- (52) Varshney, M.; Li, Y. *Biosens. Bioelectron.* **2009**, *24*, 2951–2960.
- (53) Tosar, J. P.; Branas, G.; Laiz, J. *Biosens. Bioelectron.* **2010**, *26*, 1205–1217.
- (54) Li, L.; Garden, R. W.; Sweedler, J. V. *TIBTECH* **2000**, *18*, 151–160.
- (55) Sanvicens, N.; Pastells, C.; Pascual, N.; Marco, M.-P. *Trends Anal. Chem.* **2009**, *28*, 1243–1252.
- (56) Yoon, J.-Y.; Kim, B. *Sensors* **2012**, *12*, 10713–10741.
- (57) Syed, M. A. *Biosens. Bioelectron.* **2014**, *51*, 391–400.
- (58) Raz, S. R.; Haasnoot, W. *Trends Anal. Chem.* **2011**, *30*, 1526–1537.
- (59) Foudeh, A. M.; Didar, T. F.; Veres, T.; Tabrizian, M. *Lab Chip* **2012**, *12*, 3249–3266.
- (60) Silva, D. M.; Domingues, L. *Ecotoxicol. Environ. Saf.* **2015**, *113*, 400–411.
- (61) Sun, C. P.; Liao, J. C.; Zhang, Y. H.; Gau, V.; Mastali, M.; Babbitt, J. T.; Grundfest, W. S.; Churchill, B. M.; McCabe, E. R. B.; Haake, D. A. *Mol. Genet. Metab.* **2005**, *84*, 90–99.
- (62) Walter, A.; Wu, J.; Flechsig, G. U.; Haake, D. A.; Wang, J. *Anal. Chim. Acta* **2011**, *689*, 29–33.
- (63) Kuralay, F.; Campuzano, S.; Haake, D. A.; Wang, J. *Talanta* **2011**, *85*, 1330–1337.
- (64) Ouyang, M.; Mohan, R.; Lu, Y.; Liu, T.; Mach, K. E.; Sin, M. L. Y.; McComb, M.; Joshi, J.; Gau, V.; Wong, P. K.; Liao, J. C. *Analyst* **2013**, *138*, 3660–3666.
- (65) Liao, W.-C.; Ho, J.-A. A. *Anal. Chem.* **2009**, *81*, 2470–2476.
- (66) Loaiza, Ó. A.; Campuzano, S.; Pedrero, M.; Pingarrón, J. M. *Talanta* **2007**, *73*, 838–844.
- (67) Li, F.; Yu, Z.; Qu, H.; Zhang, G.; Yan, H.; Liu, X.; He, X. *Biosens. Bioelectron.* **2015**, *68*, 78–82.
- (68) Zhou, N.; Liu, Y.; You, Y.; Luo, J.; Tian, Y. *Electrochem. commun.* **2014**, *42*, 60–63.
- (69) Zhang, W.; Luo, C.; Zhong, L.; Nie, S.; Cheng, W.; Zhao, D.; Ding, S. *Microchim. Acta* **2013**, *180*, 1233–1240.
- (70) Shiraishi, H.; Itoh, T.; Hayashi, H.; Takagi, K.; Sakane, M.; Mori, T.; Wang, J. *Bioelectrochemistry* **2007**, *70*, 481–487.
- (71) Berganza, J.; Olabarria, G.; García, R.; Verdoy, D.; Rebollo, A.; Arana, S. *Biosens. Bioelectron.* **2007**, *22*, 2132–2137.

- (72) Mai, A. T.; Duc, T. P.; Thi, X. C.; Nguyen, M. H.; Nguyen, H. H. *Appl. Surf. Sci.* **2014**, *309*, 285–289.
- (73) Wang, J.; Rivas, G.; Cai, X. *Electroanalysis* **1997**, *9*, 395–398.
- (74) Pandey, C. M.; Sumana, G.; Malhotra, B. D. *Biomacromolecules* **2011**, 2925–2932.
- (75) Carpani, I.; Conti, P.; Lanteri, S.; Legnani, P. P.; Leoni, E.; Tonelli, D. *Biosens. Bioelectron.* **2008**, *23*, 959–964.
- (76) Settu, K.; Chen, C.-J.; Liu, J.-T.; Chen, C.-L.; Tsai, J.-Z. *Biosens. Bioelectron.* **2015**, *66*, 244–250.
- (77) Settu, K.; Liu, J. T.; Chen, C. J.; Tsai, J. Z.; Chang, S. J. *Proc. Annu. Int. Conf. IEEE Eng. Med. Biol. Soc. EMBS* **2013**, 1712–1715.
- (78) Abdullah, H.; Naim, N. M.; Azmy, N. A. N.; Hamid, A. A. *J. Nanomater.* **2014**, *2014*, 1–8.
- (79) Ma, F.; Rehman, A.; Liu, H.; Zhang, J.; Zhu, S.; Zeng, X. *Anal. Chem.* **2015**, *87*, 1560–1568.
- (80) Dechtrirat, D.; Gajovic-Eichelmann, N.; Wojcik, F.; Hartmann, L.; Bier, F. F.; Scheller, F. W. *Biosens. Bioelectron.* **2014**, *58*, 1–8.
- (81) Yang, H.; Wang, Y.; Qi, H.; Gao, Q.; Zhang, C. *Biosens. Bioelectron.* **2012**, *35*, 376–381.
- (82) Ertl, P.; Wagner, M.; Corton, E.; Mikkelsen, S. R. *Biosens. Bioelectron.* **2003**, *18*, 907–916.
- (83) Ertl, P.; Mikkelsen, S. R. *Anal. Chem.* **2001**, *73*, 4241–4248.
- (84) Shabani, A.; Marquette, C. A.; Mandeville, R.; Lawrence, M. F. *Talanta* **2013**, *116*, 1047–1053.
- (85) Guo, X.; Kulkarni, A.; Doepke, A.; Halsall, H. B.; Iyer, S.; Heineman, W. R. *Anal. Chem.* **2012**, *84*, 241–246.
- (86) Hassan, A.-R. H. A.-A.; De la Escosura-Muñiz, A.; Merkoçi, A. *Biosens. Bioelectron.* **2015**, *67*, 511–515.
- (87) Yu, H.; Bruno, J. G. *Appl. Environ. Microbiol.* **1996**, *62*, 587–592.
- (88) Settingington, E. B.; Alocilja, E. C. *Biosens. Bioelectron.* **2011**, *26*, 2208–2214.
- (89) Chan, K. Y.; Ye, W. W.; Zhang, Y.; Xiao, L. D.; Leung, P. H. M.; Li, Y.; Yang, M. *Biosens. Bioelectron.* **2013**, *41*, 532–537.

- (90) Lin, Y. H.; Chen, S. H.; Chuang, Y. C.; Lu, Y. C.; Shen, T. Y.; Chang, C. A.; Lin, C. S. *Biosens. Bioelectron.* **2008**, *23*, 1832–1837.
- (91) Li, Y.; Fang, L.; Cheng, P.; Deng, J.; Jiang, L.; Huang, H.; Zheng, J. *Biosens. Bioelectron.* **2013**, *49*, 485–491.
- (92) Lee, J.-Y.; Park, E.-J.; Min, N.-K.; Pak, J. J.; Lee, C.-J.; Kim, M. J.; Kim, S.-W.; Hong, S.-I. *IEEE Sensors Conf.* **2009**, 1176–1179.
- (93) Cheng, M. S.; Lau, S. H.; Chow, V. T.; Toh, C. S. *Environ. Sci. Technol.* **2011**, *45*, 6453–6459.
- (94) Dou, W.; Tang, W.; Zhao, G. *Electrochim. Acta* **2013**, *97*, 79–85.
- (95) Wang, Y.; Ping, J.; Ye, Z.; Wu, J.; Ying, Y. *Biosens. Bioelectron.* **2013**, *49*, 492–498.
- (96) Chowdhury, A. D.; De, A.; Chaudhuri, C. R.; Bandyopadhyay, K.; Sen, P. *Sensors Actuators, B Chem.* **2012**, *171-172*, 916–923.
- (97) Barreiros dos Santos, M.; Sporer, C.; Sanvicens, N.; Pascual, N.; Errachid, A.; Martinez, E.; Marco, M. P.; Teixeira, V.; Samiter, J. *Procedia Chem.* **2009**, *1*, 1291–1294.
- (98) Dweik, M.; Stringer, R. C.; Dastider, S. G.; Wu, Y.; Almasri, M.; Barizuddin, S. *Talanta* **2012**, *94*, 84–89.
- (99) Joung, C. K.; Kim, H. N.; Im, H. C.; Kim, H. Y.; Oh, M. H.; Kim, Y. R. *Sensors Actuators, B Chem.* **2012**, *161*, 824–831.
- (100) Lu, L.; Chee, G.; Yamada, K.; Jun, S. *Biosens. Bioelectron.* **2013**, *42*, 492–495.
- (101) Joung, C. K.; Kim, H. N.; Lim, M. C.; Jeon, T. J.; Kim, H. Y.; Kim, Y. R. *Biosens. Bioelectron.* **2013**, *44*, 210–215.
- (102) Barreiros dos Santos, M.; Aguil, J. P.; Prieto-Simón, B.; Sporer, C.; Teixeira, V.; Samitier, J. *Biosens. Bioelectron.* **2013**, *45*, 174–180.
- (103) Da Silva, J. S. L.; Oliveira, M. D. L.; de Melo, C. P.; Andrade, C. A. S. *Colloids Surfaces B Biointerfaces* **2014**, *117*, 549–554.
- (104) Su, W.; Lin, M.; Lee, H.; Cho, M.; Choe, W. S.; Lee, Y. *Biosens. Bioelectron.* **2012**, *32*, 32–36.
- (105) Kim, T.; Han, J.-I. *J. Environ. Manage.* **2013**, *130*, 267–275.
- (106) Kaya, T.; Nagamine, K.; Matsui, N.; Yasukawa, T.; Shiku, H.; Matsue, T. *Chem. Commun. (Camb)*. **2004**, *1*, 248–249.
- (107) Mittelman, A. S.; Ron, E. Z.; Rishpon, J. *Anal. Chem.* **2002**, *74*, 903–907.

- (108) Serra, B.; Morales, M. D.; Zhang, J.; Reviejo, A. J.; Hall, E. H.; Pingarron, J. M. *Anal. Chem.* **2005**, *77*, 8115–8121.
- (109) Yang, Q.; Liang, Y.; Zhou, T.; Shi, G.; Jin, L. *Electrochem. commun.* **2009**, *11*, 893–896.
- (110) Tang, H.; Zhang, W.; Geng, P.; Wang, Q.; Jin, L.; Wu, Z.; Lou, M. *Anal. Chim. Acta* **2006**, *562*, 190–196.
- (111) Amemiya, S.; Bard, A. J.; Fan, F.-R. F.; Mirkin, M. V.; Unwin, P. R. *Annu. Rev. Anal. Chem. (Palo Alto, Calif.)* **2008**, *1*, 95–131.
- (112) Engstrom, R. C.; Weber, M.; Wunder, D. J.; Burgess, R.; Winquist, S. *Anal. Chem.* **1988**, *58*, 844–848.
- (113) Bard, A. J.; Fan, F. F.; Kwak, J.; Lev, O. *Anal. Chem.* **1989**, *61*, 132–138.
- (114) Bard, A. J.; Mirkin, M. V. *Scanning Electrochemical Microscopy*; second.; CRC Press, 2012.
- (115) Kranz, C. *Analyst* **2014**, *139*, 336–352.
- (116) Shoup, D.; Szabo, A. J. *J. Electroanal. Chem. Interfacial Electrochem.* **1982**, *140*, 237–245.
- (117) Heinze, J. *Angew. Chemie Int. Ed.* **1993**, *32*, 1268–1288.
- (118) Forster, R. J. *Chem. Soc. Rev.* **1994**, *23*, 289–297.
- (119) Zoski, C. G. *Electroanalysis* **2002**, *14*, 1041–1051.
- (120) Tel-Vered, R.; Walsh, D. A.; Mehrgardi, M. A.; Bard, A. J. *Anal. Chem.* **2006**, *78*, 6959–6966.
- (121) Slevin, C. J.; Gray, N. J.; Macpherson, J. V.; Webb, M. A.; Unwin, P. R. *Electrochem. commun.* **1999**, *1*, 282–288.
- (122) Zhang, X.; Zhang, W.; Zhou, X.; Ogorevc, B. *Anal. Chem.* **1996**, *68*, 3338–3343.
- (123) Li, Y.; Bergman, D.; Zhang, B. *Anal. Chem.* **2009**, *81*, 5496–5502.
- (124) Mezour, M. A.; Morin, M.; Mauzeroll, J. *Anal. Chem.* **2011**, *83*, 2378–2382.
- (125) Thakar, R.; Weber, A. E.; Morris, C. A.; Baker, L. A. *Analyst* **2013**, *138*, 5973–5982.
- (126) Potje-Kamloth, K.; Janata, J.; Josowicz, M. *Berichte der Bunsengesellschaft für Phys. Chemie* **1989**, *93*, 1480–1485.
- (127) Sklyar, O.; Treutler, T. H.; Vlachopoulos, N.; Wittstock, G. *Surf. Sci.* **2005**, *597*, 181–195.

- (128) Watkins, J. J.; Chen, J.; White, H. S.; Abruña, H. D.; Maisonhaute, E.; Amatore, C. *Anal. Chem.* **2003**, *75*, 3962–3971.
- (129) Cortés-Salazar, F.; Deng, H.; Peljo, P.; Pereira, C. M.; Kontturi, K.; Girault, H. H. *Electrochim. Acta* **2013**, *110*, 22–29.
- (130) Liu, B.; Rolland, J. P.; DeSimone, J. M.; Bard, A. J. *Anal. Chem.* **2005**, *77*, 3013–3017.
- (131) Eifert, A.; Mizaikoff, B.; Kranz, C. *Micron* **2015**, *68*, 27–35.
- (132) Shin, H.; Hesketh, P. J.; Mizaikoff, B.; Kranz, C. *Sensors Actuators, B Chem.* **2008**, *134*, 488–495.
- (133) Shin, H.; Hesketh, P. J.; Mizaikoff, B.; Kranz, C. *Anal. Chem.* **2007**, *79*, 4769–4777.
- (134) Wiedemair, J.; Moon, J. S.; Reinauer, F.; Mizaikoff, B.; Kranz, C. *Electrochem. commun.* **2010**, *12*, 989–991.
- (135) Takahashi, Y.; Shiku, H.; Murata, T.; Yasukawa, T.; Matsue, T. *Anal. Chem.* **2009**, *81*, 9674–9681.
- (136) Voronin, O. G.; Hartmann, A.; Steinbach, C.; Karyakin, A. A.; Khokhlov, A. R.; Kranz, C. *Electrochem. commun.* **2012**, *23*, 102–105.
- (137) Hirano, Y.; Kowata, K.; Kodama, M.; Komatsu, Y. *Bioelectrochemistry* **2013**, *92*, 1–5.
- (138) Demaille, C.; Brust, M.; Tsionsky, M.; Bard, A. J. *Anal. Chem.* **1997**, *69*, 2323–2328.
- (139) Wehmeyer, K. R.; Wightman, R. M. *Anal. Chem.* **1985**, *57*, 1989–1993.
- (140) MacFarlane, R.; Wong, K. Y. *J. Electroanal. Chem.* **1985**, *185*, 197–202.
- (141) Takahashi, Y.; Shevchuk, A. I.; Novak, P.; Murakami, Y.; Shiku, H.; Korchev, Y. E.; Matsue, T. *J. Am. Chem. Soc.* **2010**, 10118–10126.
- (142) Lin, Y.; Trouillon, R.; Svensson, M. I.; Keighron, J. D.; Cans, A. S.; Ewing, A. G. *Anal. Chem.* **2012**, *84*, 2949–2954.
- (143) Lugstein, A.; Bertagnolli, E.; Kranz, C.; Mizaikoff, B. *Surf. Interface Anal.* **2002**, *33*, 146–150.
- (144) Liljeroth, P.; Johans, C.; Slevin, C. J.; Quinn, B. M. *Electrochem. commun.* **2002**, *4*, 67–71.
- (145) Cortés-Salazar, F.; Trauble, M.; Li, F.; Busnel, J.; Gassner, A.; Hojeij, M.; Wittstock, G.; Girault, H. H. *Anal. Biochem.* **2009**, *81*, 6889–6896.
- (146) Momotenko, D.; Qiao, L.; Cortés-Salazar, F.; Lesch, A.; Wittstock, G.; Girault, H. H. *Anal. Chem.* **2012**, *84*, 6630–6637.

- (147) Cortés-Salazar, F.; Lesch, A.; Momotenko, D.; Busnel, J.-M.; Wittstock, G.; Girault, H. H. *Anal. Methods* **2010**, *2*, 817.
- (148) Momotenko, D.; Cortés-Salazar, F.; Lesch, A.; Wittstock, G.; Girault, H. H. *Anal. Chem.* **2011**, *83*, 5275–5282.
- (149) Wipf, D. O. *J. Electrochem. Soc.* **1991**, *138*, 469.
- (150) Whitworth, A. L.; Mandler, D.; Unwin, P. R. *Phys. Chem. Chem. Phys.* **2005**, *7*, 356–365.
- (151) Cornut, R.; Lefrou, C. *J. Electroanal. Chem.* **2008**, *621*, 178–184.
- (152) Sciutto, G.; Prati, S.; Mazzeo, R.; Zangheri, M.; Roda, A.; Bardini, L.; Valenti, G.; Rapino, S.; Marcaccio, M. *Anal. Chim. Acta* **2014**, *831*, 31–37.
- (153) Bard, A. J.; Li, X.; Zhan, W. *Biosens. Bioelectron.* **2006**, *22*, 461–472.
- (154) Schulte, A.; Nebel, M.; Schuhmann, W. *Annu. Rev. Anal. Chem. (Palo Alto, Calif.)* **2010**, *3*, 299–318.
- (155) Bergner, S.; Vatsyayan, P.; Matysik, F.-M. *Anal. Chim. Acta* **2013**, *775*, 1–13.
- (156) Zhang, Y.; Ma, J.; Zhang, Y.; Jiang, H.; Wang, X. *Nanosci. Nanotechnol. Lett.* **2013**, *5*, 182–185.
- (157) Sun, P.; Laforge, F. O.; Abeyweera, T. P.; Rotenberg, S. A.; Carpino, J.; Mirkin, M. V. *Proc. Natl. Acad. Sci. U. S. A.* **2008**, *105*, 443–448.
- (158) Kaya, T.; Torisawa, Y.; Oyamatsu, D.; Nishizawa, M.; Matsue, T. *Biosens. Bioelectron.* **2003**, *18*, 1379–1383.
- (159) Li, X.; Bard, A. J. *J. Electroanal. Chem.* **2009**, *628*, 35–42.
- (160) Koley, D.; Bard, A. J. *Proc. Natl. Acad. Sci. U. S. A.* **2012**, *109*, 11522–11527.
- (161) Kuss, S.; Cornut, R.; Beaulieu, I.; Mezour, M. A.; Annabi, B.; Mauzeroll, J. *Bioelectrochemistry* **2011**, *82*, 29–37.
- (162) Matsumae, Y.; Takahashi, Y.; Ino, K.; Shiku, H.; Matsue, T. *Anal. Chim. Acta* **2014**, *842*, 20–26.
- (163) Kuss, S.; Polcari, D.; Geissler, M.; Brassard, D.; Mauzeroll, J. *Proc. Natl. Acad. Sci. U. S. A.* **2013**, *110*, 9249–9254.
- (164) Takahashi, Y.; Shevchuk, A. I.; Novak, P.; Babakinejad, B.; Macpherson, J.; Unwin, P. R.; Shiku, H.; Gorelik, J.; Klenerman, D.; Korchev, Y. E.; Matsue, T. *PNAS* **2012**, *109*, 11540–11545.



- (165) Kurulugama, R. T.; Wipf, D. O.; Takacs, S. A.; Pongmayteegul, S.; Garris, P. A.; Baur, J. E. *Anal. Chem.* **2005**, *77*, 1111–1117.
- (166) Takii, Y.; Takoh, K.; Nishizawa, M.; Matsue, T. *Electrochim. Acta* **2003**, *48*, 3381–3385.
- (167) Liebetrau, J. M.; Miller, H. M.; Baur, J. E.; Takacs, S. A.; Anupunpisit, V.; Garris, P. A.; Wipf, D. O. *Anal. Chem.* **2003**, *75*, 563–571.
- (168) Rotenberg, S. A.; Mirkin, M. V. *J. Mammary Gland Biol. Neoplasia* **2004**, *9*, 375–382.
- (169) Liu, B.; Cheng, W.; Rotenberg, S. A.; Mirkin, M. V. *J. Electroanal. Chem.* **2001**, *500*, 590–597.
- (170) Liu, B.; Rotenberg, S. A.; Mirkin, M. V. *Proc. Natl. Acad. Sci.* **2000**, *97*, 9855–9860.
- (171) Torisawa, Y.-S.; Kaya, T.; Takii, Y.; Oyamatsu, D.; Nishizawa, M.; Matsue, T. *Anal. Chem.* **2003**, *75*, 2154–2158.
- (172) Bergner, S.; Wegener, J.; Matysik, F.-M. *Anal. Methods* **2012**, *4*, 623.
- (173) Nishizawa, M.; Takoh, K.; Matsue, T. *Langmuir* **2002**, *18*, 3645–3649.
- (174) Gac, L.; Sridhar, A.; Boer, H. L. De; Berg, A. Van Den. *PLoS One* **2014**, *9*, e93618.
- (175) Shiku, H.; Shiraishi, T.; Ohya, H.; Matsue, T.; Abe, H.; Hoshi, H.; Kobayashi, M. *Anal. Chem.* **2001**, *73*, 3751–3758.
- (176) Takahashi, R.; Zhou, Y.; Horiguchi, Y.; Shiku, H.; Sonoda, H.; Itabashi, N.; Yamamoto, J.; Saito, T.; Matsue, T.; Hisada, A. *J. Biosci. Bioeng.* **2014**, *117*, 113–121.
- (177) Shiku, H.; Shiraishi, T.; Aoyagi, S.; Utsumi, Y.; Matsudaira, M.; Abe, H.; Hoshi, H.; Kasai, S.; Ohya, H.; Matsue, T. *Anal. Chim. Acta* **2004**, *522*, 51–58.
- (178) Obregon, R.; Horiguchi, Y.; Arai, T.; Abe, S.; Zhou, Y.; Takahashi, R.; Hisada, A.; Ino, K.; Shiku, H.; Matsue, T. *Talanta* **2012**, *94*, 30–35.
- (179) Shiku, H.; Torisawa, Y.; Takagi, A.; Aoyagi, S.; Abe, H.; Hoshi, H.; Yasukawa, T.; Matsue, T. *Sensors Actuators B Chem.* **2005**, *108*, 597–602.
- (180) Zhu, L.; Gao, N.; Zhang, X.; Jin, W. *Talanta* **2008**, *77*, 804–808.
- (181) Gao, N.; Wang, X.; Li, L.; Zhang, X.; Jin, W. *Analyst* **2007**, *132*, 1139–1146.
- (182) Kim, J.; Connell, J. L.; Whiteley, M.; Bard, A. J. *Anal. Chem.* **2014**, *86*, 12327–12333.
- (183) Nebel, M.; Grützke, S.; Diab, N.; Schulte, A.; Schuhmann, W. *Angew. Chemie - Int. Ed.* **2013**, *52*, 6335–6338.
- (184) Yasukawa, T.; Kondo, Y.; Uchida, I.; Matsue, T. *Chem. Lett.* **1998**, *8*, 767–768.

- (185) Salamifar, S. E.; Lai, R. Y. *Anal. Chem.* **2013**, *85*, 9417–9421.
- (186) Zhang, M. M. N.; Long, Y.-T.; Ding, Z. *J. Inorg. Biochem.* **2012**, *108*, 115–122.
- (187) Zhao, X.; Diakowski, P. M.; Ding, Z. *Anal. Chem.* **2010**, *82*, 8371–8373.
- (188) Isik, S.; Schuhmann, W. *Angew. Chem. Int. Ed. Engl.* **2006**, *45*, 7451–7454.
- (189) Pitta Bauermann, L.; Schuhmann, W.; Schulte, A. *Phys. Chem. Chem. Phys.* **2004**, *6*, 4003.
- (190) Yasukawa, T.; Uchida, I.; Matsue, T. *Biochim. Biophys. Acta* **1998**, *1369*, 152–158.
- (191) Yasukawa, T.; Kaya, T.; Matsue, T. *Electroanalysis* **2000**, *12*, 653–659.
- (192) Zhan, D.; Li, X.; Nepomnyashchii, A. B.; Alpuche-Aviles, M. A.; Fan, F. R. F.; Bard, A. J. *J. Electroanal. Chem.* **2013**, *688*, 61–68.
- (193) Rapino, S.; Marcu, R.; Bigi, A.; Soldà, A.; Marcaccio, M.; Paolucci, F.; Pelicci, P. G.; Giorgio, M. *Electrochim. Acta* **2015**, *in press*.
- (194) Razzaghi, F.; Seguin, J.; Amar, A.; Griveau, S.; Bedioui, F. *Electrochim. Acta* **2015**, *157*, 95–100.
- (195) Xue, Y.; Ding, L.; Lei, J.; Yan, F.; Ju, H. *Anal. Chem.* **2010**, *82*, 7112–7118.
- (196) Takahashi, Y.; Miyamoto, T.; Shiku, H.; Ino, K.; Yasukawa, T.; Asano, R.; Kumagai, I.; Matsue, T. *Phys. Chem. Chem. Phys.* **2011**, *13*, 16569–16573.
- (197) Matsumae, Y.; Arai, T.; Takahashi, Y.; Ino, K.; Shiku, H.; Matsue, T. *Chem. Commun. (Camb)*. **2013**, *49*, 6498–6500.
- (198) Mauzeroll, J.; Bard, A. J.; Owhadian, O.; Monks, T. J. *Proc. Natl. Acad. Sci. U. S. A.* **2004**, *101*, 17582–17587.
- (199) Yasukawa, T.; Kaya, T.; Matsue, T. *Anal. Chem.* **1999**, *71*, 4637–4641.
- (200) Takahashi, Y.; Shevchuk, A. I.; Novak, P.; Zhang, Y.; Ebejer, N.; Macpherson, J. V.; Unwin, P. R.; Pollard, A. J.; Roy, D.; Clifford, C. A.; Shiku, H.; Matsue, T.; Klenerman, D.; Korchev, Y. E. *Angew. Chem. Int. Ed. Engl.* **2011**, *50*, 9638–9642.
- (201) Diakowski, P. M.; Ding, Z. *Phys. Chem. Chem. Phys.* **2007**, *9*, 5966–5974.
- (202) Kurulugama, R. T.; Wipf, D. O.; Takacs, S. A.; Pongmayteegul, S.; Garris, P. A.; Baur, J. E. *Anal. Chem.* **2005**, *77*, 1111–1117.
- (203) Ludwig, M.; Kranz, C.; Schuhmann, W.; Gaub, H. E. *Rev. Sci. Instrum.* **1995**, *66*, 2857–2860.
- (204) Schulte, A.; Nebel, M.; Schuhmann, W. *Methods Enzymol.* **2012**, *504*, 237–254.

- (205) Ayyar, B. V.; Arora, S.; Murphy, C.; O’Kennedy, R. *Methods* **2012**, *56*, 116–129.
- (206) Fodey, T.; Leonard, P.; O’Mahony, J.; O’Kennedy, R.; Danaher, M. *TrAC Trends Anal. Chem.* **2011**, *30*, 254–269.
- (207) Zhang, C. In *Antibody Methods and Protocols*; Proetzl, G.; Ebersbach, H., Eds.; Methods in Molecular Biology<sup>TM</sup>; Humana Press, 2012; Vol. 901, pp. 117–135.
- (208) Conroy, P. J.; Hearty, S.; Leonard, P.; O’Kennedy, R. *J. Semin. Cell Dev. Biol.* **2009**, *20*, 10–26.
- (209) Wu, A. H. B. *Clin. Chim. Acta.* **2006**, *369*, 119–124.
- (210) Mayhew, T. M. *J. Anat.* **2011**, *219*, 647–660.
- (211) Kuang, H.; Zhao, Y.; Ma, W.; Xu, L.; Wang, L.; Xu, C. *TrAC Trends Anal. Chem.* **2011**, *30*, 1620–1636.
- (212) Xu, M.; Rettig, M. P.; Sudlow, G.; Wang, B.; Akers, W. J.; Cao, D.; Mutch, D. G.; Dipersio, J. F.; Achilefu, S. *Int. J. Cancer* **2012**, *131*, 1351–1359.
- (213) Meng, M.; Xi, R. *Anal. Lett.* **2011**, *44*, 2543–2558.
- (214) Yalow, R. S.; Berson, S. A. *Lett. to Nat.* **1959**, *184*, 1648–1649.
- (215) Beloglazova, N. V.; Goryacheva, I. Y.; Niessner, R.; Knopp, D. *Microchim. Acta* **2011**, *175*, 361–367.
- (216) Nistor, C.; Emneus, J. In *Comprehensive Analytical Chemistry XLIV*; Gorton, L., Ed.; Elsevier B.V., 2005; pp. 375–427.
- (217) Crowther, J. R. In *The ELISA Guidebook*; Crowther, J. R., Ed.; Humana Press, 2009; Vol. 516, pp. 9–42.
- (218) Kim, J.; Park, H.; Ryu, J.; Jeon, O.; Paeng, I. R. *J. Immunoassay Immunochem.* **2010**, *31*, 33–44.
- (219) Kashiwakuma, T.; Hasegawa, A.; Kajita, T.; Takata, A.; Mori, H.; Ohta, Y.; Tanaka, E.; Kiyosawa, K.; Tanaka, T.; Tanaka, S.; Hattori, N.; Kohara, M. *J. Immunol. Methods* **1996**, *190*, 79–89.
- (220) Xin, T.-B.; Chen, H.; Lin, Z.; Liang, S.-X.; Lin, J.-M. *Talanta* **2010**, *82*, 1472–1477.
- (221) Yi, J.; Meng, M.; Liu, Z.; Zhi, J.; Zhang, Y.; Xu, J.; Wang, Y.; Liu, J.; Xi, R. *J. Zhejiang Univ. Sci. B* **2012**, *13*, 118–125.
- (222) Josephy, P. D.; Eling, T.; Mason, R. P. *J. Biol. Chem.* **1982**, *257*, 3669–3675.

- (223) Dill, K.; Ghindilis, A. L.; Schwarzkopf, K. R.; Fuji, H. S.; Liu, R. In *Immunoassay and Other Bioanalytical Techniques*; Van Emon, J. M., Ed.; CRC Press, 2006; pp. 445–501.
- (224) Lee, J. H.; Rho, J.-E. R.; Rho, T.-H. D.; Newby, J. G. *Biosens. Bioelectron.* **2010**, *26*, 377–382.
- (225) Zhao, L.; Sun, L.; Chu, X. *TrAC Trends Anal. Chem.* **2009**, *28*, 404–415.
- (226) Wang, C.; Wu, J.; Zong, C.; Xu, J.; Ju, H.-X. *Chinese J. Anal. Chem.* **2012**, *40*, 3–10.
- (227) Laschi, S.; Centi, S.; Mascini, M. *Bioanal. Rev.* **2010**, *3*, 11–25.
- (228) Ronkainen-Matsuno, N. J.; Halsall, H. B.; Heineman, W. R. In *Immunoassay and Other Bioanalytical Techniques*; Van Emon, J. M., Ed.; CRC Press, 2006; pp. 385–402.
- (229) Kuramitz, H. *Anal. Bioanal. Chem.* **2009**, *394*, 61–69.
- (230) Lu, A.-H.; Salabas, E. L.; Schüth, F. *Angew. Chem. Int. Ed. Engl.* **2007**, *46*, 1222–1244.
- (231) Xin, T.-B.; Wang, X.; Jin, H.; Liang, S.-X.; Lin, J.-M.; Li, Z.-J. *Appl. Biochem. Biotechnol.* **2009**, *158*, 582–594.
- (232) Dungchai, W.; Siangproh, W.; Lin, J.-M.; Chailapakul, O.; Lin, S.; Ying, X. *Anal. Bioanal. Chem.* **2007**, *387*, 1965–1971.
- (233) Winston, R. L.; Fitzgerald, M. C. *Mass Spectrom. Rev.* **1998**, *16*, 165–179.
- (234) Murphy, R. C.; Hankin, J. A.; Barkley, R. M. *J. Lipid Res.* **2009**, *50 Suppl*, S317–S322.
- (235) Mann, M.; Hendrickson, R. C.; Pandey, A. *Annu. Rev. Biochem.* **2001**, *70*, 437–473.
- (236) Lay, J. O. *Mass Spectrom. Rev.* **2001**, *20*, 172–194.
- (237) Fenn, J. B.; Mann, M.; Meng, C. K.; Wong, S. F.; Whitehouse, C. M. *Science* **1989**, *246*, 64–71.
- (238) Tanaka, K.; Waki, H.; Ido, Y.; Akita, S.; Yoshida, Y.; Yoshida, T.; Matsuo, T. *Rapid Commun. Mass Spectrom.* **1988**, *2*, 151–153.
- (239) Karas, M.; Bachmann, D.; Hillenkamp, F. *Anal. Chem.* **1985**, *57*, 2935–2939.
- (240) Karas, M.; Hillenkamp, F. *Anal. Chem.* **1988**, *60*, 2299–2301.
- (241) Awad, H.; Khamis, M. M.; El-Aneed, A. *Appl. Spectrosc. Rev.* **2014**, *50*, 158–175.
- (242) Ehring, H.; Karas, M.; Hillenkamp, F. *Org. Mass Spectrom.* **1992**, *27*, 472–480.
- (243) Vertes, A.; Balazs, L.; Gijbels, R. *Rapid Commun. Mass Spectrom.* **1990**, *4*, 263–266.

- (244) Krüger, R.; Pfenninger, A.; Fournier, I.; Gluckmann, M.; Karas, M. *Anal. Chem.* **2001**, *73*, 5812–5821.
- (245) Chang, W. C.; Huang, L. C. L.; Wang, Y.-S.; Peng, W.-P.; Chang, H. C.; Hsu, N. Y.; Yang, W. Bin; Chen, C. H. *Anal. Chim. Acta* **2007**, *582*, 1–9.
- (246) Seeley, E. H.; Oppenheimer, S. R.; Mi, D.; Chaurand, P.; Caprioli, R. M. *J. Am. Soc. Mass Spectrom.* **2008**, *19*, 1069–1077.
- (247) Lemaire, R.; Wisztorski, M.; Desmons, A.; Tabet, J. C.; Day, R.; Salzet, M.; Fournier, I. *Anal. Chem.* **2006**, *78*, 7145–7153.
- (248) Agar, N. Y. R.; Yang, H. W.; Carroll, R. S.; Black, P. M.; Agar, J. N. *Anal. Chem.* **2007**, *79*, 7416–7423.
- (249) Bouschen, W.; Schulz, O.; Eikel, D.; Spengler, B. *Rapid Commun. Mass Spectrom.* **2010**, *24*, 355–364.
- (250) Zavalin, A.; Todd, E. M.; Rawhouser, P. D.; Yang, J.; Norris, J. L.; Caprioli, R. M. *J. Mass Spectrom.* **2012**, *47*, 1473–1481.
- (251) Altelaar, A. F. M.; Klinkert, I.; Jalink, K.; De Lange, R. P. J.; Adan, R. A. H.; Heeren, R. M. A.; Piersma, S. R. *Anal. Chem.* **2006**, *78*, 734–742.
- (252) Bergquist, J. *Chromatogr. Suppl. I* **1999**, *49*, S41–S48.
- (253) Dalluge, J. J. *Fresenius. J. Anal. Chem.* **2000**, *366*, 701–711.
- (254) Ouedraogo, R.; Daumas, A.; Ghigo, E.; Capo, C.; Mege, J. L.; Textoris, J. J. *Proteomics* **2012**, *75*, 5523–5532.
- (255) Povey, J. F.; O'Malley, C. J.; Root, T.; Martin, E. B.; Montague, G. A.; Feary, M.; Trim, C.; Lang, D. A.; Alldread, R.; Racher, A. J.; Smales, C. M. *J. Biotechnol.* **2014**, *184*, 84–93.
- (256) Buchanan, C. M.; Malik, A. S.; Cooper, G. J. S. *Rapid Commun. Mass Spectrom.* **2007**, *21*, 3452–3458.
- (257) Hanrieder, J.; Wicher, G.; Bergquist, J.; Andersson, M.; Fex-Svenningsen, Å. *Anal. Bioanal. Chem.* **2011**, *401*, 135–147.
- (258) Srinivasan, M.; Sedmak, D.; Jewell, S. *Am. J. Pathol.* **2002**, *161*, 1961–1971.
- (259) Fox, C. H.; Johnson, F. B.; Whiting, J.; Roller, P. P. *J. Histochem. Cytochem.* **1985**, *33*, 845–853.
- (260) Schmiedeberg, L.; Skene, P.; Deaton, A.; Bird, A. *PLoS One* **2009**, *4*, e4636.
- (261) Lehmann, H. *Br. Med. J.* **1968**, *1*, 823.

- (262) Sung, H.-W.; Chang, Y.; Liang, I.-L.; Chang, W.-H.; Chen, Y.-C. *J. Biomed. Mater. Res.* **2000**, *52*, 77–87.
- (263) Tsai, C. C.; Huang, R. N.; Sung, H. W.; Liang, H. C. *J. Biomed. Mater. Res.* **2000**, *52*, 58–65.
- (264) Williams, Y.; Byrne, S.; Bashir, M.; Davies, A.; Whelan, Á.; Gun'ko, Y.; Kelleher, D.; Volkov, Y. *J. Microsc.* **2008**, *232*, 91–98.
- (265) Noguchi, M.; Furuya, S.; Takeuchi, T.; Hirohashi, S. *Pathol. Int.* **1997**, *47*, 685–691.
- (266) Levitt, D.; King, M. *J. Immunol. Methods* **1987**, *96*, 233–237.
- (267) Pollice, A. A.; McCoy, P. J.; Shackney, S. E.; Smith, C. A.; Agarwal, J.; Burholt, D. R.; Janocko, L. E.; Hornicek, F. J.; Singh, S. G.; Hartsock, R. J. *Cytometry* **1992**, *13*, 432–444.
- (268) Leong, A. S.; Daymon, M. E.; Milios, J. *J. Pathol.* **1985**, *146*, 313–321.
- (269) Rensing, K. H. In *Wood Formation in Trees: Cell and Molecular Biology Techniques*; Chaffey, N., Ed.; CRC Press, 2003; pp. 65–82.
- (270) Zierold, K. *J. Microsc.* **1991**, *161*, 357–366.
- (271) Yamane, Y.; Shiga, H.; Haga, H.; Kawabata, K.; Abe, K.; Ito, E. *J. Electron Microsc.* (Tokyo). **2000**, *49*, 463–471.
- (272) Braet, F.; Rotsch, C.; Wisse, E.; Radmacher, M. *Appl. Phys. A Mater. Sci. Process.* **1998**, *66*, 575–578.
- (273) Morkvėnaitė-Vilkončienė, I.; Ramanavičienė, A.; Ramanavičius, A. *Medicina (Kaunas)*. **2013**, *49*, 155–164.
- (274) Poole, K.; Müller, D. *Br. J. Cancer* **2005**, *92*, 1499–1505.
- (275) Korchev, Y. E.; Gorelik, J.; Lab, M. J.; Sviderskaya, E. V.; Johnston, C. L.; Coombes, C. R.; Vodyanoy, I.; Edwards, C. R. *Biophys. J.* **2000**, *78*, 451–457.
- (276) Novak, P.; Li, C.; Shevchuk, A. I.; Stepanyan, R.; Caldwell, M.; Hughes, S.; Smart, T. G.; Gorelik, J.; Ostanin, V. P.; Lab, M. J.; Moss, G. W. J.; Frolenkov, G. I.; Klenerman, D.; Korchev, Y. E. *Nat. Methods* **2009**, *6*, 279–281.
- (277) Nagata, Y.; Ishizaki, I.; Waki, M.; Ide, Y.; Hossen, M. A.; Ohnishi, K.; Sanada, N.; Setou, M. *Surf. Interface Anal.* **2014**, *46*, 185–188.
- (278) Singh, M.; Haverinen, H. M.; Dhagat, P.; Jabbour, G. E. *Adv. Mater.* **2010**, *22*, 673–685.
- (279) Derby, B. *Annu. Rev. Mater. Res.* **2010**, *40*, 395–414.

- (280) Fromm, J. E. *IBM J. Res. Dev.* **1984**, *28*, 322–333.
- (281) Reis, N.; Derby, B. *MRS Proc.* **2011**, *624*, 65.
- (282) Duineveld, P. C.; de Kok, M. M.; Buechel, M.; Sempel, A.; Mutsaers, K. A. H.; van de Weijer, P.; Camps, I. G. J.; van de Biggelaar, T.; Rubingh, J.-E. J. M.; Haskal, E. I. In *International Symposium on Optical Science and Technology*; Kafafi, Z. H., Ed.; International Society for Optics and Photonics, 2002; pp. 59–67.
- (283) Stow, C. D.; Hadfield, M. G. *Proc. R. Soc. A Math. Phys. Eng. Sci.* **1981**, *373*, 419–441.
- (284) Bhola, R.; Chandra, S. *J. Mater. Sci.* **34**, 4883–4894.
- (285) Cummins, G.; Desmulliez, M. P. Y. *Circuit World* **2012**, *38*, 193–213.
- (286) Komuro, N.; Takaki, S.; Suzuki, K.; Citterio, D. *Anal. Bioanal. Chem.* **2013**, *405*, 5785–5805.
- (287) Abe, K.; Kotera, K.; Suzuki, K.; Citterio, D. *Anal. Bioanal. Chem.* **2010**, *398*, 885–893.
- (288) Määttänen, A.; Vanamo, U.; Ihalainen, P.; Pulkkinen, P.; Tenhu, H.; Bobacka, J.; Peltonen, J. *Sensors Actuators B Chem.* **2013**, *177*, 153–162.
- (289) Lesch, A.; Cortés-Salazar, F.; Prudent, M.; Delobel, J.; Rastgar, S.; Lion, N.; Tissot, J.-D.; Tacchini, P.; Girault, H. H. *J. Electroanal. Chem.* **2014**, *717-718*, 61–68.
- (290) Jensen, G. C.; Krause, C. E.; Sotzing, G. A.; Rusling, J. F. *Phys. Chem. Chem. Phys.* **2011**, *13*, 4888–4894.
- (291) Zhang, H.; Xie, A.; Shen, Y.; Qiu, L.; Tian, X. *Phys. Chem. Chem. Phys.* **2012**, *14*, 12757–12763.
- (292) Abe, K.; Suzuki, K.; Citterio, D. *Anal. Chem.* **2008**, *80*, 6928–6934.
- (293) Kit-Anan, W.; Olarnwanich, A.; Sriprachuabwong, C.; Karuwan, C.; Tuantranont, A.; Wisitsoraat, A.; Srituravanich, W.; Pimpin, A. *J. Electroanal. Chem.* **2012**, *685*, 72–78.
- (294) Cinti, S.; Arduini, F.; Moscone, D.; Palleschi, G.; Killard, A. J. *Sensors (Basel)*. **2014**, *14*, 14222–14234.
- (295) Ajayan, P. M.; Zhou, O. Z. *Top. Appl. Phys.* **2001**, *80*, 391–425.
- (296) Charlier, J.-C. *Acc. Chem. Res.* **2002**, *35*, 1063–1069.
- (297) Hirsch, A. *Angew. Chem. Int. Ed. Engl.* **2002**, *41*, 1853–1859.
- (298) Dumitrescu, I.; Unwin, P. R.; Macpherson, J. V. *Chem. Commun. (Camb)*. **2009**, 7345, 6886–6901.
- (299) Byers, J. C.; Güell, A. G.; Unwin, P. R. *J. Am. Chem. Soc.* **2014**, *136*, 11252–11255.

- (300) Güell, A. G.; Meadows, K. E.; Dudin, P. V.; Ebejer, N.; Macpherson, J. V.; Unwin, P. R. *Nano Lett.* **2014**, *14*, 220–224.
- (301) Gasilova, N.; Qiao, L.; Momotenko, D.; Pourhaghighi, M. R.; Girault, H. H. *Anal. Chem.* **2013**, *85*, 6254–6263.
- (302) Lu, Y.; Prudent, M.; Qiao, L.; Mendez, M. A.; Girault, H. H. *Metallomics* **2010**, *2*, 474–479.
- (303) Abonnenc, M.; Dayon, L.; Perruche, B.; Lion, N.; Girault, H. H. *Anal. Chem.* **2008**, *80*, 3372–3378.
- (304) Zamfir, A. D.; Bindila, L.; Lion, N.; Allen, M.; Girault, H. H.; Peter-Katalinić, J. *Electrophoresis* **2005**, *26*, 3650–3673.
- (305) Prudent, M.; Méndez, M.; Roussel, C.; Su, B.; Lion, N.; Rossier, J. S.; Girault, H. H. *Chim. Int. J. Chem.* **2009**, *63*, 283–287.
- (306) Liu, Y.; Liu, B.; Yang, P.; Girault, H. H. *Anal. Bioanal. Chem.* **2008**, *390*, 227–229.
- (307) Lion, N.; Rohner, T. C.; Dayon, L.; Arnaud, I. L.; Damoc, E.; Youhnovski, N.; Wu, Z.-Y.; Roussel, C.; Josserand, J.; Jensen, H.; Rossier, J. S.; Przybylski, M.; Girault, H. H. *Electrophoresis* **2003**, *24*, 3533–3562.
- (308) Lion, N.; Reymond, F.; Girault, H. H.; Rossier, J. S. *Curr. Opin. Biotechnol.* **2004**, *15*, 31–37.
- (309) Gasilova, N.; Yu, Q.; Qiao, L.; Girault, H. H. *Angew. Chem. Int. Ed. Engl.* **2014**, *53*, 4408–4412.
- (310) Cortés-Salazar, F.; Momotenko, D.; Lesch, A.; Wittstock, G.; Girault, H. H. *Anal. Chem.* **2010**, *82*, 10037–10044.
- (311) Lesch, A.; Momotenko, D.; Cortés-Salazar, F.; Roelfs, F.; Girault, H. H.; Wittstock, G. *Electrochim. Acta* **2013**, *110*, 30–41.
- (312) Bäuerle, D. W. *Laser Processing and Chemistry*; 4th ed.; Springer-Verlag: Berlin, 2011.
- (313) Hoffmann, P.; Sidler, T. *Course of Micro-Machining with Laser*; Ecole Polytechnique Federale de Lausanne: Lausanne, 2009.



# CHAPTER II

## Scanning Electrochemical Microscopy of Alive, Fixed and Permeabilized Adherent Melanoma Cells

### Abstract

Scanning electrochemical microscopy (SECM) is a versatile technique that has been widely used for the electrochemical imaging of dynamic topographical and metabolic changes of alive adherent mammalian cells. However, extracting intracellular information by SECM is difficult, since it requires redox species to travel in and out the lipid cell membrane. Additionally, direct opening of the cell membrane could lead to the release and lost of all cell content. To alleviate such situation, biologists have developed cells fixation protocols that eliminate the biological activity, but enable the access to the preserved cellular ultrastructure as well as proteins, carbohydrates and other bio-active moieties in their original spatial organization. Herein, SECM was applied to cells fixed with formaldehyde, a procedure that does not damage lipid membranes and that can therefore be used for the SECM investigation of cells topography or the passive transport of the redox mediator into the cells. Additionally, fixed cells were permeabilized with Triton X-100 to analyse by SECM their intracellular content or to couple immunoassay strategies that allows the detection of specific biomarkers.

To investigate the potential opportunities of these approaches, alive, fixed and permeabilized WM-115 melanoma cells were studied by SECM. The influence of different experimental parameters, *e.g.* redox mediator type, probe translation speed and cells population on the obtained signal were also investigated. Thereafter, three melanoma cell lines were analysed in alive, fixed and permeabilized state for assessing the possibility to differentiate them according to their progression stage. Finally, an easy and fast approach for SECM characterization of melanoma associated marker tyrosinase expression in adherent cells was developed. For this purpose, fixed/permeabilized cells were incubated with anti-tyrosinase antibodies and the obtained immunocomplex was labelled with anti-mouse antibodies conjugated with horseradish peroxidase enzyme. On the last step tetramethylbenzidine/hydrogen peroxide substrate was added and the product of the enzymatic reaction was detected by SECM in the substrate generation – tip collection mode.

## 1. Introduction

Melanoma is one of the most lethal cutaneous malignancies that strikes thousands of people around the world.<sup>1</sup> According to the World Health Organization, about 132'000 new cases of melanoma incidence occur globally every year. Diagnosed on early stages, melanoma can be cured surgically, however its progression leads to low survival rate of patients.<sup>2,3</sup> The similarity between melanoma and innocuous skin moles can cause difficulties in cancer identification. Therefore, reliable methodologies for early diagnosis and unequivocal identification of cancer stages are of critical relevance. Currently existing approaches in this area focus on the detection of specific cancer biomarkers in serum (serological markers),<sup>4</sup> tissues and cultured cells.<sup>5,6</sup> Despite some new techniques were suggested recently (*e.g.* invasive electrical impedance spectroscopy<sup>7</sup> or non-invasive smartphone application<sup>8</sup>), the prevalent method to confirm the malignancy is still based on pathological analysis such as immunohistochemistry (IHC) of skin biopsies. IHC is commonly used in cancer diagnose due to its simplicity and availability of a wide range of antibodies (Abs) to tag various cancer biomarkers. Biomarkers are typically visualized by a secondary Abs conjugated with an enzyme (*e.g.* horse radish peroxidase, HRP) which activity can be detected optically. Nevertheless, there are some drawbacks regarding the optical interpretation of IHC results particularly when staining melanoma samples due to the high contents of the pigment melanin in the skin samples. Indeed dark colour melanin spots can resemble to the 3,3'-diaminobenzidine (DAB) colour, a universally used chromogen in IHC.<sup>9-11</sup> To overcome this limitation, fluorescent tags can be employed, however cellular autofluorescence and photobleaching can lead to wrong diagnosis also.<sup>12</sup> As a result, new strategies are required for the proper spatial characterization and readout of immunostained melanoma samples.

Scanning electrochemical microscopy (SECM) is a surface reactivity characterization technique based on an electrochemical signal recorded at a probe positioned or scanned in close proximity to a substrate.<sup>13-16</sup> Thanks to its high spatial resolution and versatility, SECM has demonstrated to be a useful tool for the electrochemical imaging and intracellular investigation of different living cell types including mammalian cells.<sup>17-22</sup> Typically, SECM experiments are performed using single cells adherently-grown on glass or plastic surfaces, however they can be also applied to high dense cell cultures that mimic better conditions experienced in real tissues. Thus, the investigation of cells layers,<sup>23,24</sup> patterns<sup>25-27</sup> and single embryos<sup>28-32</sup> has been reported by using SECM. Frequently SECM studies of cells is based on the monitoring of the respiratory activity<sup>28-30,33,34</sup> and production of different compounds,

including reactive oxygen species,<sup>35-37</sup> NO<sup>38</sup> and adrenaline,<sup>39</sup> which can be easily detected in a label-free and non-invasive way in the extracellular space. In contrast, measuring the intracellular enzymatic activity requires special redox mediators that can penetrate into the cells. For instance, it was reported that electrochemically generated FcMeOH<sup>+</sup> can penetrate through the lipid bilayer<sup>40</sup> and get reduced in alive cervical cancer cells (HeLa) without membrane permeabilization.<sup>41-43</sup> Similarly, cell membrane was shown to be permeable for the menadione/menadiol redox couple, which was employed for metastatic and non-metastatic breast cancer cell lines differentiation by SECM.<sup>44-47</sup> While hydrophobic redox mediators can penetrate into the intracellular space, the lipid membrane stays impermeable for hydrophilic compounds<sup>48</sup> and therefore charged redox mediators are often employed to elucidate cells' topography.<sup>49</sup> Additionally, alive cell membrane perforation with for instance digitonin (a non-ionic detergent) allows the investigation of the intracellular enzymes activity using also hydrophilic redox mediators, although such approach permits the release of the intracellular content.<sup>50</sup> Alternatively to label-free characterization, specific antigens at adherent cells can be labeled with enzymes. For instance, labelling of single cells has been applied by *Xue et al.* for the *in situ* electrochemical imaging of membrane glycan expression in human gastric carcinoma by staining them with HRP-conjugated lectins.<sup>51</sup> Furthermore, *Takahashi et al.* presented the immunostaining-based detection of a receptor-mediated endocytosis in Chinese hamster ovaries and human epidermoid carcinoma cells.<sup>52</sup>

In spite of many successful applications, the interpretation of experimental SECM data obtained from living cell studies is still cumbersome due to *i*) cell to cell variability in terms of metabolic activities, *ii*) possible dynamic morphological changes of cells, *iii*) experimental time restrictions (*e.g.* experimental buffer solutions and redox mediators can be toxic for cells during long term experiments) and *iv*) perturbation of cell metabolic response by the species generated or consumed at the SECM probe.

In contrast, working with fixed adherent cells (*e.g.* after treatment with fixatives) leads to the elimination of their biological activity and dynamic variability, but opens the opportunity to access more easily the preserved cellular ultrastructure as well as proteins, carbohydrates and other bio-active moieties in their original spatial organization within the cells. Indeed, cross-linking fixation has been already used in combination with some scanning probe techniques, *e.g.* in atomic force microscopy (AFM) for avoiding topographical cell changes and increasing in cell membrane elastic modulus that leads to a higher image resolution.<sup>53-55</sup> Additionally, scanning ion-conductive microscopy (SICM) has been also combined with

formaldehyde fixation for epithelial kidney cells volume quantification.<sup>56,57</sup> It is important to notice that crosslinking fixatives (*e.g.* formaldehyde) form new chemical bounds within the proteins without cell membrane permeabilization. Thus, formaldehyde fixed samples can be used for investigating the topography or the passive transport of the redox mediators through the cell membrane by SECM. Furthermore, membrane permeabilization allows the access to the intracellular compartments<sup>58</sup> for the extraction of specific intracellular information, for instance, by immunostaining. The latter is relevant for the screening of intracellular cancer biomarkers that does not only give information about the presence or absence of these compounds, but also about the heterogeneity of the biomarker expression within the same cell line.

Herein, alive, fixed and permeabilized WM-115 melanoma cells were studied by SECM to evaluate the possibility of obtaining relevant biological information from cells grown in high density cultures. Influence of different parameters, *e.g.* the redox mediator type (*i.e.* hydrophilic or hydrophobic), the probe translation speed and the cells density on the SECM signal were investigated. Thereafter, three melanoma cell lines (*i.e.* WM-239, WM-115 and Sbc12) were analysed in alive, fixed and permeabilized state. To perform SECM experiments with different cell lines and different cells density within the same sample, a custom-made disposable polyimide (PI) masks with three identical channels were fabricated. Finally, SECM was employed for the precise mapping of the melanoma biomarker tyrosinase (TyR) in adherent melanoma cells, which becomes possible by the fixation and permeabilization protocols. TyR is a multi-functional copper-containing enzyme, present in both melanocytes and melanoma cells, and which catalyses the conversion of tyrosine into highly polymerized pigment melanin.<sup>59,60</sup> This marker is highly selective for melanocytes<sup>61</sup> and can be used for melanoma diagnosis in combination with others biomarkers.<sup>62,63</sup>

## **2. Materials and methods**

### **2.1. Chemicals**

Ferrocene methanol (FcMeOH), ferrocene carboxylic acid (FcCOOH), 4-(2-hydroxyethyl)-1-piperazineethanesulfonic acid (HEPES),  $\text{KH}_2\text{PO}_4$ ,  $\text{K}_2\text{HPO}_4$ ,  $\text{K}_3\text{IrCl}_6$ ,  $\text{Na}_2\text{SO}_4$ ,  $\text{MgSO}_4$ ,  $\text{K}_2\text{SO}_4$ , citric acid, Triton X-100, bovine serum albumin (BSA), TyR (from mushroom,  $\geq 1000$  unit/mg), 3,3',5,5'-tetramethylbenzidine (TMB), and hydrogen peroxide (3 % in PBS) were purchased from Sigma – Aldrich (Schnelldorf, Switzerland). Formaldehyde solution (4% in PBS) was from AlfaAesar (Karlsruhe, Germany). Anti-TyR

monoclonal Abs T311 were obtained from BIO MEDICAL LLC., USA. Secondary anti-mouse Abs conjugated with HRP (Abs-HRP) were from Abcam (Cambridge, UK). Deionized water was produced by a Milli-Q plus 185 model from Millipore (Zug, Switzerland) and was used for all experimental solutions. Polyvinylidene fluoride (PVDF) membranes for protein blotting were purchased from Bio-Rad (Hercules, CA, USA).

WM-239, WM-115 and Sbc12 human melanoma cell lines as well as breast cancer MCF-7 and cervical cancer HeLa, were purchased from the American Type Culture Collection (ATCC).

The SECM experimental buffer was 10 mM HEPES pH 7.4, containing 75 mM Na<sub>2</sub>SO<sub>4</sub>, 1 mM MgSO<sub>4</sub> and 3 mM K<sub>2</sub>SO<sub>4</sub>. The PBS buffer (10 mM, pH 7.4) was containing NaCl 137 mM, KCl 2.7 mM, Na<sub>2</sub>HPO<sub>4</sub> 10 mM, KH<sub>2</sub>PO<sub>4</sub> 1.8 mM. As sample, washing and blocking buffers 1 % BSA in PBS and as a permeabilization buffer – 1 % Triton X-100 in PBS were used. The substrate solution was 0.2 mM TMB and 0.1 mM H<sub>2</sub>O<sub>2</sub> mixture in 0.1 M citrate-phosphate buffer, pH = 5.0.

## **2.2. Preparation of the polyimide (PI) masks**

Disposable PI masks with three parallel chambers for cell patterning were made of 125 µm-thick PI films (Kapton HN<sup>®</sup>; Goodfellow, Huntingdon, England). The PI sheet was fixed on one side of a double side tape (model 4959; Tesa SE, Beiersdorf Company). Thereafter, three parallel rectangles, 1 mm wide, 10 mm long and separated by 1 mm, were carved into a 10 mm wide and 20 mm long PI sheet by using a cutter-plotter (RoboPro CE5000-40-CRP, Graphtec Corporation, USA). The obtained PI masks were sterilized with ethanol and placed on a sterile microscopic glass slide for cell culturing (Figure 2.1a).

## **2.3. Cell culture and sample preparation**

Human melanoma cell lines WM-239, WM-115, and Sbc12 as well as cervical cancer HeLa and breast cancer MCF7 were cultured in Dulbecco's modified Eagle's medium (Gibco Life Technologies), supplemented with 10% fetal calf serum (FCS) at 37 °C in humidified atmosphere with 5% CO<sub>2</sub>. 24 hours before each experiment, 10 µL of cells suspension were plated on glass slides within the chambers of the PI mask. After the cells were attached to the surface, the glass slides were placed in cell culture dishes (35 mm × 10 mm, Nunc, Denmark) filled with the Eagle's medium. The PI mask was removed directly before the SECM experiments and the glass slides were positioned within the electrochemical cell filled with

the experimental buffer. The optical control of the cultured cells was performed before and after SECM experiments by using a laser scanning microscope (VK8700, Keyence).

Samples containing the same melanoma cell line (*i.e.* WM-115) grown at different cell densities, different melanoma cell lines (*i.e.* Sbc12, WM-115 and WM-239) as well as the different cell types (*i.e.* WM-115, HeLa and MCF-7) were prepared by using the PI mask. To obtain three cell lines with a different density various amounts of WM-115 cells were seeded into each chamber of the mask. The highest concentration ( $C1 = 5 \times 10^5$  cells/mL) was three times diluted to obtain the medium concentration (C2) and nine times diluted to obtain the lowest one (C3). The initial cells concentration (C1) was determined by cell counting and extrapolation of a representative sample under an optical microscope.

#### **2.4. Fixation and permeabilization protocol**

The fixation procedure consisted in the immersion of the glass slide with alive adherent cells into the preliminarily cooled down to +4 °C formaldehyde solution and incubating during 15 min. The permeabilization was performed by incubation the fixed cells within the permeabilization buffer during 20 min at room temperature (RT). After each of the procedures, the sample was washed by immersion into the PBS solution and incubation for 5 min. The washing step was repeated three times.

#### **2.5. Protocol for TyR immunoassay within adherent cells**

The intracellular TyR immunostaining was based on the fixation/permeabilization protocols combined with the IHC procedures. Briefly, fixed and permeabilized cells were placed into 3% H<sub>2</sub>O<sub>2</sub> solution for 15 min at RT in order to block the possible endogenous peroxidase activity. Thereafter, the sample was washed 5 times with PBS and then incubated in the blocking buffer for 30 min. In the next step, the glass slide with adherent cells was transferred into the solution of primary Abs (dilution 1 to 50 in the loading buffer), kept for 1 hour at RT and washed 5 times with the washing buffer. Then the sample was incubated for 1 hour with Abs-HRP (dilution 1 to 20000 in the sample buffer), washed 5 times with washing buffer and transferred into the electrochemical cell filled with substrate solution. The presence of TyR was established by electrochemical detection of the enzymatically produced TMB<sub>ox</sub> at the scanning microelectrode (SECM details *vide infra*). In order to investigate the presence of Abs-HRP non-specific binding the above protocol was carried out, but without the incubation step with anti-TyR Abs.

## 2.6. Immobilization of proteins on PVDF membrane

The immobilization of BSA and TyR on PVDF membrane was performed as it was described by *Lin et al.*<sup>64</sup> Briefly, the PVDF membrane was wetted by placing it in methanol (5 – 10 sec) and in deionized water (1 min), consequentially. Thereafter, 1  $\mu$ L of each protein solution (10 mg/mL) was deposited on the membrane and dried under a gentle stream of nitrogen. The protein spots were separated by 1 – 2 mm of clean PVDF membrane. In the next step, the membrane was transferred into the electrochemical cell and the SECM experiments were performed.

## 2.7. Inkjet printed (IJP) cell-like sample preparation

To mimic the topography of cells and its influence on the recorded signal, several spots were prepared on polyethylene terephthalate sheets (PET; 125  $\mu$ m thick; Goodfellow, UK) by inkjet printing of a dielectric material (*i.e.* UV curable ink JEMD6200, Sun Chemical, USA). An X-Serie CeraPrinter (Ceradrop, France) was equipped with a disposable, piezoelectric driven DMP cartridge (Dimatix Fujifilm, USA) containing 16 nozzles and providing a nominal droplet volume of 10 pL. During printing, the UV curable ink was polymerized by simultaneous UV light exposition. This was achieved by the UV LED FireEdge FE300 (380-420 nm; Phoseon Technology, USA) that was integrated into the printhead slot of the X-Serie printer and mounted slightly behind the DMP cartridge. All printing parameters, such as jetting frequency, waveform and number of active nozzles, were adjusted for optimum inkjet printing. The final patterns of insulating spots were made by printing three layers of 250  $\mu$ m separated droplets. The printed patterns were investigated by laser scanning microscopy in a reflection mode.

## 2.8. SECM measurements

SECM experiments were performed by using a custom-built SECM setup running under SECMx software<sup>65</sup> and combining a three axes positioning system (Märzhäuser, GmbH & Co. KG, Wetzlar, Germany), an electronic tilt table (Zaber Technologies Inc., Vancouver, Canada) and an Ivium potentiostat (Ivium Technologies, Netherlands). Measurements were performed in a three-electrode arrangement using a Pt UME with  $r_T = 12.5 \mu\text{m}$  and  $RG = 5$  as working electrode (WE), a Ag wire as quasi-reference electrode (QRE) and a Pt wire as counter electrode (CE). All reported potentials are given with respect to the Ag-QRE. Collected data were treated and analyzed by using Origin and MIRA.<sup>66</sup>

Prior to all SECM imaging experiments, the sample surface was levelled using a tilt table based on approach curves over insulating and cell-free regions in the presence of the corresponding redox mediator (FcMeOH or FcCOOH). Briefly, two approach curves were carried out over cell-free glass regions and with a spatial separation of 5 mm in order to determine the surface position at each location. Then by using the tilt table, the appropriate tilt correction was applied until the height difference at the employed reference points was below 1  $\mu\text{m}$ . This procedure was performed for both  $x$ - and  $y$ -axis. Then the Pt UME was positioned at a given working distance (*i.e.*  $d = 15 \mu\text{m}$ ) with respect to the glass or PET substrates and moved perpendicularly to the PI chambers direction with different translation rates (*i.e.* 5  $\mu\text{m/s}$ , 10  $\mu\text{m/s}$ , 15  $\mu\text{m/s}$  and 25  $\mu\text{m/s}$ ). To compare the electrochemical signal of the same cells in different state, fixation and permeabilization of the cells were performed directly within the levelled electrochemical cell. After each of the manipulations and before starting the SECM experiments, the cell surface was gently washed with the redox mediator solution (*i.e.* 1 time with 7 mL). FcMeOH and FcCOOH solutions (0.1 mM in SECM experimental buffer) were used as hydrophobic and hydrophilic redox mediators, respectively. At the experimental conditions (*i.e.* pH = 7.4), FcCOOH (pKa = 4.6) is present in the solution mainly as  $\text{FcCOO}^-$ .<sup>67</sup>

The PVDF membrane containing adsorbed protein spots was leveled by using the oxygen reduction current obtained from oxygen diffusing out from the membrane pores.<sup>64</sup> Thereafter, Pt UME was translated over the protein spots at  $d = 25 \mu\text{m}$  with a translation rate equal to 25  $\mu\text{m/s}$ .

For the precise mapping of the melanoma biomarker TyR in fixed and permeabilized adherent melanoma cells, after the immunostaining procedure the sample was levelled by using the TMB oxidation. Then, the Pt UME biased at the  $\text{TMB}_{\text{ox}}$  reduction potential (*i.e.* 0.05 V) was positioned at a defined  $d$  (between 15  $\mu\text{m}$  and 25  $\mu\text{m}$ ) and scanned over the cells in a substrate generation-tip collection (SG/TC) mode.

To study the working distance effect on the obtained response, a lift-off routine included in the SECMx software was employed. Briefly, the UME was kept at a working distance equal to 15  $\mu\text{m}$  during the forward scan, while it was operated at a 25  $\mu\text{m}$  distance during the reverse scan and the low frequency movement (*i.e.* move perpendicular to the line scans direction). The high frequency scans (*i.e.* lateral line scans of UME) were performed perpendicularly to the cells line patterns direction.



### 3. Results and discussion

Generally, SECM investigations of living cells are performed using alive cells grown on a single-cell level, *i.e.* the cells are clearly separated from each other. However, in reality, cells are organized in a complex and dense network where they can interact with each other. Therefore, working with dense cell cultures can provide complementary data from conditions closer to the ones observed on real tissue samples. In the present chapter, SECM was employed for the investigation of melanoma cells cultured in a high density population. For this purpose, cells were grown on a PI mask template (Figure 2.1a) to reduce the amount of cells to obtain high density cell samples, in comparison with the culturing without mask. Additionally, it facilitates the manipulation (*e.g.* transferring cells between the solutions) and patterning of different cell lines close to each other on the same substrate. The morphology of the cells cultured within the mask was checked optically and did not present any deviation in comparison with cells grown in a classical way. However, this strategy is suitable only for cell lines that can be cultured under identical conditions (*i.e.* identical medium, temperature, *etc.*).

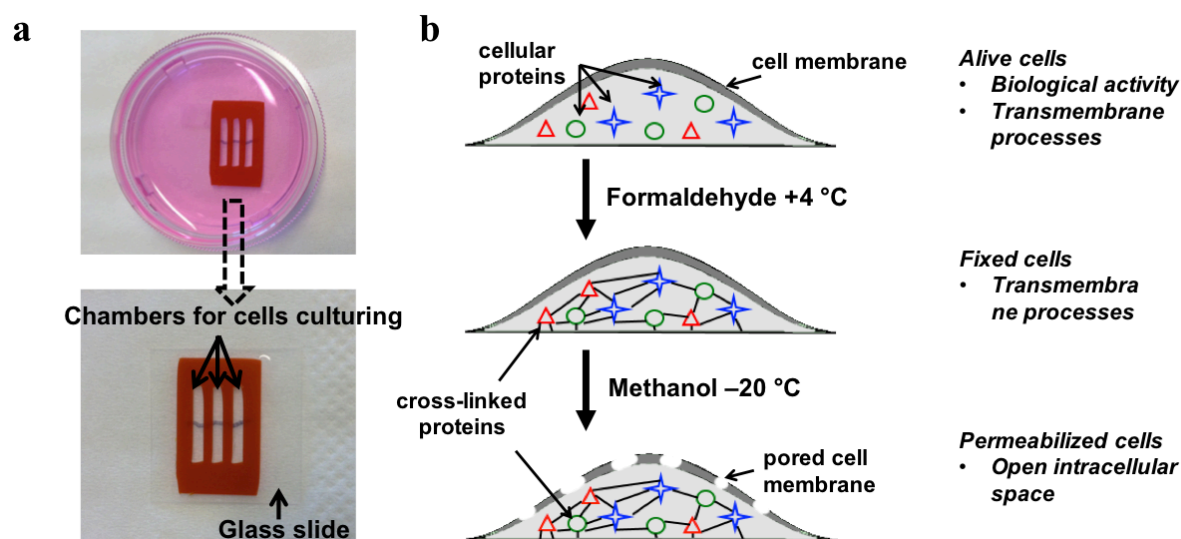


Figure 2.1. PI mask on glass surface employed to pattern different cell lines or the same cell line at different densities (a) and schematic representation of alive, fixed and permeabilized cells (b).

#### 3.1. Influence of cell density on SECM signal

In order to investigate the influence of the cells population on the SECM signal, WM-115 cells were seeded at 3 different concentrations. The optical images of the obtained cell surfaces are presented in Figures 2.2 a – c. As it can be seen, serial dilution of the initial cells culture led to a significant difference in the obtained cell surface coverage, *i.e.* population within line 1 (Figure 2.2a) < line 2 (Figure 2.2b) < line 3 (Figure 2.2c).

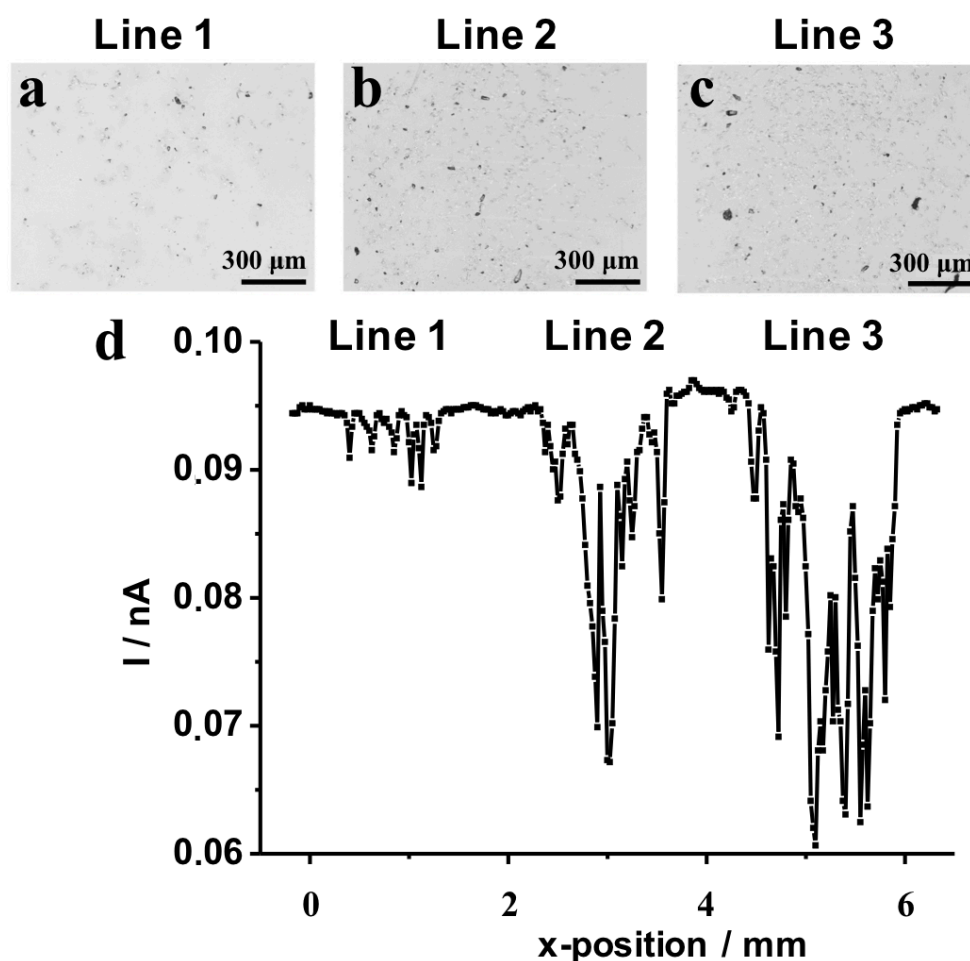


Figure 2.2. Optical images of fixed WM-115 cells at different cell populations (a) – (c). Cell surfaces (a), (b) and (c) were obtained by seeding melanoma cells with concentrations  $C_3$ ,  $C_2$  and  $C_1$  respectively, where  $9 \times C_3 = 3 \times C_2 = C_1 = 5 \times 10^5$  cells/mL. Electrochemical signal (current) obtained during SECM line scan above fixed WM-115 cells seeded at different concentrations (d). Experimental conditions: working electrode – Pt UME ( $r_T = 12.5 \mu\text{m}$ ,  $RG = 5$ ), QRE – Ag, CE – Pt, the scan rate and the working distance  $d$  were equal to  $5 \mu\text{m/s}$  and  $15 \mu\text{m}$ , respectively,  $0.1 \text{ mM FcCOOH}$  in experimental buffer ( $\text{pH} = 7.4$ ) was employed as the redox mediator.

The SECM line scan perpendicular to the direction of the mask lines was performed in order to study simultaneously all three cell regions using  $0.1 \text{ mM FcCOOH}$  as a redox mediator. As a result, a significant influence of the cell population on the magnitude of the obtained electrochemical signal was detected (Figures 2.2d). Therefore, in order to compare cell experiments in a meaningful manner, it is needed to have the same cell surface coverage. Indeed, an increase on the number of cells led to a higher decrease in the current recorded above the cells, illustrating the increased ability to block the redox mediator diffusion towards the surface of the UME due to the presence of larger cells clusters (*i.e.* numerous cells grown in contact with each other as a monolayer) and consequently higher surface coverage. Additionally, when scanning over the cluster of cells the decrease of the current remains around the same over the whole cell cluster which makes the signal more homogeneous, less likely to be affected by the cell topography. Thus, besides being closer to real tissues, higher

populated cell cultures might additionally increase the chance to obtain more clear signals. Therefore, the high-populated cell surfaces were used for all further experiments.

### **3.2. SECM of alive, fixed and permeabilized cells.**

The lipid membrane is an indispensable part of any eukaryotic cell, since it protects the intracellular components and controls the mass transport in and out the cell through active (*i.e.* with cells energy consumption) or passive (*i.e.* spontaneous or without energy consumption) processes. Previously published SECM investigations of living cells presented different ability of hydrophobic and hydrophilic redox mediators to cross through the cell membrane.<sup>40,48</sup> In the present work, FcMeOH and FcCOOH were employed as a hydrophobic and hydrophilic redox mediators, respectively. When employed for alive adherent cells investigation, FcMeOH can penetrate in the intracellular space spontaneously (*i.e.* passive transmembrane transport) and become an indicator of the intracellular biological activity. Simultaneously, active transmembrane transport and cell topography can impact on the current recorded by SECM. Alternatively, when FcCOOH is used as a redox mediator, it can penetrate inside cells only in case if an active transmembrane transport occurs. Otherwise, only cells topography will be recorded by SECM. In case of formaldehyde cells fixation, only passive transport of the redox mediator through the cells' membrane should occur. As a result, there will be no opportunity for FcCOOH to penetrate into cells and only cell topography information can be extracted by SECM. In the same time, cells will stay permeable for FcMeOH and the current recorded at UME will represent both passive transmembrane transport and cell topography. Additionally, cell membrane permeabilization will open access to the intracellular space for any compound independent on its hydrophilic properties (Figure 2.3).

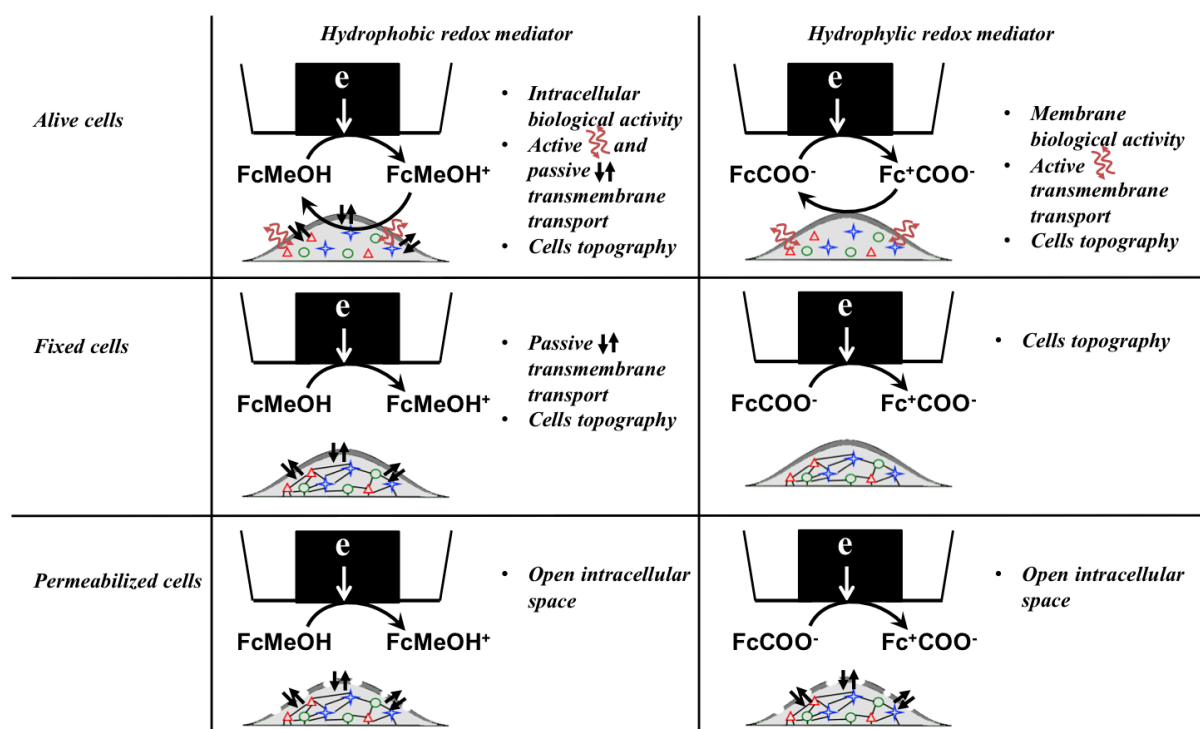


Figure 2.3. Schematic representation of the different type of information that can be extracted based on the type of redox mediator employed and the cells state (*i.e.* alive, fixed and permeabilized).

The knowledge of the sample topography is of significant importance in SECM where the recorded signal is not only related to surface reactivity, but also a function of  $d$ . Thus, for the reliable comparison of the results between cells in different states the changes in the cells size should be taken into account. Figure 2.4 represents the same cell surface when cells are alive (Figure 2.4a), fixed (Figure 2.4b) and permeabilized (Figure 2.4c). As a result, no significant morphological changes were observed. For instance, the cell marked in Figure 2.4a had a diameter equal to 22  $\mu\text{m}$ , which stayed constant during all the manipulations (Figure 2.4b and c). These results are in good agreement with the ones reported before, where no influence of cross-linking agents on cells height was reported by AFM.<sup>55</sup>

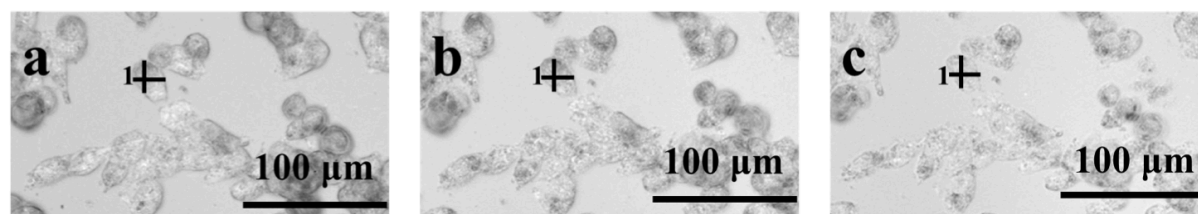


Figure 2.4. Optical images of alive (a), fixed (b) and permeabilized (c) adherent WM-115 cells.

In order to investigate any possible electrochemical activity of melanoma cells, SECM line scans above adherent WM-115 cells in alive, fixed and permeabilized state were performed using FcMeOH as a redox mediator with different UME translational rates, *i.e.* 5  $\mu\text{m/s}$ , 10  $\mu\text{m/s}$ , 15  $\mu\text{m/s}$  and 25  $\mu\text{m/s}$  (Figure 2.5).

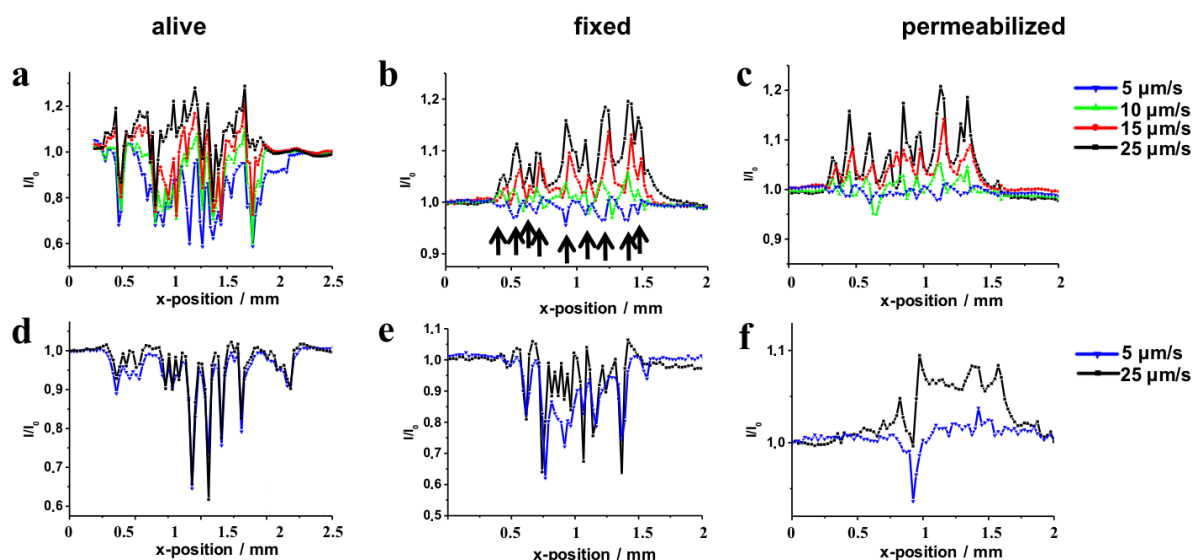


Figure 2.5. Influence of the UME translation speed on the SECM response (normalized current) provided by alive (a and d), fixed (b and e) and permeabilized (c and f) adherent WM-115 melanoma cells in presence of non-charged (a – c) and charged (d – f) redox mediators. Experimental conditions: working electrode – Pt UME ( $r_T = 12.5 \mu\text{m}$ ,  $RG = 5$ ), QRE – Ag, CE – Pt, the working distance  $d$  was equal to  $25 \mu\text{m}$ .  $0.1 \text{ mM FcMeOH}$  and  $0.1 \text{ mM FcCOOH}$  in experimental buffer ( $\text{pH} = 7.4$ ) were employed as the hydrophobic and hydrophilic redox mediators, respectively.

The current recorded at the UME when scanned above the insulating glass surface free of cells was used for normalization of the whole current profile as it was suggested before.<sup>68</sup> This normalization allows taking into account the influence of UME translation speed on the SECM current and provides a better comparison among cells generated electrochemical signal. As a result, when the translation speed was equal to  $5 \mu\text{m/s}$  the current above cells was 20-40% lower than the one over the glass. However, an increase of the UME translation speed from 5 to  $25 \mu\text{m/s}$  led to a significant change on the current profile recorded above cells consisting of a numerous current increases and decreases. Thus, for a scan rate equal to  $25 \mu\text{m/s}$  the current above cells can reach values about 20 - 25% higher and lower than the current above the glass slide (Figure 2.5a). In the same conditions, scanning above fixed cells led to a simplified electrochemical signal and a more clearly defined current profile was recorded especially at high translation rates. Thus, when the translation speed was equal to  $5 \mu\text{m/s}$  the current above cells was lower than the one over the glass. However, when the UME translation rate reached  $15 \mu\text{m/s}$  the recorded current above the fixed cells presented values between 10 to 15% higher than above the glass slide (Figure 2.5b). The nature and differences of the SECM signals obtained with alive and fixed cells might be explained by the following points: *i*) comparison of the results obtained at low scan rate (*i.e.*  $5 \mu\text{m/s}$ ) suggests the active uptake of FcMeOH by alive cells: the current decrease is much stronger when cells are alive, *ii*) comparison of the results obtained at high scan rate (*i.e.*  $15 \mu\text{m/s}$  and higher) presents

similar current increase above both alive and fixed cells, which cannot be explained by enzymatic activity (*i.e.* since fixation eliminates the biological activity of the cells). Thus other phenomena must be playing an additional role on the recorded signal, such as enhanced mass-transport due to the fast translation rate and intrinsic electrochemical reactivity within the cell (*vide infra*). Additionally, the further permeabilization of the cells did not influence drastically on the observed SECM signal.

Interestingly, when a hydrophilic redox mediator was used, both alive and fixed cells provided a significant current decrease over the cell culture, which was only slightly influenced by the UME translation speed (Figures 2.5d and e). The latter might be explained by the difficulty of the redox mediator to access the intracellular space and the absence of any cellular activity. Additionally, after scanning permeabilized cells at different translation rates, a similar behavior to the one presented in the case of hydrophobic redox mediator was observed (Figure 2.5f). By comparing the results obtained for hydrophobic and hydrophilic redox mediators, it can be suggested that when the cells are permeabilized and scanned at high translation rates, an intracellular reactivity can still be sensed.

To further compare the influence of the UME translation speed on the SECM response of alive, fixed and permeabilized cells when the hydrophobic redox mediator is used Figures 2.5 a – c were converted into the normalized peak current – translational speed coordinates (Figures 2.6 a and b). The positions of the negative current peaks, which appeared when scanning above fixed cells with the translation speed equal to 5  $\mu\text{m/s}$ , were chosen as the most representative cell points (Figure 2.5b black arrows) and these  $x$ -coordinates were used to construct the  $I/I_0 - v$  graph, as it was reported by Kuss *et al.*<sup>68</sup>

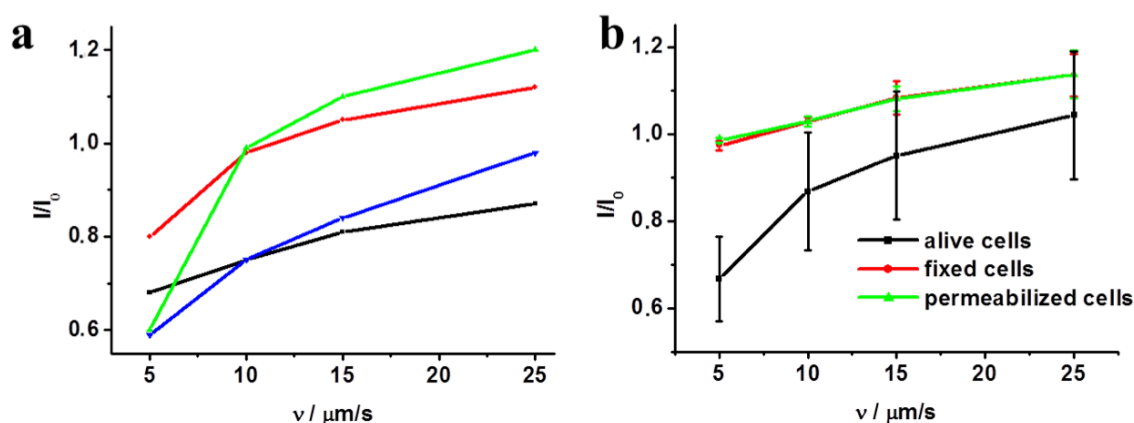


Figure 2.6. Dependence of the normalized peak current on the UME translation rate for 4 different alive cell points (a) and averaged data obtained for alive, fixed and permeabilized cells (b). The error bars represent the standard deviation of the signal. Experimental conditions: working electrode – Pt UME ( $r_T = 12.5 \mu\text{m}$ ,  $RG = 5$ ), QRE – Ag, CE – Pt, the working distance  $d$  was equal to 25  $\mu\text{m}$ , 0.1 mM FcMeOH in experimental buffer (pH = 7.4) was employed as the redox mediator.

As a result, significant differences in the behavior of alive cells were observed as it is presented in Figure 2.6a for four different reference points. The variation of the signal can be due to the presence of cells at different growth stage and due to the cell-to-cell variation of intracellular biological and electrochemical activity. Averaging these results leads to significant error bars in the cells characterization (Figure 2.6b) and illustrates the difficulties associated with SECM studies of alive cell cultured at high density. At the same time, cells fixation and permeabilization presented identical dependence of the normalized current as a function of the UME translational rate in the case of hydrophobic redox mediators (Figure 2.6b). These results suggest the fast and reproducible passive transport of FcMeOH through the cell membrane.

### 3.3. Inkjet printed cell-like sample

As it was observed in Figure 2.5, the current recorded over alive, fixed and permeabilized cells presented an increase at high UME translation rates. Such increase on the current can be explained by an increase on the mass transport due to an enhanced convection during fast scanning over non-planar samples. Additionally, the presence of an intracellular reactivity or the release of redox species can also contribute to the increase on the recorded signal. With the aim to determine the contribution to the signal due to an enhanced convection, an array of dielectric spots were inkjet printed on a glass substrate to mimic the topography of the adherent cancer cells. The prepared sample contained several spots (30  $\mu\text{m}$  diameter and approximately 6  $\mu\text{m}$  height) positioned 250  $\mu\text{m}$  from each other (Figure 2.7a – c), completely impermeable and inert to the redox mediators. The SECM images of the IJP sample using FcMeOH as the redox mediator at translation speeds equal to 5  $\mu\text{m}/\text{s}$  and 25  $\mu\text{m}/\text{s}$  are presented in Figures 2.7d and 2.7e, respectively. As expected, a clear decrease of the recorded current at the UME occurs when it is scanned over the dielectric spots for both translation speeds. However, when scanning at high translation rates a slight current increase is observed just before the drastically current decrease when the probe starts to scan the dielectric spot, which is similar to what was observed with alive and fixed cells (Figure 2.5d, 2.5e and 2.7f). The latter results confirms that forced convection introduced by the fast UME movement above the non-planar substrate has an important contribution on the recorded signal as it was reported by *Kuss et al.*<sup>68</sup> In general, the SECM image of the IJP sample correlates with the results obtained for alive and fixed cells when a hydrophilic redox mediator is employed. However, forced convection cannot explain fully the observed response when using hydrophobic redox mediators.

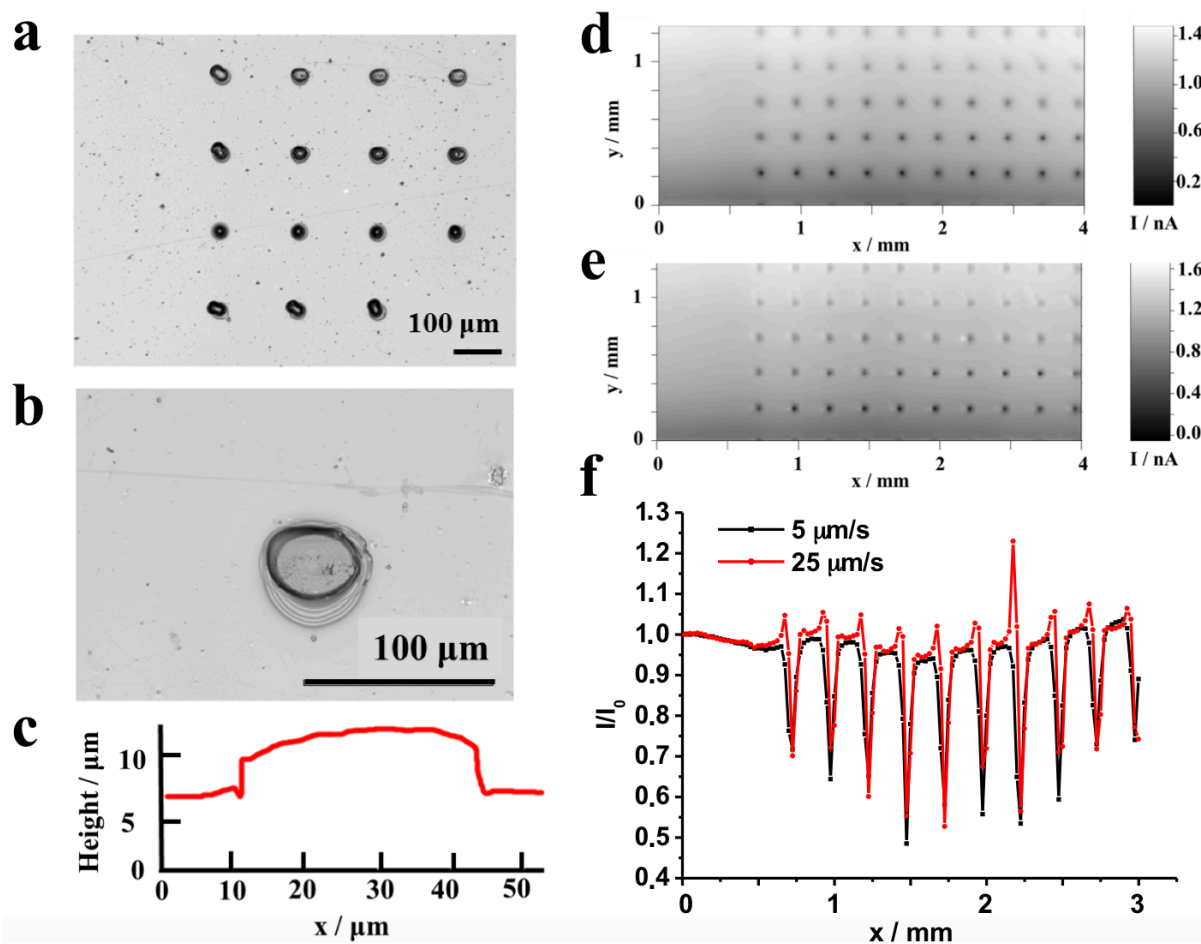


Figure 2.7. Optical images of the inkjet-printed UV-curable ink patterns (a) and (b) and the height profile of the pattern (c). 2D image (d) and (e) obtained with the translation rate  $5 \mu\text{m/s}$  and  $25 \mu\text{m/s}$  and the electrochemical signal (current) during SECM line scan (f) above the inkjet printed sample. Experimental conditions: working electrode – Pt UME ( $r_T = 12.5 \mu\text{m}$ ,  $RG = 5$ ), QRE – Ag, CE – Pt, the working distance  $d$  was equal to  $15 \mu\text{m}$ ,  $0.1 \text{ mM FcMeOH}$  in experimental buffer ( $\text{pH} = 7.4$ ) was employed as the redox mediator

### 3.4. SECM of proteins adsorbed on PVDF membrane

Indeed, the increase on the current when scanning above alive cells at high translation rates can be explained by the intrinsic biological activity of the studied cell, which could be able to release redox species into the extracellular space as a response to the external effectors (*e.g.* presence of redox mediator) or can recycle the redox species that are able to travel into the intracellular space. In the case of fixed and permeabilized cells, where no biological activity is present, the current increase can be related to the presence of various electrochemically active species (*e.g.* amino acids and hemes groups present in proteins). In order to evaluate the possible electrochemical activity of proteins, two model compounds, *i.e.* BSA and TyR, were adsorbed on a PVDF membrane and investigated under identical conditions as for the cell experiments. Both proteins contain electrochemically active amino acids (*e.g.* arginine, lysine and cysteine) and TyR contains additionally copper active center. As a result, a clear current increase was observed when scanning above both proteins,



especially at the edges of the protein spots due to the well-known “coffee ring” effect (Figure 2.8). The latter results suggest that adsorbed proteins, as well as, fixed proteins or other biopolymeric material could have an electrochemical activity that lead to the recycling of the redox mediator and as a result increase on the recorded current. The similarity of the SECM results for different proteins could be explained by the fact that peptide bonds can be also oxidized electrochemically.<sup>69,70</sup> The similarity in the SECM response provided by proteins adsorbed on a PVDF membrane and by the intracellular components can be an evidence of the biopolymeric electrochemical activity;<sup>69,70</sup> however, additional experiments are still required to determine the exact nature of the chemical reactivity observed on fixed and permeabilized cells.

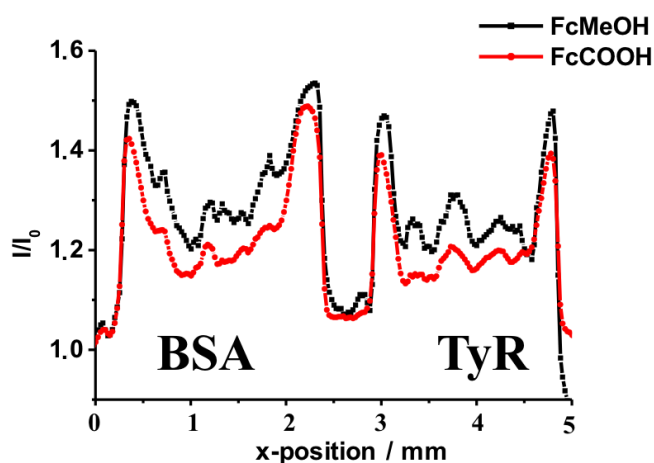


Figure 2.8. Normalized current obtained when the SECM experiments in constant height feedback mode were performed above BSA and TyR proteins spots adsorbed on PVDF membrane. Experimental conditions: working electrode – Pt UME ( $r_T = 12.5 \mu\text{m}$ ,  $RG = 5$ ), QRE – Ag, CE – Pt, the working distance  $d$  was equal to  $25 \mu\text{m}$ , the translational speed  $v$  was equal to  $25 \mu\text{m/s}$ .

### 3.5. SECM of different melanoma cell lines

Employing SECM with FcMeOH as a redox mediator allowed differentiation of MCF10A cells expressing active Ha-Ras Val12 mutant compared to normal MCF10A, apparently by measuring oxidised/reduced glutathione balance in human breast epithelial.<sup>71</sup> Therefore, it was logical to investigate whether any difference in electrochemical behavior of different stage melanoma cells can be observed. With this aim, three melanoma cell lines (*i.e.* Sbc12, WM-115 and WM-239) corresponding to the radial growth, vertical growth and metastatic phases of melanoma, respectively, were cultured on the same glass slide. SECM line scans above alive, fixed and permeabilized cells using different redox mediators and translation rates were performed. As a result, all three melanoma cell lines presented a similar behavior (Figure 2.9a and b) suggesting the impossibility to differentiate these three melanoma cell lines based on their accessible redox active content. However, as it was shown

by Liu *et al.*,<sup>72</sup> metastatic and non-metastatic breast cancer cells can be differentiated based on the SECM monitoring of the redox environment and therefore, the study of fixed and permeabilized cells might be proven useful for other cancer cell lines. Additionally, it simplifies the access into the intracellular space and can be further applied, *e.g.* for labeling of specific cancer biomarkers such as TyR.

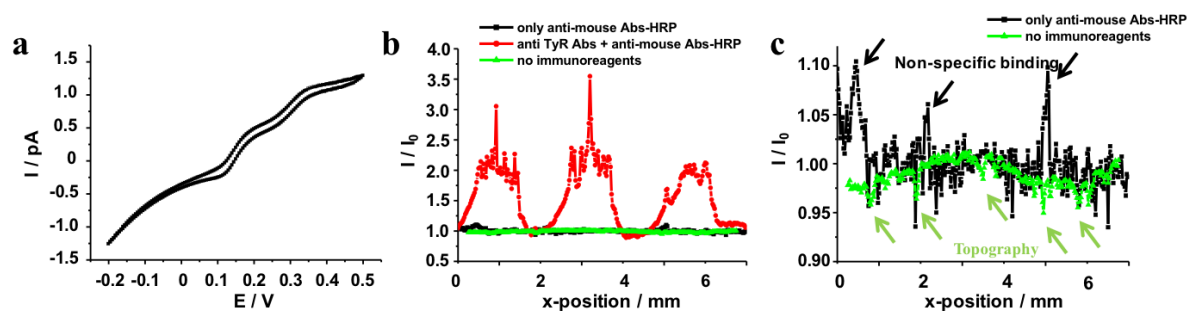


Figure 2.9. Electrochemical results obtained for three different cell lines grown within the same PI mask by SECM in the feedback mode. WM-239, WM-115 and Sbc12 cells were consequentially analyzed in alive, fixed and permeabilized state. Experimental conditions: working electrode – Pt ( $r_T = 12.5 \mu\text{m}$ ,  $\text{RG} = 5$ ), QRE – Ag, CE – Pt, the working distance  $d$  was equal to  $25 \mu\text{m}$ . The redox mediator was  $0.1 \text{ mM FcMeOH}$  in experimental buffer ( $\text{pH} = 7.4$ ) in case (a) and  $0.1 \text{ mM FcCOOH}$  in case (b). The UME translational speed was equal to  $10 \mu\text{m/s}$ .

### 3.6. Investigation of melanoma-associated tumour antigen TyR expression in adherent cells by SECM

TyR is an intracellular enzyme, which is located in the endoplasmic reticulum, Golgi and coated vesicles,<sup>73</sup> and therefore, cannot be reached by Abs within alive cells due to the inability of large proteins to penetrate across the cell membrane. However, as it was presented before, the accessibility of the intracellular space by immunoreagents and redox mediators can be performed in a simple approach based on the fixation and permeabilization of cells. Briefly, in the first step adherent cells (Figure 2.10a) were fixed with formaldehyde (Figure 2.10b) and then their lipid membranes were permeabilized by Triton X-100 (Figure 2.10c). In order to inactivate a possible intracellular peroxidase activity, the sample was incubated with  $3\% \text{ H}_2\text{O}_2$ . Additionally, the surface was blocked with BSA to prevent non-specific binding. In the next step, permeabilized cells were incubated with anti-TyR Abs (Figure 2.10d) and the obtained immunocomplex was labelled with anti-mouse Abs-HRP (Figure 2.10e). Thereafter, the TMB/ $\text{H}_2\text{O}_2$  substrate was added to the system and the product of the enzymatic reaction was detected by SECM in the SG-TC mode (Figure 2.10f).

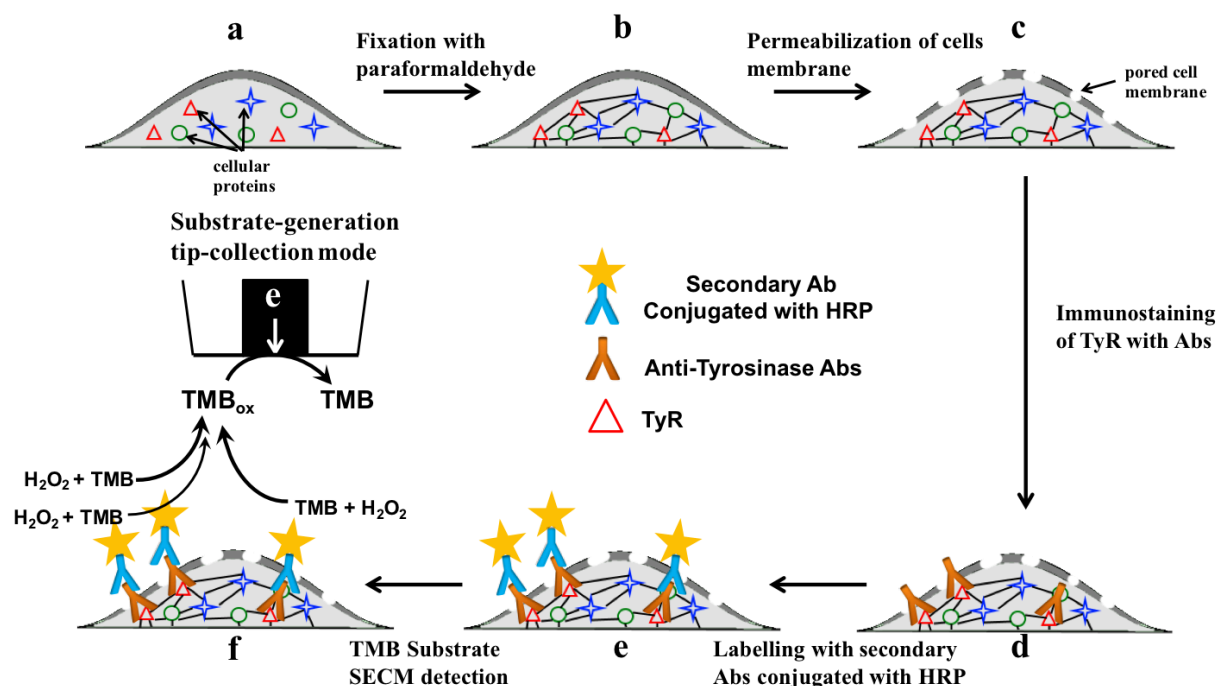


Figure 2.10. Schematic representation of TyR detection in melanoma adherent cells by SECM. Alive adherent cells (a) were fixed with formaldehyde (b) and permeabilized with Triton X-100 (c). Intracellular TyR was labelled by monoclonal Abs (d) and anti-mouse Abs conjugated with HRP (e). The HRP enzymatic activity was monitored by SECM (f).

After the immunostaining protocol was performed, the sample was placed on the SECM sample holder, levelled and then immersed into the substrate solution. Before starting the SECM experiments, the electrochemical behaviour of the employed UME was characterised by CV in presence of TMB. As it was expected, a sigmoidal electrochemical response corresponding to a two-electron transfer process was obtained with a relatively small capacitive current (Figure 2.11a). A working potential equal to 0.05 V was chosen for the TMB<sub>ox</sub> amperometric detection.

In order to investigate the influence of cell topography on the detected electrochemical signal, fixed/permeabilized cells that have not been immunostained were scanned by using an UME located at a probe-substrate distance equal to 15  $\mu\text{m}$  in presence of TMB (Figures 2.11b and 2.11c, green). Indeed, non-significant influence was observed on the SECM line scans due to the cells topography or intracellular reactivity, which suggests that under the experimental conditions SECM imaging of the immunostained intracellular TyR can be performed without any external interference.

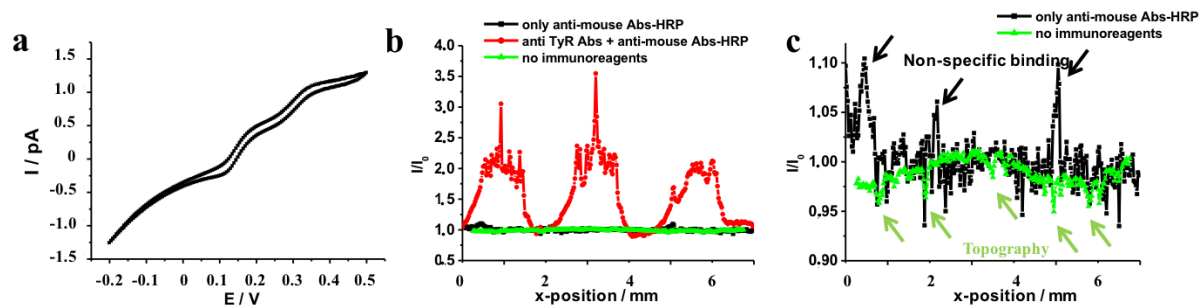


Figure 2.11. Cyclic voltammogram at a Pt UME in the presence of 0.2 mM of TMB and 0.1 mM of  $\text{H}_2\text{O}_2$  solution (a) and line scans above WM-115 cells patterns with different cell density obtained by seeding cells at different concentrations ( $C1 = 5 \times 10^5$  cells/mL,  $C1 = 3 \times C2 = 9 \times C3$ ) (b) and (c). The normalised current is presented for experiments where *i*) only Abs-HRP (b and c, black), *ii*) both primary anti-TyR Abs and secondary Abs-HRP (b, red) and *iii*) none of immunoreagents (b and c, green) were used. Experimental conditions: working electrode = Pt ( $r_T = 12.5 \mu\text{m}$ ,  $\text{RG} = 5$ ), QRE = Ag, CE = Pt. CV: performed at the bulk solution with a scan rate was equal to 25 mV/s. SECM: the working distance ( $d$ ) was equal to 15  $\mu\text{m}$  and the translation speed was equal to 25  $\mu\text{m/s}$ . The normalisation of the current was performed on a signal recorded above the cells-free glass surface during the line scan.

To evaluate the non-specific binding of anti-mouse Abs-HRP on fixed and permeabilized cells, the whole process described in Figure 2.9 except of the primary Abs step was performed. The SECM line scans above cells presented a non-significant increase on the current (*i.e.* 5-10%) indicating that the signal coming from non-specific binding is negligible in comparison with the detected analytical current when specific TyR labelling was performed (Figure 2.11b and c). Additionally, the increase of the working distance from 15  $\mu\text{m}$  to 25  $\mu\text{m}$  significantly decreases the resolution of the image (Figure 2.12a and b). Working distances smaller than 15  $\mu\text{m}$  were not tested due to the higher probability of probe-substrate crashes and the increase of the cells topographical component in the observed signal.

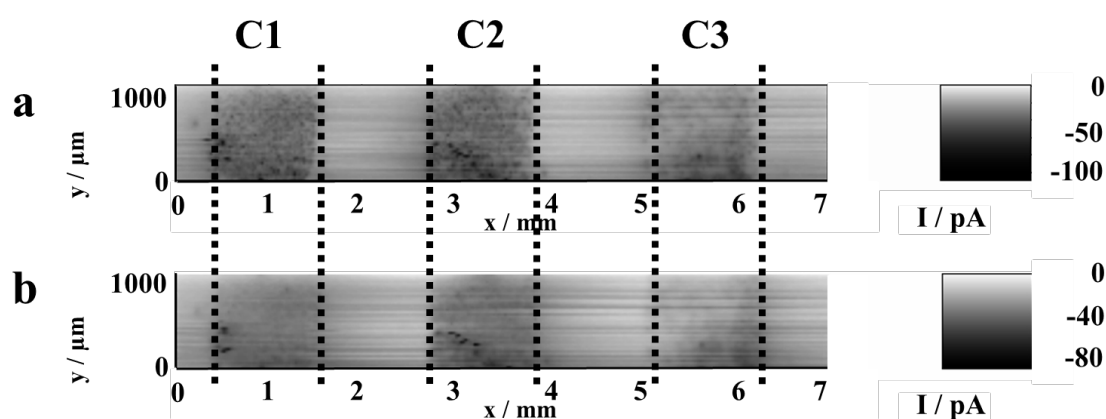


Figure 2.12. Investigation of TyR expression inside WM-115 cells by following immunostaining-SECM strategy. The adherent cells were grown at different density ( $C1 = 5 \times 10^5$  cells/mL,  $C1 = C2 \times 3 = C3 \times 9$ ). Experimental conditions: working electrode = Pt ( $r_T = 12.5 \mu\text{m}$ ,  $\text{RG} = 5$ ), working distance = 15  $\mu\text{m}$  (a) and 25  $\mu\text{m}$  (b), the translation speed was equal to 25  $\mu\text{m/s}$  and the substrate solution was containing 0.2 mM of TMB and 0.1 mM of  $\text{H}_2\text{O}_2$ .

To further assess the specificity of the immunostaining protocol employed on this chapter, the suggested strategy was applied for the staining of HeLa and MCF-7 cell lines, which do not contain TyR,<sup>74,75</sup> in contrast to human melanoma WM-115 cell line.<sup>76,77</sup> The SECM image of the TyR expression in WM-115, HeLa and MCF-7 adherent cells grown at the same cell density (*i.e.* C1) is presented in Figure 2.13a. The results of the experiment showed a good agreement with the data reported in literature, *i.e.* the value of the current provided by HeLa and MCF-7 cells was negligible in comparison with the analytical signal recorded above WM-115 cells. Additionally, a significant heterogeneity on the current recorded over the HeLa and MCF-7 cell lines shows the non-specific nature of the signal obtained for the non-melanocytic cells. Thus, the developed approach for the intracellular TyR immunostaining with SECM readout can be further applied for the investigation of this biomarker expression in different melanoma cell lines.

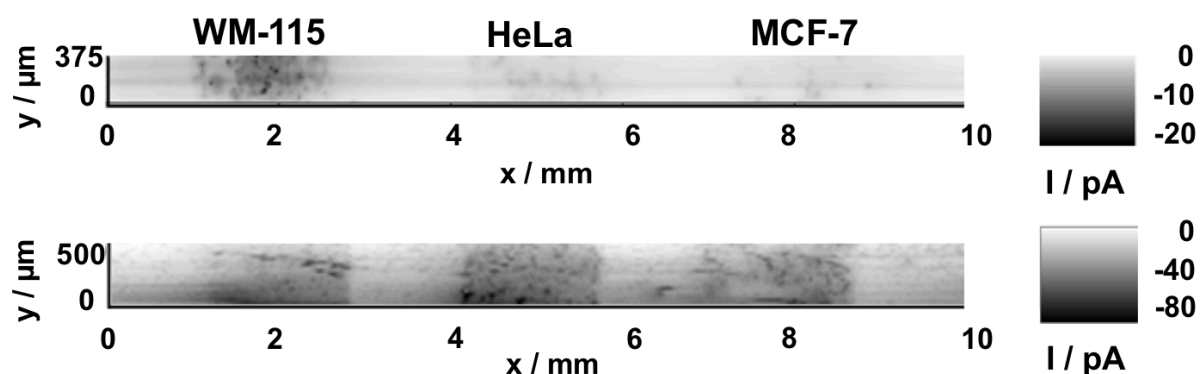


Figure 2.13. Investigation of TyR expression inside adherent cells by SECM using an immunoassay strategy. The studied sample consisting of WM-115, HeLa and MCF-7 (a) was used to evaluate the specificity of TyR detection protocol. 3 different melanoma cell lines, namely WM-239, WM-115 and Sbc12 were also studied by SECM (b). Working electrode = Pt in glass ( $r_T = 12.5 \mu\text{m}$ ,  $RG = 5$ ), working distance =  $15 \mu\text{m}$ , the translation speed was equal to  $25 \mu\text{m/s}$  and the substrate solution was containing  $0.2 \text{ mM}$  of TMB and  $0.1 \text{ mM}$  of  $\text{H}_2\text{O}_2$ .

The expression of TyR was evaluated in three different melanoma cell lines corresponding to different cancer progression stages, namely Sbc12 (intraepidermal growth during the radial-growth phase, RGP), WM-115 (dermal invasion during the vertical-growth phase, VGP) and WM-239 (metastasis). The results of the TyR immunostaining mapped by SECM are presented in Figure 2.13b. The highest TyR expression was detected in WM-115 cells line which can be assigned to the vertical-growth phase (VGP) based on the Clark model<sup>78</sup> and stage II of melanoma according to the American Joint Commission on Cancer (AJCC). The cells derived from RGP and metastatic melanomas presented lower amount of TyR.

It is also worth to notice that  $\text{TMB}_{\text{ox}}$  can be accumulated inside cells and therefore the signals detected above cells depend on the incubation time. Thus, the difference in the current in Figures 2.13a and 2.13b for the same cell line (*i.e.* WM-115) can be explained by different time spent for the sample levelling as well as for the surface imaging. The latter highlights the need to scan under the same experimental conditions all the cell lines, and also validates their differentiation based on the different TyR expression level.

#### **4. Conclusions**

The potential of SECM imaging of fixed and permeabilized cells was evaluated. For this purpose, cells were cultured within specially designed disposable PI masks and studied by SECM in alive, fixed and permeabilized state. The influence of different parameters, *e.g.* the redox mediator type (*i.e.* hydrophobic or hydrophilic), the probe translation rate and the cells population density on the SECM signal was investigated. For instance, current increases can be observed over the scanned cells when FcMeOH is used and the UME is translated with a speed equal or higher than 10  $\mu\text{m/s}$ . As it was presented in this work, this phenomenon cannot be explained only by forced convection due to the cells topography and fast translation rates, but can be also a result of the intracellular species with electrochemical activity (*e.g.* proteins).

Additionally, SECM line scans above alive melanoma cells with FcMeOH as a redox mediator presented a significant signal variation between the same cell line, which made extremely difficult the interpretation of the obtained results. In contrast, the current profile recorded above fixed and permeabilized cells is highly reproducible. Unfortunately, the direct assay of the fixed and permeabilized melanoma cells did not present any significant differences between different cell lines. Nevertheless, the fixation/permeabilization approach opens the intracellular space for performing immunostaining of the intracellular components. As a result, SECM was implemented as a tool to monitor the distribution of TyR in melanoma adherent cells by electrochemical readout of an immunoassay strategy. The specificity and validity of the protocol for TyR detection in cells has been investigated thoroughly and no significant influence on the recorded signal from non-specific binding was observed. Thereafter, this protocol was implemented for TyR imaging within different cancer progression stage cell lines as well as in non-melanotic cells. According to the obtained results, melanoma cells corresponded to stage II presented the highest expression of TyR. To the best of our knowledge, this work pioneers the SECM imaging of intracellular biomarkers using cells-fixation protocols.

## 5. References

- (1) Taylor, J.-S. *Science*. **2015**, *347*, 824.
- (2) Gray-Schopfer, V.; Wellbrock, C.; Marais, R. *Nature* **2007**, *445*, 851–857.
- (3) Rothberg, B. E. G.; Bracken, M. B.; Rimm, D. L. *J. Natl. Cancer Inst.* **2009**, *101*, 452–474.
- (4) Hartleb, J.; Arndt, R. *J. Chromatogr. B Biomed. Sci. Appl.* **2001**, *764*, 409–443.
- (5) Qendro, V.; Lundgren, D. H.; Rezaul, K.; Mahony, F.; Ferrell, N.; Bi, A.; Lati, A.; Chowdhury, D.; Gygi, S.; Haas, W.; Wilson, L.; Murphy, M.; Han, D. K. *J. Proteome Res.* **2014**, *13*, 5031–5040.
- (6) Mayer, J. E.; Swetter, S. M.; Fu, T.; Geller, A. C. *J. Am. Acad. Dermatol.* **2014**, *71*, 599.e1–e599.e12.
- (7) Mohr, P.; Birgersson, U.; Berking, C.; Henderson, C.; Trefzer, U.; Kemeny, L.; Sunderkötter, C.; Dirschka, T.; Motley, R.; Frohm-Nilsson, M.; Reinhold, U.; Loquai, C.; Braun, R.; Nyberg, F.; Paoli, J. *Ski. Res. Technol.* **2013**, *19*, 75–83.
- (8) Wolf, J. A.; Moreau, J. F.; Akilov, O.; Patton, T.; English, J. C.; Ho, J.; Ferris, L. K. *JAMA dermatology* **2013**, *149*, 422–426.
- (9) Zhang, S.; Yang, J.; Lin, J. *Bioelectrochemistry* **2008**, *72*, 47–52.
- (10) Cao, C.; Sim, S. J. *Biosens. Bioelectron.* **2007**, *22*, 1874–1880.
- (11) Bobrow, M. N.; Shaughnessy, K. J.; Litt, G. J. *J. Immunol. Methods* **1991**, *137*, 103–112.
- (12) Revin, S. B.; John, S. A. *Sensors Actuators B. Chem.* **2013**, *188*, 1026–1032.
- (13) Bard, A. J.; Denuault, G.; Lee, C.; Mandler, D.; Wipf, D. O. *Acc. Chem. Res.* **1990**, *23*, 357–363.
- (14) Bard, A. J.; Fan, F. F.; Kwak, J.; Lev, O. *Anal. Chem.* **1989**, *61*, 132–138.
- (15) Mirkin, M. V.; Nogala, W.; Velmurugan, J.; Wang, Y. *Phys. Chem. Chem. Phys.* **2011**, *13*, 21196–21212.
- (16) Bard, A. J.; Mirkin, M. V. *Scanning Electrochemical Microscopy*; second.; CRC Press, 2012.
- (17) Bard, A. J.; Li, X.; Zhan, W. *Biosens. Bioelectron.* **2006**, *22*, 461–472.
- (18) Schulte, A.; Nebel, M.; Schuhmann, W. *Annu. Rev. Anal. Chem. (Palo Alto, Calif.)*. **2010**, *3*, 299–318.
- (19) Bergner, S.; Vatsyayan, P.; Matysik, F.-M. *Anal. Chim. Acta* **2013**, *775*, 1–13.
- (20) Zhang, Y.; Ma, J.; Zhang, Y.; Jiang, H.; Wang, X. *Nanosci. Nanotechnol. Lett.* **2013**, *5*, 182–185.

- (21) Sun, P.; Laforge, F. O.; Abeyweera, T. P.; Rotenberg, S. A.; Carpino, J.; Mirkin, M. V. *Proc. Natl. Acad. Sci. U. S. A.* **2008**, *105*, 443–448.
- (22) Kaya, T.; Torisawa, Y.; Oyamatsu, D.; Nishizawa, M.; Matsue, T. *Biosens. Bioelectron.* **2003**, *18*, 1379–1383.
- (23) Torisawa, Y.-S.; Kaya, T.; Takii, Y.; Oyamatsu, D.; Nishizawa, M.; Matsue, T. *Anal. Chem.* **2003**, *75*, 2154–2158.
- (24) Bergner, S.; Wegener, J.; Matysik, F.-M. *Anal. Methods* **2012**, *4*, 623.
- (25) Nishizawa, M.; Takoh, K.; Matsue, T. *Langmuir* **2002**, *18*, 3645–3649.
- (26) Kuss, S.; Polcari, D.; Geissler, M.; Brassard, D.; Mauzeroll, J. *Proc. Natl. Acad. Sci. U. S. A.* **2013**, *110*, 9249–9254.
- (27) Gac, L.; Sridhar, A.; Boer, H. L. De; Berg, A. Van Den. *PLoS One* **2014**, *9*, e93618.
- (28) Shiku, H.; Shiraishi, T.; Ohya, H.; Matsue, T.; Abe, H.; Hoshi, H.; Kobayashi, M. *Anal. Chem.* **2001**, *73*, 3751–3758.
- (29) Takahashi, R.; Zhou, Y.; Horiguchi, Y.; Shiku, H.; Sonoda, H.; Itabashi, N.; Yamamoto, J.; Saito, T.; Matsue, T.; Hisada, A. *J. Biosci. Bioeng.* **2014**, *117*, 113–121.
- (30) Shiku, H.; Shiraishi, T.; Aoyagi, S.; Utsumi, Y.; Matsudaira, M.; Abe, H.; Hoshi, H.; Kasai, S.; Ohya, H.; Matsue, T. *Anal. Chim. Acta* **2004**, *522*, 51–58.
- (31) Obregon, R.; Horiguchi, Y.; Arai, T.; Abe, S.; Zhou, Y.; Takahashi, R.; Hisada, A.; Ino, K.; Shiku, H.; Matsue, T. *Talanta* **2012**, *94*, 30–35.
- (32) Shiku, H.; Torisawa, Y.; Takagi, A.; Aoyagi, S.; Abe, H.; Hoshi, H.; Yasukawa, T.; Matsue, T. *Sensors Actuators B Chem.* **2005**, *108*, 597–602.
- (33) Nebel, M.; Grützke, S.; Diab, N.; Schulte, A.; Schuhmann, W. *Angew. Chemie - Int. Ed.* **2013**, *52*, 6335–6338.
- (34) Yasukawa, T.; Kondo, Y.; Uchida, I.; Matsue, T. *Chem. Lett.* **1998**, *8*, 767–768.
- (35) Salamifar, S. E.; Lai, R. Y. *Anal. Chem.* **2013**, *85*, 9417–9421.
- (36) Zhang, M. M. N.; Long, Y.-T.; Ding, Z. *J. Inorg. Biochem.* **2012**, *108*, 115–122.
- (37) Zhao, X.; Diakowski, P. M.; Ding, Z. *Anal. Chem.* **2010**, *82*, 8371–8373.
- (38) Isik, S.; Schuhmann, W. *Angew. Chem. Int. Ed. Engl.* **2006**, *45*, 7451–7454.
- (39) Pitta Bauermann, L.; Schuhmann, W.; Schulte, A. *Phys. Chem. Chem. Phys.* **2004**, *6*, 4003.
- (40) Yasukawa, T.; Uchida, I.; Matsue, T. *Biochim. Biophys. Acta* **1998**, *1369*, 152–158.
- (41) Zhan, D.; Li, X.; Nepomnyashchii, A. B.; Alpuche-Aviles, M. A.; Fan, F. R. F.; Bard, A. J. *J. Electroanal. Chem.* **2013**, *688*, 61–68.
- (42) Li, X.; Bard, A. J. *J. Electroanal. Chem.* **2009**, *628*, 35–42.



- (43) Kuss, S.; Cornut, R.; Beaulieu, I.; Mezour, M. A.; Annabi, B.; Mauzeroll, J. *Bioelectrochemistry* **2011**, *82*, 29–37.
- (44) Mauzeroll, J.; Bard, A. J.; Owhadian, O.; Monks, T. J. *Proc. Natl. Acad. Sci. U. S. A.* **2004**, *101*, 17582–17587.
- (45) Koley, D.; Bard, A. J. *Proc. Natl. Acad. Sci. U. S. A.* **2012**, *109*, 11522–11527.
- (46) Matsumae, Y.; Takahashi, Y.; Ino, K.; Shiku, H.; Matsue, T. *Anal. Chim. Acta* **2014**, *842*, 20–26.
- (47) Rotenberg, S. A.; Mirkin, M. V. *J. Mammary Gland Biol. Neoplasia* **2004**, *9*, 375–382.
- (48) Amemiya, S.; Guo, J.; Xiong, H.; Gross, D. A. *Anal. Bioanal. Chem.* **2006**, *386*, 458–471.
- (49) Yasukawa, T.; Kaya, T.; Matsue, T. *Electroanalysis* **2000**, *12*, 653–659.
- (50) Gao, N.; Wang, X.; Li, L.; Zhang, X.; Jin, W. *Analyst* **2007**, *132*, 1139–1146.
- (51) Xue, Y.; Ding, L.; Lei, J.; Yan, F.; Ju, H. *Anal. Chem.* **2010**, *82*, 7112–7118.
- (52) Takahashi, Y.; Miyamoto, T.; Shiku, H.; Ino, K.; Yasukawa, T.; Asano, R.; Kumagai, I.; Matsue, T. *Phys. Chem. Chem. Phys.* **2011**, *13*, 16569–16573.
- (53) Braet, F.; Rotsch, C.; Wisse, E.; Radmacher, M. *Appl. Phys. A Mater. Sci. Process.* **1998**, *66*, 575–578.
- (54) Morkvėnaitė-Vilkončienė, I.; Ramanavičienė, A.; Ramanavičius, A. *Medicina (Kaunas)*. **2013**, *49*, 155–164.
- (55) Yamane, Y.; Shiga, H.; Haga, H.; Kawabata, K.; Abe, K.; Ito, E. *J. Electron Microsc. (Tokyo)*. **2000**, *49*, 463–471.
- (56) Korchev, Y. E.; Gorelik, J.; Lab, M. J.; Sviderskaya, E. V.; Johnston, C. L.; Coombes, C. R.; Vodyanoy, I.; Edwards, C. R. *Biophys. J.* **2000**, *78*, 451–457.
- (57) Novak, P.; Li, C.; Shevchuk, A. I.; Stepanyan, R.; Caldwell, M.; Hughes, S.; Smart, T. G.; Gorelik, J.; Ostanin, V. P.; Lab, M. J.; Moss, G. W. J.; Frolenkov, G. I.; Klenerman, D.; Korchev, Y. E. *Nat. Methods* **2009**, *6*, 279–281.
- (58) Watkins, S. *Curr. Protoc. Cytom.* **2009**, 12.16.1–12.16.10.
- (59) Xiao, L.; Matsubayashi, K.; Miwa, N. *Arch. Dermatol. Res.* **2007**, *299*, 245–257.
- (60) Hearing, V. J.; Tsukamoto, K. *FASEB J.* **1991**, *5*, 2902–2909.
- (61) Orchard, G. E. *Histochem. J.* **2000**, *32*, 475–481.
- (62) Boyle, J. L.; Haupt, H. M.; Stern, J. B.; Mulhaupt, H. A. B. *Arch. Pathol. Lab. Med.* **2002**, *126*, 816–822.
- (63) De Vries, T. J.; Fourkour, A.; Wobbles, T.; Verkroost, G.; Ruiter, D. J.; Van Muijen, G. N. P. *Cancer Res.* **1997**, *57*, 3223–3229.

- (64) Lin, T.-E.; Cortés-Salazar, F.; Lesch, A.; Qiao, L.; Bondarenko, A.; Girault, H. H. *Electrochim. Acta* **2015**.
- (65) Nunes Kirchner, C.; Hallmeier, K. H.; Szargan, R.; Raschke, T.; Radehaus, C.; Wittstock, G. *Electroanalysis* **2007**, *19*, 1023–1031.
- (66) Wittstock, G.; Asmus, T.; Wilhelm, T. *Fresenius. J. Anal. Chem.* **2000**, *367*, 346–351.
- (67) Yamada, H.; Matsue, T.; Uchida, I. *Biochem. Biophys. Res. Commun.* **1991**, *180*, 1330–1334.
- (68) Kuss, S.; Kuss, C.; Trinh, D.; Schougaard, S. B.; Mauzeroll, J. *Electrochim. Acta* **2013**, *110*, 42–48.
- (69) Permentier, H. P.; Bruins, A. P. *J. Am. Soc. Mass Spectrom.* **2004**, *15*, 1707–1716.
- (70) Roeser, J.; Permentier, H. P.; Bruins, A. P.; Bischoff, R. *Anal. Chem.* **2010**, *82*, 7556–7565.
- (71) Rapino, S.; Marcu, R.; Bigi, A.; Soldà, A.; Marcaccio, M.; Paolucci, F.; Pelicci, P. G.; Giorgio, M. *Electrochim. Acta* **2015**, *in press*.
- (72) Liu, B.; Rotenberg, S. A.; Mirkin, M. V. *Proc. Natl. Acad. Sci.* **2000**, *97*, 9855–9860.
- (73) Halaban, R.; Cheng, E.; Zhang, Y.; Moellmann, G.; Hanlon, D.; Michalak, M.; Setaluri, V.; Hebert, D. N. *Proc. Natl. Acad. Sci. U. S. A.* **1997**, *94*, 6210–6215.
- (74) Guo, J.; Wen, D. R.; Huang, R. R.; Paul, E.; Wunsch, P.; Itakura, E.; Cochran, A. J. *Exp. Mol. Pathol.* **2003**, *74*, 140–147.
- (75) McEwan, M.; Parsons, P. G.; Moss, D. J. *J. Invest. Dermatol.* **1988**, *90*, 515–519.
- (76) Al-Ghoul, M.; Bruck, T. B.; Lauer-Fields, J. L.; Asirvatham, V. S.; Zapata, C.; Kerr, R. G.; Fields, G. B. *J. Proteome Res.* **2008**, *7*, 4107–4118.
- (77) Milani, V.; Frankenberger, B.; Heinz, O.; Brandl, A.; Ruhland, S.; Issels, R. D.; Noessner, E. *Int. Immunol.* **2005**, *17*, 257–268.
- (78) Miller, A. J.; Mihm, M. C. *N. Engl. J. Med.* **2006**, *355*, 51–65.

# CHAPTER III

## Contact Mode Scanning Electrochemical Microscopy of Adherent Cancer Cells

### Abstract

Scanning electrochemical microscopy (SECM) imaging of adherent cells with a glass ultramicroelectrode (UME) requires special attention regarding the probe-sample distance in order to avoid any physical contact that can damage such delicate objects as living cells. Moreover, cells topography can lead to significant artefacts and misinterpretation of the SECM response obtained when working in a constant height mode. To alleviate these limitations hybrid techniques, such as AFM-SECM or SECM combined with shear force have been introduced. Alternatively, it has been proposed that scanning in contact mode over samples that resist the brushing-like process can reduce the topographic influence on the SECM response. Such approach is made possible by the use of the so-called soft stylus probes that are fabricated in thin polymeric materials. As a result of the probe flexibility and weak forces that it exerts on the sample surface, the soft stylus can accommodate the topography of the sample and record the reactivity of specimens without inducing scratches even over self-assembled monolayers.

In the present chapter, the potential of the soft stylus probe concept towards the scanning in contact mode of adherent living cells was investigated. For this purpose, the influence of parameters such as probe thickness and SECM translational speed was determined. As a result, a flexible probe with a significantly reduced stiffness (*i.e.* 3 times) and a slow translation speed (*i.e.* 5  $\mu\text{m/s}$ ) allowed the scanning in contact mode of adherent cells without sample destruction. The new ultra-soft probes were characterized by SECM imaging of metal-on-glass specimens and implemented for the successful and damage-free contact mode scanning of melanoma adherent cells. Still it was observed that imaging of living cells in contact mode does not eliminate completely the topography influence from the recorded signal. Independence of the observed current on the hydrophobicity of the redox mediator allows proposing the cells lipid membrane elasticity impact on the SECM signal.

## 1. Introduction

Scanning electrochemical microscopy (SECM) is a surface reactivity characterization technique where an electrochemical signal is recorded at an ultramicroelectrode (UME) positioned or scanned in close proximity to a substrate.<sup>1</sup> SECM has found a wide application for investigating electron transfer processes at liquid/liquid interfaces, homogeneous and heterogeneous kinetics and imaging the reactivity of a wide range of surfaces including living cells. Indeed, SECM has been employed for studying biological samples in constant height or constant distance mode. A constant height SECM image of alive adherent cells was first obtained by *Yasukawa et al.*<sup>2</sup> in 1998 by measuring the cells respiratory activity. Subsequently, enzymatic activity and oxygen consumption of cells were measured in a similar way.<sup>3-8</sup> However, since scanning over cells at constant height implies that the recorded signal is influenced by the changes on the working distance (due to the topography of the cell) and the reactivity of cells, several efforts have been made to differentiate these two contributions. The latter is especially relevant when the topography of the cells dominates the obtained response, which can lead to data misinterpretation. As a first approach to avoid such situations, a dual Pt microdisc electrode was employed for the simultaneous topography and photosynthetic activity imaging of a single protoplast. With this aim, the oxidation of  $\text{Fe}(\text{CN})_6^{4-}$  was detected at one UME for elucidating the cell topography, while at the other UME the reduction of oxygen was monitored for the photosynthetic activity characterization.<sup>9</sup> It has been also proposed for the separation of cells respiratory activity from cells topography to compare the SECM signal obtained when scanning over alive and killed cells.<sup>10</sup> Alternatively, scanning in a constant distance mode, which typically requires the combination of SECM with other techniques that allows an independent control of the working distance during scanning, can be employed. With this aim shear-force based techniques have been widely used, *e.g.* for the enzymatic activity detection of alkaline phosphatase, as well as for cellular respiratory activity.<sup>11-13</sup> Furthermore, the voltage-switching mode SECM (VSM-SECM) based on switching the applied voltage between potential values that allow to record a faradaic current affected by either a hindered diffusion process (for distance control and topographical imaging) or a localized surface reactivity was also applied for cells investigation. Thus, simultaneous topographical and electrochemical images of single cells was implemented for PC12 neurotransmitters detection using a nanometer sized carbon UME.<sup>14</sup> Moreover, combination of SECM with scanning ion-conductive microscopy (SICM) was also successfully implemented to perform topographical and electrochemical mapping of

adherent cells by using various tip designs.<sup>15,16</sup> Furthermore, modification of commercial atomic force microscope allowed the alternating current (AC) SECM (AC-SECM) investigation of the metabolic activity that African green monkey kidney cells (*Cos-7*) present.<sup>17</sup> Besides that, impedance-based tip-to-substrate distance control was employed for imaging PC12 cells using carbon ring and carbon fiber tips and allowed topographic images directly in the cell growth media.<sup>18</sup> Despite the use of hybrid techniques has proven to be useful for the SECM imaging of living cells, combination of different techniques is still a challenging task due to the complexity, time consuming and the need of additional equipment. Additionally, still a special attention has to be paid to the working distance, since any crashes between the hard probe body and the soft biological specimens can lead to irreparable damages. The latter does not only applies to biological samples, but also to soft samples that cannot resist a physical contact with the commonly used probes.

Recently, an alternative approach has been proposed by carrying out SECM experiments in a contact mode, which was possible by using probes with a soft and flexible polymeric body. The first soft stylus microelectrode probe was suggested for SECM investigations of rough and tilt samples in a contact mode in 2009 by *Cortés-Salazar, et al.*<sup>19</sup> Recently, other soft probes containing microfluidics, or multiplexed in linear arrays (*e.g.* fountain pen probe,<sup>20</sup> microfluidic push-pull probe,<sup>21</sup> soft linear array of microelectrodes<sup>22,23</sup>) have been implemented for extending the SECM studies to curved, vertical, large or initially dry surfaces.<sup>20–23</sup> Still the pressure applied by the soft probes on the substrate seems to be critical for scanning delicate objects such as living cells.<sup>24</sup> Herein, the potential of the soft stylus probe concept towards the contact mode scanning of adherent living cells was investigated. For this purpose, the influence of parameters such as thickness of the soft probe body and the SECM translational speed was determined. As a proof-of-concept the ultra-soft microelectrodes were implemented for the successful and damage-free contact mode scanning of adherent WM-115 melanoma cells.

## **2. Materials and methods**

### **2.1. Chemicals**

Ferrocene methanol (FcMeOH, 97%) Ru(NH<sub>3</sub>)<sub>6</sub>Cl<sub>3</sub> and D-(+)-glucose were provided by Sigma-Aldrich (St. Gallen, Switzerland). Sodium sulphate (99%), magnesium sulphate (99%), potassium sulphate (99%) and 4-(2-Hydroxyethyl)-piperazin-1-ethanesulfonic acid (HEPES, 99.5%) were provided by Fluka (St. Gallen, Switzerland). Deionized water was produced by a

Milli-Q system from Millipore (Zug, Switzerland). WM-115 human melanoma cell lines were purchased from the American Type Culture Collection (ATCC). The employed experimental buffer was composed by 10 mM HEPES pH 7.4, 10 mM glucose, 75 mM Na<sub>2</sub>SO<sub>4</sub>, 1 mM MgSO<sub>4</sub> and 3 mM K<sub>2</sub>SO<sub>4</sub>.

## **2.2. Soft stylus probe fabrication**

The ultra-soft as well as soft stylus probes were manufactured by UV-photoablation of polyethylene terephthalate films (PET, Melinex® Dupont, Wilmington, DE, USA) of different thickness (*i.e.* 30 μm and 100 μm, respectively), using a 193 nm ArF excimer laser beam (Lambda Physic, Gottingen, Germany, frequency 50 Hz, E = 250 mJ) as it was reported elsewhere.<sup>19,20</sup> The depth and width of the only fabricated microchannel was 20 μm and 30 μm, respectively. It was further manually filled with a carbon paste (Electra Polymer and Chemicals Ltd., Roughway Mill, Dunk Green, England) and cured at 80 °C to create a carbon track, which was further coated by a 2 μm thick Parylene C film, using a Parylene deposition system (Comelec SA, La Chaux-de-Fonds, Switzerland). Before each SECM experiment, the soft stylus probe was cut manually with a surgical scalpel (Swan-Morton, Sheffield, England) to obtain the V-shaped tip (0.5 – 2 mm wide) and a smooth microelectrode surface. The obtained microelectrodes were characterized optically by using a scanning laser microscope (VK8700, Keyence) and electrochemically, by performing cyclic voltammeteries (CVs) in a 2 mM FcMeOH solution prepared in the experimental buffer.

## **2.3. Cell culture and sample preparation**

Human melanoma WM-115 cell line was cultured in Dulbecco's modified Eagle's medium (Gibco Life Technologies), supplemented with 10% fetal calf serum (FCS) at 37 °C in humidified atmosphere with 5% CO<sub>2</sub>. At 24 hours before an experiment, cells were seeded in cell culture dishes (35 mm × 10 mm, Nunc, Denmark). Before each experiment, the adherent melanoma cells were washed by 2 mM FcMeOH in the experimental buffer.

## **2.4. SECM measurements**

SECM experiments were provided by a custom-built SECM setup running under SECMx software<sup>25</sup> combined with IVIUM potentiostat (Ivium Technologies, Netherlands) operating in a three-electrode setup. All the reported potentials are given with respect to the Ag quasireference electrode (Ag-QRE) and a Pt wire was used as counter electrode (CE). All obtained data were treated and analyzed by MIRA.<sup>26</sup>

Prior to all ultra-soft SECM experiments, the Pt-on-glass sample surface was levelled using a glass Pt UME ( $r_T = 12.5 \mu\text{m}$ ,  $\text{RG} = 5$ ) and 2 mM FcMeOH in the experimental buffer as the redox mediator. For this purpose, two approach curves were carried out over free glass regions and with a spatial separation of 5 mm in order to determine surface position at each location. Then by using an electronic tilt table, the appropriate tilt correction was applied until the height difference at the two recorded points was below 1  $\mu\text{m}$ . This procedure was performed for both  $x$ - and  $y$ -axis. Thereafter, the characterization of the ultra-soft stylus probes was performed by scanning in contact mode the test samples containing Pt-on-glass patterns. For this purpose, the probe was fixed by using a homemade holder with an inclination angle of 70 degree, which allowed to control the probe bending direction, while maintaining a close probe-substrate position and provides an acceptable current contrast during the SECM experiments.<sup>22</sup> It is also to be noted that when the ultra-soft probe is brought in contact with the substrate, the flexible polymeric body bends over the substrate in a way similar to the classical soft probe. In this way after contact, the tip-to-substrate distance ( $h_p$ ) can be described by  $h_p = h_A - l_T$ , where  $h_A$  is the height of the attachment point of the soft stylus probe with respect to the sample surface and  $l_T$  is the length of the probe in the unbent state.<sup>19</sup> Thus, when the probe is not in contact,  $d = h_p$ . Herein, the probe was positioned at a working distance equal to  $h_p = -50 \mu\text{m}$  and a lift-off routine included into SECMx software was employed for performing 2D SECM imaging. Briefly, the ultra-soft stylus probe was kept in contact with the surface during the forward scan (high frequency direction), while it was operated in a contact-less regime (*i.e.* 125  $\mu\text{m}$  tip-to-substrate distance) during the reverse scan and the movement towards the next scanning point (low frequency direction). Each time before starting the new line scan the probe was brought back into the contact with the surface at the same working distance. The translation rate of the probe was equal to 5  $\mu\text{m/s}$  and 50  $\mu\text{m/s}$  during the forward and reverse scan, respectively and the high and low frequency mode steps were equal to 25  $\mu\text{m}$ . The SECM image in the contact mode was constructed only from the forward line scans. Thereafter, the procedure was repeated for the probe positioned at a  $d$  equal to 25  $\mu\text{m}$  in order to obtain the 2D image of the same area in the contactless mode.

In order to simultaneously perform electrochemical and optical investigation of the cells, the culture dish with adherent cells was placed on the tilt table of the SECM setup, which has a hole where a ProScope HR digital microscope (Bodelin Technologies, Lake Oswego, OR, USA) was located. To optimize the conditions for contact-mode SECM of adherent cells, the cell culture was submerged in a solution of 2 mM FcMeOH (prepared in the experimental buffer) and soft probes of different body thickness were brought into contact with the

substrate till  $h_p = -50 \mu\text{m}$  (based on negative feedback approach curves) and then line scans were performed over the adherent cells at a defined translation speed (*i.e.* from  $5 \mu\text{m/s}$  to  $50 \mu\text{m/s}$ ). After the SECM experiments were finished, the scanned area of the sample was characterized optically by using a scanning laser microscope (VK8700, Keyence). The identification of the scanned area was made possible by different marks placed below the employed petri dish. 2D images of the adherent cells were performed in contact mode as described previously for the test samples. Due to the curved bottom of cultural dishes, only an area of  $1 \text{ mm} \times 1 \text{ mm}$  leveled and employed for SECM imaging experiments.

The reproducibility of the recorded SECM signal in contact mode ( $h_p = -50 \mu\text{m}$ ) was investigated by performing three line scans above the same area containing adherent cells. Additionally, the viability of the scanned cells was confirmed by adding trypan blue stain ( $1 \text{ mg/mL}$ ) into the petri dish directly after the SECM line scans. To investigate the influence of the redox mediator on the obtained SECM signal, similar experiments were also performed using  $2 \text{ mM Ru}(\text{NH}_3)_6\text{Cl}_3$  (prepared in the experimental buffer) as the redox mediator.

### 3. Results and discussion

The ultra-soft and soft stylus probes were fabricated by drilling a microchannel on  $30 \mu\text{m}$  or  $100 \mu\text{m}$  thick polyethylene terephthalate films, respectively, filling them with a carbon paste, curing and isolating them with a thin Parylene C coating. After exposing a cross-section of the probe by blade cutting, the shape of the obtained UME can be approximated to a half-disc shape with  $15 \mu\text{m}$  radius (Figure 3.1a). The manufactured probes were characterized by performing CVs in the presence of FcMeOH or  $\text{Ru}(\text{NH}_3)_6\text{Cl}_3$  solutions prepared in the experimental buffer. As it was expected, a sigmoidal electrochemical response indicating a clear steady-state current for the oxidation of FcMeOH and reduction of  $\text{Ru}(\text{NH}_3)_6\text{Cl}_3$  was obtained with a relatively small capacitive current (Figure 3.1b and c). Indeed, no significant differences were observed between the 1<sup>st</sup> and the 5<sup>th</sup> scan for each redox mediator, which confirms the stable electrochemical response of the carbon microelectrode.



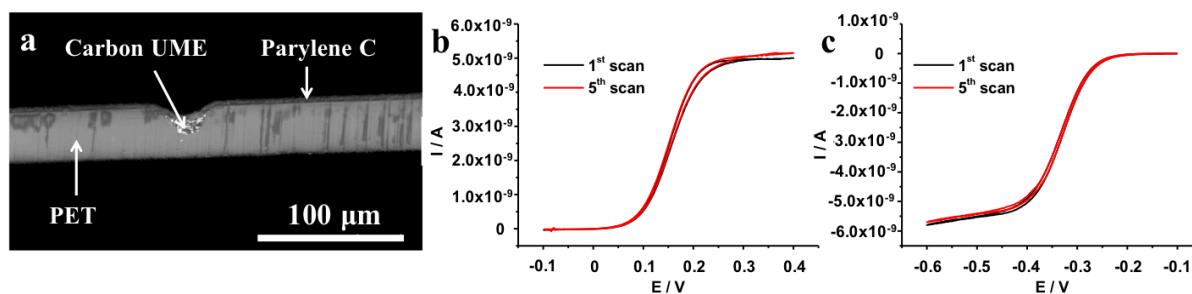


Figure 3.1 Microscopic image of the ultra-soft probe cross-section (a) and cyclic voltammograms recorded at an ultra-soft probe in presence of 2 mM FcMeOH (b) and 2 mM Ru(NH<sub>3</sub>)<sub>6</sub>Cl<sub>3</sub> (c) (prepared in the experimental buffer). Working electrode = integrated carbon paste microelectrode, counter CE = Pt, QRE = Ag wire, the scan rate was equal to 0.01 V/s.

Additional characterization of the fabricated ultra-soft stylus probe was performed by SECM imaging of a Pt-on-glass substrate in contact ( $h_p = -50 \mu\text{m}$ ) and contactless ( $d = 25 \mu\text{m}$ ) regime and using FcMeOH as a redox mediator (Figure 3.2a). Figures 3.2b and 3.2c shows the SECM images obtained during the contactless and contact scans, respectively. As it can be seen, the SECM image obtained in contact mode (Figure 3.2c) led not only to more defined features, but also to a more homogeneous current and slightly higher current contrast between the insulating and conductive regions (*i.e.* 2.2 nA and 2.0 nA for contact and contactless experiments, respectively) in comparison to the contactless SECM image (Figure 3.2b). The presence of the current heterogeneity in case of the ultra-soft probe employed in the contactless regime was observed most likely due to the strong sensitivity of the system regarding the external factors (*e.g.* vibrations) and can be explained by the softness of the probe body. The same reason does not allow collecting the images out of the reverse high frequency line scans: the pressure which appears when the probe is moved backwards is strong enough to bend the ultra-soft probe during the line scan. Therefore, uncontrolled changes of the positioning angle can take place which could lead to the variation in the working distance. As a result, in order to avoid any probe-sample contact during the reverse scan, the ultra-soft probe was always kept far from the substrate (*i.e.* 125  $\mu\text{m}$  tip-to-substrate distance). Additionally, it is worth to notice that the region where the Pt layer was isolated by a thin layer of Si<sub>2</sub>O (*i.e.* 50  $\mu\text{m}$  thick, isolated Pt), presented low current in both contact and contactless experiments confirming the damage-free contact mode scanning. Furthermore, the shift in the position of the Pt patterns between the two images (Figure 3.2b and c) appeared due to different starting point of the contact and contact-less scans (*i.e.* the probe slides on the substrate when it is brought in contact with the sample). Moreover, contact mode experiment resulted in the image with the geometry close to the real, while some blurring was observed in the contactless case.

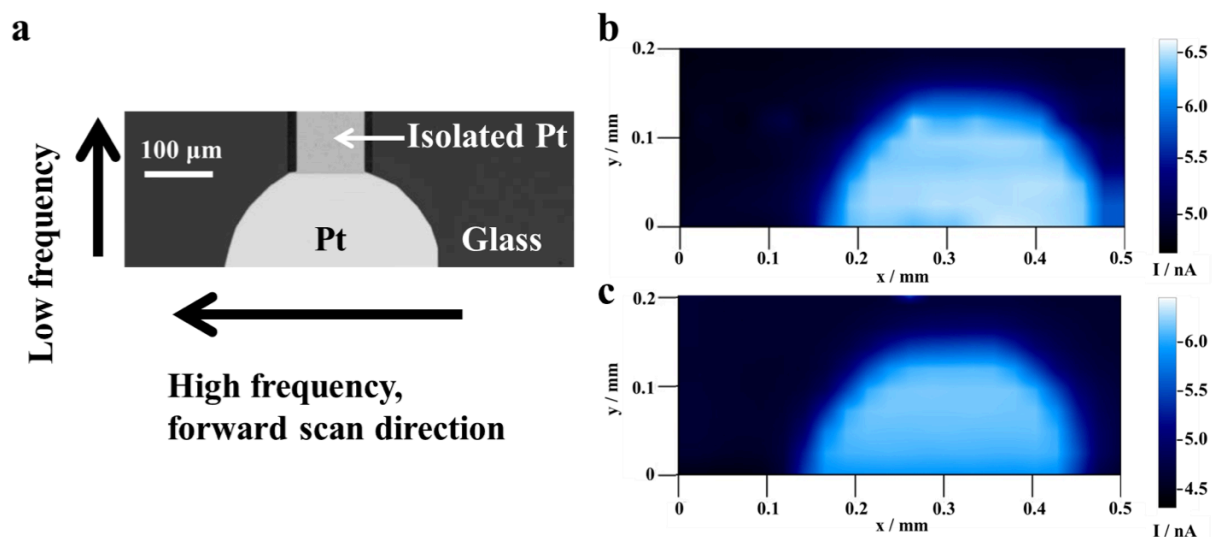


Figure 3.2. Microscopic images of Pt-on glass substrate (a) which was imaged in contactless (b,  $d = 25 \mu\text{m}$ ) and contact (c,  $h_p = -50 \mu\text{m}$ ) modes using ultra-soft stylus probe. Experimental conditions: working electrode = integrated carbon paste microelectrode of an ultra-soft probe, CE = Pt, QRE = Ag wire, the translation rate was equal to  $5 \mu\text{m/s}$ , the high and low frequency mode steps were equal to  $25 \mu\text{m}$ . A solution of  $2 \text{ mM FcMeOH}$  prepared in the experimental buffer was used as redox mediator.

To evaluate the potential ability of soft and ultra-soft probes for contact mode SECM of adherent cells, the different probes were brought into contact with the surface of a *Petri* dish ( $h_p = -50 \mu\text{m}$ ) and scanned over the adherent cells at different translation rates. As a result, the classical soft stylus probe (*i.e.*  $100 \mu\text{m}$  thick) led to the detachment of most of the scanned adherent cells independently on the employed translation speed (Figures 3.3b and 3.3c). In contrast, a significant decrease on the observed damage on the scanned cells was observed when employing the ultra-soft probe (*i.e.*  $30 \mu\text{m}$  thick) at high translation rates (Figure 3.3d). Furthermore, when scanning at low translation rates, practically no damages were observed over the scanned cells (Figure 3.3e) indicating the possibility to scan in contact mode living cells by using the ultra-soft probes.

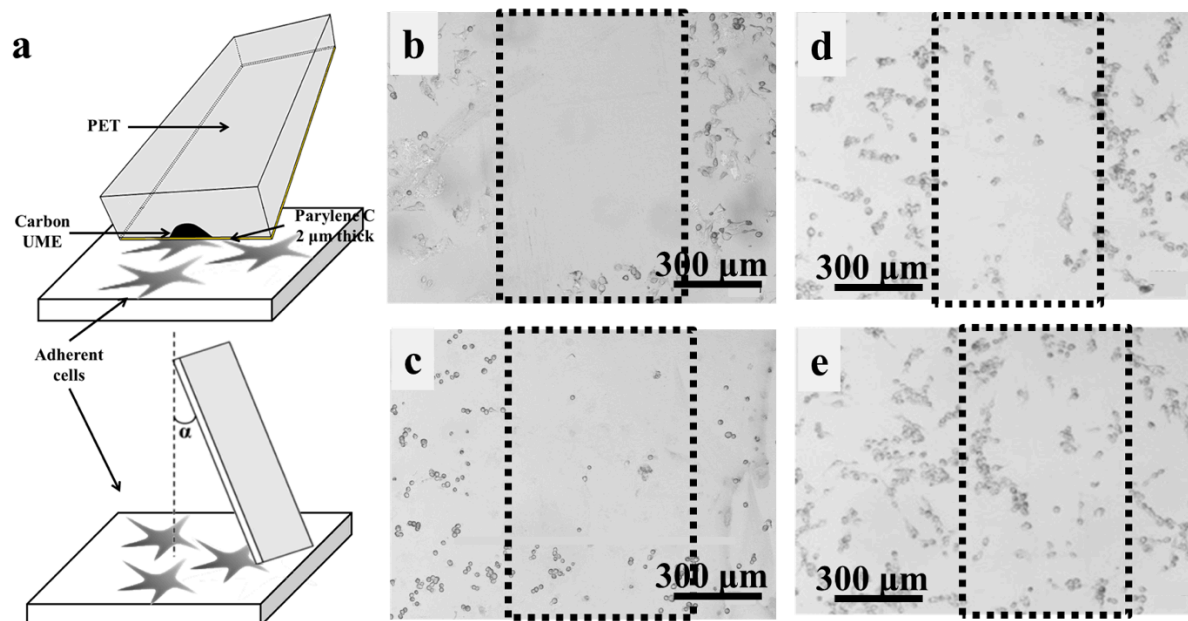


Figure 3.3. Schematic representation of the contact mode scanning of adherent WM-115 cells (a) and microscopic images of the sample surfaces after the contact mode line scans performed with 100  $\mu\text{m}$  (b and c) and 30  $\mu\text{m}$  (d and e) thick soft probes and with translation rates equal to 50  $\mu\text{m}/\text{s}$  (b and d) and 5  $\mu\text{m}/\text{s}$  (c and e). 2 mM FcMeOH in experimental buffer was used as redox mediator.

The images of the cell surface during the contact mode SECM line scan performed in optimal conditions are presented in Figures 3.4 a–c. After the ultra-soft stylus probe was brought into the contact with the cultural dish (Figure 3.4a), it was moved 1000  $\mu\text{m}$  forward with a translation speed of 5  $\mu\text{m}/\text{s}$  (Figures 3.4b and c) and the scanned cells were studied optically (Figure 3.4d). Thereafter, the probe was moved away (Figure 3.4e) and any possible perturbation on the cells viability due to the scanning in contact mode was evaluated by employing a trypan blue viability test. The latest is based on the ability of alive cells to pump out the trypan blue stain and therefore, stay uncolored while in the case when the cell lipid membrane has been damaged, the stain will be accumulated in the intracellular space and the whole cell will get a strong dark-blue color. As a result, all scanned adherent cells remained uncolored after this test, suggesting that both the membrane and viability of the cells was not perturbed by the scanning in contact mode.

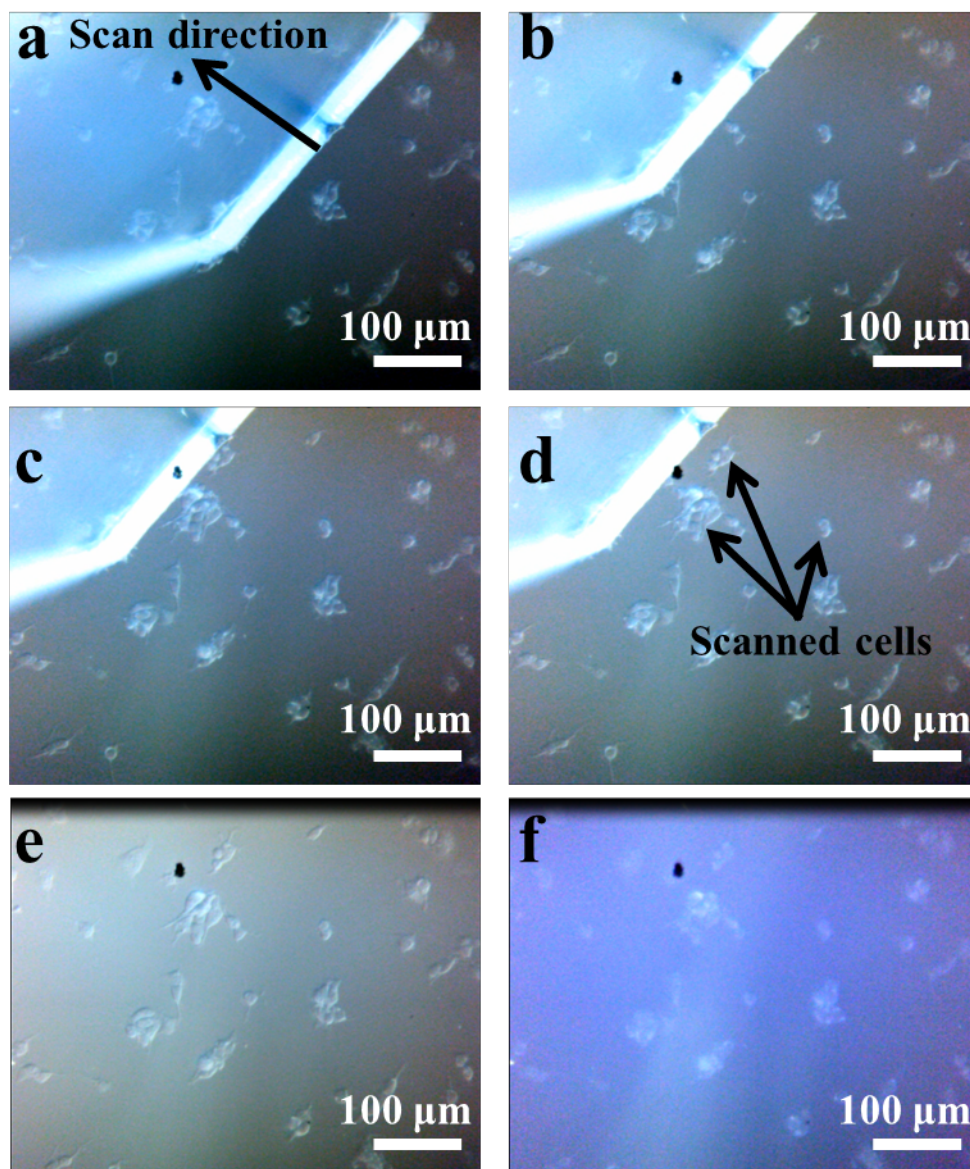


Figure 3.4. Microscopic images of adherent WM-115 cells during a SECM line scan in contact mode ( $h_p = -50 \mu\text{m}$ ) by using an ultra-soft stylus probe (a – d), as well as, before (e) and after (f) trypan blue stain addition over the scanned region. Experimental conditions: working electrode = integrated carbon paste microelectrode, CE = Pt, QRE = Ag wire. The translation rate was equal to  $5 \mu\text{m/s}$  with a step equal to  $25 \mu\text{m}$ . A solution of  $2 \text{ mM}$  FcMeOH prepared in the experimental buffer was used as redox mediator.

The electrochemical signal recorded at the ultra-soft stylus during the contact mode line scan of adherent WM-115 cells is presented in Figure 3.5a. A strong and reproducible decrease on the recorded current was observed when the UME was brushing over the adherent cells. However, during the second and third scans, the signal observed around  $x = 0.1 \text{ mm}$  on the first scan disappeared. Furthermore, a signal around  $x = 0.7 \text{ mm}$  became more clear only after the second and third scan. This fact illustrates that the employed contact mode scan is not 100% damage-free and individual cell scratches are possible, especially on the areas

where the probe is approached towards the substrate. To confirm the possibility to scan in contact mode a larger area of adherent cells with the ultra-soft stylus probe, a 2D image in contact mode of adherent cells was performed. Considering that the width of the tip of the probe was 500  $\mu\text{m}$  and the low frequency step size was 25  $\mu\text{m}$ , the average number of contact mode scans performed above each cell is equal to 20. The SECM image of adherent cells is presented in Figure 3.5b. The dark blue color corresponds to low current regions and represents the position of WM-115 cells, while the light-blue and white colors correspond to substrate regions without adherent cells. The image was obtained from the bottom to the top and presents also a decrease in cells number between  $y = 0.8 - 1$  mm. The latter indicates the decrease of cells resistance to the contact mode scanning in time due to the limited viability of adherent cells in the experimental buffer, especially when toxic redox mediators (*e.g.* FcMeOH) are used.

To investigate the nature of observed negative feedback provided by adherent cells brushed with the ultra-soft stylus probe, the hydrophobic FcMeOH redox mediator was replaced by a hydrophilic redox mediator that cannot penetrate cells membrane and therefore the recorded signals remains indifferent from any intracellular biological processes (*i.e.*  $\text{Ru}(\text{NH}_3)_6\text{Cl}_3$ ). The results of the contact mode line scan are presented in Figure 3.5c. Indeed, there is a strong similarity between the signal observed with both redox mediators indicating that the recorded signal is mainly controlled by the topography of the cells. The latter is in contradiction with the assumption that scanning in contact mode could avoid any topographical influence coming from living cells, as it is the case for non-biological samples. Such a strong difference between biological and non-biological samples can be explained by the elasticity of cells lipid membranes, which is deformed but not destroyed when the ultra-soft stylus probe is scanned over the cells. In this case, the deformed cell membrane can accommodate the UME shape (Figure 3.5c) providing a stronger diffusion blocking of the redox mediator towards the surface of the electrode. The time required for the membrane to adjust the shape during the ultra-soft probe brush can be also an explanation of the significant scan rate influence on the cells surface damaging. Thus, the slow motion provides sufficient time for the morphological adjustment and therefore, presents a smaller cells damage. Despite the fact scanning in contact mode living cells does not eliminate the topographic influence on the SECM signal, the possibility to brush cells could be an advantage for more sensitive detection of species released by the studied cells.

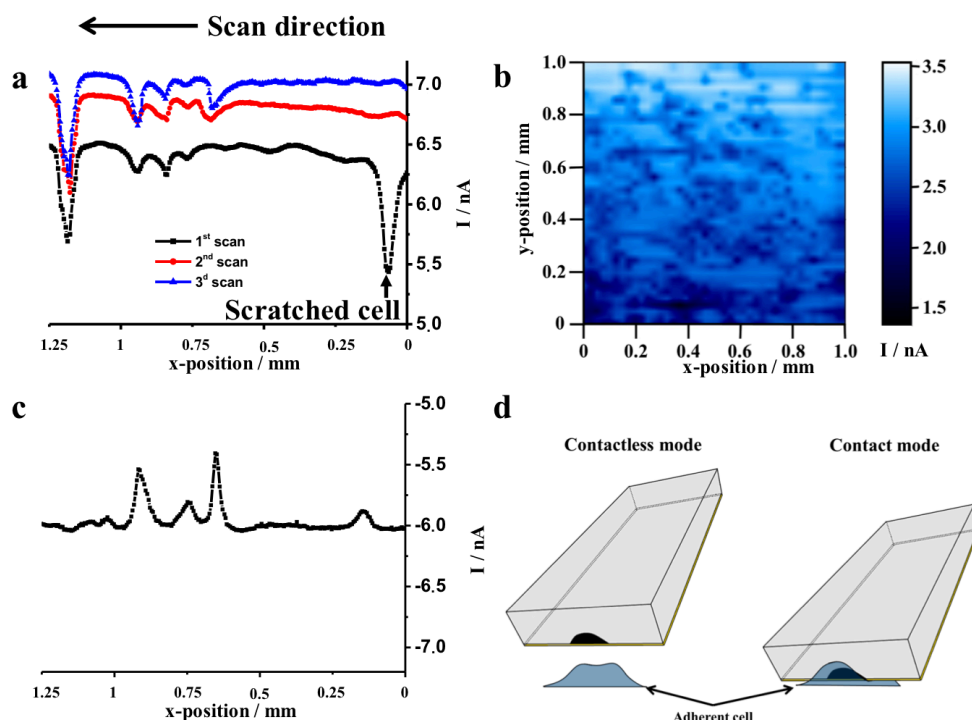


Figure 3.5. Contact mode SECM line scans recorded at the ultra-soft stylus probes (a) and (c) and the 2D SECM image of adherent WM-115 cells (b). Schematic representation of cells membrane deformation during contact mode SECM (d). Experimental conditions: working electrode = integrated carbon paste microelectrode of the ultra-soft probe, CE = Pt, QRE = Ag wire, the translation rate was equal to  $5 \mu\text{m/s}$  with a step of  $25 \mu\text{m}$ .  $2 \text{ mM FcMeOH}$  (a and b) and  $2 \text{ mM Ru}(\text{NH}_3)_6\text{Cl}_3$  (c) prepared in the experimental buffer were used as redox mediators.

#### 4. Conclusions

In the present contribution, the potential of the soft stylus probe concept towards the scanning of adherent living cells in a contact mode was investigated. Significant influence of the body stiffness and the probe translation rate was observed. As a result, the ultra-soft stylus probe (*i.e.*  $30 \mu\text{m}$  thick) was shown to be able to brush adherent WM-115 melanoma cells without damaging cells or pilling them off from the substrate surface at a translation rate of  $5 \mu\text{m/s}$ . Performing the experiment within both charged and non-charged redox mediators presented significant negative feedback when scanning in contact mode above the adherent cells. This observation suggests that imaging of living cells in contact mode does not eliminate the topography influence on the recorded signal most likely due to the specific cells lipid membrane properties (*i.e.* elasticity). Still, scanning in contact mode of living cells is possible.

## 5. References

- (1) Bard, A. J.; Fan, F. F.; Kwak, J.; Lev, O. *Anal. Chem.* **1989**, *61*, 132–138.
- (2) Yasukawa, T.; Kondo, Y.; Uchida, I.; Matsue, T. *Chem. Lett.* **1998**, *8*, 767–768.
- (3) Bard, A. J.; Li, X.; Zhan, W. *Biosens. Bioelectron.* **2006**, *22*, 461–472.
- (4) Rotenberg, S. A.; Mirkin, M. V. *J. Mammary Gland Biol. Neoplasia* **2004**, *9*, 375–382.
- (5) Takii, Y.; Takoh, K.; Nishizawa, M.; Matsue, T. *Electrochim. Acta* **2003**, *48*, 3381–3385.
- (6) Liebetrau, J. M.; Miller, H. M.; Baur, J. E.; Takacs, S. A.; Anupunpisit, V.; Garris, P. A.; Wipf, D. O. *Anal. Chem.* **2003**, *75*, 563–571.
- (7) Zhang, M.; Long, Y.-T.; Ding, Z. *Chem. Cent. J.* **2012**, *6*, 20.
- (8) Matsumae, Y.; Takahashi, Y.; Ino, K.; Shiku, H.; Matsue, T. *Anal. Chim. Acta* **2014**, *842*, 20–26.
- (9) Yasukawa, T.; Kaya, T.; Matsue, T. *Anal. Chem.* **1999**, *71*, 4637–4641.
- (10) Zhu, L.; Gao, N.; Zhang, X.; Jin, W. *Talanta* **2008**, *77*, 804–808.
- (11) Pitta Bauermann, L.; Schuhmann, W.; Schulte, A. *Phys. Chem. Chem. Phys.* **2004**, *6*, 4003.
- (12) Takahashi, Y.; Shiku, H.; Murata, T.; Yasukawa, T.; Matsue, T. *Anal. Chem.* **2009**, *81*, 9674–9681.
- (13) Nebel, M.; Grützke, S.; Diab, N.; Schulte, A.; Schuhmann, W. *Angew. Chemie - Int. Ed.* **2013**, *52*, 6335–6338.
- (14) Takahashi, Y.; Shevchuk, A. I.; Novak, P.; Babakinejad, B.; Macpherson, J.; Unwin, P. R.; Shiku, H.; Gorelik, J.; Klenerman, D.; Korchev, Y. E.; Matsue, T. *PNAS* **2012**, *109*, 11540–11545.
- (15) Takahashi, Y.; Shevchuk, A. I.; Novak, P.; Murakami, Y.; Shiku, H.; Korchev, Y. E.; Matsue, T. *J. Am. Chem. Soc.* **2010**, 10118–10126.
- (16) Takahashi, Y.; Shevchuk, A. I.; Novak, P.; Zhang, Y.; Ebejer, N.; Macpherson, J. V.; Unwin, P. R.; Pollard, A. J.; Roy, D.; Clifford, C. A.; Shiku, H.; Matsue, T.; Klenerman, D.; Korchev, Y. E. *Angew. Chem. Int. Ed. Engl.* **2011**, *50*, 9638–9642.
- (17) Diakowski, P. M.; Ding, Z. *Phys. Chem. Chem. Phys.* **2007**, *9*, 5966–5974.
- (18) Kurulugama, R. T.; Wipf, D. O.; Takacs, S. A.; Pongmayteegul, S.; Garris, P. A.; Baur, J. E. *Anal. Chem.* **2005**, *77*, 1111–1117.
- (19) Cortés-Salazar, F.; Trauble, M.; Li, F.; Busnel, J.; Gassner, A.; Hojeij, M.; Wittstock, G.; Girault, H. H. *Anal. Biochem.* **2009**, *81*, 6889–6896.
- (20) Cortés-Salazar, F.; Lesch, A.; Momotenko, D.; Busnel, J.-M.; Wittstock, G.; Girault, H. H. *Anal. Methods* **2010**, *2*, 817.

- (21) Momotenko, D.; Cortés-Salazar, F.; Lesch, A.; Wittstock, G.; Girault, H. H. *Anal. Chem.* **2011**, *83*, 5275–5282.
- (22) Cortés-Salazar, F.; Momotenko, D.; Lesch, A.; Wittstock, G.; Girault, H. H. *Anal. Chem.* **2010**, *82*, 10037–10044.
- (23) Lesch, A.; Momotenko, D.; Cortés-Salazar, F.; Wirth, I.; Tefashe, U. M.; Meiners, F.; Vaske, B.; Girault, H. H.; Wittstock, G. *J. Electroanal. Chem.* **2012**, *666*, 52–61.
- (24) Kranz, C. *Analyst* **2014**, *139*, 336–352.
- (25) Nunes Kirchner, C.; Hallmeier, K. H.; Szargan, R.; Raschke, T.; Radehaus, C.; Wittstock, G. *Electroanalysis* **2007**, *19*, 1023–1031.
- (26) Wittstock, G.; Asmus, T.; Wilhelm, T. *Fresenius. J. Anal. Chem.* **2000**, *367*, 346–351.



# CHAPTER IV

## Electrochemical Push-Pull Probe for Multimodal Altering of Cell Microenvironment

*Based on A. Bondarenko, F. Cortés-Salazar, M. Gheorghiu, S. Gaspar, D. Momotenko, L. Stanica, A. Lesch, E. Gheorghiu and H. H. Girault. Anal. Chem. 2015, 87, 4479–4486.*

### Abstract

In Chapter IV the implementation of an electrochemical push-pull probe, which combines a microfluidic system with a microelectrode, as a tool for locally altering the microenvironment of few adherent living cells by working in two different perturbation modes, namely electrochemical (*i.e.* electrochemical generation of a chemical effector compound) and microfluidic (*i.e.* infusion of a chemical effector compound from the pushing microchannel, while aspirating it through the pulling channel thereby focusing the flow between the channels) modes is presented. The effect of several parameters such as flow rate, working distance and probe inclination angle on the affected area of adherently growing cells was investigated both theoretically and experimentally. As a proof of concept, localized fluorescent labelling and pH changes were purposely introduced to validate the probe as a tool for studying adherent cancer cells through the control over the chemical composition of the extracellular space with high spatiotemporal resolution. A very good agreement between experimental and simulated results showed for instance, that the electrochemical perturbation mode enables to affect precisely only few living cells localized in a high-density cell culture.

## 1. Introduction

Essential cellular behaviors such as proliferation, apoptosis, toxicity, cytokinesis, chemotaxis, asymmetric cell division or changes in synaptic strength are hallmark processes that require well-orchestrated, spatially localized and dynamic biochemical strategies. Typically, investigating biochemical changes requires: *i*) the manipulation of cells in a fixed volume space, *ii*) the perturbation of the system by introducing an external agent (*e.g.* drug) or a new condition (*e.g.* pH or temperature) and *iii*) the detection of the cell response. Despite of all optical imaging techniques that can, for instance, reveal within a minute details of living cells interior,<sup>1-4</sup> it remains challenging to image and modify simultaneously the chemical environment around cells with a high sensitivity and resolution.<sup>1</sup> Microfabrication techniques opened new ways of studying biological processes by providing devices with capacities for growing, seeding or sorting cells and by providing microfluidic networks for controlling the extracellular environment, either fully compatible with or capable to integrate various current powerful detection techniques.<sup>5-9</sup> For instance, multipurpose scanning microfluidic probes<sup>10,11</sup> were suggested for the local assessment and perturbation of cellular environments. Similarly, new microfluidic probes consisting of three open microchannels,<sup>12-14</sup> two for aspirating and one for infusing, were introduced for single cell manipulations to analyze the enzymatic activity of kinase and house-keeping proteins present in a single cell extract.<sup>13</sup>

As it was discussed in Chapter I, SECM has been widely implemented for characterization of living cells. While most of the SECM experiments with biological specimens have been devoted to the “reading” of adherent cells, the perturbation of the cell environment through electrochemical reactions can also be implemented as shown by Bergner *et al.*<sup>15</sup> Although this task seems to be complicated for classic glass-encapsulated UMEs, it can be easily solved by employing the soft polymeric probes initially developed to carry out SECM experiments on tilted, rough and large surfaces in a contact mode.<sup>16-22</sup> Indeed, these probes can be combined with microfluidics to release locally electrolyte solutions in the gap between the sensing UME and the sample area under study as in case of the fountain pen<sup>42</sup> or, additionally, to aspirate the delivered solution as in case of the microfluidic push-pull probe.<sup>43</sup> As a result, the readout of surface reactivity at metal-on-glass structures, human fingerprints, immobilized enzymes and self-assembled monolayers have been demonstrated.<sup>23-25</sup> Furthermore, the electrochemical push-pull scanner (the modified version of the microfluidic push-pull probe) has enabled the coupling of SECM with mass spectrometry for the extraction of chemical and electrochemical surface information.<sup>23</sup>

Herein, we introduced and characterized the electrochemical push-pull probe as a precise perturbation tool for adherent cancer cells in a dual, electrochemical and microfluidic mode. More specifically, the control of the chemical composition of the extracellular space is achieved by using a microfluidic mode (*i.e.* the infusion of a chemical effector from the pushing microchannel, while aspirating it through the pulling channel) and/or an electrochemical mode (*i.e.* the electrochemical generation of a chemical effector). As a proof of concept, fluorescent labeling of adherently growing cancer cells in the microfluidic mode and their response under a locally induced pH change in the electrochemical mode were demonstrated. Finite element analysis of coupled Navier-Stokes and diffusion-convection differential equations showed a good agreement with the experimental data, confirming the unique dual electrochemical push-pull probe capabilities as a writing tool of biological samples.

## **2. Materials and methods**

### **2.1. Chemicals**

Acridine orange hydrochloride hydrate (AO), 4-(2-hydroxyethyl)piperazine-1-ethanesulfonic acid (HEPES), ferrocene methanol (FcCH<sub>2</sub>OH,  $\geq 97\%$ ), sodium chloride and sodium hydroxide were purchased from Sigma-Aldrich (Munich, Germany). All chemical reagents were of analytical grade and were used without further purification. Ultrapure water (MilliQ) was employed to prepare all solutions.

### **2.2. Cell culture preparation**

A549 cells (Human Lung Cancer Cell Line) were grown on Dulbecco-modified Eagle Medium (DMEM) supplemented with 10% fetal bovine serum (FBS) and penicillin-streptomycin (100 IU/mL) at 37 °C in a 5% CO<sub>2</sub> humidified incubator (Sanyo). Cells were split at 70% confluence using Trypsin-EDTA (0.5%) and seeded in glass bottom cell culture dishes (World Precision Instruments) at a concentration of  $18 \times 10^4$  cells/mL and grown to 80% confluence prior to experiments in DMEM. All culture media and supplements were purchased from Gibco/Invitrogen.

Before the experiments, the adherent cells were washed and the growth medium was replaced with Ringer solution that includes 130 mM NaCl, 1 mM KCl, 1 mM MgCl<sub>2</sub>, 2 mM CaCl<sub>2</sub>, 10 mM HEPES, 10 mM glucose, pH = 7.4 (adjusted with NaOH). The cell line was chosen based on its good resilience to environmental perturbations, to avoid nonspecific cellular changes during the operations with the electrochemical push-pull probe.

### 2.3. Electrochemical push-pull probe fabrication

The electrochemical push-pull probe was manufactured by UV-photoablation of 100  $\mu\text{m}$  thick polyethylene terephthalate substrate (PET, Melinex®Dupont, Wilmington, DE, USA), using a 193 nm ArF excimer laser beam (Lambda Physik, Gottingen, Germany, frequency 50 Hz, energy = 350 mJ) as it has been reported previously<sup>17,25</sup> and described in Chapter I. Briefly, 2 parallel microchannels (100  $\mu\text{m}$  width, 30  $\mu\text{m}$  depth, 60  $\mu\text{m}$  distance between channels) were fabricated on one side of a PET film. A third parallel microchannel (30  $\mu\text{m}$  width, 20  $\mu\text{m}$  depth) was ablated in-between the previous two channels, but on the opposite side of the PET film. The latter microchannel was manually filled with a carbon ink (Electra Polymer and Chemicals Ltd., Roughway Mill, Dunk Green, England) and cured at 80 °C during 1 h to create a carbon track. Furthermore, the side with 2 open microchannels was laminated with a polyethylene (PE)/PET film (Payne, Wildmere Road, Banbury, England) to create two microfluidic channels. Thereafter, the carbon track was coated by a 2  $\mu\text{m}$  thick Parylene C film using a parylene deposition system (Comelec SA, La Chaux-de-Fonds, Switzerland). Before each experiment, the probe was cut manually with a surgical scalpel blade to obtain a fresh electrode surface and a V-shaped tip (0.5 – 2 mm wide). The electrochemical response of the carbon microelectrode was verified by cyclic voltammetry (CV) in a solution of 2 mM  $\text{FcCH}_2\text{OH}$  in 0.1 M  $\text{KNO}_3$  and 10 mM HEPES buffer.

### 2.4. Computational model and numerical simulations

To estimate the size and the shape of the areas affected by the electrochemical push-pull probe operating in the microfluidic, as well as, in the electrochemical mode, finite element analysis of coupled Navier-Stokes and diffusion-convection differential equations in steady-state conditions were carried out similarly as reported previously.<sup>25</sup> The computational model of the probe assumes the probe (parallelepiped with dimensions 125  $\mu\text{m}$  thickness  $\times$  500  $\mu\text{m}$  width  $\times$  1000  $\mu\text{m}$  height) in a box-shaped domain (2000  $\mu\text{m}$  length  $\times$  2000  $\mu\text{m}$  width  $\times$  (1000  $\mu\text{m}$  +  $d$   $\mu\text{m}$ ) height, where  $d$  is the distance between the probe and the substrate) that represents the bulk solution (Figure 4.1a and 4.1b). The active area of the UME was approximated to a half-disc shape with 20  $\mu\text{m}$  radius and the simulated microchannels had a shape of an isosceles trapezium located in the opposite side of the probe (*i.e.* 70  $\mu\text{m}$  and 100  $\mu\text{m}$  bases length and 30  $\mu\text{m}$  height, and center-to-center separation of 160  $\mu\text{m}$ , Figure 4.1a).

When the finite element analysis is employed, one important factor to be considered is the mesh size. Here, the Navier-Stokes equation was solved with a fine mesh size between  $10^{-5}$  to  $10^{-6}$  m at the substrate plane, the microchannels and the electrode edge, which

corresponds to the most relevant regions in the present system. In order to optimize the calculation time, the mesh employed to map the bulk solution was on the  $7.5 \times 10^{-5}$  m range that still allows a precise characterization of the convection-diffusion process within the simulated system. It is important to notice that the above mentioned mesh sizes were found to be the optimum ones after performing several simulations with different mesh sizes and obtaining a reproducible and mesh-independent solution to the system. Numerical simulations were performed for both microfluidic and electrochemical operation modes at different flow rates, inclination angles  $\alpha$  (equal to  $90^\circ$  or  $70^\circ$ ) and working distances ( $d$ ) between the tip and the substrate surface (Figure 4.1c and 4.1d).

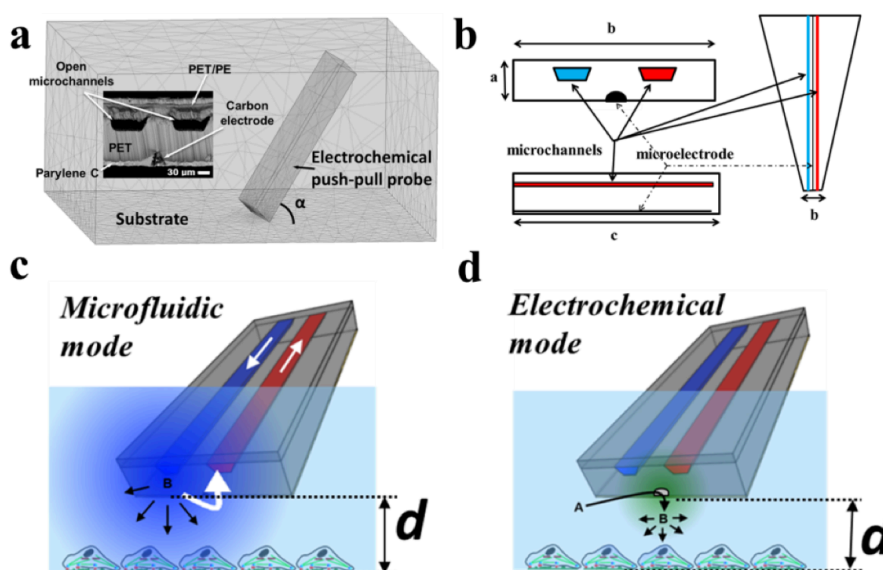


Figure 4.1. Grid for the numerical simulations of the area affected by the electrochemical push-pull probe when it is positioned above the substrate at an inclination angle  $\alpha$  and at the working distance  $d$  (a). The inset shows a microscopic image of the probe cross-section. A schematic representation (with dimensions) of the electrochemical push-pull probe (b) and the illustration of the microfluidic focusing mode (c) and the electrochemical mode (d) for the localized perturbation of living cells are also presented.

The two inclination angles employed for the simulation correspond to the most common experimental conditions in which the electrochemical push-pull probe is used for SECM experiments.<sup>25</sup> For instance, working with an inclination angle of  $70^\circ$  allows an easier positioning of the probe in a closer proximity to the substrate without scratching adherent cells. In contrast, working at  $90^\circ$  assures a more oriented perturbation. In each case, the affected substrate area was determined based on the concentration profile of a given chemical effector B (*i.e.* which can perturb cells in different manners) delivered from an open microchannel or electrochemically generated from a non-active compound A (*i.e.* which cannot perturb cells) at the microelectrode and transported to the substrate surface by

diffusion only. All simulations were run by using an initial normalized concentration of B and A equal to unity for microfluidic and electrochemical modes, respectively. ImageJ software (Wayne Rasband, Research Services Branch, National Institute of Mental Health, Bethesda, Maryland, USA) was employed to determine the whole affected area in each case.

To estimate theoretically the distribution over the sample surface of an active compound B that is delivered through the pushing channel and aspirated through the pulling channel of the electrochemical push-pull probe, the following two differential equations should be solved, namely the convection-diffusion (in steady-state conditions) equation (4.1) and the Navier-Stokes equation (4.2).

$$\nabla \cdot (-D\nabla c_B) = -\mathbf{u} \cdot \nabla c_B \quad (4.1)$$

$$\rho(\mathbf{u} \cdot \nabla)\mathbf{u} = \nabla \cdot [-p\mathbf{I} + \eta(\nabla\mathbf{u} + (\nabla\mathbf{u})^T)] + \mathbf{F} \quad (4.2)$$

where  $\nabla$  is the Laplace operator,  $c_B$  is the concentration of the compound B at a given time,  $\rho$  is the density of the solution ( $\rho = 1000 \text{ kg/m}^3$ ),  $\eta$  is the dynamic viscosity of the solution ( $\eta = 1.002 \times 10^{-3} \text{ Pa}\cdot\text{s}$ ),  $\mathbf{F}$  is a volume force,  $\mathbf{u}$  is the flow velocity and  $\mathbf{I}$  is the 3x3 identity matrix. The values of the parameters used for the simulations are presented in Table 4.1.

Table 4.1. The values of the parameters used for the simulations of the microfluidic mode

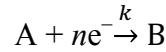
Parameter	Value [units]	Name
$\rho$	1000 [kg/m <sup>3</sup> ]	water density
$\eta$	$8.94 \times 10^{-4}$ [Pa·s]	water viscosity
flowrate	1 [μL/min]	pushing volume flow rate
A	$0.5 \times (70[\mu\text{m}] + 100[\mu\text{m}]) \times 30[\mu\text{m}]$	cross sectional surface area of the microchannels
linearFL	flowrate/A	pushing linear flow rate
linearFL2	linearFL [μL/min] × a (a = 1, 2, 3, 4, 5, 10)	aspirating linear flow rate
D	$1 \times 10^{-9}$ [m <sup>2</sup> /s]	diffusion coefficient of compound B

The numerical solution of the system of differential equations was obtained by using the direct linear system solver UMFPAK with a relative error tolerance of  $10^{-8}$  for the number of different distances between the probe and the substrate pattern. To reduce the RAM amount required for simulations and allow the numerical solution to converge, which is particularly difficult with coupled Navier-Stokes and diffusion-convection equations, the “stored solution options” were used. The boundary conditions listed in Table 4.2 were employed.

Table 4.2. The boundary conditions for the differential equations employed for the simulations of the microfluidic mode of the electrochemical push-pull probe. Herein,  $\mathbf{n}$  is the vector normal to the surface.

Surface	Navier-Stokes	Convection-diffusion B
Active surface of electrode	Wall; no slip; $\mathbf{u} = 0$	Insulation/Symmetry; $\mathbf{n} \cdot (-D\nabla c_B + c_B \mathbf{u}) = 0$
Body of the probe	Wall; no slip; $\mathbf{u} = 0$	Insulation/Symmetry; $\mathbf{n} \cdot (-D\nabla c_B + c_B \mathbf{u}) = 0$
Box planes (except reactive pattern)	Wall; no slip; $\mathbf{u} = 0$	Concentration; $c_B = 0$
Substrate pattern	Wall; no slip; $\mathbf{u} = 0$	Insulation/Symmetry; $\mathbf{n} \cdot (-D\nabla c_B + c_B \mathbf{u}) = 0$
Pushing microchannel	Inlet; Velocity; $\mathbf{u} = -U_0 \mathbf{n}$ ; $U_0 = \text{linearFL}$	Concentration; $c_B = c_{B0}$ ; $c_{B0} = 1 \text{ M}$
Aspirating microchannel	Outlet; Velocity; $\mathbf{u} = -U_0 \mathbf{n}$ ; $U_0 = \text{linearFL} \times X$ , $X=1, 2, 3, 4, 5, 10$	Convective flux; $\mathbf{n} \cdot (-D\nabla c_B) = 0$

The electrochemical operation mode of the electrochemical push-pull probe is based on the *in situ* electrochemical generation of species that can perturb adherent cells locally, *e.g.* the non-active compound A, present in the solution, is converted into an active compound B at the electrode *via* its electrochemical reduction:



where  $n$  corresponds to the number of electrons transferred. For the numerical simulations a fast kinetic rate constant (*i.e.*  $k = 10^6 \text{ m}\cdot\text{s}^{-1}$ ) was assumed. The distribution of the compound B over the sample surface can be estimated through the distribution of the non-active compound A ( $c_B = c_0 - c_A$ ). To simulate it, the Fick's second law in steady-state conditions has to be solved:

$$\nabla \cdot (-D\nabla c_A) = 0 \quad (4.3)$$

where  $D$  is the diffusion coefficient and  $c_A$  is the concentration of the compound A at a given time. The values of the parameters used for the simulations are given in Table 4.3.

Table 4.3. The values of the parameters used for the simulations of the electrochemical mode

Parameter	Value [units]	Name
$D$	$1 \times 10^{-9}$ [m <sup>2</sup> /s]	diffusion coefficient
$c_0$	1 [mol/L]	initial concentration of compound A
$k$	$1 \times 10^6$ [m/s]	kinetic rate constant at microelectrode

The boundary conditions listed in Table 4.4 were employed to solve the present model.

Table 4.4. Boundary conditions for the differential equation 4.3. Herein,  $\mathbf{n}$  is the vector normal to the surface.

Surface	Diffusion of A
Active surface of electrode	Concentration; $c_A = 0$
Body of the probe	Insulation/Symmetry; $\mathbf{n} \cdot (-D\nabla c_A) = 0$
Box planes (except reactive pattern)	Concentration; $c_A = c_0$ ; $c_0 = 1 M$
Substrate pattern	Insulation/Symmetry; $\mathbf{n} \cdot (-D\nabla c_A) = 0$
Pushing microchannel	Insulation/Symmetry; $\mathbf{n} \cdot (-D\nabla c_A) = 0$
Aspirating microchannel	Insulation/Symmetry; $\mathbf{n} \cdot (-D\nabla c_A) = 0$

## 2.5. Local perturbation of adherent cells

For each experiment, a Petri dish containing adherently growing cancer cells was positioned on top of an AxioObserver Z1 inverted microscope (Zeiss, Germany) combined with an XYZ positioning system (consisting of a DC-3K micromanipulator and a STM 3 controller from MärzhäuserWetzlar GmbH & Co. KG). The electrochemical push-pull probe was mounted on a homemade plexiglass holder with a predefined inclination angle of 70° or 90° and fixed on the above-mentioned positioning system. The microchannels were connected to a computer-controlled syringe pump (Cavro XLP 6000 from Tecan Systems, Inc.) and valve (Model M6 liquid handling pump from VICI AG International) through silica capillaries (TSP FS-Tubing, 100 μm inner diameter (ID), 363 μm outer diameter (OD) from BGB Analytik AG, Switzerland) and fittings (NanoPort Assemblies from IDEX Health & Science LLC, USA). The positioning of the probe over the adherent cancer cells at a working distance (*e.g.* 2.5 μm, 50 μm, 100 μm or 250 μm) was verified by using the optical focusing of the inverted microscope. Specifically, the objective of the microscope was focused on the cells surface and its absolute position was recorded. Thereafter, the objective was moved up by a defined value equivalent to the desired working distance (*e.g.* 2.5 μm, 50 μm, 100 μm or 250 μm) and the electrochemical push-pull probe was moved down until the plane of the microelectrode and the open microchannels was in the focus of the objective. Further, the



objective was refocused on the cell surface to confirm the working distance value. Then the probe was employed to affect the cell culture by using one of the operating modes. For instance, in the microfluidic mode, cancer cells were labeled by fluorescent AO species delivered from the electrochemical push-pull probe at a nominal pushing flow rate of 1  $\mu\text{L}/\text{min}$  (*i.e.* during 2 min) and a nominal aspirating flow rate of 0  $\mu\text{L}/\text{min}$ , 20  $\mu\text{L}/\text{min}$  or 50  $\mu\text{L}/\text{min}$ . The final image of the cell surface after perturbation was obtained employing a band pass filter for excitation (BP 450-490 nm) and a long pass filter ( $>515$  nm) for emission, in conjunction with the monochromatic iXon DU-885K EMCCD camera from Andor and analyzed by ImageJ software in order to determine the affected area (based on the pixel size calculated taking into account all magnifications). A similar procedure was followed to determine the area of the cell-covered surface affected by the electrochemical push-pull probe operated in the electrochemical mode. In such cases, the probe was positioned above adherent cells previously labeled with AO and a constant potential of  $-2$  V was applied at the UME (*vs* an Ag quasi-reference electrode, Ag-QRE) for a given time by using an Autolab potentiostat (Autolab PGSTAT101, MetrohmAutolab B.V., The Netherlands). This procedure induced a drastic increase of the local pH value, which decreased the fluorescence in the cells at the detection wavelength (*vide infra*). The electrochemical operation mode was further employed to generate a Morse code “S-O-S” signal (*i.e.* 3 short signals or “dots” for S – 3 long signals or “dash lines” for O – 3 short signals for S) by purposely controlling the fluorescence intensity of adherent cells. With this aim, the probe was positioned 7  $\mu\text{m}$  above the cell-covered surface with an inclination angle of  $70^\circ$  and the following potential step program was applied: a potential of  $-2$  V was applied during 30 s to generate the “dots”, while the “dash lines” were generated by biasing the electrode at  $-2$  V during 60 s. A potential of 0 V was applied for 60 s in between “dots” and “dashes” and for 120 s in between characters. To confirm the applied potential values, the Ag-QRE electrode was additionally characterized *vs* standard Ag/AgCl/3 M KCl electrode.

Additionally, a 10 mM NaOH solution was delivered over AO labeled cells to confirm that changes in the fluorescence, observed while using the electrochemical push-pull probe in the electrochemical operation mode, were due to local pH changes. The NaOH solution was consequently delivered over the AO fluorescent-labeled cells with a flow rate equal to 0.5  $\mu\text{L}/\text{min}$  during 50 s.

### 3. Results and discussion

#### 3.1. Computational model and numerical simulations

##### 3.1.1. Microfluidic mode

To estimate theoretically the area affected by the electrochemical push-pull probe operated in the microfluidic mode (Figure 4.1c), the computational model assumed a probe positioned with an inclination angle of  $90^\circ$  or  $70^\circ$  at a distance of  $50\ \mu\text{m}$ ,  $100\ \mu\text{m}$  or  $250\ \mu\text{m}$  above the substrate. Furthermore, a chemical effector B was delivered through the pushing channel with a flow rate equal to  $1\ \mu\text{L}/\text{min}$ , while the aspirating flow rate was varied from  $0\ \mu\text{L}/\text{min}$  to  $10\ \mu\text{L}/\text{min}$ . The system of Navier-Stokes and diffusion-convection equations was solved then to estimate the influence of the inclination angle, probe-substrate distance and aspirating flow rate on the sample affected area. The results of the numerical simulations demonstrated the significant influence of the aspirating rate on the affected area similar for both inclination angles (Figure 4.2a – s). Implementing the aspiration focuses the flow of the chemical effector B delivered by the electrochemical push-pull probe. Indeed, the affected areas shown in Figure 4.2 have a shape of an elongated oval sharpened on the side of the pulling microchannel. Varying the value of the pulling flow rate changes the shape of the global concentration gradients, which is reflected on the affected area. For instance, increasing of the pulling flow rate from  $1\ \mu\text{L}/\text{min}$  to  $5\ \mu\text{L}/\text{min}$  for the  $70^\circ$  inclination angle and  $50\ \mu\text{m}$  working distance, decreases the affected area drastically from *ca.*  $2 \times 10^6\ \mu\text{m}^2$  to  $4.5 \times 10^5\ \mu\text{m}^2$  (Figure 4.2q and 4.2d, respectively). The influence of the working distance on the affected area is more significant at high aspirating flow rates. For instance with a  $5\ \mu\text{L}/\text{min}$  aspirating flow rate, the increase of the working distance from  $50\ \mu\text{m}$  to  $100\ \mu\text{m}$  generates a decrease of the affected area about 3 times (Figure 4.2e, sample affected area *ca.*  $1.5 \times 10^5\ \mu\text{m}^2$ ). As expected, the subsequent increase of the working distance up to  $250\ \mu\text{m}$ , leads to the further decrease of the concentration of the active compound B on the substrate (Figure 4.2f, less than 10% from the initial concentration of B reaches the surface). In contrast, when the aspirating flow rate is equal to  $1\ \mu\text{L}/\text{min}$ , the affected area is very similar for all working distances. Moreover, changing the inclination angle from  $70^\circ$  to  $90^\circ$  generates slightly wider affected areas with a similar behavior when the working distance was constant.

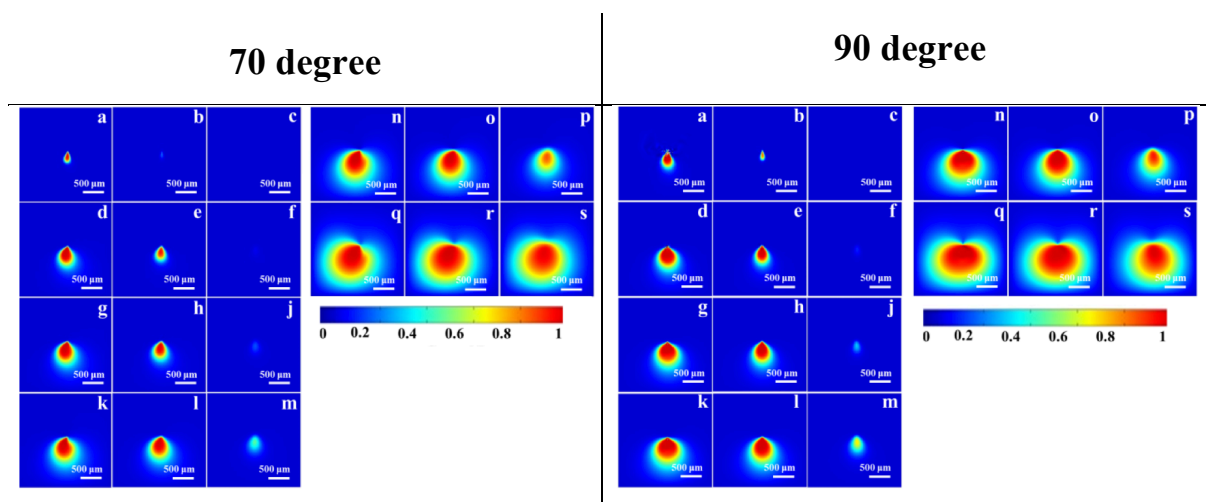


Figure 4.2. Simulated concentration profiles of the active compound B delivered over the sample surface by the electrochemical push-pull probe operated under different conditions. The pushing flow rate was 1  $\mu\text{L}/\text{min}$  for all the simulations. The aspirating flow rate and the working distance  $d$  for each case were: 10  $\mu\text{L}/\text{min}$ , 50  $\mu\text{m}$  (a); 10  $\mu\text{L}/\text{min}$ , 100  $\mu\text{m}$  (b); 10  $\mu\text{L}/\text{min}$ , 250  $\mu\text{m}$  (c); 5  $\mu\text{L}/\text{min}$ , 50  $\mu\text{m}$  (d); 5  $\mu\text{L}/\text{min}$ , 100  $\mu\text{m}$  (e); 5  $\mu\text{L}/\text{min}$ , 250  $\mu\text{m}$  (f); 4  $\mu\text{L}/\text{min}$ , 50  $\mu\text{m}$  (g); 4  $\mu\text{L}/\text{min}$ , 100  $\mu\text{m}$  (h); 4  $\mu\text{L}/\text{min}$ , 250  $\mu\text{m}$  (j); 3  $\mu\text{L}/\text{min}$ , 50  $\mu\text{m}$  (k); 3  $\mu\text{L}/\text{min}$ , 100  $\mu\text{m}$  (l); 3  $\mu\text{L}/\text{min}$ , 250  $\mu\text{m}$  (m); 2  $\mu\text{L}/\text{min}$ , 50  $\mu\text{m}$  (n); 2  $\mu\text{L}/\text{min}$ , 100  $\mu\text{m}$  (o); 2  $\mu\text{L}/\text{min}$ , 250  $\mu\text{m}$  (p); 1  $\mu\text{L}/\text{min}$ , 50  $\mu\text{m}$  (q); 1  $\mu\text{L}/\text{min}$ , 100  $\mu\text{m}$  (r); 1  $\mu\text{L}/\text{min}$ , 250  $\mu\text{m}$  (s).

### 3.1.2. Electrochemical mode

The electrochemical operation mode of the probe (Figure 4.1d) is based on the *in situ* electrochemical generation of species that can perturb adherent cells locally. The computational model in this case assumes that the non-active compound A present in the solution is converted into the chemical effector B at the UME, which then diffuses to the substrate. As in the previous case, the probe was positioned with an inclination angle of 90° or 70°, but at working distances from 2  $\mu\text{m}$  to 25  $\mu\text{m}$  above the substrate.

As in the case of the microfluidic operation mode, a similar behavior was observed when the working distance was varied for both inclination angles, therefore only the results obtained with the 70° inclination angle will be further discussed (Figure 4.3). Indeed, the working distance has a significant influence on the concentration profile of the active compound B over the substrate and on the whole affected area. For example, increasing  $d$  from 2  $\mu\text{m}$  to 15  $\mu\text{m}$  decreases the maximum concentration of B that reaches the substrate from 1 M to 0.46 M (Figure 4.3e and b, respectively). Accordingly, the whole affected area increases from 10<sup>4</sup>  $\mu\text{m}^2$  to 4 $\times$ 10<sup>4</sup>  $\mu\text{m}^2$ , due to a broader diffusion field generated, but the area affected with a concentration of active compound higher than 95% is approximately 70  $\mu\text{m}^2$  that coincides to the size of a single or few living cells. Furthermore, the affected area for the same working distance is smaller when the probe is positioned with an inclination angle equal

to 70° as compared to the case when this angle is 90°. The latter is mainly due to the diffusion profiles that in comparison with an angle equal to 90°, is developed towards the sample plane.

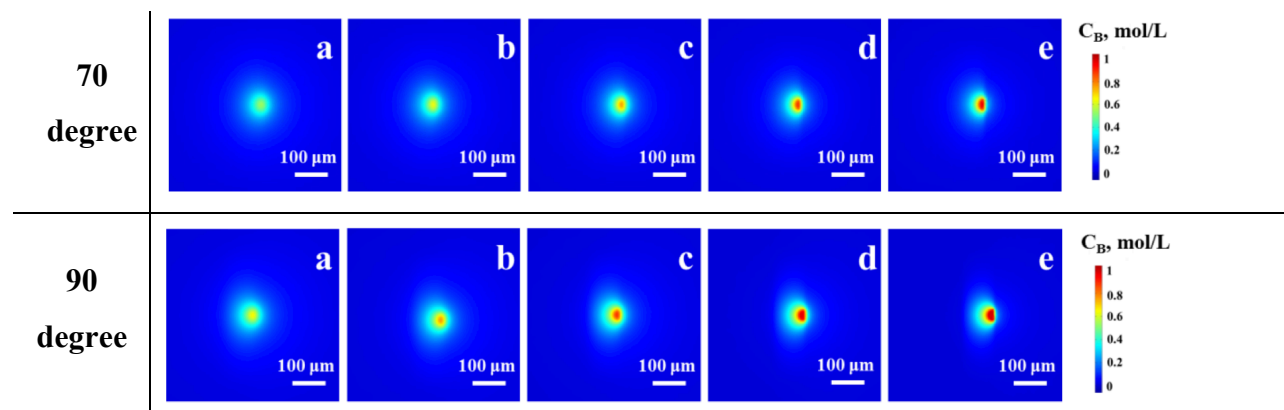


Figure 4.3. Simulated concentration profiles of the active compound B on the sample surface generated by the electrochemical push-pull probe operated in an electrochemical mode. The working distance  $d$  was 20  $\mu\text{m}$  (a); 15  $\mu\text{m}$  (b); 10  $\mu\text{m}$  (c); 5  $\mu\text{m}$  (d); 2  $\mu\text{m}$  (e).

## 3.2. Experimental perturbation of adherent cancer cells

### 3.2.1. Microfluidic mode

The electrochemical push-pull probe in the microfluidic mode was used to label adherent A549 cancer cells with AO. AO is a fluorescent dye, which has found a wide application in cellular biology due to its capability to penetrate cell membranes and bind both DNA and RNA.<sup>26</sup> Since A549 cancer cells do not have an intrinsic fluorescence, only the adherent cells that capture AO will be clearly highlighted in the fluorescence image. With this aim, a solution of AO (0.002% in Ringer buffer) was delivered by using the electrochemical push-pull probe in order to study the influence of different parameters (*e.g.* working distance, inclination angle, aspiration rate) on the affected cell area. For each experiment, AO was only delivered during the first 2 min, while the aspiration rate was kept constant along the complete duration of the experiment (*i.e.* 10 min). In order to avoid any interference from the autofluorescence of the probe materials (*i.e.* PET and PE, Figure 4.4), the probe was moved away from the field of view of the microscope before the final image of the perturbed cells was obtained. After the delivery process was activated, the area of fluorescent labeled cells grew progressively (Figure 4.4a – f), until a steady-state condition was reached (Figure 4.4g – j, *i.e.* after 60 s from starting the experiment). A period of 8 min between stopping the pushing channel and taking the final image was necessary to prevent additional cell staining when moving away the probe. The latter was required to avoid any perturbation due to the convection generated by the probe repositioning and the pressure remaining in the microfluidic system even after the pump was turned off.

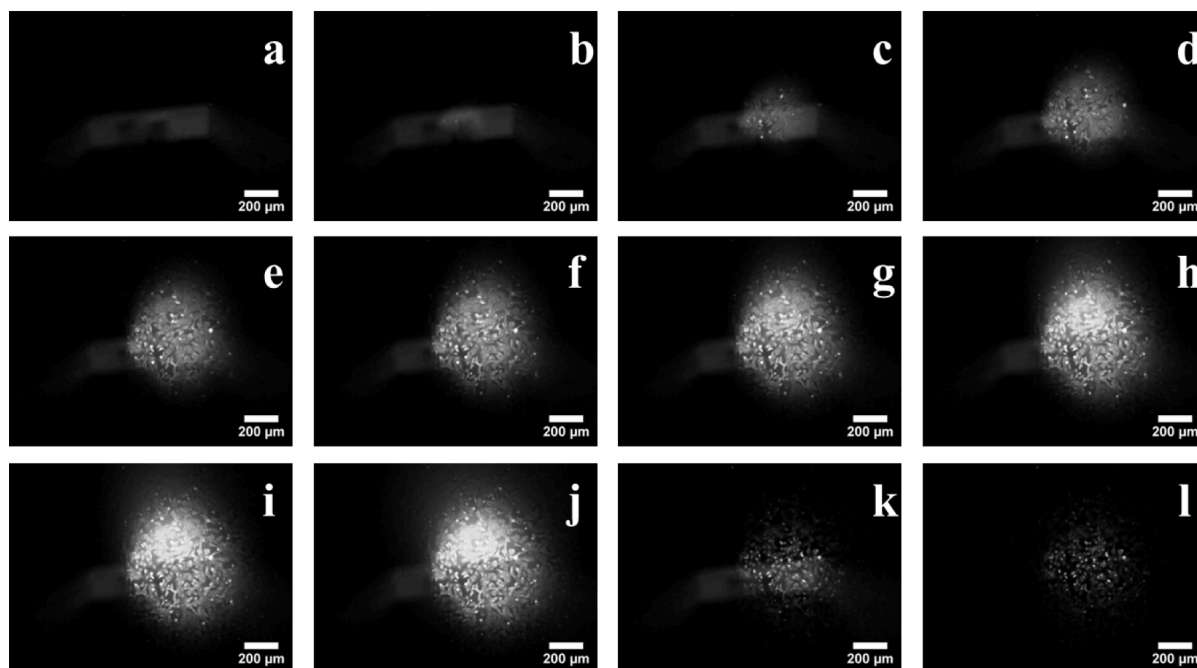


Figure 4.4. Evolution of affected area of cells as a function of time when the electrochemical push-pull probe is operated in a microfluidic mode. Fluorescence microscopy images of the cell surface taken 10 s from each other are presented in (a) to (j), 500 s after the AO delivery started is presented in (k) and the final image after removing the probe from observed area in (l). The inclination angle was equal to  $70^\circ$ , the working distance was  $100\ \mu\text{m}$ , the nominal pushing and aspirating flow rates were  $1\ \mu\text{L}/\text{min}$  and  $20\ \mu\text{L}/\text{min}$ , respectively.

After 500 s the intensity of the fluorescence decreased drastically most likely due to aspiration or partially diffusion away of the remaining AO in the solution as the pushing channel was stopped 120 s after the experiment was started (Figure 4.4k). As a result, the real affected area can be more clearly observed at times longer than 500 s. It is worth noticing that both a constant decrease of the AO fluorescence as well as a pronounced autofluorescence of the probe body (*i.e.* PET and PE) were observed during all the experiments. To overcome such situation, a precise time control of the cell perturbation was followed by the displacement of the probe from the field of view of the microscope before the final image of the perturbed cells was obtained (Figure 4.4l).

The most representative results for the perturbation of cells by the electrochemical push-pull probe operating in a microfluidic mode are presented in Figure 4.5. When the probe is employed without aspiration, the dimension of the affected area is defined mainly by the time of the assay (2 min in the present case). For instance, when AO was delivered at a working distance of  $50\ \mu\text{m}$  and with an inclination angle of  $90^\circ$ , the area of the affected cells occupied almost the entire field of view of the microscope (*i.e.*  $\text{mm}^2$  scale, Figure 4.5a). By performing the same experiment, but with a nominal aspiration flow rate of  $20\ \mu\text{L}/\text{min}$ , the labeled area presented a deformed oval shape, which was sharpened below the location of the aspirating microchannel (Figure 4.5b). Moreover, the affected area in this case corresponds to

approximately  $3.1 \times 10^5 \mu\text{m}^2$ , which was reached and kept almost constant after a period of 60 s of injection, thanks to the achievement of steady-state conditions. To investigate whether the efficiency of the aspirating microchannel can be further improved, a higher pulling flow rate was also employed while labeling cells with AO (*i.e.* 50  $\mu\text{L}/\text{min}$ , Figure 4.5c). However, no significant differences compared to the previous experiments were observed (Figure 4.5b and Figure 4.5c). This confirms that a maximum effective aspiration rate was achieved already at the nominal pulling flow rate of 20  $\mu\text{L}/\text{min}$ . Indeed, depending on the microchannel dimensions, the presence of air bubbles in the microchannels and the dead volumes of the microfluidic connections, the effective aspiration rate does not necessarily correspond to the nominal one (*i.e.* effective aspiration rate < nominal aspiration rate).

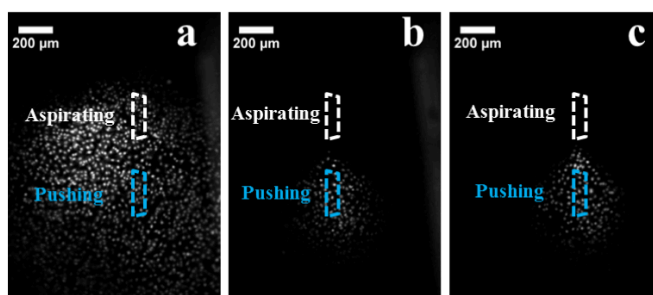


Figure 4.5. Fluorescence microscopy images of adherent cancer cells affected by the electrochemical push-pull probe operated in a microfluidic mode with an inclination angle of  $90^\circ$ . The blue and white dash lines represent the position of the pushing and aspirating microchannels, respectively. The nominal pushing flow rate was 1  $\mu\text{L}/\text{min}$  and the nominal aspirating flow rate and the working distance  $d$  were: 0  $\mu\text{L}/\text{min}$ , 50  $\mu\text{m}$  (a); 20  $\mu\text{L}/\text{min}$ , 50  $\mu\text{m}$  (b); 50  $\mu\text{L}/\text{min}$ , 50  $\mu\text{m}$  (c).

As predicted from the numerical simulations, changing the inclination angle from  $90^\circ$  to  $70^\circ$  does not introduce significant differences (Figure 4.2). However, for a 50  $\mu\text{m}$  working distance, a larger and wider oval area was obtained for a  $70^\circ$  inclination angle (*i.e.*  $6.7 \times 10^5 \mu\text{m}^2$  for  $70^\circ$  compared to  $3.3 \times 10^5 \mu\text{m}^2$  for  $90^\circ$ , see Figure 4.6a). This result can be explained mainly by the differences on the effective aspiration flow rates achieved in each experiment. By comparing the experimental results obtained with the electrochemical push-pull probe at different working distances (Figure 4.6a, 4.6b and 4.6c) and the simulated results obtained under similar conditions, it can be suggested that for  $70^\circ$  inclination angle the effective aspiration rate achieved experimentally was approximately equal to 3  $\mu\text{L}/\text{min}$ , while for  $90^\circ$  it was close to 10  $\mu\text{L}/\text{min}$  (Figure 4.6d, 4.6e and 4.6f).

The behavior observed experimentally in terms of shape and size of the affected area correlates qualitatively with the numerical results, especially for the effects caused by the working distance and inclination angle. Further increase of  $d$  up to 100  $\mu\text{m}$  (with a  $70^\circ$  inclination angle), only introduces slight changes on the shape (*i.e.* sharpened oval shape) and

size (*i.e.*  $5.3 \times 10^5 \mu\text{m}^2$ ) of the affected area (Figure 4.6b). However, when a working distance of 250  $\mu\text{m}$  was employed, the size and the intensity of the labeled area were drastically reduced (Figure 4.6c). Despite only few stained cells with very low fluorescence intensity can be observed on the final image, the labeling of cells under these conditions corresponds more to a random distribution (see also Figure 4.6f). For 90° inclination angle the similar behavior (in correspondence to the higher flow rate) was recorded.

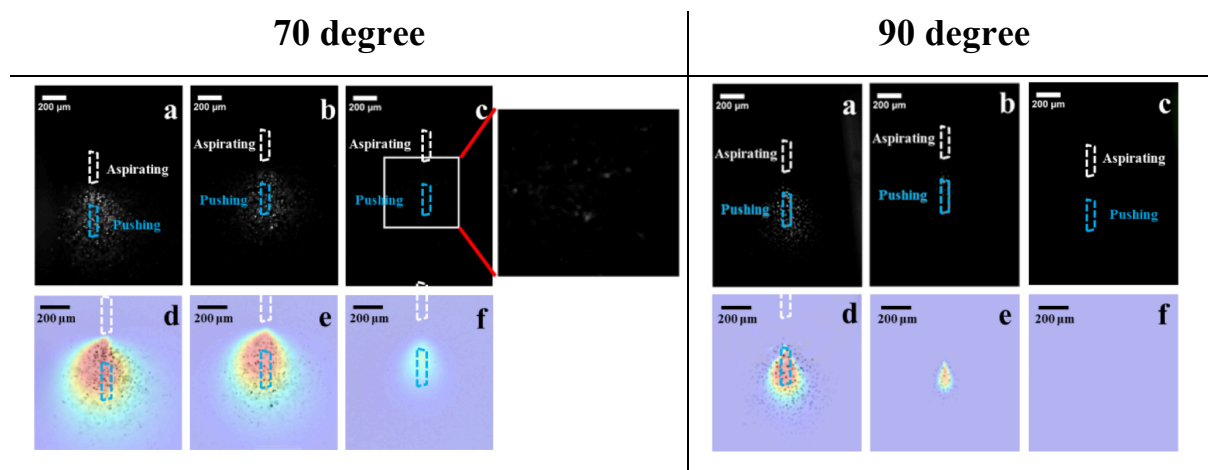


Figure 4.6. Fluorescence microscopy images of cancer cells labeled with AO (white spots) by the electrochemical push-pull probe operated in a microfluidic mode at 70° and 90° inclination angles (a), (b) and (c). The overlapping between the numerically simulated affected area (color image) and the experimental results (presented as inverted black-and-white images; labeled cells are depicted as black spots) is depicted in (d), (e) and (f). The blue and white dash lines represent the position of the pushing and aspirating microchannels, respectively. The experimental nominal aspirating flow rate was 20  $\mu\text{L}/\text{min}$ , while the one used for the simulations was 10  $\mu\text{L}/\text{min}$  and 3  $\mu\text{L}/\text{min}$  for an inclination angle of 90° and 70°, respectively. The working distance  $d$  was: 50  $\mu\text{m}$  (a) and (d); 100  $\mu\text{m}$  (b) and (e); 250  $\mu\text{m}$  (c) and (f). The pushing flow rate was 1  $\mu\text{L}/\text{min}$  for all experiments.

### 3.2.2. Electrochemical mode

Before carrying out experiments in the electrochemical mode, UME of the electrochemical push-pull probe was characterized by CV in the presence of a solution of 2 mM FcMeOH in 0.1 M  $\text{KNO}_3$ . As it was expected, a sigmoidal electrochemical response indicating a clear steady-state current for the oxidation of FcMeOH was obtained with a relatively small capacitive current (Figure 4.7). As it can be seen in Figure 4.7a, no significant difference was observed between the 1<sup>st</sup> and the 5<sup>th</sup> scan, which confirms the proper functioning of the carbon microelectrode and the possibility to generate electrochemically chemical effectors that might affect adherent cancer cells. Additionally, when the same experiment was carried out using Ag/AgCl/3 M KCl electrode the only effect observed was the shift of the potential towards more positive potentials by a value of 0.150 V.

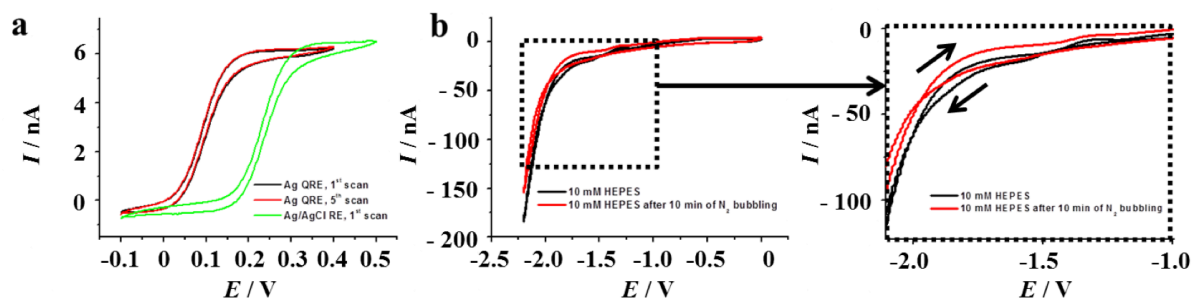


Figure 4.7. Cyclic voltammograms recorded with the electrochemical push-pull probe in 2 mM FcMeOH and 0.1 M  $\text{KNO}_3$  (a) and 10 mM HEPES buffer (b). The inset represents a zoom-in on the highlighted area in Figure 4.7b. Working electrode = integrated carbon paste microelectrode, counter electrode (CE) = Pt, scan rate = 0.01 V/s. As a reference electrode Ag wire (a and b) and Ag/AgCl/3 M KCl (a) standard electrode was used.

The optimal potential for water reduction was determined from CVs recorded with the electrochemical push-pull probe in 10 mM HEPES buffer solution, as the one shown in Figure 4.7b. The reduction of water was observed at potentials more negative than  $-1.8$  V vs Ag-QRE as indicated by a drastic increase in the cathodic current. Besides the pH increasing, it was important to avoid  $\text{H}_2$  bubble formation at the carbon UME. As a consequence, the working potential was selected only slightly more negative than  $-1.8$  V (*i.e.*  $-2$  V) vs Ag-QRE.

One of the possibilities to affect adherent cells electrochemically using the electrochemical push-pull probe is to change locally the pH of the extracellular space, for instance by carrying out the electrolysis of water at the integrated carbon UME. Moreover, local pH changes can be monitored optically by taking advantage of the pH dependence of the AO fluorescence. The fluorescence of AO loaded into cells presents a red shift when the pH of the media is increased or decreased.<sup>27–29</sup> Indeed, Figure 4.8 shows the quenching of the AO fluorescence by a local pH change, when a solution of NaOH (*i.e.* 0.01 M, flow rate 0.6  $\mu\text{L}/\text{min}$  during 50 s) is delivered over AO fluorescent-labeled cells. The decrease of the fluorescence intensity was followed by a recovery on the edge of the affected area only, while for the cells located just below the NaOH delivery zone, slight or negligible recovery was observed most likely due to the longer exposure to a high NaOH concentration that can irreversibly affect the pH cell status.



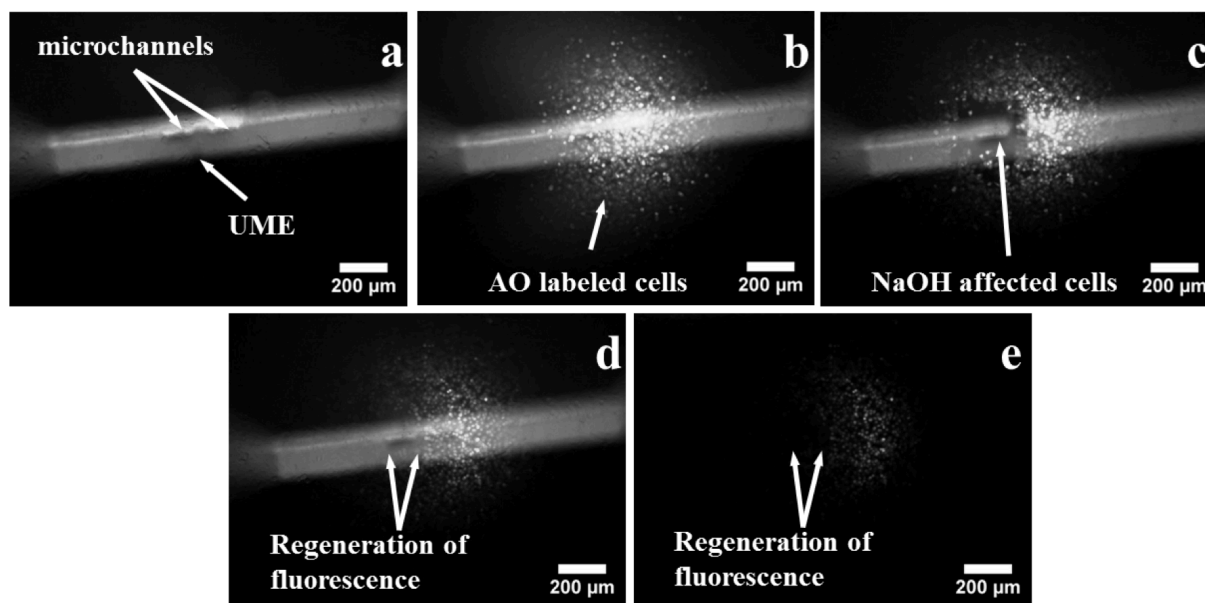


Figure 4.8. Fluorescence microscopy images of adherent cancer cells after the electrochemical push-pull probe is positioned above them (a), after pushing of AO with a flow rate of 1  $\mu\text{L}/\text{min}$  during 50 s (b), after pushing of 0.01 M NaOH with a flow rate 0.5  $\mu\text{L}/\text{min}$  during 50 s (c), 5 min after NaOH flow was stopped (d) and after moving the probe outside the view (e).

To further confirm the effect of basic pH on the fluorescence of AO, we have evaluated the emission spectra of Ringer solutions with 0.2% AO and three different pH values. As shown in Figure 4.9, the AO emission spectra (measured with a Jasco 750 spectrofluorimeter using 480 nm excitation wavelength) reveal a decrease of the fluorescence intensity as the pH of the media increases.

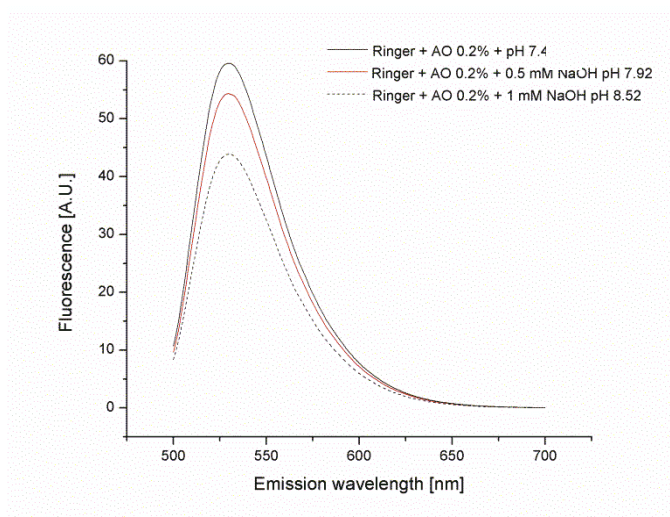


Figure 4.9. Fluorescent emission spectra of a solution of 0.2% AO in Ringer buffer at different pH values.

All these observations are in good agreement with the use of AO as a pH indicator within the cellular environments.<sup>27–29</sup> Thus, if the UME of the probe is biased to a potential of  $-2$  V, a local pH increase will be induced due to  $\text{OH}^-$  generation ( $2\text{H}_2\text{O} + 2\text{e}^- \rightarrow \text{H}_2 + 2\text{OH}^-$ ). This

can be then monitored by the quenching of AO fluorescence of the labelled cells. As shown by Cannan *et al.*, drastic pH changes (*i.e.* between 3 to 6 pH units) can be observed in the vicinities of an electrode where the consumption of  $H^+$  (or generation of  $OH^-$ ) is taking place.<sup>30</sup> In our specific case, it is expected to observe similar, but slightly compressed pH profiles due to the presence of the Ringer buffer that acts as a chemical lens to constraint the localized pH change.<sup>31</sup> Additionally, it is important to note that when applying  $-2$  V at the microelectrode not only water reduction, but also oxygen reduction can take place (Figure 4.7). This process can locally decrease the concentration of the dissolved oxygen, which can lead to apoptosis and possible morphological changes of adherent cells. However, no morphological marks of cell apoptosis were detected during the experiment. Probably, oxygen diffusion was fast enough and the time during which the local oxygen concentration was influenced by the probe was short enough not to affect irreversibly the live cells.

The affected area can be thus determined by the decrease of the fluorescence intensity of AO labeled cells. With this aim, after the electrochemical push-pull probe was employed to label the adherent cells with AO, it was brought in a close proximity of the cells (*e.g.* from a working distance of  $20\ \mu\text{m}$  to a working distance of  $2.5\ \mu\text{m}$ ) and a potential of  $-2$  V was applied during 180 s. The applied potential allowed a perturbation of AO labeled adherent cells, without generation of  $H_2$  bubbles. The latter was confirmed optically by the inverted microscope and by the stable current profiles recorded during the applied potential steps.

The experimental results obtained for the perturbation of adherent cells with the electrochemical push-pull probe operating in an electrochemical mode and with an inclination angle of  $70^\circ$  and  $90^\circ$  are shown in Figure 4.10. The results are similar for both inclination angles, however, an easier and therefore closer positioning of the probe over the cell surface was achieved when using the probe with an inclination angle of  $70^\circ$  (because aligning an edge of the probe to the cells is easier than aligning the whole cross section). Therefore, the further discussion will be focused on the  $70^\circ$  inclination angle. As it can be seen in Figure 4.10i and j, when operating the probe at a working distance of  $2.5\ \mu\text{m}$ , only few cells (*i.e.* 6 cells, sample affected area *ca.*  $9000\ \mu\text{m}^2$ ) present a decrease of their fluorescent intensity. However, only the adherent cancer cells located just below the microelectrode presents a drastic decrease of its AO fluorescence intensity. As discussed previously, the electrochemical operation mode might enable affecting areas as small as  $70\ \mu\text{m}^2$  with localized concentration profiles of up to 95% of the maximum reachable concentration of an electrogenerated compound. The latter results demonstrate the capabilities of the electrochemical push-pull probe for the precise and localized perturbation of living cells in an electrochemical operation mode.

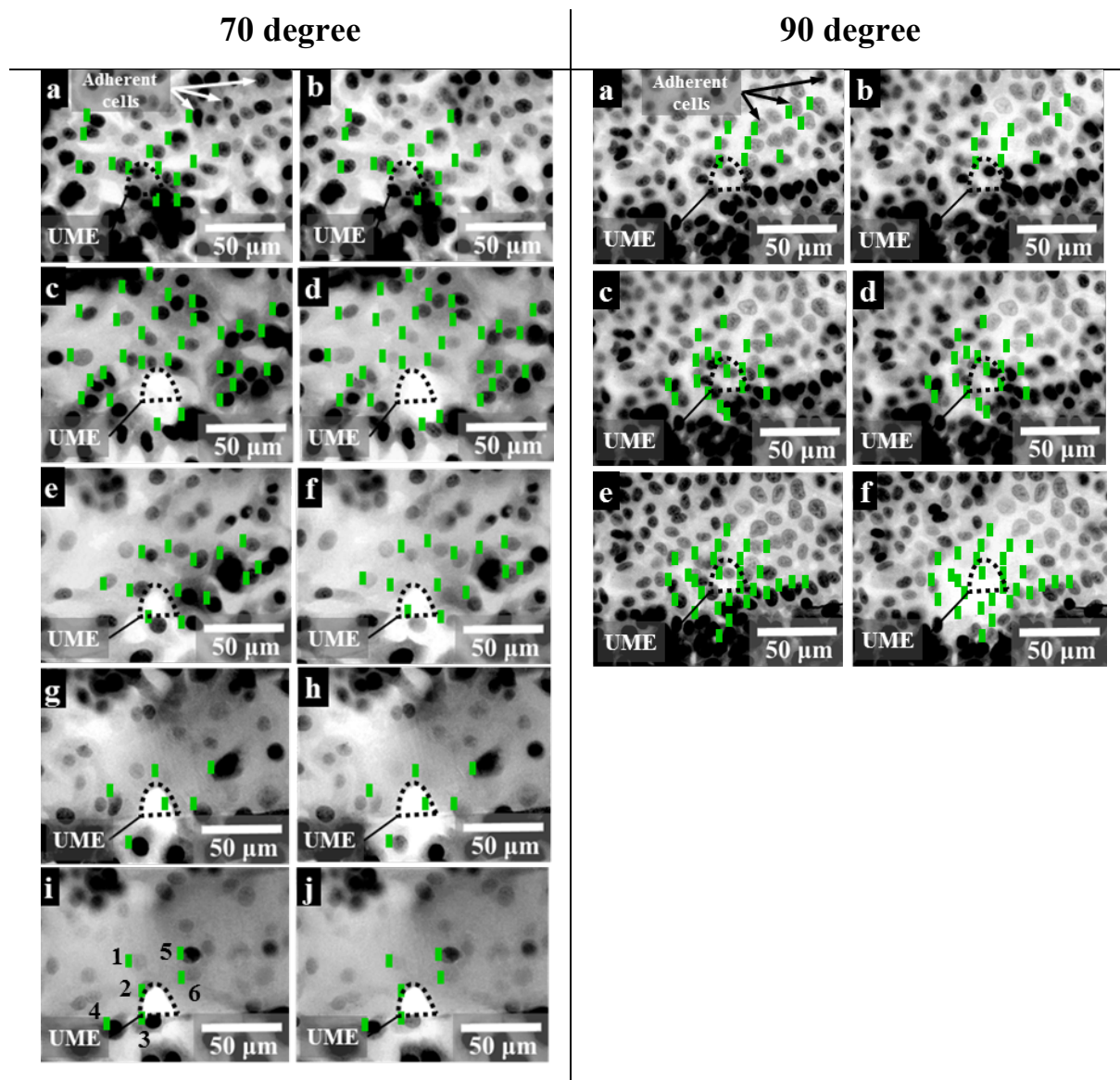


Figure 4.10. Fluorescence microscopy images of adherent cancer cells labeled with AO before ((a), (c), (e) (g) and (i)) and after ((b), (d), (f), (h) and (j)) their perturbation by using the electrochemical push-pull probe in an electrochemical mode. For a better visualization, all obtained images were converted into black-and-white, the colors were inverted and the brightness adjusted. The working distance  $d$  was  $20\ \mu\text{m}$  for (a) and (b),  $15\ \mu\text{m}$  for (c) and (d),  $10\ \mu\text{m}$  for (e) and (f)  $5\ \mu\text{m}$  for (g) and (h) and  $2.5\ \mu\text{m}$  for (i) and (j). Working electrode = integrated carbon paste UME, QRE = Ag, CE = Pt, applied potential =  $-2\ \text{V}$  during a period of 180 s. Cells marked with green were significantly affected during the experiment.

As expected, with the increase of the working distance, an increase of the affected area is observed (Figure 4.10). For instance, when increasing the working distance to  $15\ \mu\text{m}$ , approximately 30 cells are clearly affected corresponding to an area equal to  $2 \times 10^4\ \mu\text{m}^2$ . The dependency of the affected areas on the working distance can be interpreted in terms of the different extension of the truncated diffusion fields created between the probe and the substrate. Thus, a smaller distance between the probe and the substrate will generate a smaller perturbation area. The latter is in a very good agreement with the numerical simulations, where similar behavior was observed for both inclination angles (Figure 4.3). Moreover, the

numerical results reproduced qualitatively the truncated round shape of the affected areas due to the probe position and inclination. Indeed, in Figure 4.10i the cell No. 3 placed just below the edge of the UME is not drastically affected, since the diffusion of electrogenerated species is also truncated in this direction.

It is important to note that after the applied voltage was switched off, the fluorescence intensity of the AO species inside the affected cells was substantially recovered. The latter suggests the possibility to perform reversible (temporal) cell perturbations by working in an electrochemical mode that in addition can be precisely localized in a small number of cells (spatially). To demonstrate the dynamic perturbation provided by the electrochemical push-pull probe operating in an electrochemical mode, a Morse code "S-O-S" signal was generated by applying a potential step program to induce local pH changes over AO-labeled cells (see materials and methods section). The recorded video was further analyzed using ImageJ software to read the fluorescence intensity profile of the cells positioned under the UME as a function of time (Figure 4.11 and inset). The first and the last three peaks of the image correspond to the three "dots" that generate the "S" letter in Morse code. The next three broader peaks stand for the three "dashes" that generate the letter "O". The results of the experiments showed good reproducibility of the signal during the first 3 cycles, however starting from the 6th cycle significant decrease of the fluorescence was observed. The latter is most likely, as observed also when delivering NaOH through the probe (Figure 4.8), due to the long exposure of the cells to a considerable concentration of OH<sup>-</sup> that can affect drastically the cell status and that does not allow the fluorescence to recover completely before the next potential pulse is applied (*i.e.* -2 V).

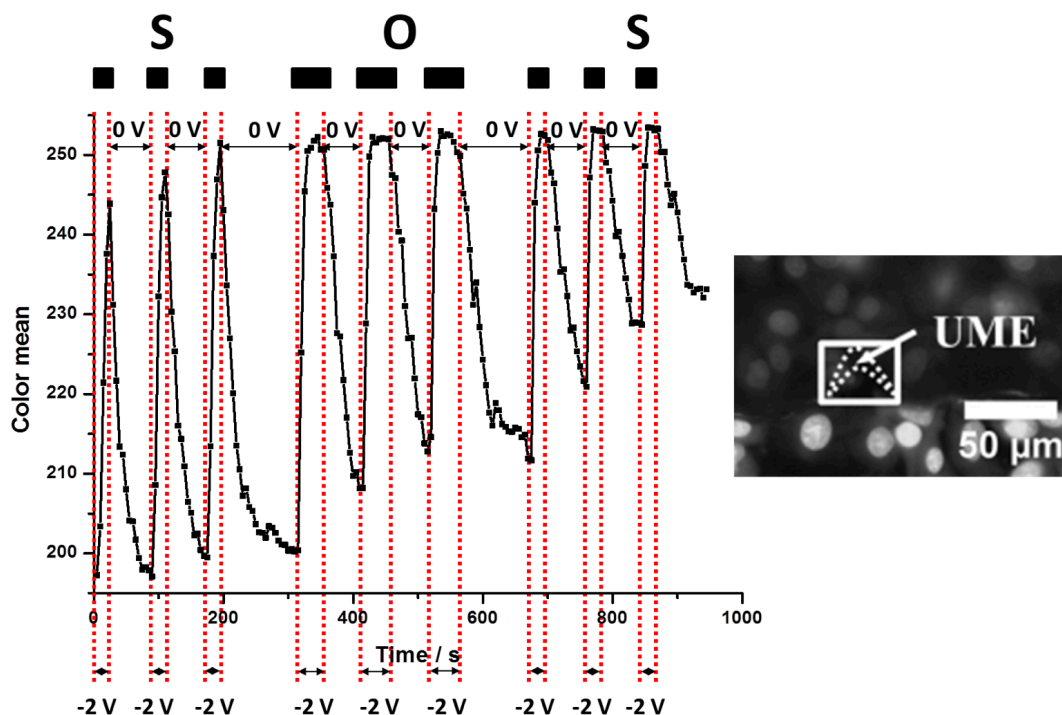


Figure 4.11. The reversed fluorescence intensity profile of the AO-labeled cells during the electrochemically induced Morse code “S-O-S” signal. Working electrode = integrated carbon paste UME, QRE = Ag, CE = Pt, applied potential =  $-2\text{ V}$ , the working distance  $d = 10\ \mu\text{m}$ . The inset shows the microscopic image of AO-labeled adherent cells with the electrochemical push-pull probe positioned above them. The white square within the inset shows the area of which fluorescence intensity was analyzed.

#### 4. Conclusions

We demonstrated the precise spatiotemporal perturbation of adherent living cells by taking advantage of the integrated electrochemical and microfluidic modes inside a soft electrochemical push-pull probe. Numerical simulations of the implemented probe and the influence of different parameters, such as aspiration rate, working distance and probe inclination angle indicated the possibility to perturb only few cells *via* the electrochemical mode and a group of few hundreds of cells by using the microfluidic mode. The latter possibility was thoroughly verified experimentally. With this aim, localized fluorescent labeling of adherently growing cells was achieved by flowing from one of the open microchannels AO, while pulling it from the other open microchannel. Furthermore, highly localized pH changes were induced by the integrated microelectrode in areas covering only few cells. Finally, the capability of our system for localized, dynamic and reversible cell perturbation was illustrated with a cell-emitted “S-O-S” signal obtained by purposely tuning the fluorescent intensity of AO-labeled cells *via* electrochemically induced spatiotemporal pH changes. This study paves the way for further applications of multiparametric cell stimulation

to study the pH influence on the growth and proliferation of malignant cancer cells as well as on analyzing the samples collected from the extracellular space through the pulling channel.

## 5. References

- (1) Toomre, D.; Bewersdorf, J. *Annu. Rev. Cell Dev. Biol.* **2010**, *26*, 285–314.
- (2) Lang, P.; Yeow, K.; Nichols, A.; Scheer, A. *Nat. Rev. Drug Discov.* **2006**, *5*, 343–356.
- (3) Fletcher, J. S. *Analyst* **2009**, *134*, 2204–2215.
- (4) Bulte, J. W. M.; Kraitchman, D. L. *NMR Biomed.* **2004**, *17*, 484–499.
- (5) Servant, G. *Science* **2000**, *287*, 1037–1040.
- (6) Kim, B. J.; Wu, M. *Ann. Biomed. Eng.* **2012**, *40*, 1316–1327.
- (7) Cimetta, E.; Figallo, E.; Cannizzaro, C.; Elvassore, N.; Vunjak-Novakovic, G. *Methods* **2009**, *47*, 81–89.
- (8) Torisawa, Y.-S.; Kaya, T.; Takii, Y.; Oyamatsu, D.; Nishizawa, M.; Matsue, T. *Anal. Chem.* **2003**, *75*, 2154–2158.
- (9) Taylor, R. J.; Falconnet, D.; Niemistö, A.; Ramsey, S. A.; Prinz, S.; Shmulevich, I.; Galitski, T.; Hansen, C. L. *Proc. Natl. Acad. Sci. U. S. A.* **2009**, *106*, 3758–3763.
- (10) Juncker, D.; Schmid, H.; Delamarche, E. *Nat. Mater.* **2005**, *4*, 622–628.
- (11) Kaigala, G. V.; Lovchik, R. D.; Drechsler, U.; Delamarche, E. *Langmuir* **2011**, *27*, 5686–5693.
- (12) Ainla, A.; Jeffries, G. D. M.; Brune, R.; Orwar, O.; Jesorka, A. *Lab Chip* **2012**, *12*, 1255–1261.
- (13) Sarkar, A.; Kolitz, S.; Lauffenburger, D. A.; Han, J. *Nat. Commun.* **2014**, *5*, 3421.
- (14) Ainla, A.; Gözen, I.; Hakonen, B.; Jesorka, A. *Sci. Rep.* **2013**, *3*, 2743.
- (15) Bergner, S.; Wegener, J.; Matysik, F. M. *Anal. Chem.* **2011**, *83*, 169–174.
- (16) Kranz, C. *Analyst* **2014**, *139*, 336–352.
- (17) Cortés-Salazar, F.; Trauble, M.; Li, F.; Busnel, J.; Gassner, A.; Hojeij, M.; Wittstock, G.; Girault, H. H. *Anal. Biochem.* **2009**, *81*, 6889–6896.
- (18) Cortés-Salazar, F.; Momotenko, D.; Lesch, A.; Wittstock, G.; Girault, H. H. *Anal. Chem.* **2010**, *82*, 10037–10044.
- (19) Cortés-Salazar, F.; Momotenko, D.; Girault, H. H.; Lesch, A.; Wittstock, G. *Anal. Chem.* **2011**, *83*, 1493–1499.
- (20) Lesch, A.; Momotenko, D.; Cortés-Salazar, F.; Wirth, I.; Tefashe, U. M.; Meiners, F.; Vaske, B.; Girault, H. H.; Wittstock, G. *J. Electroanal. Chem.* **2012**, *666*, 52–61.
- (21) Lesch, A.; Vaske, B.; Meiners, F.; Momotenko, D.; Cortés-Salazar, F.; Girault, H. H.; Wittstock, G. *Angew. Chem. Int. Ed. Engl.* **2012**, *51*, 10413–10416.
- (22) Lesch, A.; Momotenko, D.; Cortés-Salazar, F.; Roelfs, F.; Girault, H. H.; Wittstock, G. *Electrochim. Acta* **2013**, *110*, 30–41.

- (23) Momotenko, D.; Qiao, L.; Cortés-Salazar, F.; Lesch, A.; Wittstock, G.; Girault, H. H. *Anal. Chem.* **2012**, *84*, 6630–6637.
- (24) Cortés-Salazar, F.; Lesch, A.; Momotenko, D.; Busnel, J.-M.; Wittstock, G.; Girault, H. H. *Anal. Methods* **2010**, *2*, 817.
- (25) Momotenko, D.; Cortés-Salazar, F.; Lesch, A.; Wittstock, G.; Girault, H. H. *Anal. Chem.* **2011**, *83*, 5275–5282.
- (26) Zoccarato, F.; Cavallini, L.; Alexandre, A. *J. Neurochem.* **1999**, *72*, 625–633.
- (27) Kapuscinski, J.; Darzynkiewicz, Z. *J. Biomol. Struct. Dyn.* **1987**, *5*, 127–143.
- (28) Lyles, M. B.; Cameron, I. L. *Biophys. Chem.* **2002**, *96*, 53–76.
- (29) Han, J.; Burgess, K. *Chem. Rev.* **2010**, *110*, 2709–2728.
- (30) Cannan, S.; Douglas Macklam, I.; Unwin, P. R. *Electrochem. commun.* **2002**, *4*, 886–892.
- (31) Borgwarth, K.; Heinze, J. **1999**, *146*, 3285–3289.



# CHAPTER V

## The Intact Cell MALDI-MS of Melanoma

### Abstract

Mass-spectrometry (MS) combined with different separation techniques is an attractive and widely used tool for mammalian cells protein identification and thus for the discovery of possible new cancer biomarkers. However, complete cell proteome identification stays a complicated and time-consuming procedure. Alternatively, the MS analysis of the intact cells by matrix-assisted laser adsorption/ionisation MS (MALDI-MS) can be employed in order to obtain the cells MS fingerprints (*i.e.* the number of characteristic peaks) which can be further used for cell lines characterisation and identification. The ability to follow high-abundant cellular moieties, as well as, the requirement of the minimal sample preparation makes this approach attractive for fast screening of potential cancer biomarkers.

Herein, the intact cell MALDI-MS protocol for the characterization of mammalian melanoma cancer cell lines from different tumour progression stages is presented. To perform the MALDI-MS assay, melanoma cells were cultured on a flat and thin aluminium foil, which was directly transferred to the target plate for the analysis. The influence of a wide range of cells fixation protocols (*i.e.* formalin-based and alcohol-based methods) and MALDI matrices on the obtained characteristic spectra was investigated. For the optimization of the MALDI-MS analysis, the MS fingerprints of melanoma WM-239 cell line with and without an overexpressed enhanced green fluorescent protein was employed. The optimized protocol was further applied to characterise melanoma cell lines derived from different cancer stages, *i.e.* radial growth phase (Sbcl2), vertical growth phase (WM-115) and metastatic (WM-239) cells. This simple approach allowed identification of unique MS signals that can be used for the differentiation between the studied cell lines (*i.e.* molecular weight equal to 10.0 kDa and 26.1 kDa). Comparison of the obtained results with previously published proteomic characterisation of melanoma cells suggests that one of this MS peaks corresponds to the trans-membrane protein V-ATPase B2 (molecular weight equal to 26.1 kDa), which is a possible marker for melanoma progression.

## 1. Introduction

Mammalian cells cultured *in vitro* been widely employed in medicine and biology as a simple model of complex living organisms to develop new strategies of diagnostic and treatment of different diseases.<sup>1-4</sup> With this aim various approaches to characterize cells have been developed based on chemical sensing, optical microscopy and mass-spectrometry (MS).<sup>5-9</sup> In comparison with other strategies, MS is a label free technique where the analytical signal depends on the molecular weight and charge of the analysed species after ionization. Typically, MS experiments for the characterization of *in vitro* cultured cells include cell lysis followed by the MS analysis of the obtained extract with or without enzymatic protein cleavage.<sup>10</sup> However, the full cell proteome analysis is very challenging and therefore, MS is often combined with separation techniques, *i.e.* electrophoresis or liquid chromatography.<sup>11</sup> To ionize cellular constituents without fragmentation, soft ionization techniques, *e.g.* electrospray ionization (ESI)<sup>12</sup> and matrix-assisted laser desorption/ionization (MALDI)<sup>13,14</sup> are widely used.<sup>15-18</sup> Although these methods allow the detection and identification of a wide range of intracellular proteins with high sensitivity, they are complex and time-consuming.

Another approach for the analysis of *in vitro* cultured mammalian cells is the intact-cell analysis, typically performed by MALDI-MS. In this case cells can be either grown directly on a MALDI target plate<sup>19</sup> or collected by centrifugation after culturing in a classical Petri dish.<sup>11,20-23</sup> The latter allows cell pellets to be either transferred directly to the target plate, where they are dried and covered with a matrix solution,<sup>22</sup> or mixed with a matrix solution prior to the transfer.<sup>20,21,23</sup> As a result, instead of individual protein peaks, a number of signals representing the MS fingerprint characteristic for a specific cell type or physiological state can be obtained.<sup>11</sup> This approach has been successfully applied for the identification of two different pancreatic cell lines,<sup>22</sup> the differentiation between stimulated and non-stimulated macrophages,<sup>20</sup> the prediction of mammalian cell phenotypes<sup>21</sup> and the characterization of neural cell types.<sup>23</sup> Moreover, it was reported that the analysis of on-target-grown cells resulted in mass spectra of higher peak intensity in comparison to whole cells placed on top of a matrix layer and with cellular extracts analysed using the conventional sample-matrix mixture technique.<sup>19</sup> However, it is important to note, that when culturing cells directly on MALDI target plates the surface can be contaminated with high concentrations of salts present in the culturing medium, which negatively influence the ionization efficiency. Furthermore, direct sample washing with deionized water becomes difficult due to the strong osmotic pressure. In previous studies, this problem was solved by chemical fixation of cells,<sup>24</sup>

which is a well-established method in cell biology, histology and MALDI-MS imaging of tissues<sup>25–27</sup> and cells.<sup>28–30</sup> Cells, treated in such a way can be further washed without losing any intracellular protein content.

Herein, we present an intact cell MALDI-MS protocol for characterizing differences in the high-abundant protein content of human melanoma cells derived from different cancer stages. With this aim, cells were grown *in vitro* and chemically fixed on a flat and thin aluminium foil, which was directly transferred to the MALDI target plate for the MS analysis. As a proof of concept and for optimization of the sample preparation, MS fingerprints of the melanoma WM-239 cell line with and without a recombinantly overexpressed enhanced green fluorescent protein (EGFP) were recorded. Different chemical fixatives including cross-linkers (i.e. paraformaldehyde and paraformaldehyde-methanol) and dehydrators (i.e. methanol, methanol-acetone and methanol-ethanol) were tested and compared to the non-fixed cell samples. The optimized protocol was subsequently applied to investigate mass spectra differences between three melanoma cell lines, *i.e.* Sbc12, WM-115 and WM-239 corresponding to the radial growth phase (RGP), vertical growth phase (VGP) and metastatic melanoma stages, respectively.

## 2. Materials and methods

### 2.1. Chemicals

Trifluoroacetic acid (TFA) (99.0%) was obtained from Acros Organics (New Jersey, USA). Cytochrome C (CytC), trypsin, 2,5-dihydroxybenzoic acid (DHB), -cyano-4-hydroxycinnamic acid (HCCA) and sinapic acid (SA) were purchased from Sigma-Aldrich (St. Gallen, Switzerland). Methanol, acetone, ethanol and acetonitrile were obtained from Merck (Dietikon, Switzerland) and formaldehyde solution (4% in PBS) was from AlfaAesar (Karlsruhe, Germany). Deionized water was produced by Alpha Q Millipore system (Zug, Switzerland).

The matrices contained 10 mg/mL of SA, 10 mg/mL of DHB or 10 mg/mL of HCCA were prepared in the solution containing 70% of acetonitrile, 29.9% of water and 0.1% of TFA in terms of v/v.

WM-239, WM-115 and Sbc12 human melanoma cell lines were purchased from the American Type Culture Collection (ATCC).

## 2.2. Cell culture preparation

Human melanoma cell lines WM-239, WM-115, and Sbc12 as well as WM-239 with overexpressed EGFP protein were cultured in Dulbecco's modified Eagle's medium (Gibco Life Technologies, Basel, Switzerland), supplemented with 10% fetal calf serum at 37 °C in humidified atmosphere with 5% CO<sub>2</sub>. Twenty hours before an experiment, 200 µL of cell suspension were plated on a sterile aluminium foil (~ 1 cm wide and ~ 2 cm long) and incubated during 4 hours for attachment on the surface (37 °C, 5% CO<sub>2</sub>). Finally, 2 mL of medium was gently added into the system and cells were incubated overnight before starting the experiment (37 °C, 5% CO<sub>2</sub>). In order to obtain WM-239 cells with overexpressed EGFP, transient transfection was performed by using Lipofectamine 2000 (Invitrogen, Basel, Switzerland). Twenty hours before transfection WM-239 cells were split in 75 cm<sup>2</sup> T-flask (TPP, Trasadingen, Switzerland) reaching 80% confluence. The transfection mixture was obtained by mixing 24 µg of EGFP-N1 plasmid DNA (Clontech, Basel, Switzerland) in 1.5 mL of OptiMEM medium (Gibco Life Technologies, Basel, Switzerland) and 60 µL of Lipofectamine 2000 reagent in 1.5 mL of OptiMEM medium. After 20 min of incubation at room temperature (RT) the transfection mixture was added to the cells. The transfection efficiency calculated at 20 h after transfection was approximately 80%.

## 2.3. Fixation protocols

To fix cells with dehydrating agents the aluminium foil with adherent cells was submerged for 5 – 7 min in the cooled down (–20 °C) solution of pure methanol (methanol protocol), methanol/acetone (50%/50% v/v, methanol-acetone protocol) and methanol/ethanol (50%/50% v/v, methanol-ethanol protocol). Cross-linking fixation was performed by placing the aluminium foil inside an ice-cold 4% formaldehyde solution for 15 min (formaldehyde protocol). To permeabilize cells fixed with formaldehyde, the foil was additionally placed for 10 min into methanol cooled down to –20°C (formaldehyde-methanol protocol). Thereafter, all fixed samples were washed with deionized water for 5 min and finally dried at RT. In order to obtain the non-fixed samples adherent cells grown on aluminium foil were placed into the deionized water for 5 s and then dried at RT.

## 2.4. MALDI experiments

Protein mass fingerprints of melanoma cells were obtained by a Microflex MALDI-TOF instrument (Bruker Daltonics, Bremen, Germany) operated in a positive linear ion mode. Before each experiment, the samples on aluminium foil were positioned on a MALDI target

plate by using a double-side tape and flattened by pressing it with a microscopic glass slide. Thereafter, 1  $\mu\text{L}$  of CytC calibration solution was positioned into each aluminium foil in a cell-free region and dried at RT. Finally, 1  $\mu\text{L}$  of the matrix solution was deposited over the cells and the calibration spots and crystallized at RT. Calibration of the instrument was performed separately for each cells-on-aluminium sample based on CytC analytical signal,  $(\text{M}+\text{H})^+$  and  $(\text{M}+2\text{H})^{2+}$ . An average cell spectrum was collected from 500 random laser shots at 20 Hz laser frequency. The instrumental parameters were fixed as following: laser attenuator – 90% within the range of 30% to 70% laser intensity; delayed ion extraction time – 400 ns; detector gain – 19.4 $\times$ ; electronic gain – enhanced (100 mV). The ion source voltages were at the default values optimized by Bruker: ion source 1 – 20.0 kV; ion source 2 – 18.5 kV; lens – 8.5 kV. The MS spectra were analysed by mMass - Open Source Mass Spectrometry Tool ([www.mmass.org](http://www.mmass.org)). Peaks with  $\text{S/N} \geq 3$  were considered as significant. A tolerance of 500 ppm was set for identical peaks.

### 3. Results and discussion

The intact cell MALDI-MS approach is a simple method that allows distinguishing differences in the mass spectra of distinct cell types without the need of performing the full proteome identification. Whole cell fingerprints cannot only be employed to differentiate among various cells but also to detect abnormal protein expression patterns indicative of cancer development. Sample preparation for the intact cell MALDI-MS typically involves only washing of cells which are directly cultured on the target plate, as it was presented by *Bergquist et al.*<sup>19</sup> The main limitations of this strategy are related to the MALDI plate contamination, and the large consumption of reagents due to the MALDI target plate size. To overcome these problems, we herein demonstrate for the first time the concept of growing cells on a disposable thin aluminium foil for MALDI-MS experiments. Previously the aluminium foil layer has been shown as an ideal disposable substrate for MALDI MS presenting a good sensitivity for the detection of proteins and peptides.<sup>31</sup> However, this approach has thus far not yet been applied for whole cell analysis. In contrast to the on-plate cells culturing, growing mammalian cells on a disposable thin aluminium foil requires smaller amount of both cells and growth medium, and allows working with different cells types simultaneously by placing few samples on the same target plate. Furthermore, adherent cells grown on aluminium foil can be easily transferred between various solutions (*e.g.* washing and fixation solutions). However, it is of note to mention that positioning the aluminium foil on the MALDI target plate changes the distance that ions have to pass in the time-of-flight

(TOF) MS analyser, and thus the energy obtained by the ions from the extraction/acceleration electric fields. Therefore, the MALDI-TOF-MS instrument has to be calibrated for each experiment, *e.g.* by analysing a spot of CytC positioned on the same aluminium foil.

An important step for MALDI-MS experiments is the optimization of the sample ionization, which can be significantly influenced by *i)* the applied MALDI matrix, *ii)* the presence of salts in the sample and *iii)* the application of organic solvents. With the aim to optimize the ionization process of adherent cells deposited on aluminium foils, the MS-spectra of genetically modified WM-239 cells to overexpress the EGFP (M = 26.9 kDa) were collected for several matrices combinations (*i.e.* SA, DHB and HCCA) and cell fixation protocols (*i.e.* formaldehyde, formaldehyde-methanol, methanol, methanol-acetone and methanol-ethanol). Additionally, non-fixed cells directly washed with deionized water were also analysed by MALDI-MS (Figure 5.1). As it was discussed in Chapter I, fixation procedures will trap proteins, lipids and carbohydrates in a matrix of insoluble proteins and therefore, allow to immobilize cells on the surface and wash them in order to remove salts present in the grow medium without risk of sample destruction. In contrast, washing of alive cells should be performed fast and gently in order to minimise detaching and destroying of cells that can lead to loss of intracellular information. Still, fixation solutions can affect drastically the final ionization efficiency and therefore, the most widely used fixation solutions were tested in order to determine the optimal one for the intact cells MALDI-MS.

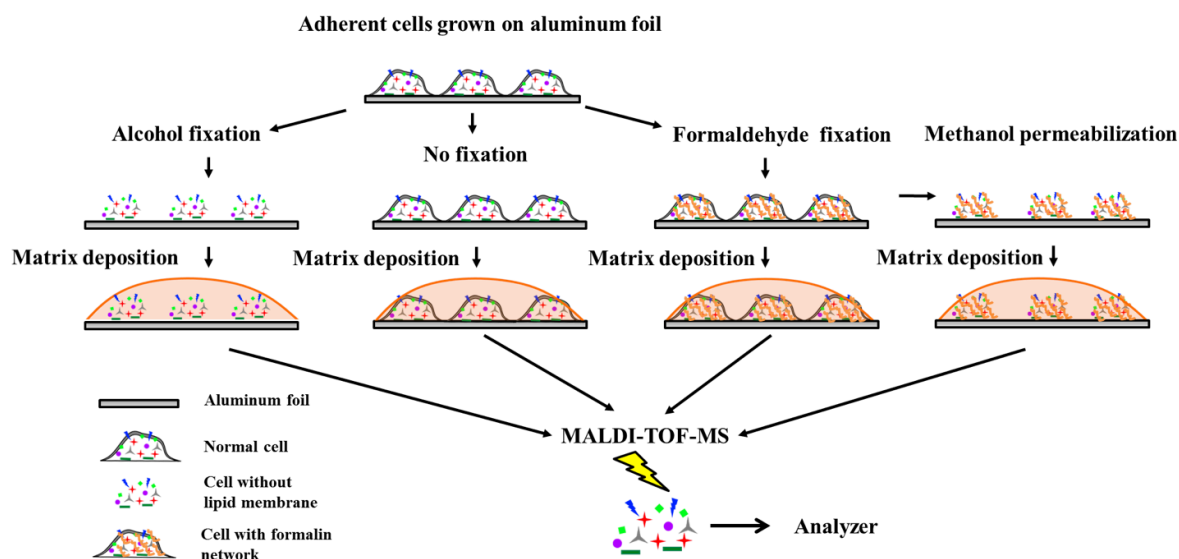


Figure 5.1. Schematic representation of different sample preparation protocols applied for MALDI-MS analysis of mammalian cells grown on disposable aluminium foils.

As it can be seen from the spectra collected for different matrix and fixation combinations (Figure 5.2 and Appendix I), independently on the fixation method when

HCCA or DHB matrices are applied no ionization of molecules with molecular weight higher than 15 kDa was observed (Figure 5.2 columns 2 and 3). Additionally, poor ionization efficiency was also obtained when DHB matrix was used (Figure 5.2 column 2, Appendix I column 2), *i.e.* the highest number of peaks of most of the observed signals was observed when analysing methanol and methanol-acetone fixed samples and was equal to 20. In contrast, SA matrix showed both the highest ionization efficiency and number of detected species within the  $m/z$  range from 4 to 40 kDa (Figure 5.2 column 1), *i.e.* up to 50 well resolved peaks can be distinguished depending on the fixation protocol.

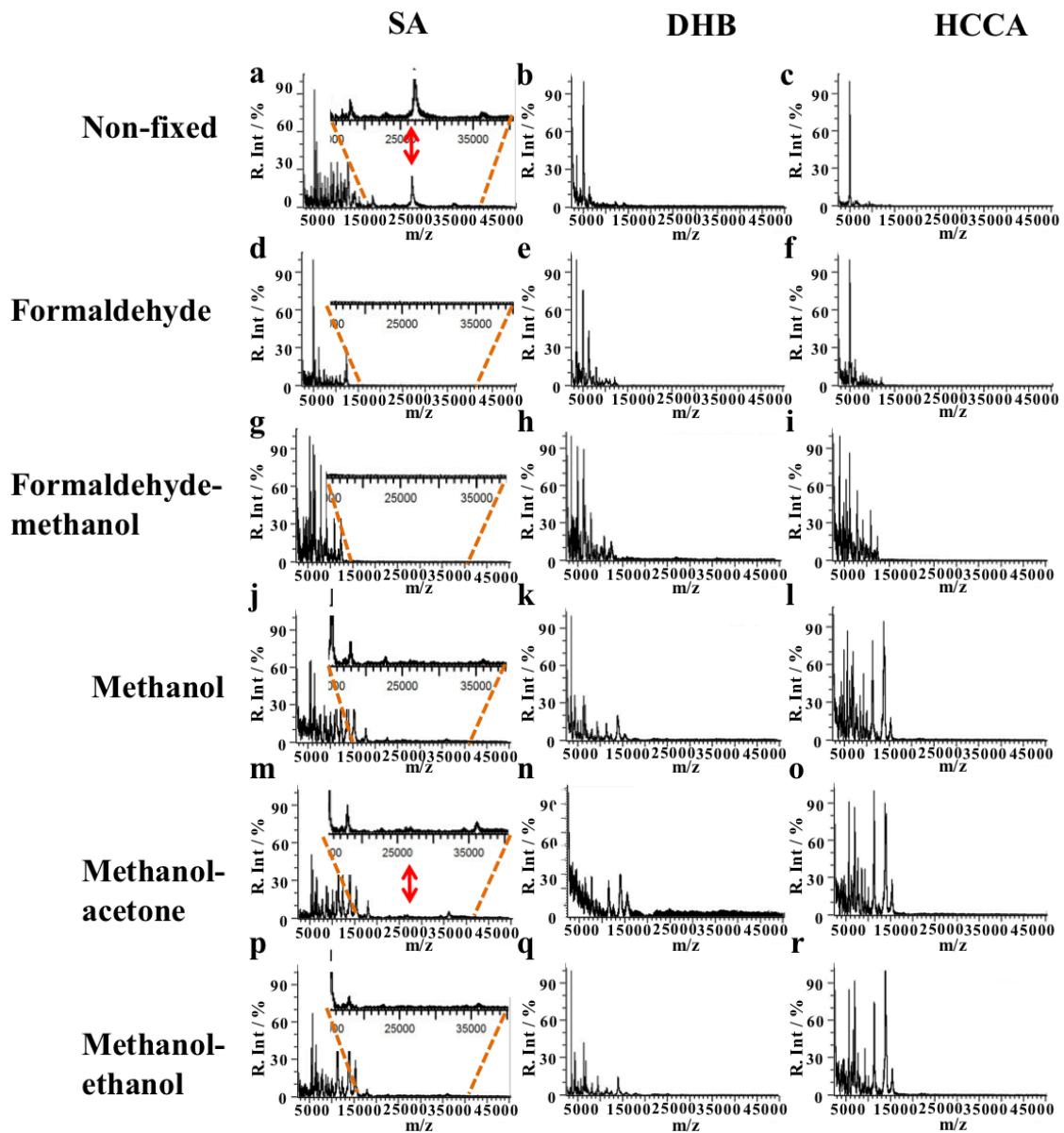


Figure 5.2. Optimization of MALDI matrices and cells fixation protocols for obtaining characteristic MS fingerprints of WM-239 melanoma cell lines with an overexpressed EGFP protein. MALDI matrices were SA (a, d, g, j, m and p), DHB (b, e, h, k, n and q) and HCCA (c, f, i, l, o and r). Fixation protocols were: non-fixed cells (a – c), formaldehyde (d – f), formaldehyde-methanol (g – i), methanol (j – l), methanol-acetone (m – o) and methanol-ethanol (p – r).

Indeed, the fixation protocols present a significant influence on the obtained results. For instance, formaldehyde fixation with and without permeabilization were not suitable for the detection of molecules with molecular weight higher than 15 kDa (Figure 5.2 d and g), while all types of alcohol fixation (Figures 5.2 j, m and p) and the non-fixed samples (Figure 5.2 a) allowed the detection of species within the 25000 – 40000 Da  $m/z$  range. The latter is due to the different nature of the formaldehyde and alcohol fixation, *i.e.* chemical cross-linking and physical precipitation, respectively. Moreover, when working with formaldehyde fixed cells, the molecular weight of the cross-linked proteins might be too high and its concentration too low to be detected by MALDI-MS.

It is also worth to notice that the overexpressed EGFP protein was detected only when the non-fixed and the methanol-acetone permeabilized cells were analysed (Figure 5.2 red arrows). Despite the highest EGFP peak intensity is observed with the non-fixed sample, the reproducibility of the signal becomes an issue when the cells are not fixed.

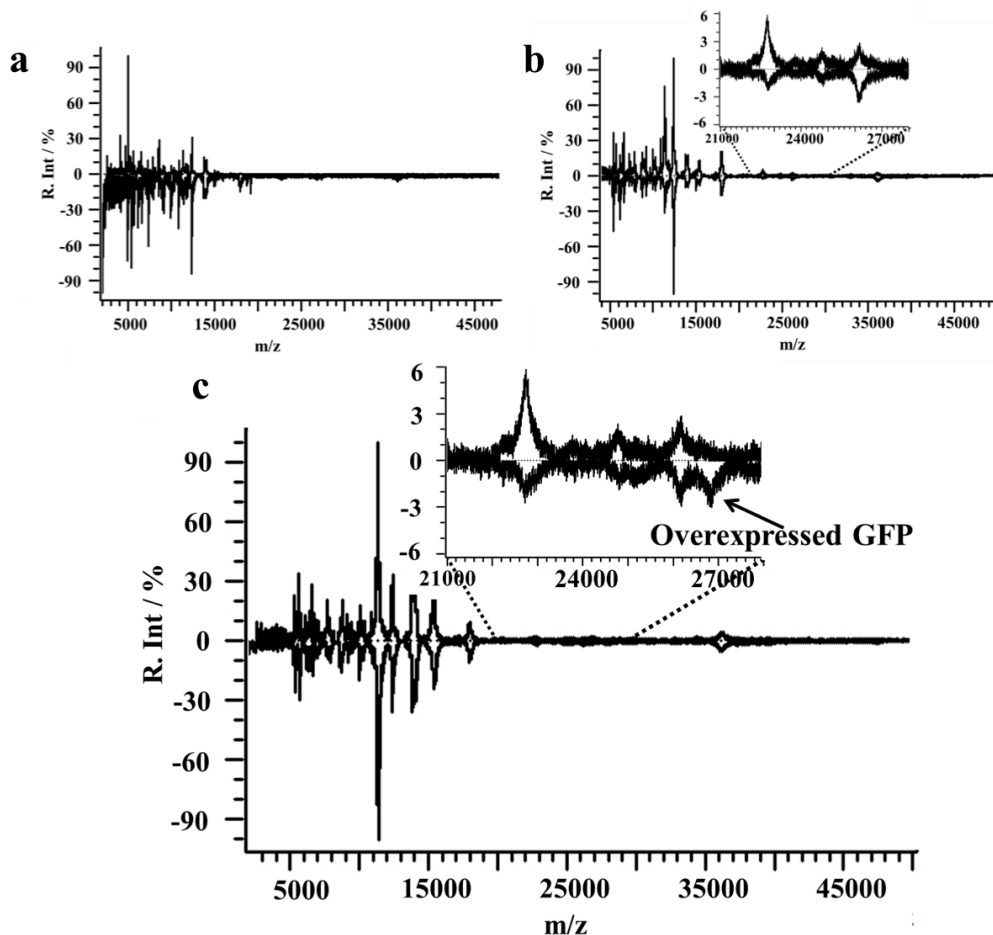


Figure 5.3. Reproducibility of the MS spectra obtained for non-fixed (a) and methanol-acetone fixed (b) cells. The upper and lower spectra represent MALDI-MS results for 2 samples prepared in the same way (*i.e.* culturing conditions, fixation and washing). SA was employed as MALDI matrix. Characteristic MALDI-MS fingerprints of WM-239 cells without (upper spectrum) and with (lower spectrum) the overexpressed EGFP in the optimized conditions (*i.e.* methanol-acetone fixation protocol and SA MALDI matrix) are presented in (c).



Indeed, the MALDI-MS fingerprints obtained from a set of non-fixed WM-239 cells-on-aluminium samples showed significant differences in the ionization efficiency and MS spectra (Figure 5.3a). Thus, only 22 well-resolved peaks with  $S/N \geq 3$  can be distinguished on the upper spectrum in Figure 5.3a, while 37 peaks are presented on the lower one. The latter can be explained by the strong influence of the salts present in the analysed sample and the irreproducibility on the cells washing step due to the time-restrictions when working with alive cells. At the same time, alcohol fixation procedure leads to a good reproducibility of 45 resolved peaks with a signal to noise ratio equal or higher than 3 in all collected spectra (Figure 5.3b). Therefore, the intact cell MALDI-MS of samples pretreated with a methanol-acetone solution can be compared in a more reliable way.

The intact cell MALDI-MS fingerprints of WM-239 cell line with and without overexpressed EGFP are presented in Figure 5.3c. An additional peak corresponding to a molecular weight equal to 26.9 kDa with a 3% relative abundance can be clearly detected, confirming the potential ability of the suggested approach to detect differences in the intracellular proteins profiles.

The optimized protocol for the intact cell MALDI-MS on aluminium foil was further applied to characterize three melanoma cell lines, *i.e.* Sbc12, WM-115 and WM-239 derived from RGP, VGP and metastatic melanomas, respectively. The obtained spectra are presented in pairs (*i.e.* Sbc12 vs WM-115, Sbc12 vs WM-239) for an easier comparison of the protein profiles (see Figure 5.4).

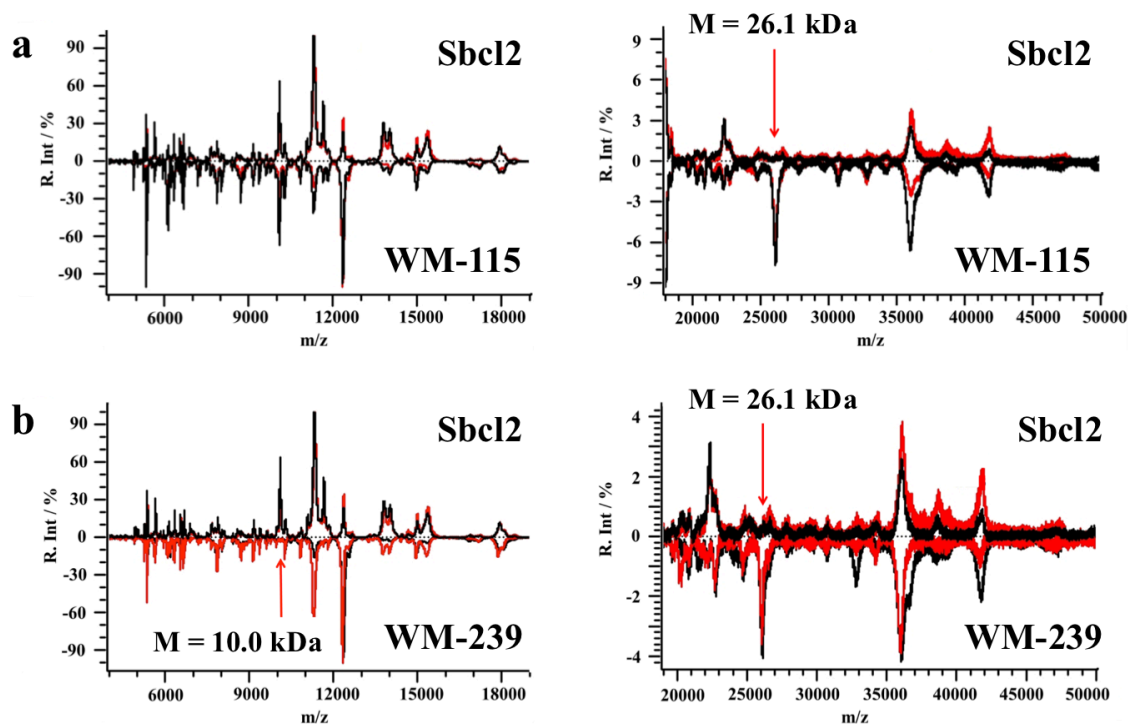


Figure 5.4. The characteristic MALDI-MS fingerprint spectra obtained for Sbc12, WM-115 and WM-239 melanoma cell lines representing cancer progression (RGP, VGP and metastatic, respectively). For better visualisation of the obtained MS spectra, the obtained full spectra are separated in 2 (i.e.  $m/z$  intervals from 5 to 19k and from 19 to 50k), and data are presented as the following pairs: Sbc12 vs WM-115 (a and b) and Sbc12 vs WM-239 (c and d). Two independently collected MS spectra of the same cell line sample (but from different spot) are presented in black and red colour, respectively. Experimental conditions: methanol/acetone fixation, SA matrix.

The obtained MALDI-MS fingerprints were highly reproducible independently on the cell line that is demonstrated by the good overlapping between the MS spectra collected for the same cell line, but at a different region of the same studied sample (black and red continuous lines). All melanoma cell lines presented a very similar peak distribution except for 2 peaks of  $m/z$  ratio equal to 10.0 kDa and 26.1 kDa (the full list of the resolved peaks for each cell line is presented in Appendix II). Interestingly, the  $m/z$  equal to 10.0 kDa was only detected in the primary melanoma stages (i.e. RGP and VGP), but not in metastatic one (Figure 5.4 a and c). Furthermore, the signal of 26.1 kDa  $m/z$  was absent only in the RGP stage.

The comparison of the results obtained in this work with previously published characterisation of melanoma cell lines showed similar results. Thus, northern blot analysis presented a significant expression of the S100 family proteins mRNAs in the primary melanoma stages (i.e. Sbc12 and WM-115), while a lower level was detected in the metastatic WM-239 cell line.<sup>31</sup> The molecular weight of S100 proteins is 10 kDa which correlates to the characteristic MS peak with  $m/z$  equal to 10.0 kDa. In its turn, the 26.1 kDa peak could be the

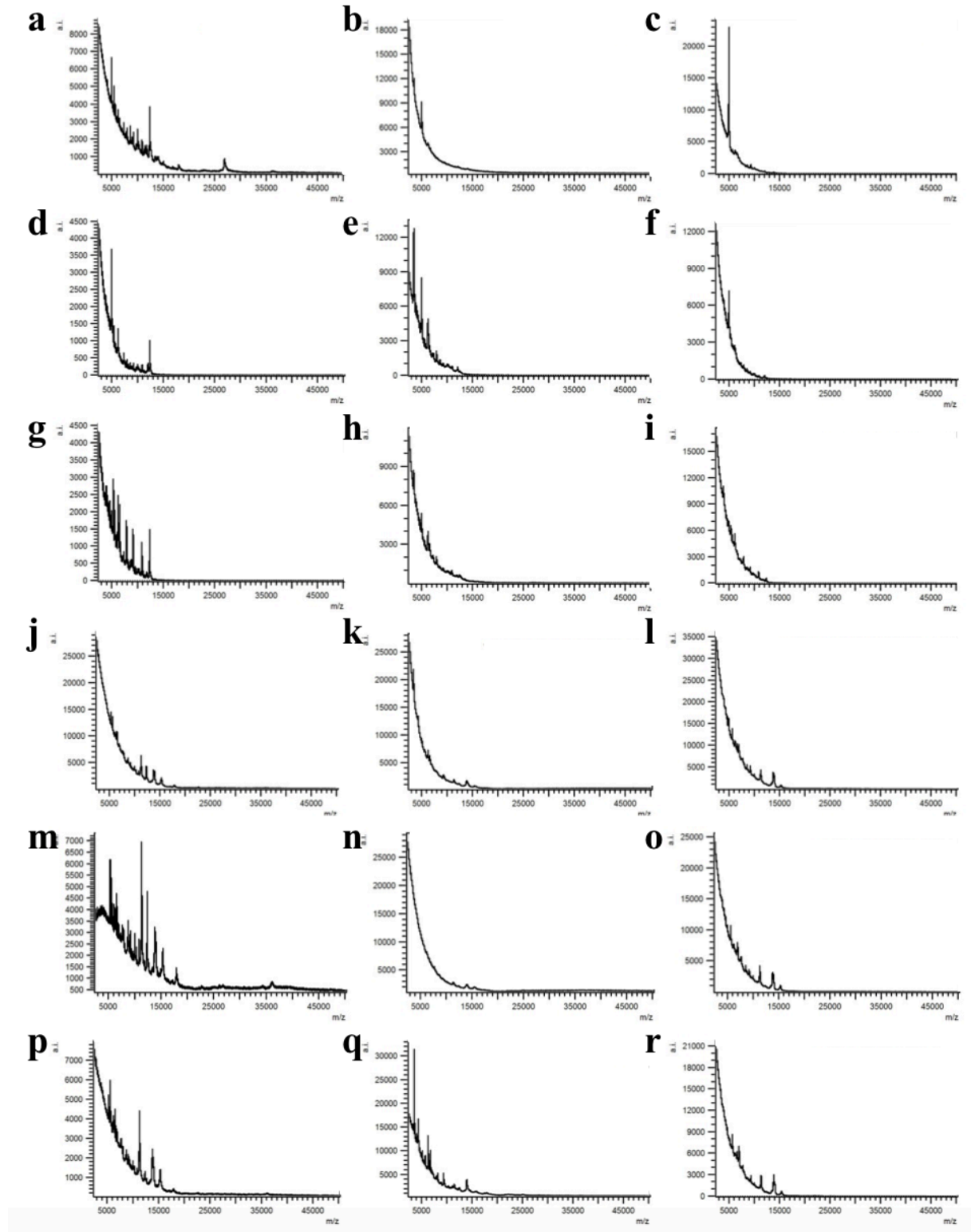
trans-membrane protein so-called V-ATPase B2 identified by *Baruthio et al.* by liquid chromatography coupled to MS/MS in the late primary and metastatic cancer stages (*i.e.* WM-115 and WM-239), but not in the early tumour cells (*i.e.* Sbc12) and which was suggested as a potential cancer progression biomarker.<sup>32</sup> The ability to follow its expression by the intact cell MALDI-MS approach was first time presented in this work and can be beneficial for establishing the aggressiveness of melanoma cells due to the simplicity and much shorter time of the assay in comparison with full MS proteomics. Additionally, the intact cell MALDI-MS can be a useful tool for searching new biomarkers which can be further directly detected in tissues without any special pre-treatment.

#### **4. Conclusions**

A fast and simple intact cell MALDI-MS approach was successfully implemented as a tool for fast screening of highly abundant cell biomarkers. For this purpose, cells were cultured on disposable aluminium foils which allowed direct transfer of different adherent cell lines to the MALDI target plate for their consecutive analysis. The influence of a wide range of cells fixation protocols (*i.e.* formalin-based and alcohol-based methods) as well as the MALDI matrices on the obtained characteristic spectra was investigated. Optimization of the intact cell MALDI-MS protocol was performed based on the MS fingerprints of the melanoma WM-239 cell line with and without overexpression of EGFP (molecular weight equal to 26.9 kDa). It was found that the methanol-acetone fixation protocol coupled with the use of SA matrix allowed the reliable and reproducible detection of the overexpressed EGFP protein. The optimized protocol was further applied to differentiate melanoma cell lines derived from different cancer stages, *i.e.* RGP, VGP and metastatic cells. This simple approach allowed the identification of different signals only present on the earlier or latest melanoma stages, which can be used for their clear differentiation. Comparison of the obtained results with previously published reports of melanoma cells suggested that one of the unique observed peaks could be the trans-membrane protein V-ATPase B2 (molecular weight equal to 26.1 kDa), a possible marker of melanoma tumour progression. Identification of cancer biomarkers which can be directly detected by MALDI-MS can be important for further fast cancer diagnosis.

**Appendix I**

Optimization of MALDI matrices and cells fixation protocols for obtaining characteristic fingerprints of WM-239 melanoma cell line with an overexpressed EGFP protein. MALDI matrices were SA (a, d, g, j, m and p), DHB (b, e, h, k, n and q) and HCCA (c, f, i, l, o and r). Fixation protocols were: non-fixed cells (a – c), formaldehyde (d – f), formaldehyde-methanol (g – i), methanol (j – l), methanol-acetone (m – o) and methanol-ethanol (p – r).



**Appendix II**The full list of the resolved peaks ( $S/N \geq 3$ ) obtained for melanoma cells by the intact cell MALDI

<b>Sbcl2, <math>m/z</math> / kDa</b>	<b>WM-115, <math>m/z</math> / kDa</b>	<b>WM-239, <math>m/z</math> / kDa</b>
5,27	5,27	5,27
5,36	5,36	5,36
5,65	5,65	5,65
5,95	5,95	5,95
6,09	6,09	6,09
6,13	6,13	6,13
6,18	6,18	6,18
6,57	6,57	6,57
6,67	6,67	6,67
6,73	6,73	6,73
6,89	6,89	6,89
7,14	7,14	7,14
7,18	7,18	7,18
7,27	7,27	7,27
7,38	7,38	7,38
7,5	7,5	7,5
7,65	7,65	7,65
7,87	7,87	7,87
8,02	8,02	8,02
8,41	8,41	8,41
8,58	8,58	8,58
8,67	8,67	8,67
8,72	8,72	8,72
8,83	8,83	8,83
8,95	8,95	8,95
9,15	9,15	9,15
9,37	9,37	9,37
9,63	9,63	9,63
9,77	9,77	9,77
9,98	9,98	9,98
<b><u>10,01</u></b>	<b><u>10,01</u></b>	
10,28	10,28	10,28
10,84	10,84	10,84
11,06	11,06	11,06
11,34	11,34	11,34
11,66	11,66	11,66
11,82	11,82	11,82
12,35	12,35	12,35
14,04	14,04	14,04
14,97	14,97	14,97
15,36	15,36	15,36
17,2	17,2	17,2
17,95	17,95	17,95
22,7	22,7	22,7
	<b><u>26,11</u></b>	<b><u>26,11</u></b>
36,1	36,1	36,1

## 5. References

- (1) Gerecht-Nir, S.; Ziskind, A.; Cohen, S.; Itskovitz-Eldor, J. *Lab. Investig.* **2003**, *83*, 1811–1820.
- (2) Muruganandam, A.; Herx, L.; Monette, R.; Durkin, J.; Stanimirovic, D. *FASEB J* **1997**, *11*, 1187–1197.
- (3) Romano, B.; Pagano, E.; Montanaro, V.; Fortunato, A. L.; Milic, N.; Borrelli, F. *Phyther. Res.* **2013**, *27*, 1588–1596.
- (4) De Clercq, E. *Curr. Opin. Microbiol.* **2005**, *8*, 552–560.
- (5) Giaever, I.; Keese, C. R. *Nature* **1993**, *363*, 591–592.
- (6) Pemberton, R. M.; Cox, T.; Tuffin, R.; Drago, G. A.; Griffiths, J.; Pittson, R.; Johnson, G.; Xu, J.; Sage, I. C.; Davies, R.; Jackson, S. K.; Kenna, G.; Luxton, R.; Hart, J. P. *Sensors* **2014**, *14*, 20519–20532.
- (7) Fan, Y.; Chen, Z.; Ai, H.-W. *Anal. Chem.* **2015**, *87*, 2802–2810.
- (8) Ulber, R.; Frerichs, J. G.; Beutel, S. *Anal. Bioanal. Chem.* **2003**, *376*, 342–348.
- (9) Janshoff, A.; Galla, H. J.; Steinem, C. *Angew. Chemie - Int. Ed.* **2000**, *39*, 4004–4032.
- (10) Fenn, J. B.; Mann, M.; Meng, C. K.; Wong, S. F.; Whitehouse, C. M. *Science* **1989**, *246*, 64–71.
- (11) Tanaka, K.; Waki, H.; Ido, Y.; Akita, S.; Yoshida, Y.; Yoshida, T.; Matsuo, T. *Rapid Commun. Mass Spectrom.* **1988**, *2*, 151–153.
- (12) Karas, M.; Bachmann, D.; Hillenkamp, F. *Anal. Chem.* **1985**, *57*, 2935–2939.
- (13) Winston, R. L.; Fitzgerald, M. C. *Mass Spectrom. Rev.* **1998**, *16*, 165–179.
- (14) Murphy, R. C.; Hankin, J. A.; Barkley, R. M. *J. Lipid Res.* **2009**, *50 Suppl*, S317–S322.
- (15) Mann, M.; Hendrickson, R. C.; Pandey, A. *Annu. Rev. Biochem.* **2001**, *70*, 437–473.
- (16) Lay, J. O. *Mass Spectrom. Rev.* **2001**, *20*, 172–194.
- (17) Merlos Rodrigo, M. A.; Zitka, O.; Krizkova, S.; Moulick, A.; Adam, V.; Kizek, R. *J. Pharm. Biomed. Anal.* **2014**, *95*, 245–255.
- (18) Dalluge, J. J. *Fresenius. J. Anal. Chem.* **2000**, *366*, 701–711.
- (19) Bergquist, J. *Chromatogr. Suppl. I* **1999**, *49*, S41–S48.
- (20) Ouedraogo, R.; Daumas, A.; Ghigo, E.; Capo, C.; Mege, J. L.; Textoris, J. *J. Proteomics* **2012**, *75*, 5523–5532.
- (21) Povey, J. F.; O'Malley, C. J.; Root, T.; Martin, E. B.; Montague, G. A.; Feary, M.; Trim, C.; Lang, D. A.; Alldread, R.; Racher, A. J.; Smales, C. M. *J. Biotechnol.* **2014**, *184*, 84–93.
- (22) Buchanan, C. M.; Malik, A. S.; Cooper, G. J. S. *Rapid Commun. Mass Spectrom.* **2007**, *21*, 3452–3458.

- (23) Hanrieder, J.; Wicher, G.; Bergquist, J.; Andersson, M.; Fex-Svenningsen, Å. *Anal. Bioanal. Chem.* **2011**, *401*, 135–147.
- (24) Brock, R.; Hamelers, I. H. L.; Jovin, T. M. *Cytometry* **1999**, *35*, 353–362.
- (25) Seeley, E. H.; Oppenheimer, S. R.; Mi, D.; Chaurand, P.; Caprioli, R. M. *J. Am. Soc. Mass Spectrom.* **2008**, *19*, 1069–1077.
- (26) Lemaire, R.; Wisztorski, M.; Desmons, A.; Tabet, J. C.; Day, R.; Salzet, M.; Fournier, I. *Anal. Chem.* **2006**, *78*, 7145–7153.
- (27) Agar, N. Y. R.; Yang, H. W.; Carroll, R. S.; Black, P. M.; Agar, J. N. *Anal. Chem.* **2007**, *79*, 7416–7423.
- (28) Bouschen, W.; Schulz, O.; Eikel, D.; Spengler, B. *Rapid Commun. Mass Spectrom.* **2010**, *24*, 355–364.
- (29) Zavalin, A.; Todd, E. M.; Rawhouser, P. D.; Yang, J.; Norris, J. L.; Caprioli, R. M. *J. Mass Spectrom.* **2012**, *47*, 1473–1481.
- (30) Altelaar, A. F. M.; Klinkert, I.; Jalink, K.; De Lange, R. P. J.; Adan, R. A. H.; Heeren, R. M. A.; Piersma, S. R. *Anal. Chem.* **2006**, *78*, 734–742.
- (31) Maelandsmo, G. M.; Flørenes, V. A.; Mellingsaeter, T.; Hovig, E.; Kerbel, R. S.; Fodstad, O. *Int. J. cancer* **1997**, *74*, 464–469.
- (32) Baruthio, F.; Quadroni, M.; Rüegg, C.; Mariotti, A. *Proteomics* **2008**, *8*, 4733–4747.





# CHAPTER VI

## Inkjet Printed Carbon Nanotubes Based Multiplexed Electrochemical Sensor for Environmental and Clinical Applications

*The Chapter has been done as a part of the project with Bürkert Fluid Control Systems (Triembach au val, France)*

### Abstract

In this chapter a fast, simple and cost-efficient way of manufacturing multiplexed electrochemical sensors that enables the reproducible implementation of a broad spectrum of immunoassays with amperometric detection is presented. The multiplexed sensor device consists of 16 independent electrochemical cells fabricated by sequential inkjet printing (IJP) of silver, carbon nanotubes (CNTs) and an insulator on a polyimide substrate. The manufacturing process is completed by mounting plastic wells on top of the inkjet printed patterns to obtain a 16-well microchip. Each well of the microchip has a volume capacity of 50  $\mu\text{L}$  and represents an electrochemical cell composed by stand-alone CNTs working electrode, an Ag reference/counter electrode and an insulating layer that precisely defines the working electrode surface area. The IJP microchip presented a highly reproducible response among the individual wells (4.5% of deviation) due to the accuracy of the IJP process and fast electrode kinetics achieved at the CNTs working electrodes. The IJP microchip was implemented as a detection platform for different magnetic beads-based immunoassay formats, namely, competitive enzyme immunoassay (for atrazine (ATR) detection in water), sandwich enzyme immunoassay (for thyroid-stimulating hormone (TSH) detection in urine) and label-free non-competitive immunoassay (for *Escherichia coli* (*E. coli*) detection in water). Indeed, the achieved limits of detection for ATR (*i.e.* 0.05  $\mu\text{g/L}$ ), TSH (*i.e.* 0.5 mUI/L) and viable *E. coli* ( $10^6$  cells/mL) demonstrated the potential of the IJP microchips for environmental and biological quantification of various compounds in a very reliable, portable and high throughput platform.

## 1. Introduction

Carbon nanotubes (CNTs) discovered in 1991<sup>1</sup> represent an ideal and perfectly ordered carbon network with  $sp^2$ -hybridised carbon atoms, forming individual (single-walled, SWCNTs) or concentric (multi-walled, MWCNTs) graphene cylinders.<sup>2,3</sup> CNTs demonstrated remarkable properties, such as metallic conductivity, chemical and thermal stability, high flexibility, ability to sorb gas molecules and simple strategies for its surface modification.<sup>4</sup> Several techniques have been introduced to manufacture CNTs devices including spray coating,<sup>5,6</sup> filtering and transferring,<sup>7,8</sup> laser ablation,<sup>9</sup> screen printing<sup>10</sup> and inkjet printing (IJP).<sup>11</sup> Among these strategies, IJP has recently become a powerful tool for the deposition of various functional materials (*e.g.* nanoparticles, organometallic, conductive polymers, graphene oxide, CNTs, protein microarrays and living cells)<sup>12-14</sup> thanks to its accuracy, micrometer resolution, mask-less and contact-less approach and scalability from laboratory to industrial production level. As a result, IJP has been used for the fabrication of (bio)chemical sensors on paper<sup>15,16</sup> and polymeric substrates,<sup>17,18</sup> in a single<sup>19</sup> or multiplexed concept,<sup>18</sup> designed for the simultaneous detection of one<sup>15</sup> or multiple analytes<sup>20</sup> and combined with other microfabrication techniques.<sup>21,22</sup> Despite the current debate whether CNTs represent efficient electrocatalysts as stand-alone films,<sup>23-25</sup> this material has been widely used as active layer in electronic and electrochemical devices. For instance, flexible stand-alone CNTs electrodes were fabricated recently by a multilayer IJP process showing a catalytic effect and faster kinetics compared to carbon paste electrodes for the amperometric detection of antioxidants in blood bags.<sup>17</sup> Such encouraging results suggest that IJP CNTs electrodes can be employed for the detection of other relevant target analytes such as pollutants, biomarkers or bacteria.

Amperometric sensors employed for the detection of electrochemically not active compounds are often combined with immunoassay strategies based on two main approaches, namely electrode modification with various capturing agents (*e.g.* antibodies (Abs), aptamers, specific proteins) or magnetic beads based assays (MBs).<sup>26-28</sup> The MB based immunoassays have the advantage of having commercially available MBs with a wide range of surface chemical modifications for both covalent and non-covalent binding interactions.<sup>29</sup> Furthermore MBs based immunoassays are often characterized by high sensitivity, selectivity, rapidity, simplicity and low cost.<sup>30</sup>

Herein, a multilayer IJP process for the batch production of multiplexed electrochemical microchips (*i.e.* 16 independent two-electrode electrochemical cells) for environmental and

clinical applications is presented. The IJP process comprises the deposition of an entire electrical circuit including also the reference/counter electrode made of Ag (first layer), a stand-alone CNTs working electrode (second layer) and an insulating layer (third layer) that defines precisely the CNTs working electrode area. In order to create a microtiter plate like device, plastic wells were mounted on the top of the IJP electrochemical cells. Finally, the IJP CNTs multiplexed sensor was successfully coupled with different formats of MBs-based immunoassays: *i*) competitive enzyme immunoassay for atrazine (ATR) detection in water, *ii*) sandwich enzyme immunoassay for thyroid-stimulating hormone (TSH) analysis in urine and *iii*) label-free immunoassay for *Escherichia coli* (*E.coli*) detection in water.

ATR is a micropollutant of both ground and surface water that was widely used in agriculture as an herbicide due to its high effectiveness and low cost.<sup>31</sup> However, the utilization of ATR was forbidden in Europe in 2003 due to its possible carcinogenic, endocrine disruptor and teratogenic effects.<sup>32–35</sup> It was allowed to be used until 2010 in order to finish existing stocks and therefore, significant amounts can be still detected in the water of several European countries. Furthermore, ATR is poorly eliminated by classical wastewater treatment plants, since ozonation and advanced oxidation processes are required for its efficient removal.<sup>36,37</sup> Furthermore, the maximum residue level (MRL) of ATR in water defined by the WHO (*i.e.* 0.1 ng/mL) requires sensitive analytical tools for its fast and reliable detection. Among the present analytical techniques for ATR screening, MBs-based immunoassay is a very attractive approach.<sup>30</sup>

TSH is a glycoprotein stimulating thyroidal thyroxin and triiodothyronine in the human organism<sup>38</sup> and can be a marker of different diseases, *i.e.* subclinical thyroid disease<sup>39</sup> or iodine deficiency disorders.<sup>40</sup> Normal TSH levels in blood according to the American Association of Clinical Endocrinologists (AACE) ranges from 0.4 to 2.5 milli-international units per liter (mIU/L) for adults and can be as high as 16 mIU/L for newborns. The sandwich enzyme immunoassay is a well-known method for TSH detection in clinical investigations.<sup>41</sup>

*E. coli* is a well-known bacteria type within the family *Enterobacteriaceae* and the tribe *Escherichia*. In spite the most of *E. coli* strains are harmless and widely used in biotechnology<sup>42,43</sup> the virulent serotypes can cause significant problems for food and medical industry.<sup>44</sup> Virulent *E. coli* typically causes infection through the colonization of a mucosal site, evasion of host defenses, multiplication and finally host damage.<sup>44</sup> Additionally, *E. coli* can be found in intestines of a large number of warm-blood animals and therefore, it can be used as an indicator of water safety regarding fecal contamination.<sup>45</sup> Besides, the natural  $\beta$ -galactosidase activity present on this bacteria can be employed to detect in a label-free format

the presence of *E. coli*.<sup>46–48</sup> This approach is of significant interest due to capability to only quantify alive bacteria with a high sensitivity that can be tuned by increasing the time of substrate – *E. coli* incubation, for instance. Due to the commercial availability of anti-*E. coli* Abs, this label-free approach can be easily combined with MBs-based immunoassay and therefore, transferred into a multiplexed format for high throughput analysis.

## 2. Materials and methods

### 2.1. Chemicals

Jettable nano silver EMD5603 (Ag 20% w/w) and jettable insulator EMD6201 were both purchased from Sun Chemical (Carlstadt, USA) and the CNT dispersion BSI.B12212 was received from Brewer Science (Rolla, USA). Goat anti-rabbit Abs conjugated with HRP (Abs-HRP) were from Invitrogen, Life Technologies (Zug, Switzerland), rabbit anti-Bovine Abs conjugated with ALP (Abs-ALP) were from Sigma-Aldrich (Buchs, Switzerland). Ferrocene methanol (FcMeOH) was purchased from Sigma-Aldrich reagents (Buchs, Switzerland). 10 mM PBS, containing 1 mM MgCl<sub>2</sub>, 1mM CaCl<sub>2</sub>, 4 mM KCl, 136 mM NaCl, 7 mM Na<sub>2</sub>HPO<sub>4</sub> and 3 mM NaH<sub>2</sub>PO<sub>4</sub>, was prepared from Sigma-Aldrich reagents (Buchs, Switzerland) and deionized water produced with a Mili-Q plus 185 model from Millipore (Zug, Switzerland).

The immunoassay kit for ATR detection was from Abraxis (Warminster, USA) and consisted of ATR standard solutions, washing buffer solution, 3,3',5,5'-Tetramethylbenzidine (TMB) substrate solution (mixture of TMB with H<sub>2</sub>O<sub>2</sub>), MBs coated with Abs against ATR (MBs-Ab<sub>ATR</sub>) and ATR-HRP conjugate solution. Water samples from the Lake Geneva were taken, filtered with a 0.2 μm filter and used freshly without any additional pretreatment.

Urine samples and ELISA kit for TSH detection were kindly provided by DiagnoSwiss (Monthey, Switzerland). The kit consisted of TSH standard solutions, washing buffer solution, 4-aminophenyl phosphate (PAPP) substrate solution (2.5 mg/mL), MBs coated with Abs against TSH (MBs-Ab<sub>TSH1</sub>) and Abs against TSH conjugated with ALP (Ab<sub>TSH2</sub>-ALP) solution. Super paramagnetic beads coated with Proteins A and G (MBs-ProteinAG) were kindly offered by Merck Chimie SAS (Fontenay-sous-Bois, France).

Wild *E.coli* (ATCC 8739) as well as monoclonal Abs against it (Ab<sub>*E.coli*</sub>) were kindly provided by Bürkert Fluid Control Systems (Triembach au val, France). Isopropyl-beta-D-thiogalactopyranoside (IPTG), polymixin B, lysozyme (Lys) and 4-aminophenyl β-D-Galactopyranoside (PAPG) were also purchased from Sigma-Aldrich reagents (Buchs,

Switzerland). The LB medium for bacteria cultivation contained 10 g of tryptone, 5 g of yeast extract, and 10 g of NaCl dissolved in 950 mL of deionized water. Before using, it was sterilized by autoclaving.

## **2.2. *E. coli* culturing**

A single colony of *E. coli* was grown as a pre-culture at 37 °C in 2 mL of LB medium for 6 h with continuous shaking (250 rpm). The day before the experiment, 3 mL of LB medium was inoculated with 100 µL of the bacteria pre-culture and incubated overnight at 37 °C with shaking (250 rpm). Before the experiments, the concentration of the overnight *E. coli* culture was measured optically by absorbance at 600 nm.

## **2.3. Microchip fabrication**

The IJP CNTs microchips were fabricated on a 125 µm-thick polyimide (PI) substrate (Kapton HN<sup>®</sup>; Goodfellow, Huntingdon, England) using the drop-on-demand DMP-2831 materials printer and a 10 pL cartridge DMC-11610 (Dimatix Fujifilm, Santa Clara, CA, USA). For each ink, the printing parameters such as jetting frequency, voltage, cartridge temperature and cleaning cycles were adjusted as described elsewhere.<sup>17</sup> In brief, the substrate temperature was increased for the IJP of both Ag and CNTs inks to ensure highly resolved patterns. Afterwards, patterns were cured at 200 °C and 120 °C during 30 min for the Ag and CNTs (2 °C/min heating/cooling rate), respectively. The insulating UV curable ink was printed under simultaneous UV exposition thanks to a light guide integrated into the DMP-2831 printer head and connected to an Omnicure<sup>®</sup> S2000 mercury UV lamp. The optical characterization of the fabricated sensors was performed by laser scanning microscopy using a Keyence VK 8700 (Keyence, Osaka, Japan).

## **2.4. Electrochemical characterization of IJP sensors**

To characterize the IJP CNTs microchips electrochemically and to investigate the influence of MBs on the electrochemical signal, cyclic voltammetry (CV) in PAPP and TMB substrate solutions was performed in the presence and absence of MBs. For that purpose, 50 µL of each MBs commercial suspension was transferred into a vial, sedimented and separated from the supernatant using a magnetic separation stand from Promega (Dubendorf, Switzerland). Subsequently, MBs were resuspended in 50 µL of PAPP or TMB solution and transferred into the microchip wells together with 50 µL of each substrate without beads. CV experiments were carried out using an Ivium compactstat (Ivium Technologies, Netherlands) with a scan rate of 0.05 V/s.

The signal reproducibility was determined by the amperometric detection of para-aminophenol (PAP). For this purpose, 1 mL of PAPP was incubated with 1  $\mu$ L of Ab-ALP stock solution overnight to complete the enzymatic reaction that produces PAP. Thereafter, 50  $\mu$ L of the obtained solution was transferred into each well of the microchip and the electrochemical signal was read out simultaneously in all 16 wells at the optimal potential (*i.e.*  $E = 0.05$  V) during 120 s using the ImmuDrop<sup>TM</sup> potentiostat (DiagnoSwiss; Monthey, Switzerland). The latter potentiostat contains an integrated magnet located directly below the microchip holder in order to bring close to, but not over, the electrode the magnetic beads. Additionally it allows simultaneous measurement of 16 individual electrochemical cells.

## **2.5. Electrochemical characterization of MBs by SECM**

SECM was employed to determine if the MBs presented any electrochemical activity that can influence the signal recorded at the IJP microchips. Experimentally, 2.5  $\mu$ L of the suspensions of MBs-ProteinAG (dilution 1 to 20 in PBS), MBs-Ab<sub>TSH1</sub> and MBs-Ab<sub>ATR</sub> were transferred into an electrochemical cell filled with 2 mM FcMeOH solution in 10 mM PBS and installed above a magnet so that the MBs formed small plugs positioned in one line. SECM experiments were provided by a custom-built SECM setup running under SECMx software<sup>49</sup> combined with an Ivium potentiostat operating in a three-electrode mode. An Ag wire was used as a quasi-reference electrode (QRE) and a Pt wire – as a counter (CE). All the reported further potentials are given with respect to the Ag-QRE. The surface of the electrochemical cell was levelled based on negative feedback approach curves performed at a potential equal to 0.25 V with a glass Pt UME (diameter of Pt = 10  $\mu$ m, RG = 7). Due to the fact the magnetic bead plugs presented a pronounced topography, the UME was positioned 200  $\mu$ m above the substrate and the current was recorded during scanning above the sample surface at a constant height with a step of 10  $\mu$ m and a translation speed of 10  $\mu$ m/s.

## **2.6. Influence of the enzyme concentration on the electrochemical signal**

To investigate the influence of the enzyme concentration on the electrochemical signal, MBs-ProteinAG were incubated with different concentrations of Abs-HRP. Briefly, 50  $\mu$ L of MBs suspensions were loaded into several vials, sedimented and separated from the supernatant. Thereafter, 50  $\mu$ L of Abs-HRP solutions with different enzyme concentrations were added and incubated for 30 min at room temperature (RT) under stirring (1000 rpm). Next, 100  $\mu$ L of the washing solution was employed to rinse the system. The washing step was repeated 3 times, using a magnetic separation stand to trap magnetic beads bound with

the Abs-HRP and to separate them from the supernatant. Finally, 50  $\mu\text{L}$  of the TMB substrate solution was added into each vial, the suspension was transferred into a respective microchip well and a given potential was applied for the amperometric detection of  $\text{TMB}_{\text{ox}}$ . The same protocol was applied for Abs-ALP using the PAPP solution as a substrate.

## 2.7. Detection of ATR and TSH

### 2.7.1. Optimization of the immunoassay procedure

In order to implement and optimize the amperometric detection process of ATR in the microchip format, blank ATR (0  $\mu\text{g/L}$ ) and ATR-HRP solutions were mixed with a MBs- $\text{Ab}_{\text{ATR}}$  suspension (see below the employed volumes), placed into vials and incubated during 30 min at RT under stirring (1000 rpm). Thereafter, the system was rinsed 3 times with the washing solution, using a magnetic separation rack to trap the MBs with the immunocomplex and to separate them from the supernatant. Finally, 50  $\mu\text{L}$  of the TMB substrate solution was added into each vial, the suspension was transferred into the microchip and the optimal potential was applied (*vide infra*). The initial volumes of the immunoreagents were: a) 25  $\mu\text{L}$  of ATR (blank) with 25  $\mu\text{L}$  of ATR-HRP with 50  $\mu\text{L}$  of MBs- $\text{Ab}_{\text{ATR}}$  (Procedure A), b) 50  $\mu\text{L}$  of ATR (blank) with 50  $\mu\text{L}$  of ATR-HRP with 100  $\mu\text{L}$  of MBs- $\text{Ab}_{\text{ATR}}$  (Procedure B), c) 100  $\mu\text{L}$  of ATR (blank) with 100  $\mu\text{L}$  of ATR-HRP with 200  $\mu\text{L}$  of MBs- $\text{Ab}_{\text{ATR}}$  (Procedure C), and d) 250  $\mu\text{L}$  of ATR (blank) with 250  $\mu\text{L}$  of ATR-HRP with 500  $\mu\text{L}$  of MBs- $\text{Ab}_{\text{ATR}}$  (Procedure D). Volumes of the washing solution were adjusted based on the initial volumes of the immunoreagents: a) 1 step 100  $\mu\text{L}$ , 2 step 100  $\mu\text{L}$ , 3 step 50  $\mu\text{L}$ , b) 1 step 200  $\mu\text{L}$ , 2 step 100  $\mu\text{L}$ , 3 step 50  $\mu\text{L}$ , c) 1 step 400  $\mu\text{L}$ , 2 step 200  $\mu\text{L}$ , 3 step 100  $\mu\text{L}$ , d) 1 step 1000  $\mu\text{L}$ , 2 step 500  $\mu\text{L}$ , 3 step 100  $\mu\text{L}$ , respectively. Finally, MBs were resuspended in 50  $\mu\text{L}$  of TMB solution and transferred into the electrochemical well. In each case the current was recorded during 120 s at the potential equal to  $-0.1\text{ V}$ .

To optimize the TMB solution volume, four vials containing each one of them 250  $\mu\text{L}$  of blank ATR (0  $\mu\text{g/L}$ ), 250  $\mu\text{L}$  of ATR-HRP solutions and 500  $\mu\text{L}$  of MBs- $\text{Ab}_{\text{ATR}}$  suspension were incubated during 30 min at RT under stirring (1000 rpm). Thereafter, the system was rinsed 3 times with the washing solution, using a magnetic separation rack to precipitate the MBs with the immunocomplex and to separate them from the supernatant. Finally, 50  $\mu\text{L}$ , 100  $\mu\text{L}$ , 250  $\mu\text{L}$ , 500  $\mu\text{L}$  of the TMB substrate solution was added into the corresponding vial, incubated during 15 min at RT and 50  $\mu\text{L}$  of each suspension was transferred into the microchip. In each case the current was recorded during 120 s at a potential equal to  $-0.1\text{ V}$ .

The kit for TSH quantification was designed based on the amperometric detection of PAP within 30  $\mu\text{L}$  volume and did not require any additional optimization.

### **2.7.2. MBs based immunoassay protocols**

To obtain the calibration curve for ATR detection, 100  $\mu\text{L}$  of standard ATR solutions with different concentrations, 100  $\mu\text{L}$  of ATR-HRP solution and 200  $\mu\text{L}$  of MBs-Ab<sub>ATR</sub> suspension were added into the vials and incubated during 30 min at RT with stirring (1000 rpm). Thereafter, the system was rinsed with 400  $\mu\text{L}$ , 200  $\mu\text{L}$  and 100  $\mu\text{L}$  of the washing solution. Finally, 100  $\mu\text{L}$  of the TMB substrate solution was added into each vial, the different suspensions were transferred into their respective wells in the microchip and the current was monitored while applying a potential equal to  $-0.1\text{ V}$ . To confirm the ability of analyzing real samples, a water sample from lake Geneva spiked with 0.1  $\mu\text{g/L}$  and 0.05  $\mu\text{g/L}$  of ATR was analyzed in triplicates.

Calibration curves for TSH detection were obtained, following the commercial protocol. Briefly, 10  $\mu\text{L}$  of standard solution of TSH, 10  $\mu\text{L}$  of Ab<sub>TSH2</sub>-ALP solution and 10  $\mu\text{L}$  of MBs-Ab<sub>TSH1</sub> suspension were added into the vials and incubated during 30 min at RT with stirring (1000 rpm). The system was then rinsed 3 times with 30  $\mu\text{L}$  of the washing solution, 50  $\mu\text{L}$  of the PAPP substrate solution was added into each vial, the suspension was transferred into the microchip and a potential equal to 0.05 V was applied to detect the presence of PAP. To confirm the ability of analyzing real samples and evaluate the influence of samples with complex matrices, the calibration curve was also performed in urine. Thereafter, the urine samples spiked with 1 mUI/L, 5 mUI/L and 10 mUI/L of TSH were analyzed in triplicates.

### **2.8. *E.coli* detection protocol**

To perform the immunoassay, *E. coli* samples were prepared in water at different concentrations:  $10^8$  cells/mL,  $10^6$  cells/mL and 0 cells/mL. MBs-ProteinAG suspension (0.5 mg/mL) was sedimented and resuspended in an equivalent volume of Abs<sub>*E.coli*</sub> solution (dilution 1/10 in PBS). Thereafter, 50  $\mu\text{L}$  of the MBs-ProteinAG-Abs<sub>*E.coli*</sub> suspension was transferred into each bacteria sample (volume 1 mL) and incubated during 1 hour at RT under stirring (950 rpm). On the next step, MBs with the captured *E.coli* were separated from the supernatant, washed with 1 mL of PBS, resuspended in 1 mL of 0.5 mM IPTG in LB solution and incubated during 2 hours at 37 °C under stirring (950 rpm). Further, MBs were separated from the supernatant, wash with 1 mL of PBS, resuspended in 1 mL of polymyxin B (10  $\mu\text{g/mL}$ ) and Lys (25  $\mu\text{g/mL}$ ) in LB solution and incubated during 40 min at 30 °C under



stirring (950 rpm). Thereafter, MBs were washed with 200  $\mu\text{L}$  of PBS and 50  $\mu\text{L}$  of PAPG (1 mg/mL) in PBS solution was added. The suspension was incubated at 37  $^{\circ}\text{C}$  under stirring (950 rpm) during 15 min, 30 min or 60 min, transferred into the IJP microchip for the electrochemical monitoring of the produced PAP at an applied voltage of 0.05 V during 120 s.

### 3. Results and discussions

#### 3.1. IJP CNTs microchip characterization

Multiplexed electrochemical sensors were printed on PI by taking advantage of a multi-layer inkjet printing process (*vide supra*). The outcome of the three subsequent printing steps is shown in Figure 6.1, *i.e.* the silver layer for the electrical connections and counter-reference electrode fabrication (Figure 6.1a), 4 inkjet printed layers of CNTs for the working electrode (Figure 6.1b) and the insulator defining precisely the active working electrode area (Figure 6.1c). A whole batch of printed electrodes (Figure 6.1d) was further cut manually and covered with plastic wells to obtain microchips with 16 independent two-electrode electrochemical cells (Figure 6.1e) containing the CNTs working and the Ag reference/counter electrodes (Figure 6.1f).

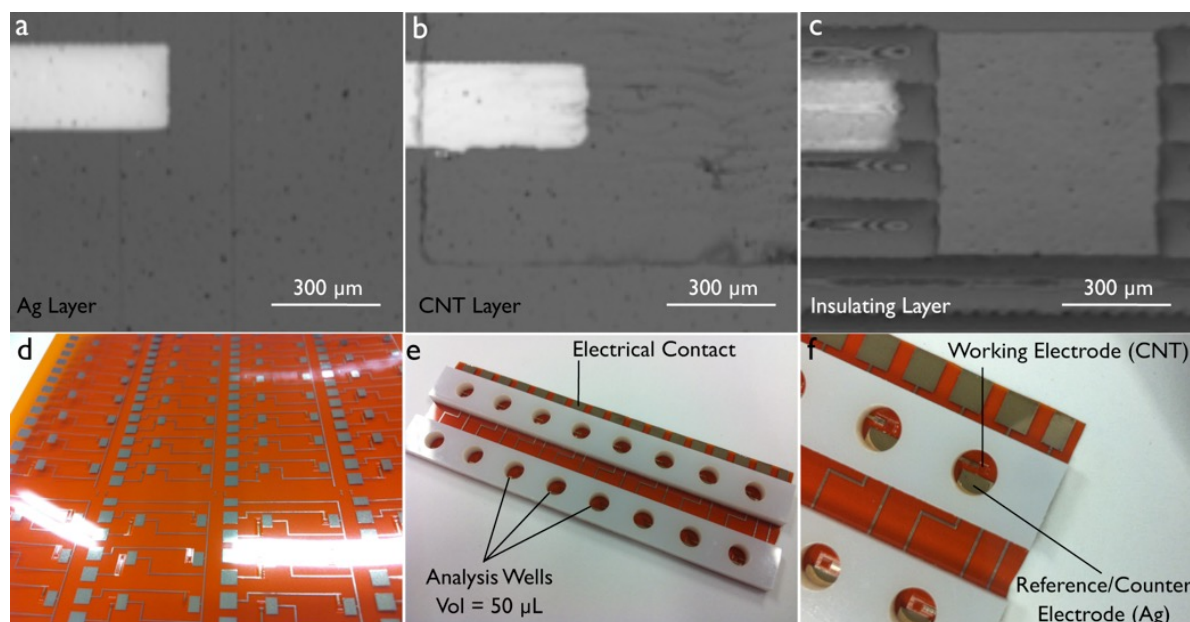


Figure 6.1. Optical images of the multilayer process employed for the microfabrication of multiplexed electrochemical sensors prepared by printing a silver layer for electrical connections and as reference/counter electrode (a), depositing a CNTs layer as working electrode (4 inkjet-printed layers) (b) and printing an insulating layer for defining precisely the active working electrode area (c). Batch production of microchips (d) followed by positioning of the plastic wells on top (e). Optical image of an exemplary two-electrode cell within the multiplexed microchip with a predefined maximum analysis volume equal to 50  $\mu\text{L}$  (f).

The fabricated microchips were further characterized electrochemically, using TMB and PAPP substrate solutions as redox mediators in the presence and absence of different MBs. The CVs for the TMB solution (Figure 6.2a) presented basically two oxidation peaks during the forward scan around 0.1 V and 0.25 V and two reduction peaks during the reverse scan around 0.2 V and 0.025 V, which is in good agreement with the reported two-electron transfer reaction of TMB.<sup>50</sup> When adding MBs into the system the measured redox potentials of TMB is shifted to higher values by approximately 0.1 V and 0.075 V for Abraxis and DiagnoSwiss MBs, respectively. Independent of this phenomena, the amperometric detection of TMB<sub>ox</sub> produced by HRP (*i.e.* the analytical signal of the ATR immunoassay) can be performed at – 0.1 V.

Figures 6.2b and 6.2c show the first and second scans recorded at the IJP CNTs microchips in the presence of PAPP, respectively. Briefly, PAPP is irreversibly oxidised at the working electrode to para-iminoquinone (PIQ) at around 0.5 V, which is electrochemically reduced to PAP at –0.05 V (Figure 6.2b). In the second CV scan, PAP is electrochemically oxidised at around 0.025 V (Figure 6.2c). The addition of MBs to the PAPP solution did not present any influence on the CVs and the quantitative PAP detection can be performed at a potential equal to 0.05 V.

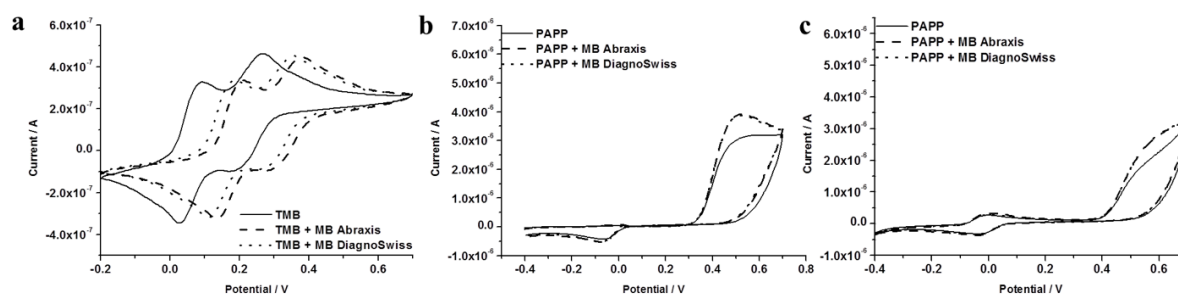


Figure 6.2. Cyclic voltammetry at the IJP CNTs microchip in the presence of TMB (a) and PAPP (b, 1<sup>st</sup> scan and c, 2<sup>nd</sup> scan) substrate solutions with or without MBs. Scan rate was 0.05 V/s.

In order to investigate whether the MBs coating has any impact on the potential shift observed for the TMB redox mediator, for instance by participating on other electrochemical reactions with the substrate solution, MBs were characterised electrochemically using SECM. In terms of SECM, scanning above the plug of well-coated and therefore isolated MBs should provide a negative feedback due to the blocking of the diffusion of the redox mediator (*i.e.* FcMeOH) towards the surface of the microelectrode. As a result, SECM line scans above MBs-Ab<sub>TSH1</sub> and MBs-ProteinAG presented the expected decrease on the recorded current profile, however an increase on the current at the UME when it was scanned above the MBs-

Ab<sub>ATR</sub> plug was observed (Figure 6.3). The latter indicates that the MBs-Ab<sub>ATR</sub> are not completely insulated and therefore allows the Fe<sub>3</sub>O<sub>4</sub> core to react with FcMeOH<sup>+</sup>. Still, since the potential peak shift was observed with all the MBs, a poor insulation of the MBs cannot be employed to justify the results presented in Figure 6.2a. Taking into account that the potential shift was only observed with TMB but not with PAPP, it could be suggested that such behaviour is due to an induced pH change that is fully covered by the alkaline buffer solution of the ALP assay (*i.e.* pH = 9.5), but not by the HRP one (*i.e.* pH = 5). Additionally, the commercial TMB solution also contains H<sub>2</sub>O<sub>2</sub> as an important component of the enzymatic reaction, which can also plays a role on the electrochemical detection potential of TMB<sub>ox</sub>.

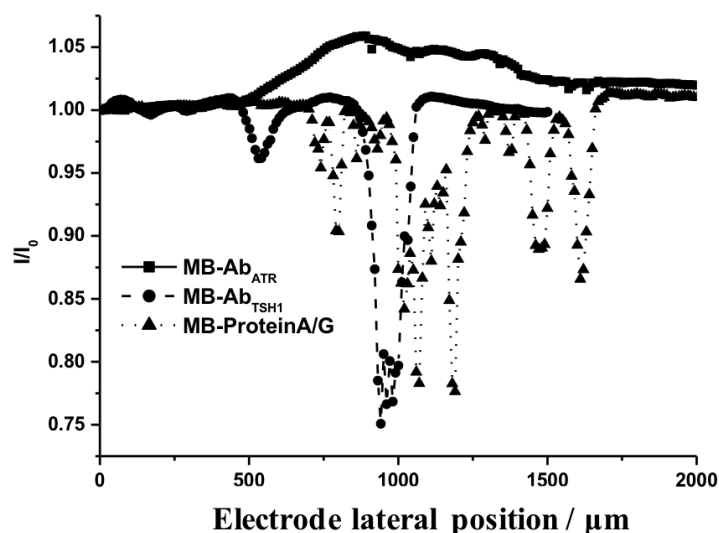


Figure 6.3. SECM line scan (normalized current) obtained during lateral movement of the electrode above the MBs plugs at a constant distance.  $E = 0.250$  V, QRE = Ag, CE = Pt, working electrode = Pt UME. 2 mM FcMeOH in 0.1 M KNO<sub>3</sub> was used as a redox mediator.

The IJP microchip was further characterized in terms of the reproducibility of the electrochemical signal by detecting simultaneously in all the microchip wells the PAP produced by the enzymatic reaction between PAPP and ALP (Figure 6.4a). Standard deviations of the detected current varied only by 4.5%, which represents an acceptable variation for commercial multiplexed immunoassays. In order to determine the relation between the measured signals and the HRP concentration, MBs-ProteinAG were incubated with different concentrations of Abs-HRP. The enzymatic production of TMB<sub>ox</sub> was monitored amperometrically at a potential equal to  $-0.1$  V and the recorded currents were in a good agreement with the HRP dilutions (Figure 6.4b).

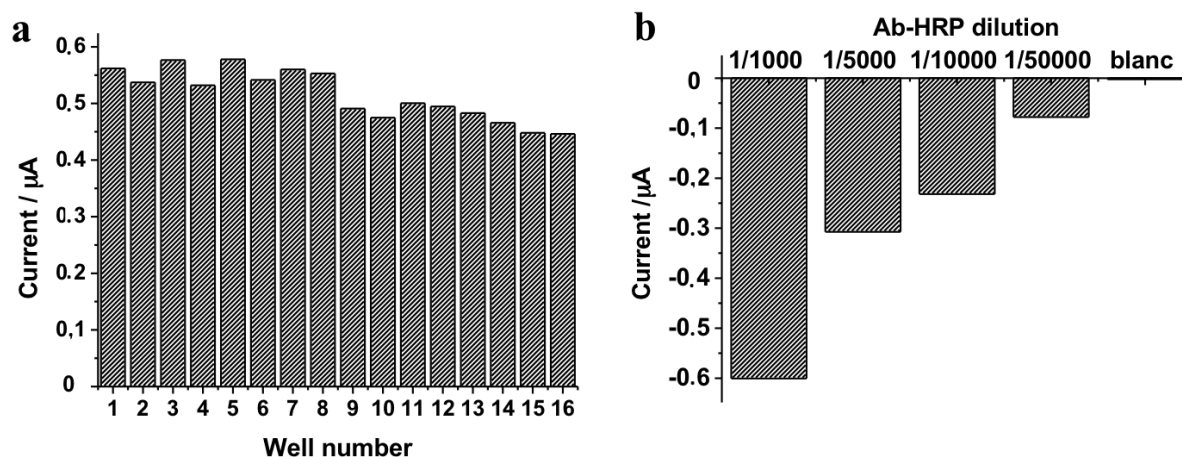


Figure 6.4. Reproducibility of the electrochemical signal for the inkjet-printed microchip based on the amperometric detection of PAP (at 0.05 V during 120 s (a)). Analysis of HRP dilutions.  $\text{TMB}_{\text{ox}}$  produced in the reaction between TMB and  $\text{H}_2\text{O}_2$  catalyzed by HRP was electrochemically detected at  $-0.1$  V during 120 s (b). Abs-HRP dilutions were 1/1000, 1/5000, 1/10000 and 1/50000 in PBS.

### 3.2. IJP microchip for ATR immunoassay

The ATR detection kit was designed as a competitive immunoassay (Figure 6.5a), where the Abs against ATR were bound to a support ( $\text{MBs-Ab}_{\text{ATR}}$ ) and the ATR presented in the sample competes with the ATR-HRP conjugate for binding the Abs. When the analyzed sample contains no ATR, the amount of ATR-HRP bound to MBs will be the maximum. Therefore, the amperometric signal is inversely proportional to the ATR concentration.

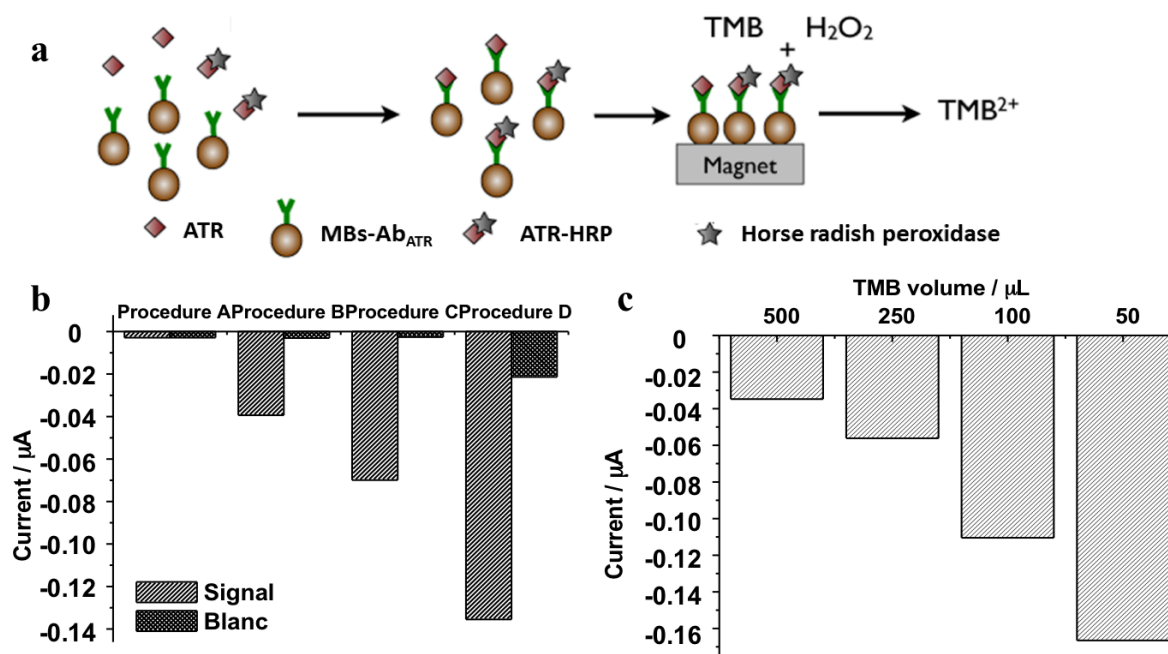


Figure 6.5. Optimization of the immunoreagents volumes for the amperometric detection of ATR (a) and of the TMB volume for the amperometric detection of ATR (b). Electrochemical experiments were performed by applying  $-0.1$  V potential during 120 s at the IJP CNTs microchip.

The commercial kit for ATR detection was designed by the provider for the colorimetric detection of TMB<sub>ox</sub>, therefore it is required to optimize the protocol of the assay for the amperometric detection at the IJP microchip. Thus, the volumes of the immunoreagents were adjusted by the proportional decrease of all components of the assay by factors of 2.5, 5 and 10 times (procedures C, B and A, respectively). In this way the sensitivity of the competitive immunoassay remained intact. In addition, as it can be seen in Figure 6.5b, when the procedure A was performed the amperometric signal from ATR-HRP bound to MBS-Ab<sub>ATR</sub> does not present any difference from the background signal. However, increasing the volumes of the immunoreagents increases the electrochemical signal and for procedure B the signal reaches already a 10 times higher value than the background and increases for both procedures C and D. Consequently, procedure D was chosen as the optimum one for the further experiments.

The ATR commercial kit involves the addition of 1 mL of the immunoreagents (250  $\mu$ L of ATR with 250  $\mu$ L of ATR-HRP with 500  $\mu$ L of MBS-Ab<sub>ATR</sub>) and 500  $\mu$ L of the TMB/H<sub>2</sub>O<sub>2</sub> solution. However, the volume of each IJP CNT microchip well is equal to 50  $\mu$ L and therefore, the protocol of the immunoassay should be optimized. As it can be seen in Figure 6.5c, when 500  $\mu$ L of the TMB substrate solution was added to the system the amperometric signal from ATR-HRP bound to MBS-Ab<sub>ATR</sub> present a very low amperometric signal. However, decreasing the volumes of TMB increases the electrochemical signal, for instance addition of 50  $\mu$ L of the TMB solution result in 16 times increase on the signal to noise ratio due to a concentration effect. Still 100  $\mu$ L of TMB was chosen as the optimal volume for the immunoassay protocol in order to eliminate any possible artifacts coming from the evaporation of the solutions observed when using 50  $\mu$ L TMB solution.

Based on the optimizations on the immunoassay protocol, a calibration curve for ATR detection was performed. It showed a limit of detection equal to the one announced for the commercial kit for an optical detection, *i.e.* 0.02  $\mu$ g/L, while the range of the concentrations which can be detected electrochemically was smaller than for the colorimetric detection, *i.e.* from 0  $\mu$ g/L and 0.5  $\mu$ g/L for the IJP sensor (Figure 6.6) *vs* from 0  $\mu$ g/L and 1  $\mu$ g/L for the commercial protocol.

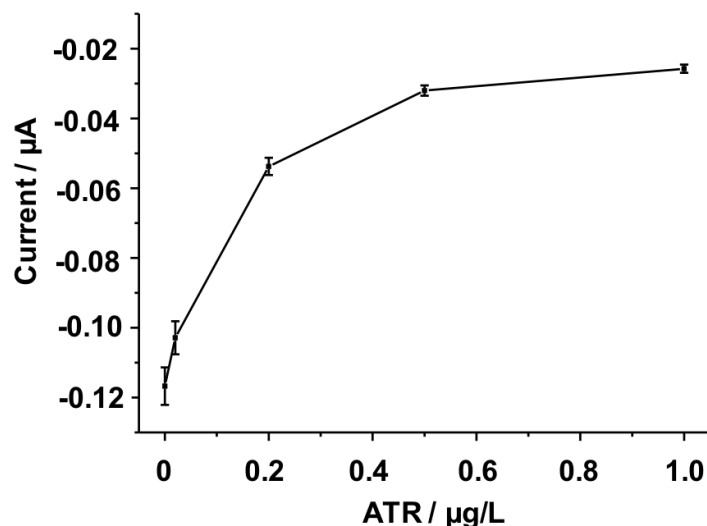


Figure 6.6. Calibration curve for amperometric detection of ATR.

Water samples from the lake of Geneva were spiked with known amounts of ATR and further analyzed in triplicates using the optimized immunoassay protocol. The ATR concentrations were further evaluated based on the obtained calibration curve. The results of the experiment presented values of ATR higher than the spiked amount, presenting possible contamination of water however, the herbicide concentration ( $0.01 \mu\text{g/L}$ ) is significantly smaller than the MRL. These results are in good agreement with previously reported data, where ATR was detected in the lake of Geneva.<sup>51</sup>

Table 6.1. Results of the recovery test of ATR in real samples analyzed by the immunoassay with amperometric detection in the inkjet-printed microchips.

Analyzed sample	Spiked concentration	Detected concentration	Detected concentration
Water from Lake Geneva	$0.1 \mu\text{g/L}$	$0.11 \pm 0.005 \mu\text{g/L}$	110%
Water from Lake Geneva	$0.05 \mu\text{g/L}$	$0.051 \pm 0.002 \mu\text{g/L}$	102%
Water from Lake Geneva	$0 \mu\text{g/L}$	Not detected	Not detected

### 3.3. IJP microchip for TSH immunoassay

The TSH detection kit was designed as the classical sandwich immunoassay (Figure 6.7a), where one type of Ab against TSH is bound to a support (MBS-Ab<sub>TSH1</sub>) and another type is labeled with an enzyme (Ab<sub>TSH2</sub>-ALP). When the analyzed sample contains TSH, an immunocomplex composed by TSH and both Abs will be formed and as a consequence the ALP bound to MBs as well as the recorded amperometric signal will increase directly proportional to the TSH concentration. A calibration curve for TSH detection based on the

commercial TSH immunoassay kit and the IJP microchips is presented on Figure 6.7b. In comparison with the analytical characteristics of the kit, the sensitivity of the assay was not affected by the modification and the limit of detection stayed equal to 0.5 mIU/L while the TSH detection range was from 0.5 to 30 mIU/L. Thereafter, in order to analyze TSH in complex matrices such as urine samples, the calibration curve was performed in urine instead of the model buffer (Figure 6.7b). Indeed, the obtained results show a slight matrix interference on the sensitivity of the assay at high TSH concentrations which is expected for such complex and variable matrix. To confirm this point, 2 different urine samples were spiked with different TSH amounts and the TSH concentration was evaluated based on the calibration curve in urine presented in Figure 6.7b. As a result, a high recovery rate (Table 6.2) was obtained for all samples however, it is clear that depending on the sample origin a different recovery rate was obtained. Nevertheless, the IJP CNTs electrodes are sensitive enough to not only see such differences, but also to sense TSH in a reliable way within the biological relevant range and thus open the door for a potential commercialization.

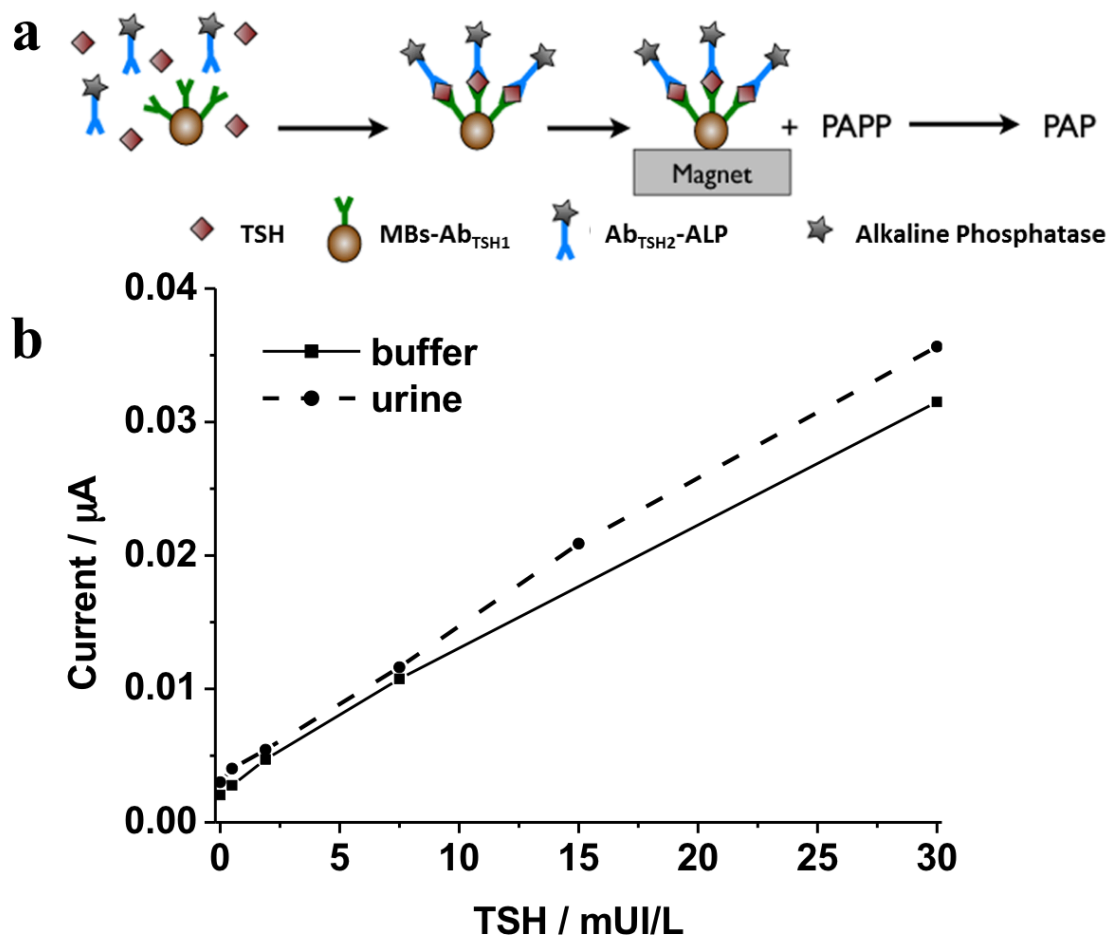


Figure 6.7. Scheme of the sandwich immunoassay for TSH detection (a). Calibration curves for the amperometric detection of TSH in buffer and urine (b).

Table 6.2. Results of the recovery test of TSH in real samples analyzed by the immunoassay with amperometric detection in the inkjet-printed microchips.

Analyzed sample	Spiked TSH concentration	Detected TSH concentration	Recovery %
Urine (sample 1)	10 mUI/L	9.7 ± 0.5 mUI/L	97%
Urine (sample 1)	1 mUI/L	1.1 ± 0.1 mUI/L	110%
Urine (sample 1)	0 mUI/L	Not detected	Not detected
Urine (sample 2)	10 mUI/L	8.3 ± 0.5 mUI/L	83%
Urine (sample 2)	1 mUI/L	0.8 ± 0.1 mUI/L	80%
Urine (sample 2)	0 mUI/L	Not detected	Not detected

### 3.4. IJP microchip for *E. coli* detection

The proposed labelled-free detection strategy of *E. coli* based on the previous reports<sup>52–55</sup> is presented in Figure 6.8a. Briefly, MBs-ProteinAG are incubated with Abs<sub>*E. coli*</sub> to form the non-covalent MBs-Abs complex which is further employed for immunocapturing bacteria in water samples. Thereafter, the trapped *E. coli* are separated from the sample media, and the expression of relevant enzymes such as β-GAL is induced by the addition of IPTG. To facilitate the transport of the PAPG substrate into the cell, the cell membrane is permeabilized by polymixin B and Lys. On the final step, the PAPG substrate is added and the whole suspension is transferred into the corresponding IJP CNTs microchip well to detect the amount of produced PAP that is transported out of the bacteria.

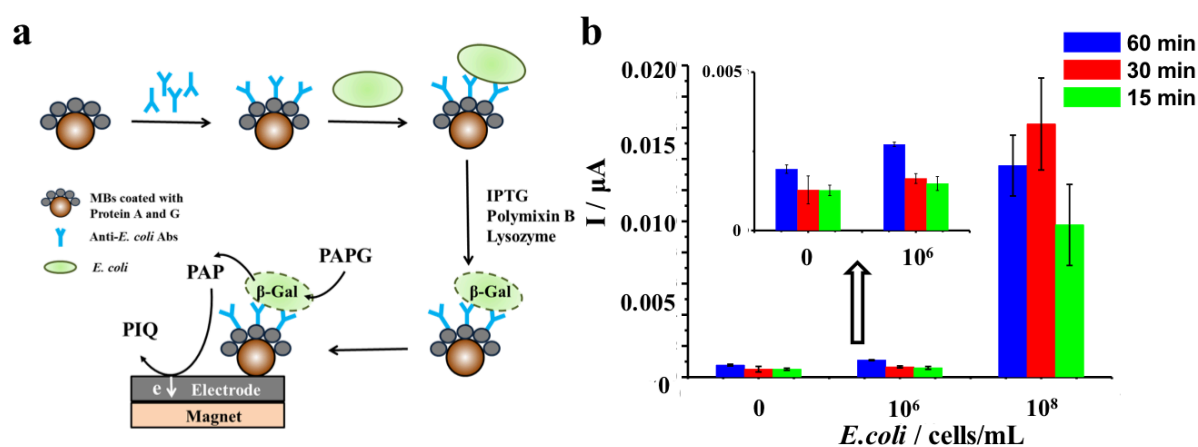


Figure 6.8. Schematic representation of the proposed label-free MBs-based immunoassay with amperometric detection for the detection of *E. coli* cells (a) and the experimental results obtained for bacteria in water at different incubation times with PAPG (i.e. 15 min, 30 min and 60 min) (b).



*E. coli* induction and permeabilization time was equal to the optimal conditions presented elsewhere,<sup>52-55</sup> while the incubation time between the trapped *E. coli* cells and PAPG was investigated. As it is shown in Figure 6.8b, for high concentrations of bacteria (*i.e.*  $10^8$  cells/mL) increasing the substrate reaction time leads to an increase on the detected currents (from 15 min to 30 min), but reach a plateau after 30 min. The latter is most likely due to a full conversion of PAPG into PAP by the highly populated *E. coli* culture, as well as, due to the death of the microorganisms. When a lower concentration of *E. coli* (*i.e.*  $10^6$  cell/mL) was used, the analytical signal different from the background was detected only after 60 min of incubation with PAPG confirming that the sensitivity of the assay can be influenced by the time of the enzymatic reaction due to continuous enzymatic activity of living organisms.

Thus, *E. coli* can be detected in water by using IJP CNT microchip coupled with MBs-based label-free immunoassay in a relatively short time (approximately 5 hours) in comparison with classical microbiological methods, which often require overnight incubation. In comparison with other instrumental methods, the label-free immunoassay is cheap and simple and, additionally, detects only viable bacteria. Furthermore, it can be fast transferred into the semi-quantitative format, when only positive/negative response regarding the concentration of interest (*e.g.*  $10^6$  cells/mL) is required.

#### 4. Conclusions

A microchip consisting of 16 independent electrochemical cells fabricated by an IJP multilayer process was proposed. The different IJP layers based on Ag, stand-alone CNTs and an insulator were employed as counter/reference electrode and electrical connections, working electrode and for precisely defining the exposed electrode areas. The IJP microchip was characterized electrochemically presenting a highly reproducible signal between the wells (4.5%) and a clear ability to detect electrochemically PAP and TMB. The conditions for the amperometric detection of HRP and ALP enzymatic activity were optimized and the IJP microchips were further successfully implemented as a highly sensitive detection platform for different MBs-based immunoassay formats, namely, competitive enzyme immunoassay for ATR detection in water, sandwich enzyme immunoassay for TSH detection in urine and label-free non-competitive immunoassay for *E. coli* detection in water. Thus, the developed IJP microchip can be used as an unified platform for the electrochemical readout of several analytes based on immunoassay detection protocols. The high reproducibility of the analytical signal, the simple way of microchip manufacturing and the versatility of the microchip make it a promising device for a further commercial application.

## 5. References

- (1) Iijima, S. *Lett. to Nat.* **1991**, *354*, 56–58.
- (2) Ajayan, P. M.; Zhou, O. Z. *Top. Appl. Phys.* **2001**, *80*, 391–425.
- (3) McCreery, R. L. *Chem. Rev.* **2008**, *108*, 2646–2687.
- (4) Hirsch, A. *Angew. Chem. Int. Ed. Engl.* **2002**, *41*, 1853–1859.
- (5) Schrage, C.; Kaskel, S. *ACS Appl. Mater. Interfaces* **2009**, *1*, 1640–1644.
- (6) Zhao, X.; Chu, B. T. T.; Ballesteros, B.; Wang, W.; Johnston, C.; Sykes, J. M.; Grant, P. S. *Nanotechnology* **2009**, *20*, 065605.
- (7) Kim, M. J.; Shin, D. W.; Kim, J.-Y.; Park, S. H.; Han, I. T.; Yoo, J. B. *Carbon N. Y.* **2009**, *47*, 3461–3465.
- (8) Zhou, Y.; Hu, L.; Grüner, G. *Appl. Phys. Lett.* **2006**, *88*, 123109.
- (9) Saran, N.; Parikh, K.; Suh, D.; Mun, E.; Kolla, H.; Manohar, S. K. *J. Am. Chem. Soc.* **2004**, *126*, 4462–4463.
- (10) Lee, H. J.; Moon, S. I.; Kim, J. K.; Lee, Y. D.; Nahm, S.; Yoo, J. E.; Han, J. H.; Lee, Y. H.; Hwang, S. W.; Ju, B. K. *J. Appl. Phys.* **2005**, *98*, 016107.
- (11) Tortorich, R.; Choi, J.-W. *Nanomaterials* **2013**, *3*, 453–468.
- (12) Cummins, G.; Desmulliez, M. P. Y. *Circuit World* **2012**, *38*, 193–213.
- (13) Dias, A.; Kingsley, D.; Corr, D. *Biosensors* **2014**, *4*, 111–136.
- (14) Romanov, V.; Davidoff, S. N.; Miles, A. R.; Grainger, D. W.; Gale, B. K.; Brooks, B. D. *Analyst* **2014**, *139*, 1303–1326.
- (15) Abe, K.; Kotera, K.; Suzuki, K.; Citterio, D. *Anal. Bioanal. Chem.* **2010**, *398*, 885–893.
- (16) Määttänen, A.; Vanamo, U.; Ihalainen, P.; Pulkkinen, P.; Tenhu, H.; Bobacka, J.; Peltonen, J. *Sensors Actuators B Chem.* **2013**, *177*, 153–162.
- (17) Lesch, A.; Cortés-Salazar, F.; Prudent, M.; Delobel, J.; Rastgar, S.; Lion, N.; Tissot, J.-D.; Tacchini, P.; Girault, H. H. *J. Electroanal. Chem.* **2014**, *717-718*, 61–68.
- (18) Jensen, G. C.; Krause, C. E.; Sotzing, G. A.; Rusling, J. F. *Phys. Chem. Chem. Phys.* **2011**, *13*, 4888–4894.
- (19) Zhang, H.; Xie, A.; Shen, Y.; Qiu, L.; Tian, X. *Phys. Chem. Chem. Phys.* **2012**, *14*, 12757–12763.
- (20) Abe, K.; Suzuki, K.; Citterio, D. *Anal. Chem.* **2008**, *80*, 6928–6934.
- (21) Kit-Anan, W.; Olarnwanich, A.; Sriprachuabwong, C.; Karuwan, C.; Tuantranont, A.; Wisitsoraat, A.; Srituravanich, W.; Pimpin, A. *J. Electroanal. Chem.* **2012**, *685*, 72–78.
- (22) Cinti, S.; Arduini, F.; Moscone, D.; Palleschi, G.; Killard, A. J. *Sensors (Basel)*. **2014**, *14*, 14222–14234.
- (23) Dumitrescu, I.; Unwin, P. R.; Macpherson, J. V. *Chem. Commun. (Camb)*. **2009**, 7345, 6886–6901.
- (24) Byers, J. C.; Güell, A. G.; Unwin, P. R. *J. Am. Chem. Soc.* **2014**, *136*, 11252–11255.
- (25) Güell, A. G.; Meadows, K. E.; Dudin, P. V.; Ebejer, N.; Macpherson, J. V.; Unwin, P. R. *Nano Lett.* **2014**, *14*, 220–224.

- (26) Hayat, A.; Catanante, G.; Marty, J. *Sensors* **2014**, *14*, 23439–23461.
- (27) Mistry, K. K.; Layek, K.; Mahapatra, A.; RoyChaudhuri, C.; Saha, H. *Analyst* **2014**, *139*, 2289–2311.
- (28) Bunyakul, N.; Baeumner, A. *Sensors* **2014**, *15*, 547–564.
- (29) Lu, A.-H.; Salabas, E. L.; Schüth, F. *Angew. Chem. Int. Ed. Engl.* **2007**, *46*, 1222–1244.
- (30) Liang, H. C.; Bilon, N.; Hay, M. T. *Water Environ. Res.* **2013**, *85*, 2114–2138.
- (31) Schwarzenbach, R. P.; Escher, B. I.; Fenner, K.; Hofstetter, T. B.; Johnson, C. A.; Von Gunten, U.; Wehrli, B. *Science* **2006**, *313*, 1072–1077.
- (32) Sass, J. B.; Colangelo, A. *Int. J. Occup. Environ. Health* **2013**, *12*, 260–267.
- (33) Dich, J.; Zahm, S. H.; Hanberg, A.; Adami, H. O. *Cancer Causes Control* **1997**, *8*, 420–443.
- (34) Hamlin, H. J.; Guillette, L. J. *Birth Defects Res. C. Embryo Today* **2011**, *93*, 19–33.
- (35) Fan, W.; Yanase, T.; Morinaga, H.; Gondo, S.; Okabe, T.; Nomura, M.; Komatsu, T.; Morohashi, K.-I.; Hayes, T. B.; Takayanagi, R.; Nawata, H. *Environ. Health Perspect.* **2007**, *115*, 720–727.
- (36) Luo, Y.; Guo, W.; Ngo, H. H.; Nghiem, L. D.; Hai, F. I.; Zhang, J.; Liang, S.; Wang, X. C. *Sci. Total Environ.* **2014**, *473-474*, 619–641.
- (37) Udiković-Kolić, N.; Scott, C.; Martin-Laurent, F. *Appl. Microbiol. Biotechnol.* **2012**, *96*, 1175–1189.
- (38) Soldin, O. P.; Chung, S. H.; Colie, C. *J. Thyroid Res.* **2013**, *2013*, 148157.
- (39) Ortiz, E.; Daniels, G. H.; Sawin, C. T.; Cobin, R. H.; Franklyn, J. A.; Hershman, J. M.; Burman, K. D.; Denke, M. A.; Cooper, R. S.; Weissman, N. J. *J. Am. Med. Assoc.* **2004**, *291*, 228–238.
- (40) Delange, F. *Thyroid* **1994**, *4*, 107–128.
- (41) Shamsi, M. H.; Choi, K.; Ng, A. H. C.; Wheeler, A. R. *Lab Chip* **2014**, *14*, 547–554.
- (42) Belkin, S. *Curr. Opin. Microbiol.* **2003**, *6*, 206–212.
- (43) Cortés-Salazar, F.; Beggah, S.; Van der Meer, J. R.; Girault, H. H. *Biosens. Bioelectron.* **2013**, *47*, 237–242.
- (44) Nataro, J. P.; Kaper, J. B. *Clin. Microbiol. Rev.* **1998**, *11*, 142–201.
- (45) Lopez-Roldan, R.; Tusell, P.; Courtois, S.; Cortina, J. L. *Trends Anal. Chem.* **2013**, *44*, 46–57.
- (46) Yang, Q.; Liang, Y.; Zhou, T.; Shi, G.; Jin, L. *Electrochem. commun.* **2009**, *11*, 893–896.
- (47) Serra, B.; Morales, M. D.; Zhang, J.; Reviejo, A. J.; Hall, E. H.; Pingarron, J. M. *Anal. Chem.* **2005**, *77*, 8115–8121.
- (48) Mittelman, A. S.; Ron, E. Z.; Rishpon, J. *Anal. Chem.* **2002**, *74*, 903–907.
- (49) Nunes Kirchner, C.; Hallmeier, K. H.; Szargan, R.; Raschke, T.; Radehaus, C.; Wittstock, G. *Electroanalysis* **2007**, *19*, 1023–1031.
- (50) Volpe, G.; Compagnone, D.; Draisci, R.; Palleschi, G. *Analyst* **1998**, *123*, 1303–1307.

- (51) Fankhauser, S. *La Lettre du Léman*; 2009.
- (52) Geng, P.; Zheng, J.; Zhang, X.; Wang, Q.; Zhang, W.; Jin, L.; Feng, Z.; Wu, Z. *Electrochem. commun.* **2007**, *9*, 2157–2162.
- (53) Abu-Rabeah, K.; Ashkenazi, A; Atias, D.; Amir, L.; Marks, R. S. *Biosens. Bioelectron.* **2009**, *24*, 3461–3466.
- (54) Boyaci, I. H.; Aguilar, Z. P.; Hossain, M.; Halsall, H. B.; Seliskar, C. J.; Heineman, W. R. *Anal. Bioanal. Chem.* **2005**, *382*, 1234–1241.
- (55) Kaya, T.; Nagamine, K.; Matsui, N.; Yasukawa, T.; Shiku, H.; Matsue, T. *Chem. Commun. (Camb)*. **2004**, *1*, 248–249.

# CHAPTER VII

## General Conclusions and Future Perspectives

In this thesis the potential of a number of bioanalytical approaches towards sensing, imaging and perturbing of adherent cells was evaluated. With this aim as it is presented in Chapter II, SECM was combined with cell fixation strategies to open the intracellular space for performing immunostaining of the intracellular components. As a result, SECM was implemented as a tool to monitor the distribution of TyR in melanoma adherent cells by electrochemical readout of horse radish peroxidase (HRP) activity (*i.e.* immunoassay strategy). Indeed, this approach can be easily extended to various melanoma markers (*e.g.* S100, gp100)<sup>1,2</sup> as well as to different cancer types. Alternatively to HRP, others types of labels, *e.g.* quantum dots (QDs) and metal nanoparticles (NPs) can be also detected electrochemically. For instance, Au NPs-modified with Abs were reported to produce *p*-aminophenol (PAP) from *p*-nitrophenol in the presence of NaBH<sub>4</sub>.<sup>3</sup> Additionally, *Polsky et al.* suggested reagentless immunoassay using Au/Pt NPs labelled Abs.<sup>4</sup> Indeed since the Au/Pt NPs catalyse the O<sub>2</sub> reduction, their presence can be detected electrochemically. Furthermore, implementing QDs as a label would allow simultaneous optical and electrochemical detection of biomarkers by combination SECM setup with a laser fluorescent microscope.

In Chapter III the potential of the soft stylus probe concept towards the scanning of adherent living cells in a contact mode was investigated. The ultra-soft stylus probe (*i.e.* 30 μm thick) was shown to be able to brush adherent WM-115 melanoma cells without damaging cells or pilling them off from the substrate surface at a translation rate of 5 μm/s. Despite imaging of living cells in contact mode does not eliminate the topography influence on the recorded signal (most likely due to cells lipid membrane elasticity), it can be further tested in order to read out the metabolic response of adherent cells or the signal coming from a immunostaining process. In such case, an ultra-soft stylus probe with two working electrodes can be implemented for the complete differentiation of topography and surface reactivity by using two redox mediators (*i.e.* one for chemical imaging and another one cells topography characterization, Figure 7.1).

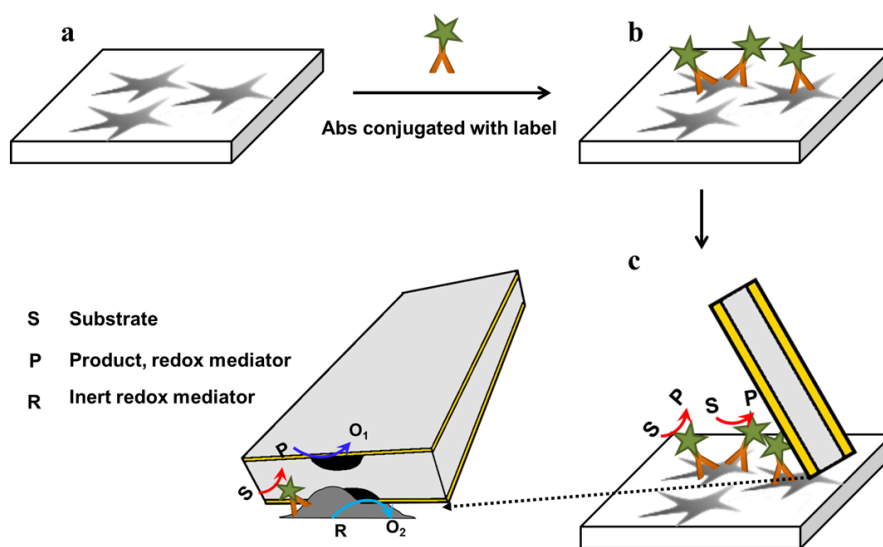


Figure 7.1. Schematic representation of simultaneous detection of topography and electrochemical activity of immunostained cells by SECM in a contact mode. Fixed and permeabilized adherent cells (a) immunostained with Abs-label (b). The products of the reaction catalyzed by the label (c) can be monitored by SECM simultaneously with the topography by employing the inert (*i.e.* does not react with S, P and O<sub>1</sub>) redox mediator (d).

In Chapter IV, the precise spatiotemporal perturbation of adherent living cells (*i.e.* localized fluorescent labeling and pH changes) was performed by taking advantage of the integrated electrochemical and microfluidic modes at a soft electrochemical push-pull probe. This study paves the way for investigating real cancer progression processes, *e.g.* for monitoring the *in vitro* hypoxic tumour models towards potentially therapeutic compounds and localized pH changes (Figure 7.2). Hypoxic tumour cells (*e.g.* present in colon, cervical, breast and renal carcinomas, and brain tumors) are characterized by a low pH microenvironment that is related to their characteristic resistance to classical chemo- and radiotherapies, as well as, a poor prognosis.<sup>5,6</sup> Indeed, it has been reported that carbonic anhydrase (CA) IX, a metallo-enzyme that catalyzes the rapid conversion of carbon dioxide to bicarbonate and protons, plays a prominent role in the acid-base balance of hypoxic tumors where it is typically overexpressed.<sup>5,6</sup> Therefore, evaluating the potential of CA IX inhibitors as anti-cancer drugs is of high relevance. With this aim, the push-pull system can be implemented for the localized delivery of CA IX inhibitors through one of the open microchannels, while any species released from the cells as their biological response can be aspirated and further analyzed by mass spectrometry by the use of the additional open microchannel. Complementary, the integrated carbon microelectrode can be employed for the electrochemical readout of the cancer cells after perturbation, for instance by its functionalization with Prussian Blue to selectively and sensitively detect H<sub>2</sub>O<sub>2</sub>.<sup>7</sup>

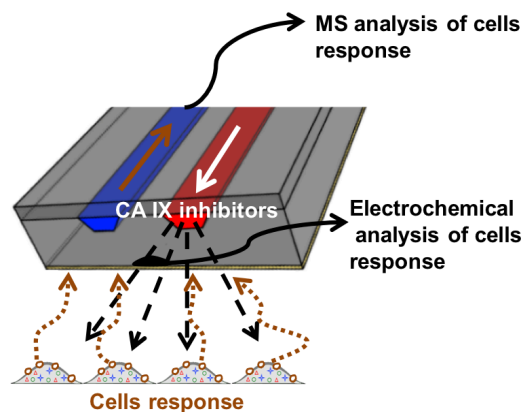


Figure 7.2. Schematic representation of electrochemical push-pull probe applied for *in vitro* monitoring of anti-cancer drugs.

In chapter V of this thesis, melanoma cells differentiation based on MALDI MS analysis was evaluated. A fast and simple intact cell MALDI-MS approach was combined with various cell fixation techniques in order to acquire the MS fingerprints of melanoma cells. As a result, a possible marker of melanoma tumour progression with a  $m/z$  equal to 26.1 kDa was detected.<sup>8</sup> Such strategy can be further extrapolated to cancer diagnosis in real tissues samples. Besides cancer diagnosis, intact cell MALDI MS can be further implemented for investigation of stem cells proteome modifications during the processes of their dynamic transformation in other cell types.

In the final part of this thesis (Chapter VI), an IJP multiplexed platform was developed for the monitoring of biological and environmental relevant samples. The IJP microchip presented a highly reproducible signal between the wells and was successfully implemented as a highly sensitive detection platform for different MBs-based immunoassay formats. The 16-well microchip format can be easily transferred into a 32- or a 96-well platform in order to increase the screening capabilities of such approach.

All in all, this work has demonstrated that SECM offers an interesting tool to visualize particular cell compartments and could be further implemented for medical diagnostics and *in vitro* manipulations with adherent cells and additionally, can be extended for tissue analysis.

**References**

- (1) Boyle, J. L.; Haupt, H. M.; Stern, J. B.; Multhaupt, H. A. B. *Arch. Pathol. Lab. Med.* **2002**, *126*, 816–822.
- (2) De Vries, T. J.; Smeets, M.; De Graaf, R.; Hou-Jensen, K.; Bröcker, E. B.; Renard, N.; Eggermont, A. M. M.; Van Muijen, G. N. P.; Ruiter, D. J.; Vries, T. J. De; Smeets, M.; Graaf, R. De; Hou-Jensen, K.; Bro, E. B.; Renard, N.; Eggermont, A. M. M.; Muijen, G. N. P. Van; Ruiter, D. J. *J. Pathol.* **2001**, *193*, 13–20.
- (3) Selvaraju, T.; Das, J.; Han, S. W.; Yang, H. *Biosens. Bioelectron.* **2008**, *23*, 932–938.
- (4) Polsky, R.; Harper, J. C.; Wheeler, D. R.; Dirk, S. M.; Rawlings, J. A; Brozik, S. M. *Chem. Commun. (Camb).* **2007**, *1*, 2741–2743.
- (5) Winum, J.; Rami, M.; Scozzafava, A.; Montero, J.; Supuran, C. *Med. Res. Rev.* **2008**, *28*, 445–463.
- (6) Shin, H.-J.; Rho, S. B.; Jung, D. C.; Han, I.-O.; Oh, E.-S.; Kim, J.-Y. *J. Cell Sci.* **2011**, *124*, 1077–1087.
- (7) Pribil, M. M.; Cortés-Salazar, F.; Andreyev, E. A.; Lesch, A.; Karyakina, E. E.; Voronin, O. G.; Girault, H. H.; Karyakin, A. A. *J. Electroanal. Chem.* **2014**, *731*, 112–118.
- (8) Baruthio, F.; Quadroni, M.; Rüegg, C.; Mariotti, A. *Proteomics* **2008**, *8*, 4733–4747.



Alexandra **BONDARENKO**

**Date and place of birth: October 23, 1988, Rudny, Kazakhstan**

**Rue de l'Alpe 31**

**1003 Lausanne, Switzerland**

**+41 76 44 99 020**

**[alexandra.bondarenko@epfl.ch](mailto:alexandra.bondarenko@epfl.ch)**

**EDUCATION**

---

- 2011 – Present    **PhD in Analytical Chemistry**  
Thesis title: Electrochemical sensing and imaging of biological samples  
Supervisor Prof. Hubert H. Girault  
Co-supervisor Dr. Fernando Cortés Salazar  
Laboratory of Physical and Analytical Electrochemistry, Institute of Chemistry and Chemical Engineering, Ecole Polytechnique Fédérale de Lausanne, Switzerland
- 2005 – 2010    **Specialist (equivalent of M. Sc.) in Chemistry**  
Thesis title: Development of fluorescence polarization immunoassay (FPIA) for mycotoxins detection in food  
Supervisor Prof. Sergei A. Eremin  
Group of Immunochemical Methods of Analysis, Division of Chemical Enzymology, Department of Chemistry, Lomonosov Moscow State University, Russia

**PROFESSIONAL EXPERIENCE**

---

- 2012 – 2014    **Teaching Assistant (Ecole Polytechnique Fédérale de Lausanne, Switzerland)**  
Practical course in analytical chemistry for bachelor students
- 2012 – 2014    **Consultancy to Bürkert Fluid Control Systems (Triembach au val, France)**  
Development of magnetic beads – based immunoassays
- 2011 (2 months)    **Internship at the Institute for Agricultural and Fisheries Research - ILVO (Oostende, Belgium)**  
Supervisor Dr. Johan Robbens  
Training course on chemical, genetic and biochemical analysis
- 2010 – 2011    **Technician at XEMA Co. Ltd. (Moscow, Russia)**  
Development of ELISA kits for mycotoxins detection
- 2010 (1 month)    **Internship at the Department of Biomedical Sciences, Chung Shan Medical University (Taichung, Taiwan)**  
Supervisor Prof. Feng-Yih Yu  
Development of fluorescence polarization immunoassay for mycotoxins' and microcystins' detection

2008 (2 months) **Internship at the Laboratory of Food Analysis, Ghent University jointly with Antwerp University (Belgium)**

Supervisors: Prof. Sarah De Saeger and Dr. Johan Robbens

Determination of zearalenone and deoxynivalenol's toxicity in river's water using daphnia-test and algae-test.

2007 (1 months) **Internship at the Laboratory of Food Analysis, Ghent University (Belgium)**

Supervisors: Prof. Sarah De Saeger

Development of immunofiltration tests for mycotoxins detection

## **PRACTICAL EXPERIENCE AND SKILLS**

---

### ***Immunoassays***

Enzyme-linked immunosorbent assay (ELISA), fluorescence polarization immunoassay (FPIA), lateral through immunoassay, magnetic beads-based immunoassay

### ***Electrochemical techniques***

Scanning Electrochemical Microscopy (SECM), amperometric sensors development

### ***Mass-spectrometry (MS)***

Matrix-assisted laser desorption /Ionization (MALDI) MS, Electrospray ionization (ESI) MS

### ***Others***

Microfluidics design and implementation; *In vitro* experiments with adherent cancer cells; Microfabrication by laser ablation and inkjet printing; Focused Ion Beam (FIB); COMSOL simulations

## **PUBLICATIONS**

---

1. Bondarenko, A.; Cortés-Salazar, F.; Gasilova, N.; Lesch, A.; Qiao, L.; Girault, H.H. Analytical Chemistry at the Laboratoire d'Electrochimie Physique et Analytique. *CHIMIA*, 2015, 69 (5), 290-293.
2. Lin T. E.; Cortés-Salazar F.; Lesch A.; Qiao, L.; Bondarenko A.; Girault H. H. Multiple SECM mapping of tyrosinase in micro-contact printed fruit samples on PVDF membrane. *Electrochim. Acta*. 2015, 179, 57–64.
3. Bondarenko A.; Cortés-Salazar F.; Gheorghiu M.; Gáspár S.; Momotenko D.; Stanica L.; Lesch A.; Gheorghiu E.; Girault H. H. Electrochemical push-pull probe: from scanning electrochemical microscopy (SECM) to multimodal altering of cell microenvironment. *Anal. Chem.* 2015, 87, 4479–4486.
4. Qiao L.; Tobolkina E.; Lesch A.; Bondarenko A.; Zhong X.; Liu B.; Pick H.; Vogel H.; Girault H. H. Electrostatic Spray Ionization Mass Spectrometry Imaging. *Anal. Chem.* 2014, 86, 2033–2041.
5. Bondarenko A.; Eremin S. A. Determination of Zearalenone and Ochratoxin A Mycotoxins in Grain by Fluorescence Polarization Immunoassay. *J. Anal. Chem.* 2012, 67 (9), 790–794.

## CONTRIBUTION IN INTERNATIONAL CONFERENCES

---

SECM 2015: 8th International Workshop on Scanning Electrochemical Microscopy: Microsystems, Micromanipulation and Microfabrication (October 9 – 13, 2015, Xiamen, China)

Poster presentation: Bondarenko, A.; Lin, T.-E.; Pick, H.; Lesch, A.; Cortés-Salazar, F.; Girault, H. H. *Detection of Melanoma-Associated Tumor Antigen Tyrosinase in Adherent Cells by Scanning Electrochemical Microscopy.*

ISE 2015: 66th Annual International Society of Electrochemistry Meeting (October 4 – 9, 2015, Taipei, Taiwan)

Oral presentation: Bondarenko, A.; Lin, T.-E.; Pick, H.; Lesch, A.; Cortés-Salazar, F.; Girault, H. H. *Scanning electrochemical microscopy of adherent melanoma cells: alive, fixed and permeabilized.*

SMOBE 2015: Summer meeting on bioelectrochemistry (August 17 – 20, 2015, Antwerp, Belgium)

Oral presentation: Bondarenko, A.; Lin, T.-E.; Pick, H.; Lesch, A.; Cortés-Salazar, F.; Girault, H. H. *Scanning electrochemical microscopy of alive, fixed and permeabilized melanoma cells.*

ISE 2014: 65th Annual International Society of Electrochemistry Meeting (August 31 – September 5, 2014, Lausanne, Switzerland)

Poster presentation: Bondarenko, A.; Pick, H.; Lin, T.-E.; Lesch, A.; Cortés-Salazar, F.; Wittstock, G.; Vogel, Horst.; Girault, H. H. *Contact Mode SECM Imaging of Living Cells: An Ultra-Soft Story*

ElecNano 2014: Electrochemistry in Nanoscience – 6 (May 26 – 28, 2014, Paris, France)

Oral presentation: Bondarenko, A.; Pick, H.; Lin, T.-E.; Lesch, A.; Cortés-Salazar, F.; Wittstock, G.; Vogel, Horst.; Girault, H. H. *Contact mode scanning of biological samples with ultra-soft stylus probes.*

ISE 2013: 64th Annual International Society of Electrochemistry Meeting (September 8 – 13, 2013, Santiago de Queretaro, Mexico)

Poster presentation: Bondarenko, A.; Momotenko, D.; Cortés Salazar, F.; Gaspar, S.; Gheorghiu, M.; Gheorghiu, E.; Girault, H. H. *Microfluidic push-pull device for surface modification: Numerical simulations and experimental verification.*

SSE 2013: Summer School on Electrochemistry for Environmental and Biomedical Applications (June 17 – 21, 2013, Cluj-Napoca, Romania)

Poster presentation: Bondarenko, A.; Momotenko, D.; Cortés Salazar, F.; Gaspar, S.; Gheorghiu, M.; Gheorghiu, E.; Girault, H. H. *Microfluidic push-pull device for surface modification: Numerical simulations and experimental verification.* Best poster award.

MSB 2012: 27<sup>th</sup> international Symposium on MicroScale Bioseparations and Analysis (February 12 – 15, 2012, Geneva, Switzerland)

Poster presentation: Bondarenko, A.; Gassner, A.-L.; Girault, H. H. *“Double bubble” system for capillary electrophoresis.*

BIONANOTOX 2011: Biomaterials and Nanobiomaterials: Recent Advances and Safety-Toxicology Issues (May 5 – 12, 2011, Heraklion, Crete, Greece)

Oral presentation: Bondarenko, A.; Eremin S. A. *Express detection of mycophenolic acid in serum using method of fluorescence polarization immunoassay.*

LOMONOSOV 2010: International Scientific Conference of Students, PhD Students and Young Scientists (April 12 – 15, 2010, Moscow, Russia)

Oral presentation: Bondarenko, A.; Eremin S. A. *Determination of mycotoxins in corn by fluorescence polarization immunoassay.* Best oral presentation award

## **AWARDS**

---

- 2015** Excellent Talk at the student short presentation session, Bioelectrochemistry Symposium at the 66<sup>th</sup> Annual Meeting of the International Society of Electrochemistry (October 4 – 9, 2015, Taipei, Taiwan)
- 2013** Best Poster Award, Summer School on Electrochemistry for Environmental and Biomedical Applications (June 17 – 21, 2013, Cluj-Napoca, Romania)
- 2010** Diploma cum laude of a Specialist in Chemistry (Moscow State University, Moscow, Russia)
- 2010** Best Oral Presentation Award, International Scientific Conference of Students, PhD Students and Young Scientists LOMONOSOV (Moscow, Russia)
- 2009** Best student Scientific Research awarded by I. V. Berezin Foundation (Moscow, Russia)

## **LANGUAGES**

---

<i>Russian</i>	native
<i>English</i>	fluent
<i>French</i>	intermediate